



Amphotericin B Incorporated in Liquid Crystals  
for Lung Fungal Infection Treatment

Rabkwan Chuealee

A Thesis Submitted in Fulfillment of the Requirements for the Degree of

Doctor of Philosophy in Pharmaceutical Sciences

Prince of Songkla University

2009

Copyright of Prince of Songkla University

**Thesis Title** Amphotericin B Incorporated in Liquid Crystals for Lung  
Fungal Infection Treatment

**Author** Mrs. Rabkwan Chuealee

**Major Program** Pharmaceutical Sciences

---

**Major Advisor**

.....  
(Assoc. Prof. Dr. Teerapol Srichana)

**Examining Committee**

.....Chairperson  
(Prof. Dr. Vimon Tantishaiyakul)

**Co-advisor**

.....  
(Prof. Dr. Timothy S. Wiedmann)

.....  
(Prof. Dr. Narong Sarisuta)

.....  
(Assist. Prof. Dr. Sanae Kaewnopparat)

.....  
(Assoc. Prof. Dr. Teerapol Srichana)

.....  
(Assoc. Prof. Dr. Pornanong Aramwit)

The Graduate School, Prince of Songkla University, has approved this thesis as fulfillment of the requirements for the Doctor of Philosophy Degree in Pharmaceutical Sciences

.....  
(Assoc. Prof. Dr. Kerkchai Thongnoo)  
Dean of Graduate School

**Thesis Title:** Amphotericin B Incorporated in Liquid Crystals for Lung Fungal Infection Treatment

**Author:** Mrs. Rabkwan Chuealee

**Major Program:** Pharmaceutical Sciences

**Academic Year:** 2008

## **ABSTRACT**

Cholesteryl carbonate esters, cholesteryl palmityl carbonate (CPC), dicholesteryl carbonate (DCC) and sodium cholesteryl carbonate (SCC) were synthesized as thermotropic liquid crystals in this research work. The phase behavior of these compounds were characterized by using differential scanning calorimetry (DSC), transmission electron microscopy (TEM), polarized light microscope (PLM), small angle X-ray diffraction (SAXD) and solid state nuclear magnetic resonance spectroscopy (ssNMR). CPC, DCC and SCC are stable crystals over wide range of temperatures and exhibited liquid crystal phase at temperature higher than 25 °C. Thus, those compounds provide a desirable feature for their use in dry powder drug delivery systems.

Amphotericin B (AmB) in cholesteryl carbonate esters dry powders were prepared by using solvent evaporation method. All formulations were evaluated for content uniformity and delivery efficiency to lower airways by Andersen cascade impactor (ACI). The results were calculated as the mass median aerodynamic diameter (MMAD), fine particle fraction (FPF) and emitted dose (ED). The results suggest that AmB in liquid crystal dry powder formulations are uniform and stable within the

storage period of 6 months. MMAD of all AmB dry powder formulations were obtained between 4–8  $\mu\text{m}$ . The different types and ratios of liquid crystal to AmB gave significantly different of MMAD ( $p\text{-value} < 0.01$ ). In addition, higher content of liquid crystal in AmB formulation (12:1, mole ratio) tends to decrease MMAD. All AmB in liquid crystals formulations against *Saccharomyces cerevisiae* ATCC 9763 gave higher potency than that of standard AmB ( $p\text{-value} < 0.05$ ). Lower MICs and MFCs of AmB in liquid crystals against *S. cerevisiae* ATCC 9763, *Cryptococcus neoformans* and *Candida albicans* (2–4 times) were obtained as compared to pure AmB. All pure liquid crystals and AmB in liquid crystal dry powder formulations were not toxic to human red blood cells and respiratory cell lines including small airway epithelial and alveolar macrophage cell lines. Furthermore, they did not activate AMs to produce inflammatory mediators including interleukin-1 $\beta$ , tumor necrosis factor- $\alpha$  or nitric oxide at any concentrations tested. This indicates that AmB in liquid crystal as dry powder formulations are potential candidates to be used in lung fungal infectious.

## ACKNOWLEDGEMENTS

This Thesis could not be successfully completed without the help of many persons. First of all, I would like to express my sincere gratitude and deep appreciation to my advisor, Assoc. Prof. Dr. Teerapol Srichana for all of the valuable advice and giving me the opportunity to get the Royal Golden Jubilee Ph.D. Program scholar. I am grateful for his support and guidance while I worked with him. I admire him as an educator and advisor. I learned a great deal from him.

Special thanks and admiration go to Prof. Dr. Timothy S. Wiedmann University of Minnesota for his helpful advices and supports especially warm welcome when I worked in his research group in the USA.

Special thanks and appreciation go to Assist. Prof. Dr. Sanae Kaewnopparat, Assoc. Prof. Dr. Pornanong Aramwit, Prof. Dr. Vimom Tantishaiyakul and Prof. Dr. Narong Sarisuta for their helpful advices. My grateful appreciation also goes to Prof. Dr. L.A. Damani for editing the manuscript.

I offer special thanks to the Department of Pharmaceutical Technology, the Faculty of Pharmaceutical Sciences, Prince of Songkla University and the Institute of Technology Characterization Facility, University of Minnesota for their contribution and use of facilities throughout this study.

For granting financial support in the past 5 years, I would like to thank Thailand Research Fund through the Royal Golden Jubilee Ph.D. Program under Grant No. PHD/0098/2547 and the Nanotechnology Center (NANOTEC) of excellence at PSU.

I would like to thank friends and staffs in the Drug Delivery System Research Center and Department of Pharmaceutical Technology, Prince of Songkla University, with special appreciations go to Ms. Supreedee Sungkarak, Ms. Khemmarat Buaking, Ms. Narumon Changsan and Ms. Titpawan Nakpeng for their assistance, helpful advice and meaningful friendship.

Throughout my graduate work, my beloved son, my daughter and my husband, shared with me the best and most frustrating moments. I am fulfilled with their love and their support.

Finally, my love and gratitude go to my parents, my older sisters and my younger brother who always give me forever love. I am grateful for everything that they have done for me.

Rabkwan Chuealee

# CONTENTS

	<b>Page</b>
•???	iii
<b>ABSTRACT</b>	v
<b>ACKNOWLEDGEMENTS</b>	vii
<b>CONTENTS</b>	ix
<b>LIST OF TABLES</b>	xv
<b>LIST OF ILLUSTRATIONS</b>	xvii
<b>ABBREVIATION AND SYMBOLS</b>	xxv
<b>CHAPTER</b>	
<b>1. GENERAL INTRODUCTION</b>	1
<b>2. LITERATURE REVIEW</b>	
<b>2.1 Liquid crystals</b>	8
<b>2.2 Types of liquid crystals</b>	
2.2.1 The lyotropic liquid crystals	9
2.2.2 The thermotropic liquid crystals	12
<b>2.3 Phases of thermotropic liquid crystals</b>	
2.3.1 Discotic phase	13
2.3.2 Columnar phase	14
2.3.3 Smectic phase	14
2.3.4 Nematic phase	16
2.3.5 Cholesteric phase	16

## CONTENTS (continued)

	<b>Page</b>
<b>2.4 Physicochemical characterization of liquid crystal</b>	
2.4.1 Microscopy	18
2.4.2 X-ray Diffraction	19
2.4.3 Differential Scanning Calorimetry	21
2.4.4 solid state Nuclear Magnetic Resonance Spectroscopy	22
<b>2.5 Respiratory tract</b>	22
<b>2.6 Lung fungal infections</b>	25
2.6.1 Histoplasmosis	25
2.6.2 Aspergillosis	26
2.6.3 Coccidioidomycosis	27
2.6.4 Other fungi	27
<b>2.7 Treatments of lung fungal infection</b>	
2.7.1 Fungal cell structure and targets	28
2.7.2 Amphotericin B (AmB)	29
2.7.3 Mechanism of action of AmB	30
<b>2.8 Formulations of AmB for lung infection</b>	
2.8.1 Conventional AmB formulation	32
2.8.2 Lipids based AmB	33
<b>2.9 Aerosol formulation</b>	42
2.9.1 Factors affecting particle deposition in the lung	43



## CONTENTS (continued)

	<b>Page</b>
2.9.2 Particle size analysis of aerosol	44
<b>2.10 Development of AmB aerosols</b>	<b>46</b>
<b>3. SYNTHESIS AND CHARACTERIZATION OF CHOLESTERIC LIQUID CRYSTALS</b>	
<b>3.1 Introduction</b>	<b>49</b>
<b>3.2 Materials and methods</b>	
3.2.1 Synthesis of cholesteryl carbonate esters	51
3.2.2 Characterization of cholesteryl carbonate esters	55
<b>3.3 Results and discussions</b>	<b>57</b>
<b>3.4 Conclusions</b>	<b>77</b>
<b>4. INTERACTION OF AMPHOTERICIN B WITH CHOLESTERYL CARBONATE ESTERS</b>	
<b>4.1 Introduction</b>	<b>78</b>
<b>4.2 Materials and methods</b>	
4.2.1 Materials	79
4.2.2 Sample preparation	79
4.2.3 Differential Scanning Calorimetry	81
4.2.4 Transmission Electron Microscopy	81
4.2.5 Polarized Light Microscope	81
4.2.6 Small Angle X-ray Diffraction	82

## CONTENTS (continued)

	<b>Page</b>
4.2.7 solid state Nuclear Magnetic Resonance Spectroscopy	82
<b>4.3 Results and discussions</b>	
4.3.1 Differential Scanning Calorimetry Studies	82
4.3.2 Transmission Electron Micrographs	89
4.3.3 Polarized Light Microscopic Studies	90
4.3.4 State diagram analysis	92
4.3.5 Small Angle X-ray Diffraction Patterns	96
4.3.6 solid state Nuclear Magnetic Resonance Spectra	100
<b>4.4 Conclusions</b>	105
<b>5. AMPHOTERICIN B IN LIQUID CRYSTALS AS DRY POWDER AEROSOLS</b>	
<b>5.1 Introduction</b>	106
<b>5.2 Materials and methods</b>	
5.2.1 Validation of HPLC method for determination of AmB	108
5.2.2 Preparations of AmB in cholesteryl carbonate esters dry powder	110
5.2.3 Content uniformity of AmB in cholesteryl carbonate esters dry powders	110
5.2.4 Solubility studies of AmB in cholesteryl carbonate esters	111
5.2.5 Dissolution studies of AmB in cholesteryl carbonate esters	111

## CONTENTS (continued)

	<b>Page</b>
5.2.6 <i>In vitro</i> deposition of AmB in cholesteryl carbonate esters dry powder by Andersen Cascade Impactor	112
5.2.7 Statistical analysis	112
<b>5.3 Results and discussions</b>	
5.3.1 Method validation of AmB	113
5.3.2 Calibration curve for standard AmB	115
5.3.3 Stability of AmB in cholesteryl carbonate esters formulations	116
5.3.4 Solubility of AmB formulations	117
5.3.5 Dissolution profiles of AmB in cholesteryl carbonate esters	118
5.3.6 Aerosolization of AmB in cholesteryl carbonate esters dry powder	121
<b>5.4 Conclusions</b>	126
<b>6. BIOACTIVITY AND TOXICITY STUDIES OF AMPHOTERICIN B INCORPORATED IN LIQUID CRYSTALS</b>	
<b>6.1 Introduction</b>	127
<b>6.2 Materials and methods</b>	
6.2.1 Potency of AmB in cholesteryl carbonate esters dry powders	129
6.2.2 Evaluation of AmB formulations potency	129
6.2.3 Broth microdilution for antifungal susceptibility testing	131

## **CONTENTS (continued)**

	<b>Page</b>
6.2.4 Hemolysis of AmB in cholesteryl carbonate esters dry powders	133
6.2.5 Cytotoxicity and determination of cytokines and nitric oxide productions	134
6.2.6 Statistical analysis	139
<b>6.3 Results and discussions</b>	
6.3.1 Activity of AmB in cholesteryl carbonate ester dry powder against fungal cells	140
6.3.2 Hemolysis of AmB in cholesteryl carbonate ester dry powder	143
6.3.3 Cytotoxicity of AmB in cholesteryl carbonate ester to the respiratory tract cell lines	149
6.3.4 Immunological response of AMs to AmB in cholesteryl carbonate ester dry powder	153
<b>6.4 Conclusions</b>	158
<b>7. CONCLUSIONS</b>	159
<b>BIBLIOGRAPHY</b>	161
<b>APPENDIX</b>	179
<b>VITAE</b>	218

## LIST OF TABLES

<b>Table</b>		<b>Page</b>
<b>1.1</b>	Average cost of Amphotericin B therapy in various formulations for one week	3
<b>2.1</b>	Industrial formulations of Amphotericin B	39
<b>2.2</b>	Advantages and disadvantages of dry powder inhalers	43
<b>3.1</b>	Characteristic functional group of cholesteryl carbonate esters	59
<b>3.2</b>	Thermotropic phase transition temperatures of sodium cholesteryl carbonate (SCC), cholesteryl palmityl carbonate (CPC), dicholesteryl carbonate (DCC) cholesteryl oleoyl carbonate (COC) and cholesteryl myristate (CM)	64
<b>3.3</b>	Spacing of X-ray diffraction peaks of sodium cholesteryl carbonate (SCC), cholesteryl myristate (CM) and cholesteryl oleyl carbonate (COC) obtained at the indicated temperatures	71
<b>4.1</b>	$^{13}\text{C}$ chemical shift (ppm) of pure cholesteryl palmityl carbonate (CPC) and binary mixture of AmB and CPC (1:3, mole ratio) at various physical states	104
<b>5.1</b>	Linearity of Amphotericin B standard curve determined by HPLC	114

## LIST OF TABLES (continued)

		<b>Page</b>
<b>5.2</b>	Accuracy of Amphotericin B standard curve determined by HPLC	115
<b>5.3</b>	Composition and % drug content of Amphotericin B in cholesteryl carbonate ester dry powders	116
<b>5.4</b>	Solubility of Amphotericin B and Amphotericin B formulations containing 0.25% w/v SDS in phosphate buffer saline pH 7.4	117
<b>5.5</b>	The aerodynamic characteristics of Amphotericin B in cholesteryl carbonate ester dry powders	125
<b>6.1</b>	Potency, minimum inhibitory concentration (MIC) and minimum fungicidal concentration (MFC) of Amphotericin B in cholesteryl carbonate ester dry powders	142

## LIST OF ILLUSTRATIONS

<b>Figure</b>		<b>Page</b>
<b>2.1</b>	Formation of lyotropic liquid crystal	10
<b>2.2</b>	Formation of lyotropic liquid crystal at various concentrations of amphiphilic molecules	11
<b>2.3</b>	Molecular arrangement of thermotropic liquid crystal	12
<b>2.4</b>	Schematic representation of the discotic nematic phase	13
<b>2.5</b>	Schematic representation of the columnar nematic phase and the hexagonal columnar phase	14
<b>2.6</b>	The layer arrangement of rod-like molecules in smectic liquid crystals	15
<b>2.7</b>	The orientational order in a nematic liquid crystal made of rod-like molecules	16
<b>2.8</b>	The arrangement of molecules in cholesteric liquid crystal phase	17
<b>2.9</b>	Anatomy of respiratory tract	23
<b>2.10</b>	A schematic representation of airway branching in the human lung	24
<b>2.11</b>	The chemical structure of ergosterol	28
<b>2.12</b>	The chemical structure of Amphotericin B (AmB)	29
<b>2.13</b>	Model illustrating the possibility for the formation of channels by AmB interacting with sterol containing membranes	31
<b>2.14</b>	Schematic representation of hydrogen bond formation	32

## LIST OF ILLUSTRATIONS (continued)

		<b>Page</b>
<b>2.15</b>	Schematic representation of possible locations of a liposome– associated with AmB	34
<b>2.16</b>	Structure feature of AmB interacted with cholesteryl sulfate	35
<b>2.17</b>	AmB and lipid arrangement in 1:1 interdigitated complex Abelcet <sup>™</sup>	37
<b>2.18</b>	Mechanisms of anticellular action of AmB: the formation of transmembrane pores.	40
<b>2.19</b>	Mechanisms of anticellular action of liposomal AmB	41
<b>3.1</b>	Synthesis route of sodium cholesteryl carbonate (SCC)	52
<b>3.2</b>	Synthesis route of cholesteryl palmityl carbonate (CPC)	53
<b>3.3</b>	Synthesis route of dicholesteryl carbonate (DCC)	54
<b>3.4</b>	A plot of the excess heat capacity as a function of temperature for SCC, cholesteryl myristate (CM) and cholesteryl oleyl carbonate (COC)	60
<b>3.5</b>	A plot of the excess heat capacity as a function of temperature of CPC	62
<b>3.6</b>	A plot of the excess heat capacity as a function of temperature of DCC	63
<b>3.7</b>	Photographs of SCC crystals using polarizing lenses at various temperatures	65



## LIST OF ILLUSTRATIONS (continued)

		<b>Page</b>
<b>3.8</b>	Photographs of CPC using polarizing lenses at various temperatures	66
<b>3.9</b>	Photographs of DCC using polarizing lenses at various temperatures	67
<b>3.10</b>	Photographs of COC using polarizing lenses at various temperatures	68
<b>3.11</b>	A plot of the X-ray diffractometry intensity as a function of $q$ ( $1/\text{\AA}$ ) obtained at 25 °C for SCC	68
<b>3.12</b>	A plot of the X-ray diffractometry intensity as a function of $d$ ( $\text{\AA}$ ) obtained at 25 °C for SCC	70
<b>3.13</b>	A plot of the X-ray diffractometry intensity as a function of $d$ ( $\text{\AA}$ ) for SCC at indicated temperatures	72
<b>3.14</b>	A plot of the X-ray diffraction intensity as a function of $q(1/\text{\AA})$ for CM at the indicated temperature	73
<b>3.15</b>	A plot of the X-ray diffraction intensity as a function of $d$ ( $\text{\AA}$ ) for COC at the indicated temperature	74
<b>4.1</b>	Chemical structures of CPC, DCC, SCC and cholesterol	80
<b>4.2</b>	A plot of the excess heat capacity as a function of temperature (heating process) for AmB in CPC at mole ratios; 0:1, 1:12, 1:6, 1:3, 1:2, 1:1 and 1:0	83

## LIST OF ILLUSTRATIONS (continued)

		<b>Page</b>
<b>4.3</b>	A plot of the excess heat capacity as a function of temperature (cooling process) for AmB in CPC at mole ratios; 0:1, 1:12, 1:6, 1:3, 1:2 and 1:1	84
<b>4.4</b>	A plot of the excess heat capacity as a function of temperature (heating process) for AmB in DCC at mole ratios; 0:1, 1:12, 1:6, 1:3, 1:2, 1:1 and 1:0	85
<b>4.5</b>	A plot of the excess heat capacity as a function of temperature (cooling process) for AmB in DCC at mole ratios; 0:1, 1:12, 1:6, 1:3, 1:2 and 1:1	87
<b>4.6</b>	A plot of the excess heat capacity as a function of temperature (heating process) for AmB in SCC at mole ratios; 0:1, 1:12, 1:6, 1:3, 1:2, 1:1 and 1:0	88
<b>4.7</b>	A plot of the excess heat capacity as a function of temperature (cooling process) for AmB in SCC at mole ratios; 0:1, 1:12, 1:6, 1:3, 1:2 and 1:1	89
<b>4.8</b>	TEM micrographs of AmB in DCC with different mole ratios; 1:3, 1:6, 1:12 and pure DCC	90
<b>4.9</b>	PLM micrographs of pure CPC, AmB in CPC, pure DCC, AmB in DCC, pure SCC and AmB in SCC	91
<b>4.10</b>	State diagram of binary mixture of AmB in CPC	93
<b>4.11</b>	State diagram of binary mixture AmB in DCC	94

## LIST OF ILLUSTRATIONS (continued)

		<b>Page</b>
<b>4.12</b>	State diagram of binary mixture AmB in SCC	95
<b>4.13</b>	A plot of the X-ray diffractometry intensity as a function of $2\theta$ for pure CPC	97
<b>4.14</b>	A plot of the X-ray diffractometry intensity as a function of $2\theta$ for pure CPC during cooling down process	98
<b>4.15</b>	A plot of the X-ray diffractometry intensity as a function of $2\theta$ for binary mixture of AmB in CPC (1:3, mole ratio) during heating up process	98
<b>4.16</b>	A plot of the X-ray diffractometry intensity as a function of $2\theta$ for AmB in CPC (1:3, mole ratio) during cooling down process	99
<b>4.17</b>	$^{13}\text{C}$ MASNMR spectra of pure CPC	102
<b>4.18</b>	$^{13}\text{C}$ MASNMR spectra of binary mixture of AmB in CPC (1:3, mole ratio)	103
<b>5.1</b>	Andersen cascade impactor and respiratory airways	113
<b>5.2</b>	Precision of AmB analysis; intra-day and inter-day	114
<b>5.3</b>	Standard curve of AmB	115
<b>5.4</b>	<i>In vitro</i> release of AmB in CPC formulations in phosphate buffer saline pH 7.4 containing 0.25% w/v SDS	119
<b>5.5</b>	<i>In vitro</i> release of AmB in DCC formulations in phosphate buffer saline pH 7.4 containing 0.25% w/v SDS	120

## LIST OF ILLUSTRATIONS (continued)

	<b>Page</b>
<b>5.6</b> <i>In vitro</i> release of AmB in SCC formulations in phosphate buffer saline pH 7.4 containing 0.25% w/v SDS	120
<b>5.7</b> <i>In vitro</i> release of AmB in cholesterol formulations in phosphate buffer saline pH 7.4 containing 0.25% w/v SDS	121
<b>5.8</b> Size distribution of AmB in CPC and AmB in DCC dry powder formulations on each stage of the ACI after aerosolization at a flow rate of 60 L/min	122
<b>5.9</b> Size distribution of AmB in SCC and AmB in cholesterol dry powder formulations on each stage of the ACI after aerosolization at a flow rate of 60 L/min	123
<b>6.1</b> Sandwich enzyme linked immunosorbent assay	138
<b>6.2</b> Griess reaction	139
<b>6.3</b> <i>In vitro</i> hemolysis after incubation with pure CPC, pure DCC, pure SCC, pure cholesterol and pure AmB	144
<b>6.4</b> <i>In vitro</i> hemolysis after incubation with AmB in CPC formulations	145
<b>6.5</b> <i>In vitro</i> hemolysis after incubation with AmB in DCC formulations	146
<b>6.6</b> <i>In vitro</i> hemolysis after incubation with AmB in SCC formulations	147

## LIST OF ILLUSTRATIONS (continued)

		<b>Page</b>
<b>6.7</b>	<i>In vitro</i> hemolysis after incubation with AmB in cholesterol formulations	148
<b>6.8</b>	Viability of SAEC and AMs after they have been incubated with pure CPC, pure DCC, pure SCC, pure cholesterol and untreated cell line	150
<b>6.9</b>	Viability of SAEC and AMs after they have been incubated with pure AmB and AmB in CPC formulations	151
<b>6.10</b>	Viability of SAEC and AMs after they have been incubated with pure AmB and AmB in DCC formulations	151
<b>6.11</b>	Viability of SAEC and AMs after they have been incubated with pure AmB and AmB in SCC formulations	152
<b>6.12</b>	Viability of SAEC and AMs after they have been incubated with pure AmB and AmB in cholesterol formulations	152
<b>6.13</b>	The level of inflammatory cytokine IL-1 $\beta$ , TNF- $\alpha$ and nitric oxide produced from AMs after exposure with AmB in CPC formulations	154
<b>6.14</b>	The level of inflammatory cytokine IL-1 $\beta$ , TNF- $\alpha$ and nitric oxide produced from AMs after exposure with AmB in DCC formulations	155

## LIST OF ILLUSTRATIONS (continued)

		<b>Page</b>
<b>6.15</b>	The level of inflammatory cytokine IL-1 $\beta$ , TNF- $\alpha$ and nitric oxide produced from AMs after exposure with AmB in SCC formulations	156
<b>6.16</b>	The level of inflammatory cytokine IL-1 $\beta$ , TNF- $\alpha$ and nitric oxide produced from AMs after exposure with AmB in cholesterol formulations	157

## ABBREVIATIONS AND SYMBOLS

Å	=	angstrom
% RSD	=	Percentage of relative standard deviation
°C	=	Degree Celsius
ΔH	=	Enthalpy
ΔS	=	Entropy
μL	=	microliter
μm	=	micrometer
μM	=	micromolar
1-D	=	one dimensional
2-D	=	two dimension
ABCD	=	Amphotericin B colloidal dispersion
ABLCL	=	Amphotericin B lipid complex
ACI	=	Andersen Cascade Impactor
AIDS	=	Acquired immunodeficiency syndromes
AmB	=	Amphotericin B
AMs	=	alveolar macrophages
ANOVA	=	analysis of variance
API	=	active pharmaceutical ingredients
ATCC	=	American Type Cell Culture Collection
<i>BL</i>	=	bilayer
BMT	=	bone marrow transplantation

## ABBREVIATIONS AND SYMBOLS (continued)

cryo-TEM	=	Cryo-transmission electron microscope
<sup>13</sup> C-NMR	=	Carbon-13 nuclear magnetic resonance
cal/mole-K	=	calory/mole-Kelvin
CDCl <sub>3</sub>	=	deuteriochloroform
CE	=	cholesteryl ester
CFU	=	colony forming unit
Chol	=	cholesterol
CHC	=	cholesteryl hexyl carbonate
CMC	=	critical micelle concentration
CFC	=	chlorofluorocarbon
CO	=	cholesteryl oleate
COC	=	cholesteryl oleyl carbonate
CPC	=	cholesteryl palmityl carbonate
CP	=	cross polarization
D <sub>ae</sub>	=	aerodynamic diameter
DEPT	=	Distortionless Enhancement by Polarization Transfer
DFM	=	dimethylformamide
DMPC	=	dimyristoylphosphatidylcholine
DMPG	=	dimyristoylphosphatidylglycerol
DMSO	=	dimethylsulfoxide
DPIs	=	dry powder inhalers
DSC	=	differential scanning calorimetry



## ABBREVIATIONS AND SYMBOLS (continued)

DSPG	=	disteroylphosphatidylcholine
ED	=	emitted dose
EDTA	=	ethylenediamine tetraacetic acid
e.g.	=	<i>ilocal gratia</i>
ELISA	=	enzyme-linked immunosorbent assay
ESI	=	electrospray ionization
FBS	=	fetal bovine serum
FPF	=	fine particle fraction
FTIR	=	Fourier transform infrared spectroscopy
FWHM	=	full widths at half maximum
g	=	gram
GSD	=	geometric standard deviation
h	=	hour
<sup>1</sup> H-NMR	=	proton nuclear magnetic resonance
HEPES	=	4-(2-hydroxyethyl)-1-piperazineethanesulfonic acid
HEPES-BSS	=	4-(2-hydroxyethyl)-1-piperazineethanesulfonic acid – Buffered Saline Solution
HPLC	=	high performance liquid chromatography
HSPC	=	Hydrogenated soy phosphatidylcholine
Hz	=	hertz
i.d.	=	internal diameter
i.e.	=	<i>id est</i>

## ABBREVIATIONS AND SYMBOLS (continued)

IgE	=	Immunoglobulin E
IgG	=	Immunoglobulin G
IL-1 $\beta$	=	interleukine-1 $\beta$
iNOS	=	inducible nitric oxide synthase
kcal/mole	=	kilocalories/mole
kHz	=	kilohertz
kV	=	kilovolt
kW	=	kilowatt
L	=	liter
LDL	=	low density lipoprotein
LOD	=	limit of detection
LOQ	=	limit of quantification
LNS	=	lipid nanosphere
LPS	=	lipopolysaccharide
m <sup>2</sup>	=	square meter
M	=	mole
mA	=	milliampere
MASNMR	=	magic angle sample spinning nuclear magnetic resonance
mbar	=	millibar
MDIs	=	metered dose inhalers
MFCs	=	minimum fungicidal concentrations
mg	=	milligram

## ABBREVIATIONS AND SYMBOLS (continued)

MHz	=	megahertz
mL	=	milliliter
MICs	=	minimum inhibitory concentrations
min	=	minute
mL	=	milliliter
<i>ML I</i>	=	monolayer type I
<i>ML II</i>	=	monolayer type II
mm	=	millimeter
mM	=	millimolar
MMAD	=	mass median aerodynamic diameter
MPS	=	mononuclear phagocyte system
MS	=	Mass spectrometry
MTT	=	(3-(4,5-dimethylthiazole-2-yl)-2 diphenyltetrazolium bromide
MW	=	molecular weight
N <sub>2</sub>	=	nitrogen gas
NED	=	N-(1-naphthyl)-ethylenediamine dihydrochloride
nm	=	nanometer
NMR	=	nuclear magnetic resonance
NO	=	nitric oxide
PBS	=	phosphate buffer solution
PC	=	phosphatidylcholine
PG	=	propylene glycol

## ABBREVIATIONS AND SYMBOLS (continued)

PLM	=	polarized light microscope
pMDI	=	pressurized meter-dose inhaler
ppm	=	part per million
RBC	=	red blood cells
rpm	=	round per minute
RT	=	room temperature
s	=	second
SAEC	=	small airway epithelial cell
SAGM	=	small airway growth media
SAXD	=	small angle X-ray diffraction
SCC	=	sodium cholesteryl carbonate
SD	=	standard deviation
SDA	=	Sabouraud dextrose agar
SDS	=	sodium dodecylsulfate
SmA	=	Smectic A
SmC	=	Smectic C
SPC	=	soybean phosphatidylcholine
spp.	=	species
ssNMR	=	solid-state nuclear magnetic resonance
TEM	=	transmission electron microscopy
TLC	=	Thin-layer chromatography
T <sub>k</sub>	=	Kraft temperature

## ABBREVIATIONS AND SYMBOLS (continued)

TMS	=	tetramethylsilane
TNF- $\alpha$	=	tumor necrosis factor- $\alpha$
T <sub>p</sub>	=	transition temperature
USA	=	United States of America
USFDA	=	United States Food and Drug Administration
VEM	=	video-enhanced microscope
UV	=	ultraviolet
UV/VIS	=	ultraviolet/visible
v/v	=	volume by volume
WXR	=	wide angle X-ray diffraction
w/v	=	weight by volume
XRD	=	X-ray diffraction

# CHAPTER 1

## GENERAL INTRODUCTION

### 1.1 Rationale

Fungal infections have emerged as a worldwide health-care problem in the last decade (Horn *et al.*, 1985; Harvey and Myers, 1987; Fraser *et al.*, 1992; Henderson and Hirvela, 1996) particularly from the attendant feature in immunodeficiency patients. The infectious fungi are significant cause of morbidity and mortality in seriously ill and immunocompromised patients (Hay, 1999). In the United States, the nosocomial infections of fungal origin increased by 40% from 1980 to 1989. The organisms causing systemic fungal infections include *Candida albicans* (80%), *Aspergillus fumigatus* (15%), *Candida tropicalis* and *Cryptococcus neoformans* (Brykier, 2005).

Treatment of systemic fungal infection is complicated and often prolonged, because the clinical presentation of invasive fungal and bacterial infections is similar, and this may lead to a delay in diagnosis and treatment. Systemic fungal infection may result from breathing in the spores of fungi, which normally live in environment or as opportunistic disease in immunocompromised individuals.

Amphotericin B (AmB) is a broad spectrum antifungal drug and also used as the drug of choice in systemic fungal infections (Walsh and Pezzo, 1988). AmB is an antifungal produced as a fermentation by-product of *Streptomyces nodosus*, a

soil actinomycetes (Abu-Salah, 1996). The chemical structure features include a large lactone ring of 37 carbon atoms in which one side of the ring is a hydrophobic conjugated heptane chain and the other side is hydrophilic due to the presence of seven hydroxyl groups. The macrolide ring also contains a six-membered ketalic ring to which the aminosugar, mycosamine, is bonded through an  $\alpha$ -linkage. The dual hydrophobic-hydrophilic or amphipathic nature of AmB promotes the complexation with other moieties that can result in altered pharmacokinetics and pharmacodynamics. For its mechanism of action, AmB is believed to bind with sterols in cell membranes thereby forming pores to cause cell lysis (Clements and Peacock, 1990). Drug toxicity, especially nephrotoxicity, is a significant problem as AmB also damages mammalian cell membranes. The major adverse effects limit the dose that may be given.

AmB is a yellow or orange powder, and is practically insoluble in water, soluble in dimethylsulphoxide (DMSO) and in propylene glycol (PG), slightly soluble in dimethylformamide (DMF), very slightly soluble in methanol, and practically insoluble in alcohol. It is sensitive to light in dilute solutions and is inactivated at low pH values. AmB should be stored in a well-sealed, temper-proof container, protected from light at a temperature of 2 to 8°C.

The recent advances in drug delivery techniques have resulted in the development of lipid-based formulations of AmB. These formulations, which include liposomes, micellar solutions, and emulsion systems, have been shown to have reduced toxicity. These complex formulations of AmB (AmBisome<sup>®</sup>, Amphocil<sup>®</sup> and Abelcet<sup>™</sup>) are also commercially available. The toxicity of AmB can be reduced by incorporation into liposomes or by complexation with various lipids. All these formulations enhance the therapeutic index of AmB by decreasing its toxicity (Szoka and Tang, 1993;

Hiemenz and Walsh, 1998). However, several severe side effects, albeit infrequent, have been reported in patients; including allergic reactions and cardiopulmonary toxicity (Walsh and Pezzo, 1988; Gallis, *et al.*, 1990; Schaffner and Roland, 2000). The comparable efficacy of lipid-based AmB can be achieved only when they are administered at a higher dose than conventional formulation (Fungizone®). Furthermore, lipid complex formulations are much more expensive than conventional formulation. The high cost is a significant issue when using lipid-AmB formulations, but clinical studies have shown that the risk of nephrotoxicity outweighs the cost of treatment with lipid formulation (Table 1.1).

**Table 1.1** Average cost of AmB therapy in various formulations for one week (Antoniadou and Dupont, 2005).

Total cost	Conventional AmB		Lipid-AmB formulation	
	Fungizone®	AmBisome®	Amphocil®	Abelcet™
Typical daily dose (mg/kg)	1	5	4	5
Estimate weekly cost (US \$)	260	5800	3360	9200

The mortality and cause of renal failure associated with AmB therapy were reported among 707 admissions treated with AmB, 30% developed acute renal failure resulting in prolonged hospitalization (8.2 days), higher mortality and increased cost per episode (\$30,000) (Robinson and Nahata, 1999). Lipid formulations of AmB and conventional AmB were compared in terms of effectiveness and tolerability in patients with systemic fungal infections. It was noted that there was no difference in efficacy. Nephrotoxicity risk was reduced by 58% in patients treated with lipid



formulation, and more importantly mortality was reduced by 28% in the same group (31 patients treated with lipid formulation AmB) (Antoniadou and Dupont, 2005).

Therefore, the lipid-based AmB formulations that were developed in an attempt to reduce the side effects associated with the conventional AmB formulation largely achieved the goal. While the pharmacokinetic properties of the lipid-based formulations are highly variable, it is accepted that lipid-based formulations do reduce nephrotoxicity. The current paradigm is that lipids provide a protective effect based on the altered affinity of AmB for human cell membranes while preserving the affinity of AmB for fungal membranes (Sawaya *et al.*, 1995). There is still a drawback, as lipid-based formulations are less stable, less potent and require 6-10 fold greater dosages than conventional to achieve a similar therapeutic effect (Plotnick, 2000; Bennett, 2001). Furthermore, neither the rationale for the pharmacokinetic profile of AmB (especially lipid-based formulation) nor the cause of its high variability has established (Carver, 1999; Santangelo *et al.*, 2000).

Given this background there is continued interest in developing a new AmB formulation that maintains the potency with fewer side effects and has low cost. A promising approach is to alter the administration method and deliver therapeutic agent directly to the respiratory tract. Dry powder inhalers (DPI) are commonly used for this purpose. Local delivery of medication to the lung is highly desirable, especially in patients with specific pulmonary disease like cystic fibrosis, asthma, chronic pulmonary infections, or lung cancer. The principal advantages of local delivery include reduced systemic side effects and higher dose levels of the applicable medication at the site of drug action (Bennett *et al.*, 2002).

The most prevalent and important fungal infections in lung-transplanted

patients are caused by *Aspergillus* spp., which give rise to considerable morbidity and mortality. Nebulized AmB has been used successfully in the rat model of invasive aspergillosis and in human (Monforte *et al.*, 2001). Aerosolized AmB prophylaxis may be efficient and safe in preventing *Aspergillus* infection in lung-transplanted and AIDS patients (Conneally *et al.*, 1990; Beyer *et al.*, 1993; Monforte *et al.*, 2001; Ruijgrok *et al.*, 2001). Sorensen and coworkers (1993) used aerosolization of liposomal (AmBisome<sup>®</sup>) and non-liposomal (Fungizone<sup>®</sup>) AmB for pulmonary fungal infection treatment. Liposomal AmB (AmBisome<sup>®</sup>) was shown to be more amenable for nebulization than non-liposomal (Fungizone<sup>®</sup>). The small multilamellar AmB liposomes were successfully prepared by a reverse phase evaporation technique and then stabilized by lyophilization. The resulting liposomal dry powder inhaler formulation had a shelf life over 1 year with refrigerated storage (Shah and Misra, 2004). However, liposomal AmB dry powder inhaler gave a fine particle fraction of only 25%. This is quite low and would be expected to result in low deposition in the lung and high deposition in the upper respiratory tract with the expected consequence of reduced efficacy and increased side effects.

In an effort to develop a formulation that superior properties, saturated cholesteryl carbonate esters were examined. Certain of these lipids are known to form liquid crystals upon temperature changes (thermotropic mesogen), which was of interest for their potential as liquid crystal microparticle formulation. It was postulated that a low temperature, highly ordered crystal matrix could provide a chemical environment of enhance chemical and physical stability of AmB as a dry powder inhaler formulation. Moreover, the low polarity of the molecules was believed to be a desirable feature for preparing an aerosol formulation that had a high fine particle fraction. Following

administration to the lung, the elevated temperature would result in a transition from the stable crystal to a liquid crystalline phase. The formation of a liquid crystalline state was then expected to modulate the *in vivo* release of AmB. Because the interaction of AmB with membranes critically depends on cholesterol, cholesterol carbonate esters were hypothesized to favorably affect the pharmacokinetic distribution and thereby the pharmacodynamic interactions to increase the efficacy and reduce the toxicity.

However, the physicochemical properties of cholesteryl carbonate ester were not well characterized, despite the fact that cholesteryl oleyl carbonate (COC) is a commercially available cholesteryl carbonate that forms a thermotropic liquid crystal. It is found in a variety of applications such as biosensors, pressure indicator, thermometers, and drug delivery systems (Crissey *et al.*, 1965; Elser and Ennular, 1976; Lin *et al.*, 1996). COC undergoes a smectic C-phase to a cholesteric phase transition at 18.3 °C, and then another transition to an isotropic phase (35.1 °C) when heated from low temperature. The degree of unsaturated of the acyl chain in COC affects the molecular motions (Croll *et al.*, 1987). Whereas, saturated acyl chain cholesteryl carbonate esters of the same length exhibited only solid crystal phase at the room temperature.

Cholesteryl carbonate esters are lipid compounds with the carbonate moiety as the sole polar functional group. Incorporation of active ingredients into the solid lipid matrix offers protection against chemical degradation of the active compound (Jenning and Gohla, 2001), as well as allowing either immediate or sustained release, depending on the polymorphic transition of lipid matrix (Jenning *et al.*, 2000). The highly ordered crystal packing of saturated cholesteryl carbonate microparticles leads to drug expulsion but also increase physical stability.

Conventional AmB (Fungizone<sup>®</sup>) often causes serious side effects whereas lipid-based AmB formulations require complex manufacturing methods with high cost. The development of new pharmaceutical formulations of AmB would therefore be desirable. In this study lipid based, cholesteryl carbonate derivatives, were synthesized, characterized and used to prepare AmB dry powders. It was hypothesized that particulate systems would improve stability, improve efficiency and reduce toxicity of AmB.

## **1.2 The objective of the studies**

1. Synthesize cholesteryl carbonate derivatives (cholesteryl palmityl carbonate; CPC, dicholesteryl carbonate; DCC and sodium cholesteryl carbonate; SCC) and characterize their thermotropic phase behavior
2. Study interaction of AmB with cholesteryl carbonate ester
3. Characterize the interaction of AmB in cholesteryl carbonate ester as dry powders
4. Evaluate *in vitro* efficacy of AmB dry powder in cholesteryl carbonate esters against *Saccharomyces cerevisiae*, *C. neoformans* and *C. albicans*
5. Examine the toxicity of AmB in cholesteryl carbonate ester dry powder in respiratory-associated cell lines
6. Determine the immunological response of alveolar macrophage to AmB dry powders

## CHAPTER 2

### LITERATURE REVIEW

#### 2.1. Liquid crystals

Liquid crystals are aggregated organic compounds that are in a state between liquid and solid forms. They flow like liquids, often being viscous and jellylike, but behave as crystals in other properties (light scattering and reflection). Typical liquid crystals have either a rodlike or a disclike shape, although many exceptions to this basic motif have been described (Friberg, 2000). Most liquid crystals are neutral organic compounds. In addition, metallomesogens are liquid crystals that have one or more metals incorporated into the liquid-crystalline aggregate. Also, minerals or inorganic compounds can form liquid crystalline phases (Binnemans, 2005). The driving force for the formation of a liquid crystalline phase (mesophase) is primarily entropic, since there is considerably more disorder in comparison to the solid crystalline phase. The interactions among the anisometric molecules (dipole-dipole interactions, van der Waal interactions,  $\pi$ - $\pi$  stacking) are also important and are stronger than that seen in the pure liquid phase (Saeva, 1979). The liquid crystals are anisotropic materials and their properties vary according to the average alignment with the director. If the alignment is large, the material is very anisotropic. When the alignment is small, the material is almost isotropic.

## 2.2 Types of liquid crystals

### 2.2.1 The lyotropic liquid crystal

Lyotropic liquid crystals are formed when certain compounds, (amphiphilic or amphiphile molecules) are treated with a solvent. These compounds are characterized by a sort of split personality; one end of the molecule is polar and attracted to water while the other end is non-polar and attracted to hydrocarbons, or lipophilic. Figure 2.1, shows amphiphilic molecules orientate themselves such that either the polar ends are dissolved in a polar solvent. While the non-polar ends are kept isolated from unlike solvent. The phase diagram shows the changes in structure as the concentration of amphiphilic molecules increases (Figure 2.1). The concentration at which micelles form in solution is called the critical micelle concentration (CMC) (Figure 2.1, is shown as a dotted line). The solid line is the solubility of the amphiphile and the temperature at which the solubility line intersects the CMC is referred to the Kraft point ( $T_k$ ). Below the Kraft point, the concentration of the amphiphile is too low and so no micelles or liquid crystals are formed.

At low concentrations of amphiphiles, micelles are generally the first type of aggregate that is formed. According to Gibbs phase rule, micellar solutions are one phase and represent a uniform, macroscopic state. At a microscopy (actually nanometer scale), the molecules are seen to form aggregates, often with fairly consistent aggregation numbers (i.e. the number of molecules/aggregate). Micelles are often nearly spherical in shape to minimize the contact between the aggregate and water.

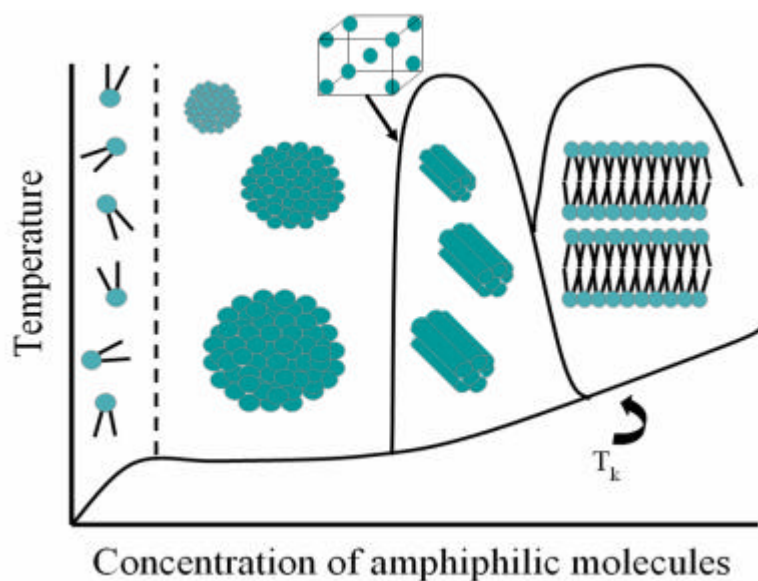


**Figure 2.1** Formation of lyotropic liquid crystal (adapted from <http://plc.cwru.edu/tutorial/enhanced/files/llc/phase/phase.htm>)

As the concentration is increased further, a body-centered cubic crystal structure, rod-shaped micelles may be formed and often assemble into hexagonal arrays made out of six rods grouped around a central one for a total of seven as shown in Figure 2.2 (A), (B) and (C), in respective order. Close inspection of a single rod reveals that the micelle surface is composed of hydrophilic heads. The hydrophobic tails are facing inward and are thereby isolated from the solvent. Hexagonal liquid crystals generally exist in solutions that are 40-70% amphiphile. The phase boundaries of the liquid crystals are sensitive to amphiphile concentration as well as the presence of salt or nonionic components (e.g., drugs).

At even higher concentrations, the molecules typically transform into another liquid crystalline phase; the lyotropic liquid crystal bilayer (Figure 2.2 (C)). This structure has a double layer of molecules arranged a bit like a sandwich with polar heads taking the place of the bread and non-polar tails as the filling. This pattern is

similar to the smectic liquid crystals in the thermotropic type. On account of the sheet-like appearance, layers can slide easily past each other. This phase is less viscous than the hexagonal phase and has a lower water content. The bilayer or lamellar phase exhibits a focal conic texture when viewed with polarized light. Another structure, the ribbon phase, may be the precursor to the bilayer. Ribbon phases involve finite bilayers that end in cylindrical half micelles. Bilayers may form when these ribbons fuse together. If the amphiphile concentration is lowered, the mixture may revert to a hexagonal phase or a solution of micelles.

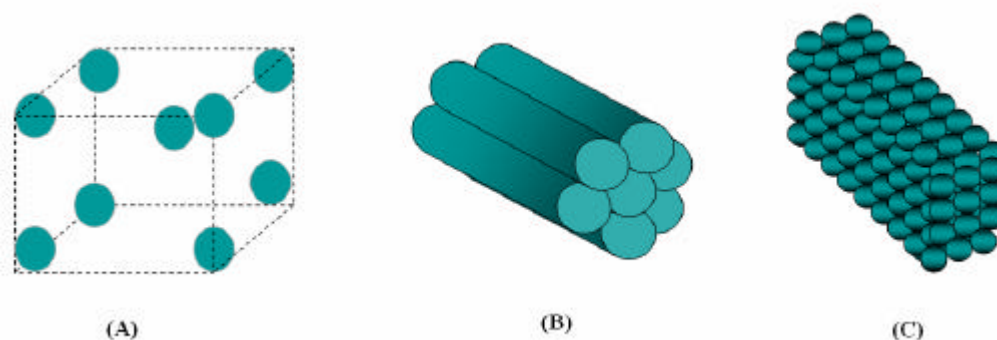


**Figure 2.2** Formation of lyotropic liquid crystal at various concentration of amphiphilic molecules

In case of the amphiphile molecules are dissolved in a non-polar solvent, the aggregation behavior occurs in similar measure as when they dissolved in water. The difference is that the non-polar tails are in contact with the solvent and the polar heads are isolated in the centers of the micelles or bilayers. When the solution contains both water and a high concentration of non-polar solvent, the inverse micelles are formed with water droplets entrapped inside the micelle and non-polar solvent on the



outside. Finally, if weaker amphiphile molecules and simple salts are dissolved together in water, lyotropic nematic phases can be formed.

### 2.2.2 The thermotropic liquid crystal

The thermotropic type of liquid crystals is formed by temperature changes above which the crystal lattice is no longer stable (Tyle, 1988; Muller-Goymann, 2004). One can arrive at the liquid crystalline state either by increasing the temperature of a solid or reducing the temperature of a liquid (Figure 2.3). Thermotropic liquid crystals phase can occur as either stable phases or metastable states. A stable mesophase is called an enantiotropic liquid crystals, which can be changed into the liquid crystal state from both lowering the temperature of a liquid and raising the temperature of a solid. Whereas, metastable mesophase also known as a monotropic liquid crystals, which can only be changed into the liquid crystal state either an increase the temperature of a solid or a decrease the temperature of a liquid (Ginsburg, 1984). In general, thermotropic mesophases occur because of anisotropic dispersion forces between the molecules and packing interactions. Many thermotropic liquid crystals pass through more than one mesomorphic phase and are called polymorphic.

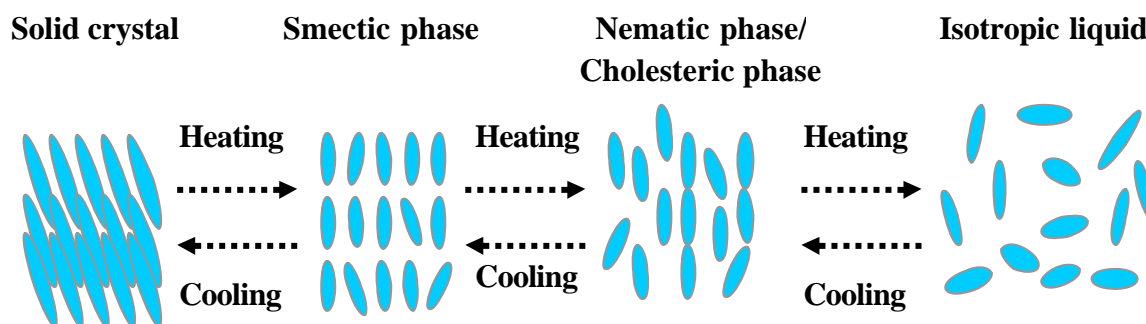


**Figure 2.3** Molecular arrangement of thermotropic liquid crystal

Thermotropic liquid crystals are classified as calamitic (i.e., made of rod-shape molecules) or discotic (i.e., made up of disc-shaped molecules). Depending on the degree of anisotropy, calamitic liquid crystals are further classified as nematic, smectic or cholesteric phases, and discotic liquid crystals are classified as nematic discotic or columnar discotic.

## 2.3 Phases of thermotropic liquid crystals

### 2.3.1 Discotic phase

Discotics are flat disc-like molecules consist of a core of adjacent aromatic rings. This phase also exhibits the nematic phase in which the director is defined as the average orientation direction of the symmetry axes of the disc is aligned normal to the disk plane (Chandrasekhar *et al.*, 1977) (Figure 2.4).



**Figure 2.4** Schematic representation of the discotic nematic phase (adapted from Binnemans, 2005)

### 2.3.2 Columnar phase (calamitic phase)

In the columnar phase, the discs are stacked one on top of another to form columns. The columns are arranged in different two-dimensional lattices. In the column nematic phase, short columns are ordered in a nematic way (Figure 2.5 (A)). This phase is also called nematic columnar phase. In hexagonal columnar phase, the molecules are stacked into columns that are further arranged into a hexagonal lattice (Figure 2.5 (B)). Other types of columnar phases are the rectangular columnar phase and oblique columnar phase. In some types of columnar phases, the order of the molecules within the columns is a periodical (disordered columnar phase), while in other cases there is an ordered, regular stacking inside the columns (ordered columnar phase).

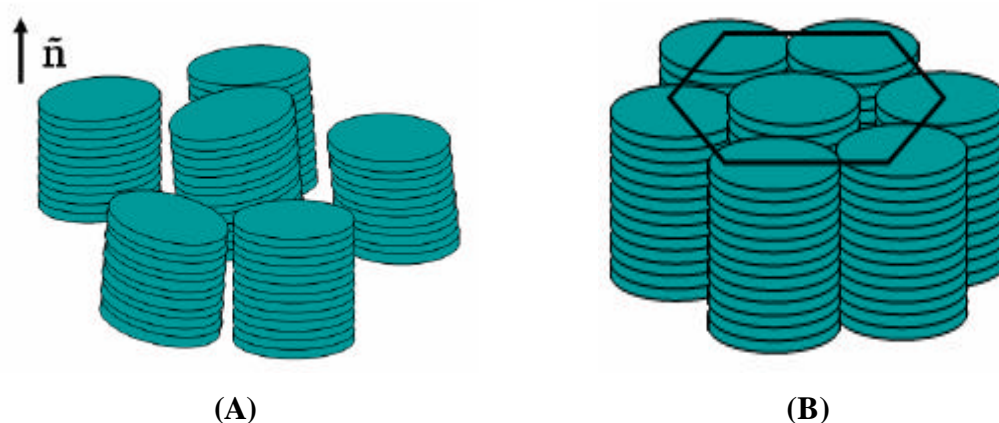


**Figure 2.5** Schematic representation of the columnar nematic phase (A) and the hexagonal columnar phase (B) (adapted from Binnemans, 2005)

### 2.3.3 Smectic phase

In the smectic phase, molecules maintain not only orientational order, but also tend to align themselves in layers or planes. Motions are restricted within these

planes and separate planes are observed to flow past each other. The increased order means that smectic state is more “solid like” than the nematic (Binnemans, 2005). They are characterized by a translational periodicity indicated by the wave vector  $\mathbf{q}$  with magnitude  $2\pi/d$ , where  $d$  is the layer spacing. The medium is called smectic A (SmA) if  $\tilde{\mathbf{n}}$  is parallel to  $\mathbf{q}$ , and smectic C (SmC) if there is a tilt angle  $\theta$  between the two vectors (Figure 2.6) (Madhusudana, 2001).

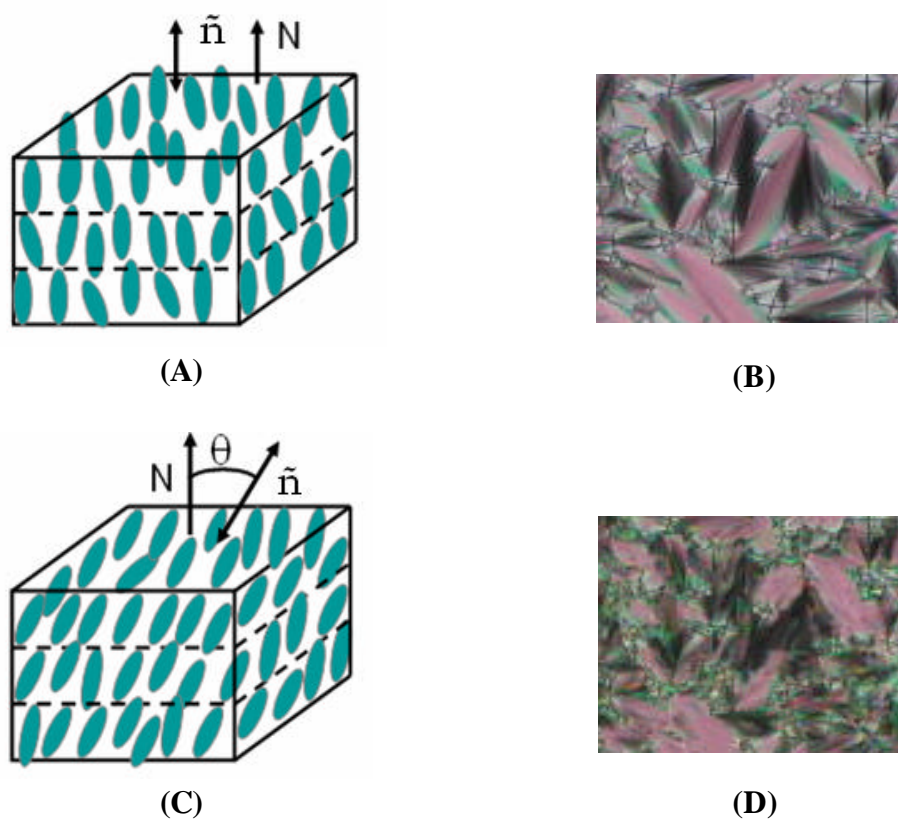


**Figure 2.6** The layer arrangement of rod-like molecules in smectic liquid crystals; smectic A (A), the layer normal  $N$  is parallel to the director  $\tilde{\mathbf{n}}$ ; smectic C (B), there is a tilt angle between them; texture of Smectic A(C) phase and Smectic C (D) phase were observed under polarized light microscope (adapted from Madhusudana, 2001)

### 2.3.4 Nematic phases

The simplest liquid crystal is the nematic (N), in which characterized by molecules that has no positional order but tend to point in the same direction (along the director). In this case, the molecules point vertically but are arranged with no particular phase (Figure 2.7).

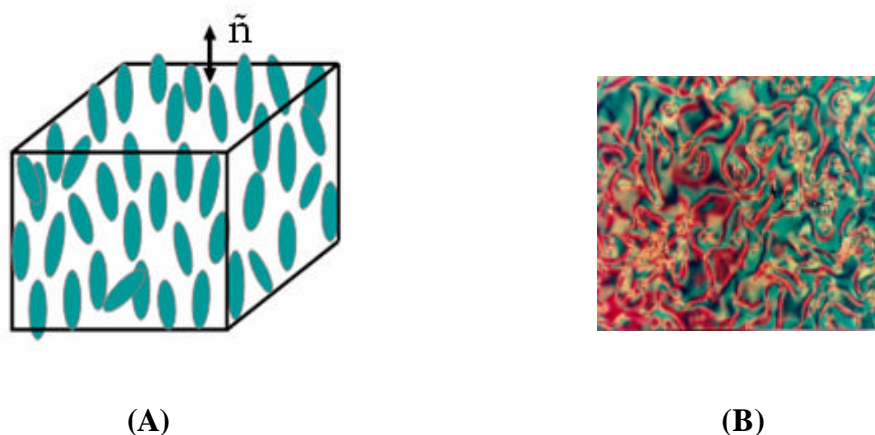


**Figure 2.7** The orientational order in a nematic liquid crystal made of rod-like molecules (A) and texture of nematic phase was observed under polarized light microscope (B). The director  $\hat{\mathbf{n}}$  represents the average orientation of the molecules (adapted from Madhusudana, 2001)

### 2.3.5 Cholesteric phase

The cholesteric (or chiral nematic) liquid crystal phase is typically composed of nematic mesogenic molecules containing a chiral center which produces intermolecular forces that alignment between molecules at the slight angle to one another. This leads to the formations of a structure that can be visualized as a stack of very thin 2-D nematic like layers with the director in each layer twisted (Friberg, 2000). Therefore, the molecules are chiral, the intermolecular interaction produces a helical

arrangement of the director  $\hat{\mathbf{n}}$  (Figure 2.8), and the pitch  $P$  is usually of the order of 0.5  $\mu\text{m}$ , i.e. wavelengths of visible light. This effect is exploited in thermography.

Another interesting property of cholesteric liquid crystals is that they selectively reflect bright colors. The wavelength of selective reflection  $\lambda$  is related to the pitch of  $P$  and can be described by following equation (Reinitzer, 1888):

$$I = (nP \cos q) \dots \dots \dots \text{Equation 2.1}$$

Where :  $n$  is the mean refractive index

:  $P$  is the pitch

:  $\theta$  is the viewing angle with respect to the surface normal

:  $\lambda$  is the reflected wavelength

If the cholesteric liquid crystal sample is right-handed, most of the right-handed component of the incoming wave is reflected while the left-handed is transmitted. The opposite is true for a left-handed cholesteric liquid crystal.

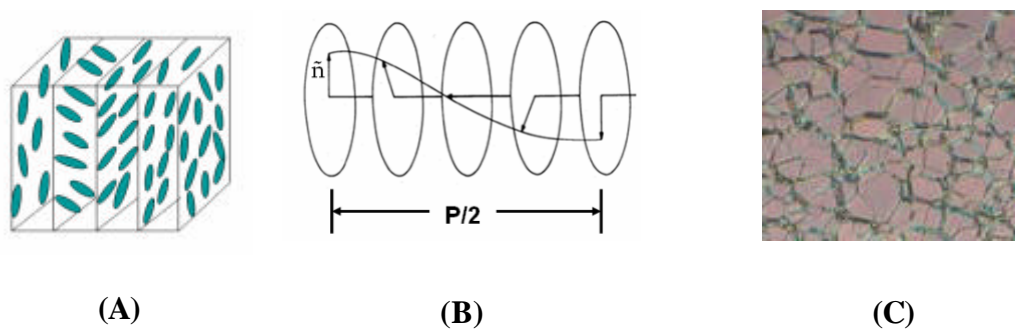


**Figure 2.8** The arrangement of molecules in cholesteric liquid crystal phase (A), the helical arrangement of the director in a cholesteric liquid crystal made of chiral molecules (B) and texture of cholesteric phase was observed under polarized light microscope (C) (Madhusudana, 2001)

## **2.4 Physicochemical characterization of liquid crystal**

Several methods are used to investigate and characterize liquid crystals. Those are frequently used in pharmaceutical product development.

### **2.4.1 Microscopy**

#### **A) Polarized Light Microscopy (PLM)**

Polarized light microscopy (PLM) is suitable for detection of liquid crystals (except cubic mesophases). The optical properties of liquid crystal phases often directly reflect the symmetry of their structures. Anisotropy of the refractive index, or birefringence, is one of the physical properties of liquid crystals. It allows for the visualization of the macroscopic molecular orientation. The thin liquid crystal sample cells are placed between two crossed polarizers under an optical microscope, and a variety of textures and birefringence colors can be observed (Demus and Richter, 1978). Hexagonal mesophases can be recognized by their typical fan shape texture. Lamellar mesophases typically show oily streaks with inserted Maltese crosses. The latter results from defect structures called confocal domains. That arises from concentric rearrangement of plane layers. These properties, the textures and colors, can provide a great deal of information about the macroscopic structure of the liquid crystal phases.

#### **B) Transmission Electron Microscopy (TEM)**

The microstructure of liquid crystals can be visualized with a high-magnification power of the electron microscope. However, aqueous samples do not survive the high vacuum of an electron microscope and water loss occurs leading to

microstructure changes. Therefore, special techniques of sample preparation are necessary prior to electron microscopy. Freeze fracture has proven to be successful in overcoming these problems (Mueller-Goymann, 2001).

#### 2.4.2 X-ray Diffraction

With X-ray diffraction experiments, characteristic interferences are generated from an ordered structure (Fontell, 1974). A typical interference pattern arises from specific repeat distances of the associated interlayer spacing ( $d$ ) can be calculated according to Bragg's Equation 2.2 (Bragg, 1913):

$$d = \left( \frac{n\lambda}{2 \sin \theta} \right) \dots \dots \dots \text{Equation 2.2}$$

Where:  $\lambda$  is the wavelength of the X-ray being used

:  $n$  is an integer and nominates the order of the interference

:  $\theta$  is the angle under which the interference occurs (reflection conditions are fulfilled).

From Bragg's equation, it can be seen that the interlayer spacing  $d$  is inversely proportional to the angle of reflection ( $\theta$ ). Large values of  $d$  in the region of long-range order can be measured by small angle X-ray diffraction (SAXD), while small values of  $d$  in the region of short-range order can be investigated by wide angle X-ray diffraction (WAXD). SAXD is the most appropriate technique for the exact determination of the distances of interlayer spacing of liquid crystalline systems. Subsequently interlayer spacing of the crystalline material and type of ordering can be measured (Luzzati *et al.*, 1960; Fontell *et al.*, 1968).



In X-ray diffraction (XRD), the scattered intensity depends on the Lorentz-Polarization factor, which is essentially equal to 1 below  $6^\circ 2\theta$ . For disorganized systems, the multiplicity factor is 1 and the structure factor,  $|F^2|$ , generally does not reflect order but involves only a form factor for the nano-scale structures that give rise to scattering, i.e., regions of differing electron density (Beaucage, 1996). In XRD, the atomic scattering factor,  $f^2$ , is equal to the square of the number of electrons in an atom at low angle,  $n_e^2(1/q)$ , where  $q$  is  $4\pi\sin(\theta)/\lambda$ . Additionally, the intensity of scattering is known to be proportional to the number of scattering elements in the irradiated volume,  $N_p(1/q)$ . For small angle scattering, we can consider a generalized rule that describes the behavior of scattered intensity as a function of Bragg size “ $d$ ” or “ $r$ ” that is observed at a given scattering angle  $2\theta$ , where  $r = 1/q$ .

$$I(q) = N_p(1/q)n_e^2(1/q) \dots \dots \dots \text{Equation 2.3}$$

From this simplified rule of thumb, most of the general rules of small angle scattering can be derived in a less rigorous manner. This approach is extremely useful for a simple understanding of small angle scattering. Scattering laws in small angle regime describe two main features that are observed in a log intensity versus log  $q$  plot (Beaucage, 1995). First, typical scattering patterns display power-law decays in intensity reflecting power-law scaling features of many materials. Secondly, power-law decays begin and end at exponential regimes that appear as knees in a log-log plot. These exponential knees reflect a preferred size as described by  $r = 1/q$  for the knee regime.

All scattering patterns in the small angle regime reflect a decay of intensity in  $q$  and this can be easily described by considering that at decreasing size

scales the number of electrons in a particle is proportional to the decreasing volume, while the number of such particles increases with 1/volume. Then, the scattered intensity by Equation 2.3 is proportional to the decay of the particle volume with the size.

The position and width of the diffraction peak are obtained by fitting a Lorentzian function (Moncton and Pindak, 1979) to the experimental data as Equation 2.4

$$I_{\text{obs}}(q) \propto [\varepsilon^2 (q-q_c)^2 + 1]^{-1} \dots\dots\dots \text{Equation 2.4}$$

Where :  $q_c$  is the center of peak position

:  $\varepsilon$  is a parameter specifying the width

### 2.4.3 Differential Scanning Calorimetry (DSC)

Phase transitions are accompanied by free energy changes and can be further assessed by the alterations in the enthalpy ( $\Delta H$ ) or entropy ( $\Delta S$ ) of the system. Enthalpy changes result in either endothermic or exothermic signals, depending on whether the transition is due to consumption of energy, e.g., melting of a solid, or a release of energy, e.g., recrystallization of an isotropic melt. It should be mentioned that the transition from the crystalline to amorphous phase requires a high energy input. In spite of crystalline to liquid crystalline and liquid crystalline to amorphous transitions as well as changes between different liquid crystalline phases, which all require lower amounts of energy. Therefore, it is necessary to ensure that the measuring device is sufficiently sensitive to reveal the transition (Shin *et al.*, 1992). Second order phase transitions may be recognized by a change in baseline slope due to a change in the specific heat capacity.

#### **2.4.4 solid state Nuclear Magnetic Resonance Spectroscopy (ssNMR)**

NMR spectroscopy is remarkable for its ability to observe each segment of the molecule in any physical state. Molecular arrangements in different phases can be detected by the value of the chemical shift and inferred molecular motions by relaxation time measurements or orientational ordering parameters. High-resolution  $^{13}\text{C}$ NMR spectroscopy has provided details about the molecular motions and intermolecular interactions of compounds in liquid and liquid crystal phases (Hamilton *et al.*, 1977; Ginsburg *et al.*, 1982; Croll *et al.*, 1986). However, the characterization of mesophases was limited by extensive line broadening and the consequent loss of spectral information. Historically, no spectral information was obtained from crystal and liquid crystal. However, introduction of the technique of NMR with magic angle sample spinning (MASNMR) can potentially eliminate the extensive line broadening in  $^{13}\text{C}$  spectra of ordered/anisotropic systems and yield high-resolution spectra from which chemical shift and relaxation measurements can be obtained.

#### **2.5 Respiratory tract**

Inhalation of air is necessary to meet the daily gas exchange requirement approximately of 10,000 L for the adult human lung. The normal lung has an extraordinary respiratory reserve. Arterial oxygenation commonly improves with exercise, and even under heavy work conditions, pulmonary gas exchange in a normal adult is rarely a cause of limitation to aerobic performance. To accomplish the efficient extraction of oxygen and exchange of carbon dioxide, the lung has an internal surface area approximately equal to that of a tennis court (Notter, 2000). The upper and lower respiratory tracts act to condition the inhaled air, and the lung has developed unique

defense pathway to allow it to maintain its fine, delicate gas exchange surface while being continuously exposed to potentially injurious reactive or infectious agent from inhaled air. Figure 2.9 shows anatomy of respiratory tract.

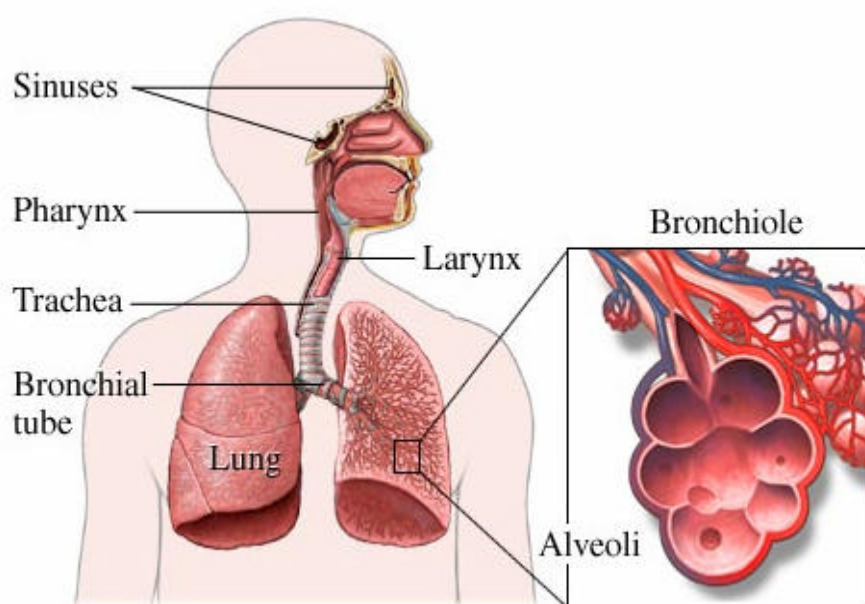


**Figure 2.9** Anatomy of respiratory tract (<http://www.nucleusinc.com>)

The airways are often described as a pulmonary tree (Figure 2.10). The tree trunk is analogous to the trachea of the airways that bifurcates to form main bronchi. These divide to form smaller bronchi that lead to individual lung lobes. Inside each lobe, the bronchi undergo further divisions to form new generations of smaller caliber airways: the bronchioles. This process continues through the terminal bronchioles, the respiratory bronchiole, alveolar ducts and terminates with alveolar sacs. The model proposes the existence of 24 airway generations in total, with the trachea

being generation 0 and the alveolar sacs being generation 23 (Hickey and Thompson, 1992).

In passing from the trachea to the alveolar sac, two physical changes occur in the airways that are important in influencing airway function. Firstly, the airway diameter decreases with increasing generations. Secondly, the surface area of the airway increases with each generation to the extent that the total area at the level of the human alveolus is in the order of  $140 \text{ m}^2$ . Various levels of the airways may be categorized functionally as being either conducting or respiratory. Conducting airways do not participate in gas exchange and extend from the trachea to the terminal bronchioles. The respiratory zone includes airways involved with the gas exchange and comprises respiratory bronchiole, alveolar duct, and the alveolar sacs (Hickey and Thompson, 1992).

conducting zone	generation	diameter (cm)	length (cm)	number	total cross sectional area ( $\text{cm}^2$ )	Powder deposition by particle diameter	
	trachea	0	1.80	12.0	1	2.54	2-10 $\mu\text{m}$
bronchi	1	1.22	4.8	2	2.33		
	2	0.83	1.9	4	2.13		
	3	0.56	0.8	8	2.00		
bronchioles	4	0.45	1.3	16	2.48		
	5	0.35	1.1	32	3.11		
terminal bronchioles	16	0.06	0.2	$6 \times 10^4$	180.0		
transitional and respiratory zones	respiratory bronchioles	17	↓	↓	↓	0.5- 2 $\mu\text{m}$ and < 0.25 $\mu\text{m}$	
		18	↓	↓	↓		
		19	0.05	0.1	$5 \times 10^5$		$10^3$
	alveolar ducts	20	↓	↓	↓		
		21	↓	↓	↓		
alveolar sacs	22	↓	↓	↓	↓		
	23	0.04	0.05	$8 \times 10^6$	$10^4$		

**Figure 2.10** A schematic representation of airway branching in the human lung (Koning, 2001).

## 2.6 Lung fungal infections

Infection by fungi generally occurs by inhalation. Thus, the lungs are the organs most frequently encountering these microorganisms and most often demonstrate the pathologic changes of fungal disease. Generalized dissemination of the fungus may cause spread of the infection from the lung to the rest of the body as part of process that has been called primary infection and postprimary dissemination. In this process, the immune system is involved in a complicated series of reactions reflecting innate factors as well as humoral and cell mediated immunity. In general, the resistance of the body to infections by fungi, characterized as saprophytic, is excellent; in fact, these fungi rarely cause significant infection in healthy humans. A group of more aggressive fungi regularly cause primary infection in healthy human subjects, but this infection is limited and not associated with significant disease, even when the postprimary dissemination occurs (Baum and Rhodes, 1998). The fungi making up diseases include *Histoplasma capsulatum*, *Aspergillus* species, *Blastomyces dermatitidis*, *Cryptococcus neoformans*, *Candida albicans* and *Coccidioides immitis*.

### 2.6.1 Histoplasmosis

*Histoplasmosis* is caused by fungus *Histoplasma capsulatum*. *Hitoplasma* is a dimorphic fungus, meaning that it exhibits two types of morphologies, depending on the conditions for growth. In soil, the organism takes the form of branching hyphae; in the body at 37 °C, it appears as a round or oval yeast. After an individual has been exposed and *H. capsulatum* has entered the lung, the organism (at body temperature) undergoes conversion to the yeast phase. An inflammatory response ensues in the lung parenchyma with recruitment of phagocytic cells (macrophages).

Commonly, there is also spread of the organism to the regional lymph nodes. Within 3 weeks, delayed hypersensitivity against *Histoplasma* generally has developed, and the pathologic response becomes granulomatous in nature.

Treatment of pulmonary histoplasmosis also depends on the particular type of infection. Acute histoplasmosis generally requires no therapy and is self-limited illness. Disseminated histoplasmosis requires treatment with either of two antifungal agents, Amphotericin B (AmB) or ketoconazole, depending on the pace of the illness and the immunologic status of host. Chronic pulmonary histoplasmosis is generally also treated with either AmB or ketoconazole.

### **2.6.2 Aspergillosis**

*Aspergillus* species are widespread throughout nature and are not limited to particular geographic areas. *Aspergillus* species are not dimorphic in appearance but always occur as mycelia, that is branching hyphal forms. Since virtually everyone is exposed to the organism, it is clear that disease must be associated with certain predisposing factors, which are now quite well-defined.

Invasive aspergillosis is certainly the most life-threatening manifestation of *Aspergillus* infection, occurring almost exclusively in patients with marked impairment of host immune defense mechanisms. The most important risk factor is neutropenia, that is, insufficient numbers of polymorphonuclear leukocytes, but patients often also have impairment of cellular immunity as a consequence of treatment with chemotherapeutic agents. Pathologically, the organism invades and spreads through lung tissue, but it also tends to invade blood vessels within the lung. As a result of

vascular involvement by the fungus, vessels can become occluded and areas of pulmonary infarction can develop.

Diagnosis of invasive aspergillosis generally requires isolation of the organism, for example, by methenamine silver staining, on a biopsy specimen of the lung tissue. Treatment consists of AmB, but even with appropriate use of this agent the mortality is extremely high.

### **2.6.3 Coccidioidomycosis**

*Coccidioidomycosis* also affects normal hosts and may have its clinical consequences altered in special categories of patients, especially those with impairment of host defense mechanisms. The causative organism, *Coccidioides immitis*, is also dimorphic fungus. Mycelia are present in soil, whereas staining of tissue specimens shows characteristic round, thick-walled structures called spherules, which often contain multiple endospores.

Treatment considerations are similar to those for histoplasmosis. Primary infections generally do not require therapy, whereas disseminated disease is treated with AmB. Chronic pulmonary disease frequently requires therapy with AmB, but occasionally surgery plays a role in specific clinical settings.

### **2.6.4 Other fungi**

The remaining fungi are less frequent causes of respiratory infections. *Blastomycosis* is seen in normal hosts and is associated with pulmonary disease, as well as with potential problems with other organ systems. *Candida albicans*, although an extraordinarily common contaminant of sputum (particularly in the patient treated with



antibiotics), is an uncommon cause of pneumonia, even in immunosuppressed patients. *Cryptococcus neoformans* is found primarily in immunosuppressed patients, in whom it causes lung disease as well as meningitis. Finally, *Mucor* is an opportunistic fungus that may cause pulmonary infection in the immunocompromised host.

## 2.7 Treatments of lung fungal infection

### 2.7.1 Fungal cell structure and targets

The cell membrane contains lipid particle called sterol. The sterol in fungus is different from that of mammalian cell membrane. The ergosterol (Figure 2.11) is the main sterol in fungal membranes, whereas cholesterol is contained in mammalian cell. Several classes of antifungal agents including the polyene, azole and allylamines have exploited the difference in sterol content as the target action (Russell, 2007).

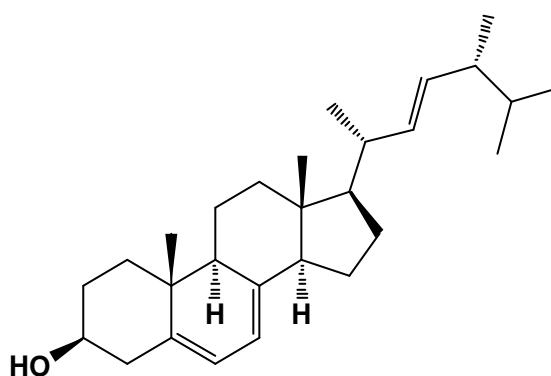


**Figure 2.11** The chemical structure of ergosterol

### 2.7.2 Amphotericin B (AmB)

Fungal infections are a significant cause of mortality and morbidity in seriously ill and immunocompromised patients. Their frequency has risen because of changes in the epidemiology of predisposing disease such as the spread of AIDS, or in management, including the development of techniques such as bone marrow transplantation (BMT) (Hay, 1999). Treatment of systemic fungal infection is complicated and often prolonged, because the infections are difficult to diagnose. Thus early detection and treatment of suspected fungal infections, especially in febrile neutropenic patients, is an important goal in current antifungal therapy. AmB has been the mainstay of systemic antifungal therapy for over 30 years. It is the most potent antifungal agent and the drug of choice in serious fungal infections (Gallis *et al.*, 1990). AmB is an antifungal antibiotic produced as a fermentation by-product of *Streptomyces nodosus*, soil actinomycetes (Abu-Salah, 1996).

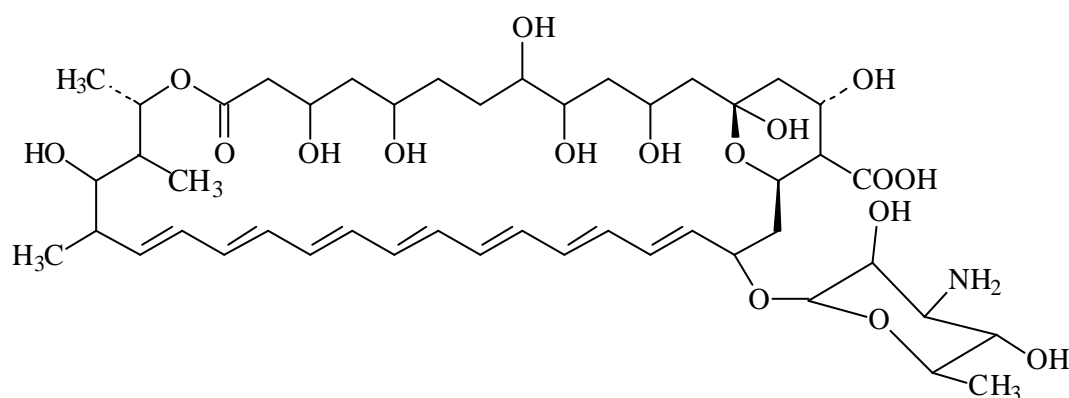


**Figure 2.12** The chemical structure of Amphotericin B (AmB)

The chemical structure (Figure 2.12) shows a large lactone ring of 37 carbon atoms in which one side of the ring is a hydrophobic, conjugated heptane chain and the other side is hydrophilic containing seven hydroxyl groups. The macrolide ring also contains a six-membered ketalic ring to which the aminosugar mycosamine is bonded through an  $\alpha$ -linkage. The amphipathic nature of AmB (hydrophobic tail and hydrophilic head) allows it to be complex with other moieties to alter its pharmacokinetics and pharmacodynamics.

AmB is a yellow or orange powder, practically insoluble in water, soluble in dimethylsulphoxide (DMSO) and in propylene glycol (PG), slightly soluble in dimethylformamide (DMF), very slightly soluble in methanol, practically insoluble in alcohol. It is sensitive to light in dilute solutions and is inactivated at low pH values. AmB should be kept in a well-closed container, protected from light at a temperature of 2 to 8°C and temper-proof container. The general understanding, AmB binds directly with sterols in cell membrane and forms pore to cause cell lysis (Clements and Peacock, 1990). Drug toxicity, especially nephrotoxicity is a significant problem as AmB damage mammalian cell membrane. The major adverse effects limit dose that may be given.

### **2.7.3 Mechanism of action of AmB**

The AmB molecular mechanism of action has still not been understood well enough to make rational design of new derivatives. It has been known that AmB interacts with the components of cell membrane and forms ion channel (Baginski *et al.*, 2002). These ion channels disrupt membrane functions and cause uncontrolled cation transport (through an increase in cell membrane permeability) leading to the leakage of

sodium, potassium and hydrogen ion, where it associates with membrane sterols to form pores which damage the cell ions, and eventual cell death. According to the widely accepted sterol hypothesis, the presence of sterol in the membrane is necessary for AmB to be able to form conducting channels. Its primary mechanism of action is via binding to ergosterol, the most abundant sterol found in the cell membrane of sensitive fungi, and the creation of a barrel pore (Fournier *et al.*, 1998) (Figure 2.13).

The binding of AmB with fungal cell membrane involves in the hydrogen bonds between the hydroxyl groups of the sterol and the carboxyl group at C18 of the AmB molecule. The strong intermolecular AmB–sterol interactions within the channel are responsible for its stability (Cotero *et al.*, 1998). This binding is strengthened by participation of the amino group of the amino sugar as shown in Figure 2.14.

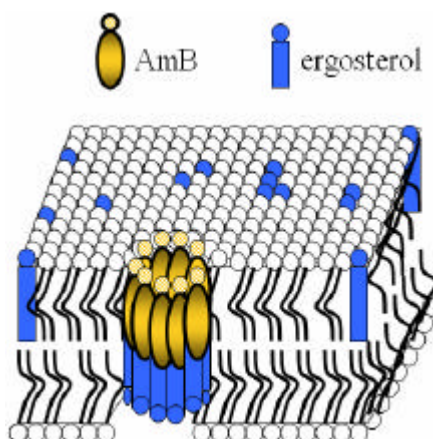


**Figure 2.13** Model illustrating the possibility for the formation of channels by AmB interacting with sterol containing membranes (adapted from Mouritsen and Bloom, 1984)

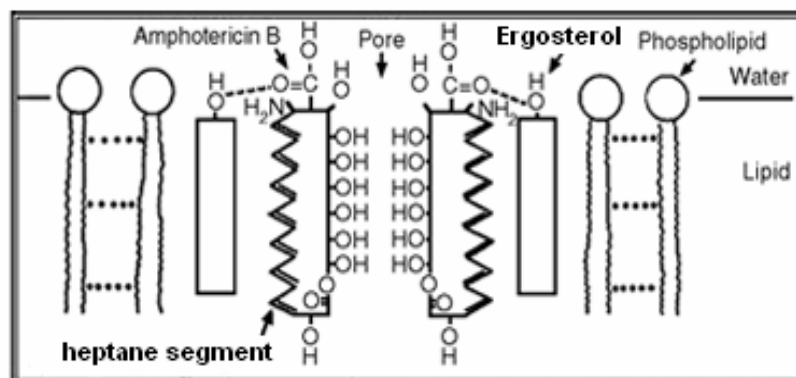


**Figure 2.14** Schematic representation of hydrogen bond formation (Brajtburg *et al.*, 1990).

## 2.8 Formulations of AmB for lung infection

### 2.8.1 Conventional AmB formulation

The conventional formulation of AmB, Fungizone<sup>®</sup>, was used in invasive fungal infection for more than four decades. Fungizone<sup>®</sup> consists of AmB complexed with the bile salt deoxycholate as a solubilizing agent. Each vial of Fungizone<sup>®</sup> (Bristol-Myers Squibb, USA) containing 50 mg of AmB with 41 mg of sodium deoxycholate and 20.2 mg of sodium phosphate. The clinical use of conventional AmB has a number of side effects such as phlebitis at injection site, fever, chills, electrolyte imbalance and nephrotoxicity, making long-term treatment difficult, due to its water-insoluble and its precipitation upon dilution. This may be related to its acute toxicity (Yu *et al.*, 1998). Nephrotoxicity is the most severe side effect and often limits the dose (Deray, 2002).

### 2.8.2 Lipids based AmB

Recent advances in drug delivery technology have resulted in the development of lipid formulations of AmB; liposomes (AmBisome<sup>®</sup>), colloidal dispersion (Amphocil<sup>®</sup>), and lipid complex (Abelcet<sup>®</sup>).

AmBisome<sup>®</sup>, the first to be licensed was a unilamellar liposome (Figure 2.15) of about 80 nm in diameter. This formulation employed saturated (rigid) phospholipids with cholesterol to stabilize the liposomal membrane. Charged phospholipids (phosphatidylglycerol) were also included to stabilize the AmB liposomes through ionic interactions. Further stabilization could result from the direct interaction of AmB with the cholesterol via its sterol binding region. Finally, it was anticipated that the small size of these liposomes (< 100 nm) would provide stabilization *in vivo* and prolong the circulation of drug-containing liposome in the plasma.

Initial studies demonstrated that AmBisome<sup>®</sup> was stable, causing little or no hemolysis (Adler-Moore and Proffitt, 1998) and was shown to have a higher therapeutic index in animal models of systemic fungal infection, largely as a result of increased safety. The product is supplied in lyophilized form for reconstitution. The drug appears to be effective in a range of systemic mycoses including aspergillosis and cryptococosis in patients who have either failed on conventional AmB or been unable to continue through toxicity (Ringden *et al.*, 1991). AmBisome<sup>®</sup> is currently the only antifungal product approved in the USA for empirical therapy of febrile neutropenic patients. It is also approved in the USA for second-line use in aspergillosis, candidiasis and cryptococosis, and for similar indications in Europe, Asia and Latin America (Meyerhoff, 1999).

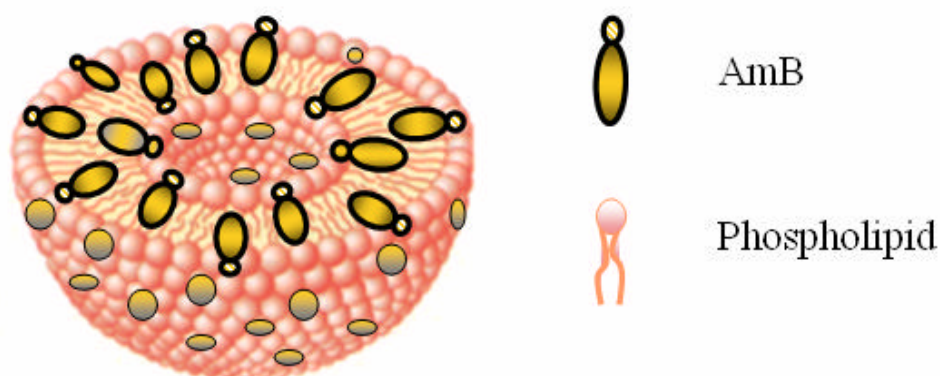


**Figure 2.15** Schematic representation of possible locations of a liposome-associated with AmB (adapted from <http://www.rxlist.com/ambisome-drug.htm>)

The second AmB lipid preparation is AmB colloidal dispersion, Amphocil<sup>®</sup>. This formulation is based on the specific interaction of AmB with sterol (Figure 2.16). The sodium salt of cholesteryl sulfate forms a stable colloidal complex with AmB at a 1:1 drug to lipid molar ratio. Negative staining of the complex by electron microscopy revealed the presence of uniquely thin discs of highly uniform diameter (Guo *et al.*, 1991). The nonliposomal structure of Amphocil<sup>®</sup> was confirmed by showing that these disc-shaped particles do not have an entrapped aqueous volume. The estimated dimensions of particles indicate the discs are about 120 nm in diameter and 4 nm thick. The properties of these discs suggest that they are stable, bilayer-like structures that are unable to curve sufficiently to form liposomes because of the rigidity of their component (Guo *et al.*, 1991). This unique colloidal formulation was shown to reduce the hemolysis, acute toxicity and lipoprotein binding of AmB (Guo *et al.*, 1991).

The improved safety profile of Amphocil<sup>®</sup> over conventional AmB was confirmed in repeated-dose studies in animals, in which it was also shown to reduce

toxicity to the kidneys by 5-8 folds (Fielding *et al.*, 1992; Wang *et al.*, 1995). The studies also demonstrated that Amphocil<sup>®</sup> was rapidly cleared from the circulation, especially into mononuclear phagocyte system tissue (liver and spleen) where it accumulates in a relatively non-toxic form. The increased safety of Amphocil<sup>®</sup> was also reflected in an increase in its therapeutic index in animal models of infection, against a range of fungi including *Aspergillus*, *Candida*, *Cryptococcus* and *Coccidioides* spp. (Guo and Working, 1993). For clinical trial patients were tolerated to Amphocil<sup>®</sup> at doses higher than conventional AmB, with a similar pattern of acute side effects (chills and fever), but less renal toxicity (Sanders *et al.*, 1991).

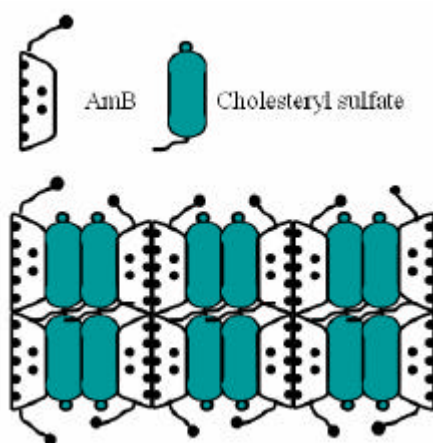


**Figure 2.16** Structure feature of AmB interacted with cholesterol sulfate (adapted from Guo *et al.*, 1991)

A third preparation is AmB lipid complex formation (Abelcet<sup>™</sup>), which appears as ribbon-like structures. Figure 2.17 shows the putative structure of Abelcet<sup>™</sup> proposed by Janoff *et al.* (1993). AmB and lipid are arranged in a phase-separated 1:1 interdigitated complex. One possible arrangement would require AmB-lipid pairs to be arranged in cylinders. The hydrophobic polyene region of AmB (Figure 2.12) would be



aligned with the lipid hydrocarbon chains, and the polar hydroxyl groups would face towards the center of the cylinder pore. The cylinders would align side by side and would have to possess two polar ends. Abelcet™ was subsequently shown to be considerably less toxic in acute and chronic animal studies, which a maximum tolerated dose up to ten-fold higher than conventional AmB (Janoff *et al.*, 1993). In animal studies Abelcet™ also retained the activity of AmB against a range of systemic pathogens, including *Candida*, *Aspergillus*, *Blastomyces*, *Cryptococcus* and *Histoplasma* spp. (Janoff *et al.*, 1993).

Pharmacokinetic studies showed that Abelcet™ was rapidly cleared from the plasma into tissue, lung, liver and spleen. The rapid clearance of Abelcet™ suggests that it is efficiently taken up by phagocytic cells. In human studies have demonstrated activity of Abelcet™ against infections cause by *Candida*, *Aspergillus*, *Cryptococcus* and *Coccidioides* spp. The pharmacokinetics of Abelcet™ in humans was found to be similar to that in animals, with rapid plasma clearance into tissue. After receiving initial approval for second-line treatment of aspergillosis, the US FDA approved indications for Abelcet™ have been expanded to include the treatment of all invasive fungal infections in patients refractory or intolerant to conventional AmB therapy. The recommended regimen is 5 mg/kg/day (Bekersky *et al.*, 1999).

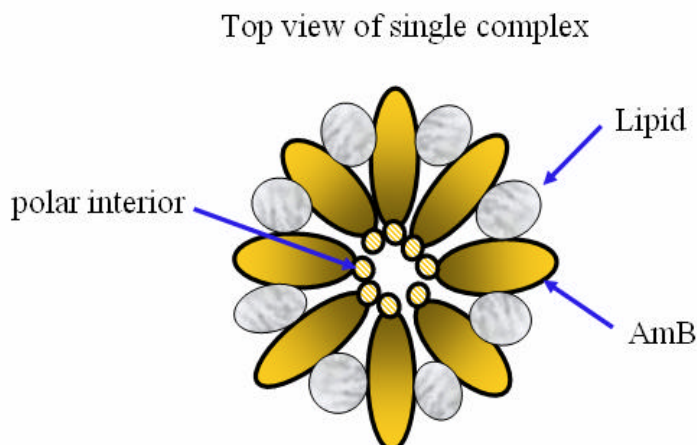


**Figure 2.17** AmB and lipid arrangement in 1:1 interdigitated complex of Abelcet™  
(adapted from Janoff *et al.*, 1993)

*In vitro* studies have shown that, most of the time, AmB in lipid formulations retained all or part of its antifungal activity, whereas its toxicity is greatly reduced or abolished. Two hypotheses have been formulated for the origin of this increase *in vitro* selectivity (Figure 2.18). According to the first hypothesis, selective transfer of the drug occurs to fungal but not to mammalian cells (Jullien *et al.*, 1990; Adler-Moore and Proffitt, 1993). The second hypothesis is based on the notion that only free (unbound to the lipid carrier) AmB damages cells (Jullien *et al.*, 1990) and that AmB is gradually released from a liposomal formulation with increased dilution (Figure 2.19). Fungi, being more sensitive to AmB than mammalian cells, are susceptible at the lower range of total AmB concentrations, a range where AmB is totally dissociated from deoxycholate in Fungizone® or from the carrier in the other formulations (Hartsel and Bolard, 1996). Despite mammalian cells are affected only by higher free-AmB

concentrations, which are never attained with lipid formulations, in contrast to Fungizone<sup>®</sup>.

All lipid-based formulations of AmB were developed to reduce the side effects associated with conventional AmB (Fungizone<sup>®</sup>), especially the nephrotoxicity. While the pharmacokinetics of lipid-based formulations are highly variable, they are accepted that the lipid-based formulations do reduce renal toxicity. This probably, that lipid-based may provide a protective effect based on the altered affinity of AmB to human cell membranes while preserving the affinity of AmB to fungal membranes (Sawaya *et al.*, 1995). Recently lipid-based formulations (AmBisome<sup>®</sup>, Amphocil<sup>®</sup>, Abelcet<sup>™</sup>) are less stable, less potent and require dose 6-10 folds greater than conventional AmB to achieve a similar therapeutic effect (Plotnick, 2000; Bennett, 2001). However, a high-dose therapeutic system is not necessary. Since, the increased doses of AmB administered will accumulate in the body because of its low rate of elimination (Atkinson and Bennett, 1978). The basic pharmacokinetic measurements of AmB (particularly lipid-based formulation) vary from study to study. No therapeutic index, equivalent doses, toxic doses or maximum therapeutic doses have been accepted (Carver, 1999; Santangelo *et al.*, 2000). One reference goes so far to state that measuring blood concentrations to monitor efficacy and toxicity is impractical due to the variation from subject to subject (Schaffner and Roland, 2000). This poses a dilemma, particularly when a physician attempts to switch a patient from one dosage form to another. In addition, these lipid-based formulations are substantially more expensive than Fungizone<sup>®</sup> and the higher cost are a major limitation in clinical practices (Persson *et al.*, 1992).

Pharmaceutical characteristics of AmB formulations are shown in Table 2.1. Those formulations differ widely in their composition and physicochemical properties: one has a mixed micelle structure, and the others are AmB-lipid formulations (liposomal bilayer, disc-like and ribbon-like structure).

**Table 2.1** Industrially produced intravenous formulations of AmB (Storm and van Etten, 1997).

<b>Formulation</b>	<b>Manufacturer</b>	<b>Carrier</b>	<b>Particle type</b>
Fungizone <sup>®</sup>	Bristol Myers-Squibb	sodium-deoxycholate	micelle
AmBisome <sup>®</sup>	NeXstar Pharmaceuticals	HSPC/DSPG/cholesterol	unilamellar
Amphocil <sup>®</sup> (ABCD)	Sequus Pharmaceuticals	cholesteryl sulfate	disc complex
Abelcet <sup>™</sup> (ABLC)	The Liposome Company	DMPC/DMPG	ribbon

ABCD: AmB colloidal dispersion, ABLC: AmB lipid complex, DMPC: dimyristoylphosphatidylcholine, DMPG: dimyristoylphosphatidylglycerol, HSPC: hydrogenated soy phosphatidylcholine, DSPG: distearoylphosphatidylglycerol

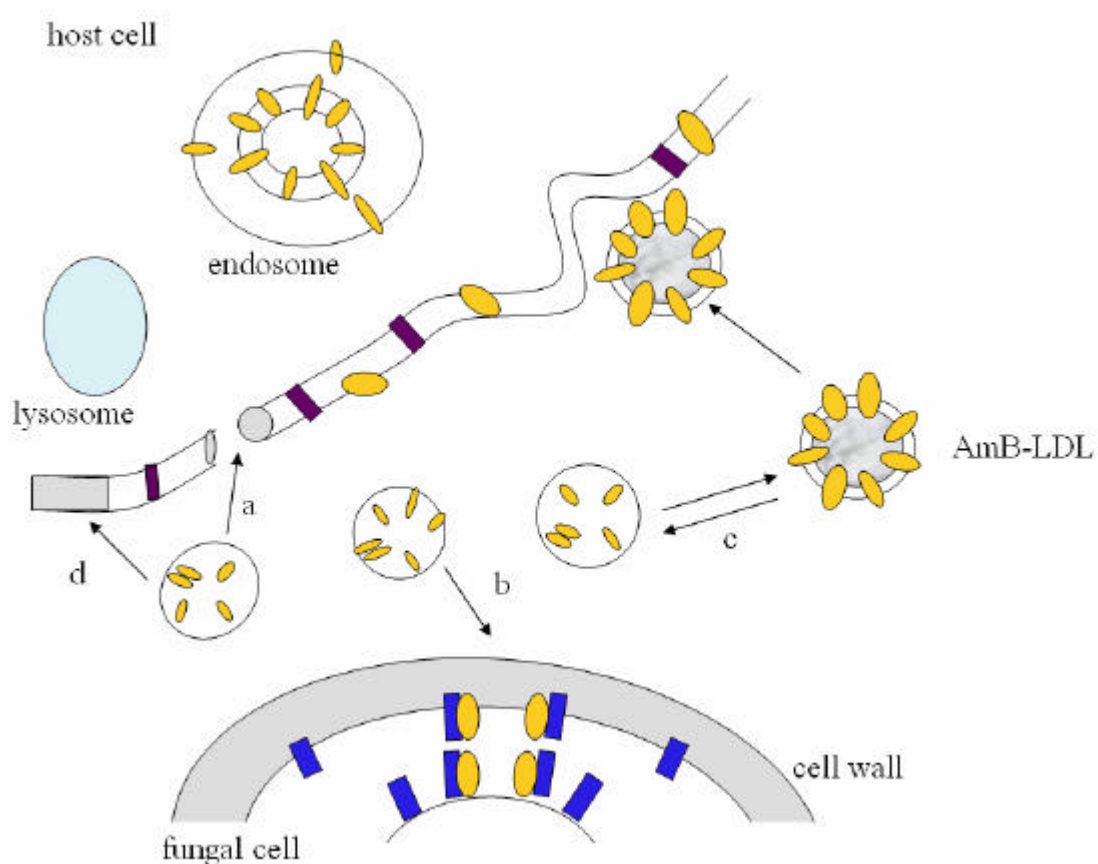


**Figure 2.18** Mechanisms of anticellular action of AmB: the formation of transmembrane pores. **a**: with mammalian cells this formation only occurs for AmB concentrations above the threshold of drug self-association, whereas **b**: with fungal cells it may occur much below the threshold. Strong evidence of sterol-AmB complexation is only indicated for ergosterol-containing membranes. Endocytosis through LDL (low density lipoprotein) receptors. **c**: AmB bound to LDL is internalized. **d**: Lipid peroxidation makes membranes more fragile. AmB (●), cholesterol (■), ergosterol (■) (adapted from Hartsel and Bolard, 1996)

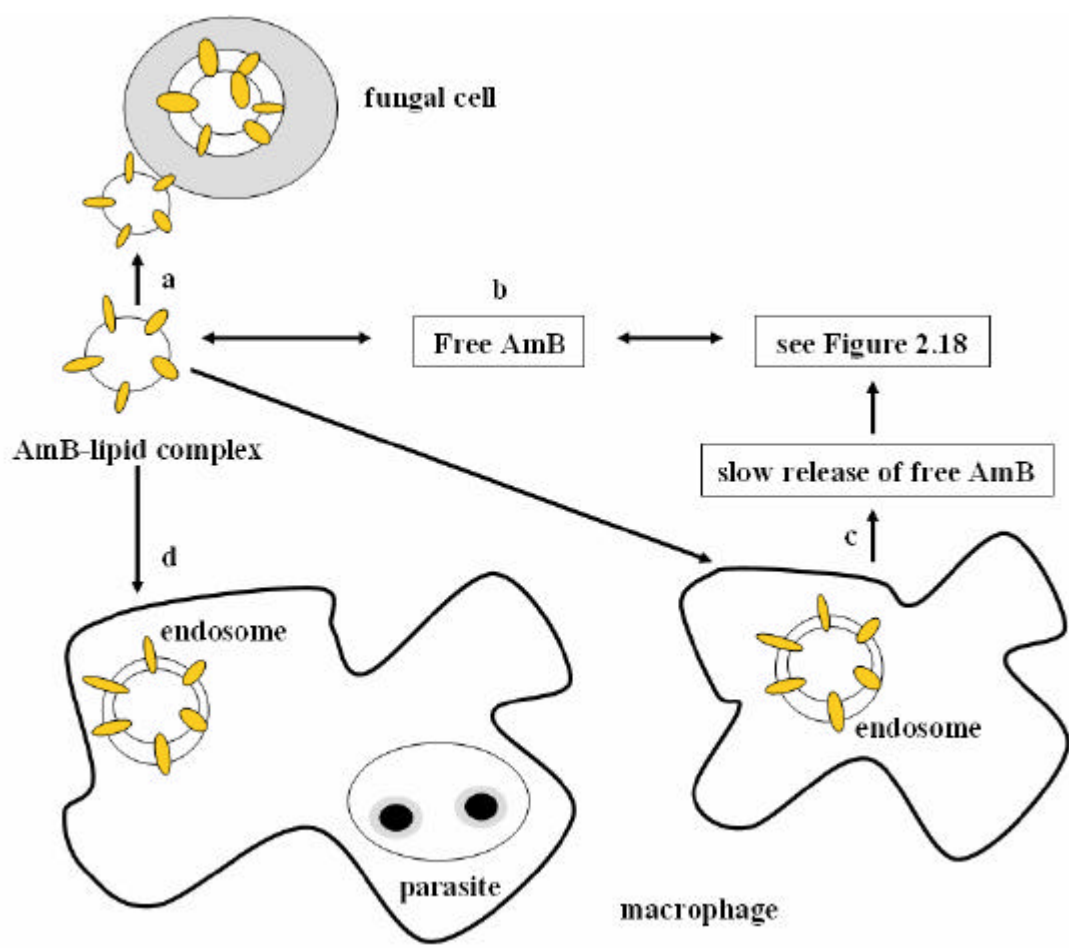


**Figure 2.19** Mechanisms of anticellular action of liposomal AmB. AmB-containing formulations may **a**: adhere to fungal cells or **b**: release free-AmB upon dilution. They also may be internalized by macrophages. In the latter case AmB can be **c**: release progressively from them, or **d**: directly kill parasites inside them. Note: it is generally true that AmB inhibits endosome-lysosome fusion and then AmB must be transferred to phagolysosomes containing parasites by a mechanism other than fusion. It may be that, at a suitable concentration, AmB can be internalized and kill the parasite but not block the fusion. AmB (🟡) (adapted from Hartsel and Bolard, 1996)

## 2.9 Aerosol formulation

Inhalation drug delivery have been used for many years for the delivery of pharmacologically active agents to treat respiratory disease, asthma therapy with bronchodilators, steroid, mast cell stabilizer and anticholinergic drug has primarily used in the pressurized meter-dose inhaler (pMDI). However, this delivery system is now under increasing threat from the environmental concern regarding chlorofluorocarbon (CFC) propellants. A range of alternative devices, such as dry powder inhalers, which do not contain propellants, are being evaluated and developed.

Dry powder inhalers are versatile delivery systems which may require some degree of dexterity to operate. Its formulation may consist of drug alone, or of drug blended with a carrier material which is usually lactose (Prime *et al.*, 1997). The advantages and disadvantages of dry powder inhalers are summarized in Table 2.2. Dry powder inhalers in common use today are breath actuated, and the energy for dry powder dispersion and generation of the aerosol are derived from the patient's inhalation. This method alleviates the problem of coordination of actuation and inhalation that many patients have with pMDIs but several studies have shown the dosing performance of some dry powder inhalers in terms of total dose or fine particle dose emitted from the device, is dependent on inspiratory flow rate (Dolovich and Ramsdale, 1990). One of the key factors involved in optimizing dry powder inhalers performance is the precision particle engineering required to produce a powder formulation that delivers accurate, consistent, efficient dose of drug (Hinds, 1982; Hickey *et al.*, 1990).

**Table 2.2** Advantages and disadvantages of dry powder inhalers (adapted from Ashurst *et al.*, 2000).

Advantages	Disadvantages
<ul style="list-style-type: none"> <li>- propellant-free</li> <li>- less need for patient coordination</li> <li>- less potential for formulation problems</li> <li>- less potential for extractable from device component</li> </ul>	<ul style="list-style-type: none"> <li>- dependency on patient's inspiratory flow rate and profile</li> <li>- device resistance and other design issue</li> <li>- greater potential problem in dose uniformity</li> <li>- less protection from environmental effects and patient abuse</li> <li>- more expensive than pMDI</li> <li>- not available worldwide</li> </ul>

### 2.9.1 Factors affecting particle deposition in the lung

Accurate assessments of drug deposition in respiratory tract are critical parameters in evaluating all inhalation drug delivery systems. The factor affecting these can be divided into two groups: the properties of the aerosol themselves and the patient (Timsina *et al.*, 1994).

- 1) The physical properties of the aerosol formulation (Gonda, 1992; Taylor, 2002)
- 2) There are three main mechanisms responsible for particulate deposition in the lung: gravitational sedimentation, impaction and diffusion. Key factors that contribute to the aerodynamic properties are found in Stoke's law. These factors may be monitored or controlled to optimize drug delivery to the lungs (Gonda, 1992; Crowder *et al.*, 2002; Taylor, 2002).



3) The patient; patient-dependent factors, such as breathing pattern, lung physiology and lung disease state affect particle aerodynamic behaviors and hence affecting deposition.

Lower the rate and longer breath-holding after inhalation, and greater volume of inhaled air enhance the deposition in the peripheral lung. Deposition by gravitational sedimentation increases as the airflow velocity decreases, so that forceful inhalation followed by a period of long breath-holding at total lung capacity maximizes aerosol deposition in the lungs. However, it should be noted that changes in the airways resulting from the disease state (i.e., airway obstruction) may affect the deposition profile of an inhaled aerosols (Gonda, 1992; Timsina *et al.*, 1994).

### **2.9.2 Particle size analysis of aerosol**

The drug particle size is recognized to play an important role in defining the location of aerosol particles deposition in the respiratory tract (Hickey and Jones, 2000). Therefore, a reliable technique is required in order to measure the particle size of inhaled aerosols and assess the drug deposition profiles both in terms of the quantity of the drug reaching the respiratory tract and its depth of penetration. When considering lung deposition, the aerodynamic diameter ( $D_{ae}$ ) is of great interest. This is defined as the diameter of a unit density sphere with the same terminal settling velocity as the particle being studied (Hickey and Jones, 2000; Mitchell and Nagel, 2004).

There are two main techniques used to analyze the particles size of aerosol, direct imaging and inertial impaction (Hickey and Jones, 2000).

a) Direct imaging based on microscopy

This method involves the viewing the particles and measuring the physical diameter. However, the subjective nature of the dimension and the largely unrealistic and unrepresentative of airway deposition are the limitation of this technique (Hickey and Jones, 2000).

#### b) Inertial sampling

This is the most widely used particle-size analysis method for inhaler output. Various instruments have been used to determine the particle size distribution of aerosols within a model respiratory tract designed to reproduce the anatomical dimension of an average healthy human airway. The instruments vary among inertial samplers, air inlet dimensions, the sampling airflow rate (12.5 to 120 L/min), the number of collecting stages (i.e., particle size ranges for collection within the distribution which varies from 2 to 8 stages), and the nature of the collection surface (liquid for impinger and uncoated or coated solid surfaces for impactor). The drug is collected and washed from these stages and analyzed by chromatographic and spectrophotometric means to determine its mass (Hickey and Jones, 2000).

A two stage device was developed as a quality control tool to predict the proportion of the fine particles present in the distribution. The most frequency used *in vitro* method is a multiple-stage impactor because more information is recovered about the range of particle sizes within the distribution. The cascade impactor utilizes the relationship between velocity and mass where larger particles with sufficient inertia are impacted on the upper stages whereas finer particles penetrate to the lower stages of the separator. Cascade impactors provide a useful aerodynamic measure of the particle size distribution, which can be used to compare devices and formulations. However, the

disadvantages of this method are the narrow range of discriminated sizes, typically at values of  $D_{ae}$  from 0.2 to 10  $\mu\text{m}$  and the considerable labor required to perform the time-consuming analyses, which are subject to operator variability and error (Hickey and Jones, 2000).

There are no pharmacopoeial monographs to fit the specific quality assurance requirements of dry powder inhalers. However, *in vitro* tests for DPIs should include uniformity of dose and respirable fraction in the aerosol clouds (Hickey and Jones, 2000).

## **2.10 Development of AmB aerosols**

The most prevalent and important organism causing fungal infections in lung-transplanted patients is *Aspergillus* spp. that remains the leading cause of morbidity and mortality after lung transplantation. Current treatment involves administration of AmB but serious adverse complications related to dose-dependent acute and chronic toxicity are seen. The rational approach to the problems requires that the drug should be targeted to the macrophages in such a way that the interaction of the free drug with non-target tissue could be minimized. The maximum tolerated dose of AmB is low in mice. The  $LD_{50}$  is 1.2 mg/kg, and doses higher than 1.6 mg/kg causes acute toxic reactions following by cardiac-respiratory arrest (Lopez-Berestein *et al.*, 1983). Whereas, treatment of disseminated fungal infections by liposomal AmB results in a lower toxicity and significantly increased survival time (Brajtburg *et al.*, 1990). It is probably that increased concentrations of drug in macrophages through passive liposomal uptake may improve its therapeutic index (Janknegt *et al.*, 1992; De Marie *et al.*, 1994). Thus, it is expected that ligand-mediated active targeting to the macrophages

would significantly increase the rate and extent of macrophage accumulation of drug. This may reduce the required doses of liposomal AmB in pulmonary aspergillosis.

Nebulized AmB has been used successfully in the rat model of invasive aspergillosis, and in human, nebulized AmB prophylaxis may be efficient and safe in preventing *Aspergillus* infection in lung-transplanted patients (Monforte *et al.*, 2001). Aerosolized AmB has been used in the treatment of pulmonary fungal infections as well as intravenous AmB. In particular, prophylactic use of AmB aerosol is effective in the prevention of pulmonary aspergillosis in an experimental animal model and humans (Conneally *et al.*, 1990; Beyer *et al.*, 1993). Sorensen and coworkers (1993) have used aerosolization of liposomal (AmBisome<sup>®</sup>) and non-liposomal (Fungizone<sup>®</sup>) AmB for pulmonary fungal infection. Liposomal AmB (AmBisome<sup>®</sup>) was able to nebulize much better than non-liposomal (Fungizone<sup>®</sup>) and to be highly effective as a prophylactic treatment in an immune compromised murine model of pulmonary aspergillosis. In addition, the pharmacokinetics of nebulized AmB was studied by Koizumi *et al.* (1998). The results showed the peak AmB concentration in bronchial-wash fluid was observed at 30 min. After that, AmB was slowly eliminated over 24 h. AmB is still the most effective agent currently available for the treatment and prevention of serious fungal infection but it must be more clinical and experimental studies to determine the best tolerated and effective regimen of AmB.

The small multilamellar AmB liposomes were successfully prepared by reverse phase evaporation technique (Shah and Misra, 2004). Liposomal dry powder inhaler was chosen to stabilize the liposomal system. Drug lipid ratio was 1:10 with membrane composition of hydrogenated soyphosphatidylcholine, cholesterol and either saturated soyphosphatidylglycerol (7:3:0.5) or stearylamine (1:1:0.1) were used to

prepare negatively and positively charged liposomes, respectively. The shelf life of the powder was over 1 year at refrigerated condition (2–8°C).

Effective chemotherapy through drug targeting to alveolar macrophages can be practically implemented particularly in pulmonary aspergillosis using ligand-anchored liposomes. Aerosolized liposomal AmB has also been reported for treatment of pulmonary fungal infections (Gilbert *et al.*, 1992; Allen *et al.*, 1994; Ruijgroka *et al.*, 2001). The encapsulation of AmB into the liposome with modification of liposomal surface by anchoring lung macrophages-specific ligands will certainly improve efficacy against pulmonary aspergillosis (Vyas *et al.*, 2005).

# CHAPTER 3

## SYNTHESIS AND CHARACTERIZATION OF CHOLESTERYL CARBONATE ESTERS

### 3.1 Introduction

There is continued interest in developing biocompatible, lipid-based systems, which exhibit liquid crystalline behavior (Tyle, 1988; Fairhurst *et al.*, 1998; Mahusudana, 2001; Hwang *et al.*, 2002; Muller-Goymann, 2004). In particular, lipid systems that are amenable for drug delivery are particularly important due to the more common discovery of active pharmaceutical ingredients (API) that have low water solubility. For this use, not only must the components be biologically acceptable but by-products of degradation must also be nontoxic. Another pharmaceutical requirement is chemical stability so that an extended shelf-life may be obtained, and the drug product can be stored for at least 2 yrs.

A relatively large number of materials have been investigated, which are often naturally occurring. Perhaps the most commonly used species are phospholipids, with phosphatidylcholines (PC) being most frequent (Small, 1986). PC's may also be used to prepare liposomes or stabilize dispersed products such as emulsions or suspensions. Triglycerides, cholesterol, cholesterol esters (CE), and fatty acids are also often used in oral or externally applied products. A shortcoming of PC's and CE's is that these species contain an ester functional group, which is chemically unstable in

water. Thus, identification of lipid excipients that have good chemical stability would be of value.

Over the last decade, the oleyl carbonate ester of cholesterol (COC) has been studied as a possible material that can be used to prepare liquid crystalline based systems (Lin *et al.*, 1995; Lin *et al.*, 2000). COC undergoes a reversible smectic-cholesteric transition near 18 °C and a cholesteric to isotropic liquid transition near 40 °C (Lin *et al.*, 2000). Despite the chemical similarity to the corresponding cholesterol ester, cholesterol oleate (CO), the behavior of the cholesterol carbonate appears to be quite distinct. For example, CO undergoes the smectic to cholesteric and the cholesteric to isotropic phase transitions at 41 and 47.5 °C (Ginsburg *et al.*, 1985) respectively, which is much higher than the carbonate derivative. COC has been studied in combination with cholesterol nonanoate (a nine carbon fatty acid ester-linked to cholesterol) in order to identify a mixture that would have a liquid crystalline to isotropic phase transition near 34-36 °C (Lin *et al.*, 2000). It was proposed that such a mixture could then be used for drug delivery applications to the skin where the surface temperature is slightly lower than the typical 37 °C body temperature. Moreover, the room temperature liquid crystalline phase would provide enhanced chemical stability in comparison to the isotropic phase.

The long term goal of this effort is to identify and develop chemically stable systems that can be used for inhalation drug delivery. For this purpose, we have compared the properties of sodium cholesteryl carbonate (SCC), cholesteryl palmityl carbonate (CPC) and dicholesteryl carbonate (DCC) as well as the unsaturated oleyl carbonate ester and the cholesterol ester, cholesterol myristate (CM). Thus, this study

investigated thermotropic phase behaviors of SCC, CPC and DCC in details by several analytical techniques in comparison with COC and CM.

### **3.2 Materials and methods**

Cholesteryl myristate was purchased from Aldrich Chemical Company, St Louis, MO, USA. Cholesterol chloroformate, cholesterol oleyl carbonate from Sigma-Aldrich Chemie, Munich, Germany. Cholesterol was obtained from Merck & Co Inc., Cincinnati, OH, USA.

#### **3.2.1 Synthesis of cholesteryl carbonate esters**

##### **A) Sodium cholesteryl carbonate (SCC)**

Cholesteryl chloroformate (5.57 mM, 2.50 g) was dissolved in 25.0 mL of dichloromethane in a round bottom flask on ice bath. Triethylamine (1.0 mL) was added, and the solution was stirred for 10 min (adapted from Suh *et al.*, 1988). Purified water (5.57 mM, 0.1 mL) was added dropwise into the flask. The reaction vessel was removed from an ice bath and was continuously stirred for 20 h at room temperature (RT). Sodium hydroxide was added to neutralize the cholesteryl carboxylate and taken a final product of sodium cholesteryl carbonate (SCC). The resulting suspension was filtered and extracted with distilled water. The organic phase was collected, and water was removed with anhydrous sodium sulfate. The organic phase was dried using a rotary film evaporator. The purity of the liquid crystals was assessed with two different thin-layer liquid chromatography (TLC) systems, petroleum ether-diethyl ether-acetic acid 80:20:1 (v/v) and hexane-chloroform 40:10 (v/v) using iodine vapor detection.



Silica gel flash column chromatography was employed to purify the sodium cholesteryl carbonate. The scheme of reaction is shown in Figure 3.1.

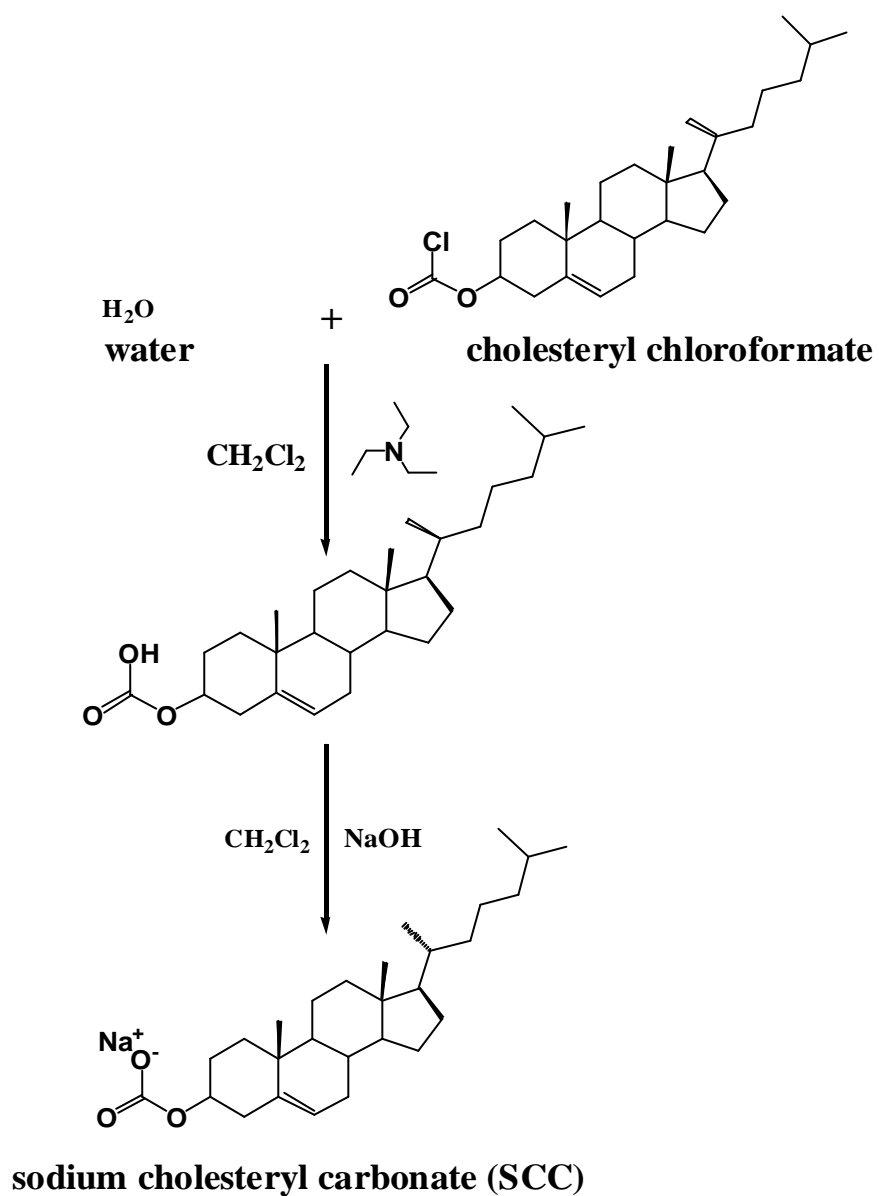


**Figure 3.1** Synthesis route of sodium cholesteryl carbonate (SCC).

### B) Cholesteryl palmityl carbonate (CPC)

Cholesteryl chloroformate (5.57 mM, 2.50 g) was dissolved in 25.0 mL of dichloromethane in a round bottom flask. Pyridine (1.0 mL) was added, and the solution was stirred for 10 min. Palmityl alcohol (5.57 mM, 1.35 g) was dissolved in 10.0 mL of dichloromethane added dropwise (1/5 s) with a dropping funnel. The reaction vessel was continuously refluxed for 20 h at room temperature (RT). The final suspension was purified and identified as described in section 3.2.1 A).

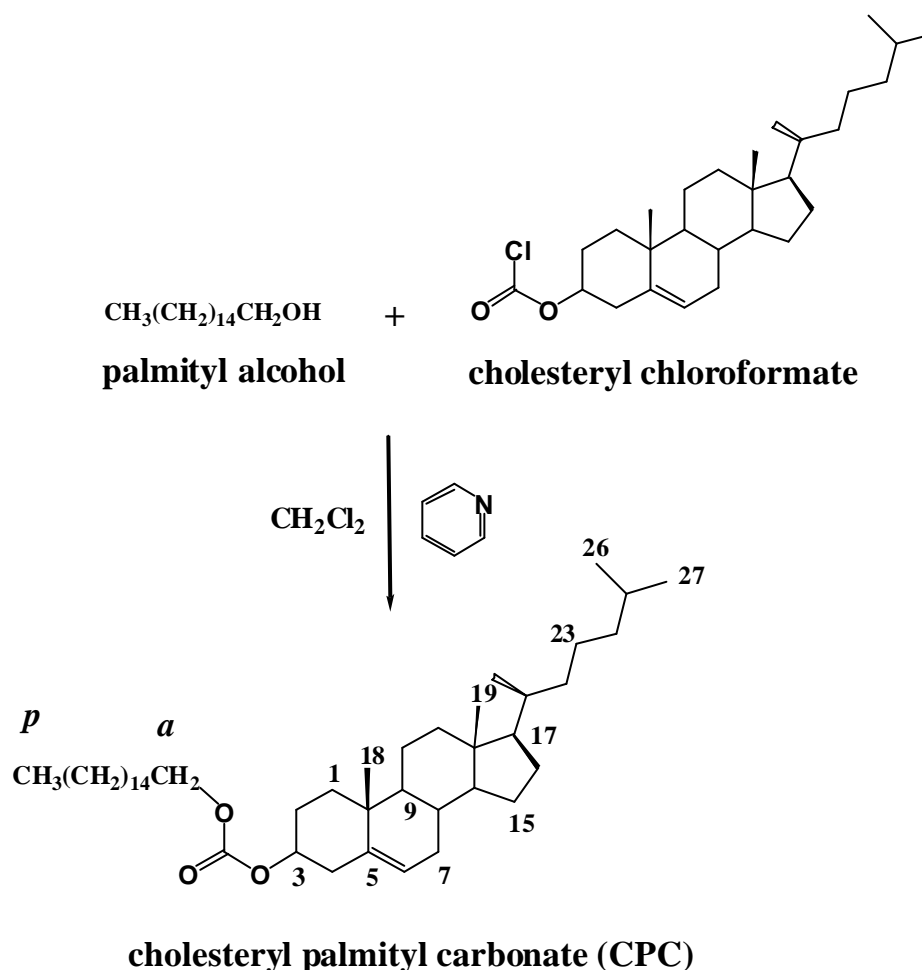


**Figure 3.2** Synthesis route of cholesteryl palmityl carbonate (CPC)

### C) Dicholesteryl carbonate (DCC)

The synthesis was prepared as cholesteryl palmityl carbonate but; cholesterol (5.57 mM, 2.15 g) was used instead palmityl alcohol in the same of mole ratio. The synthesis method and identification of product were already described in section 3.2.1 B).

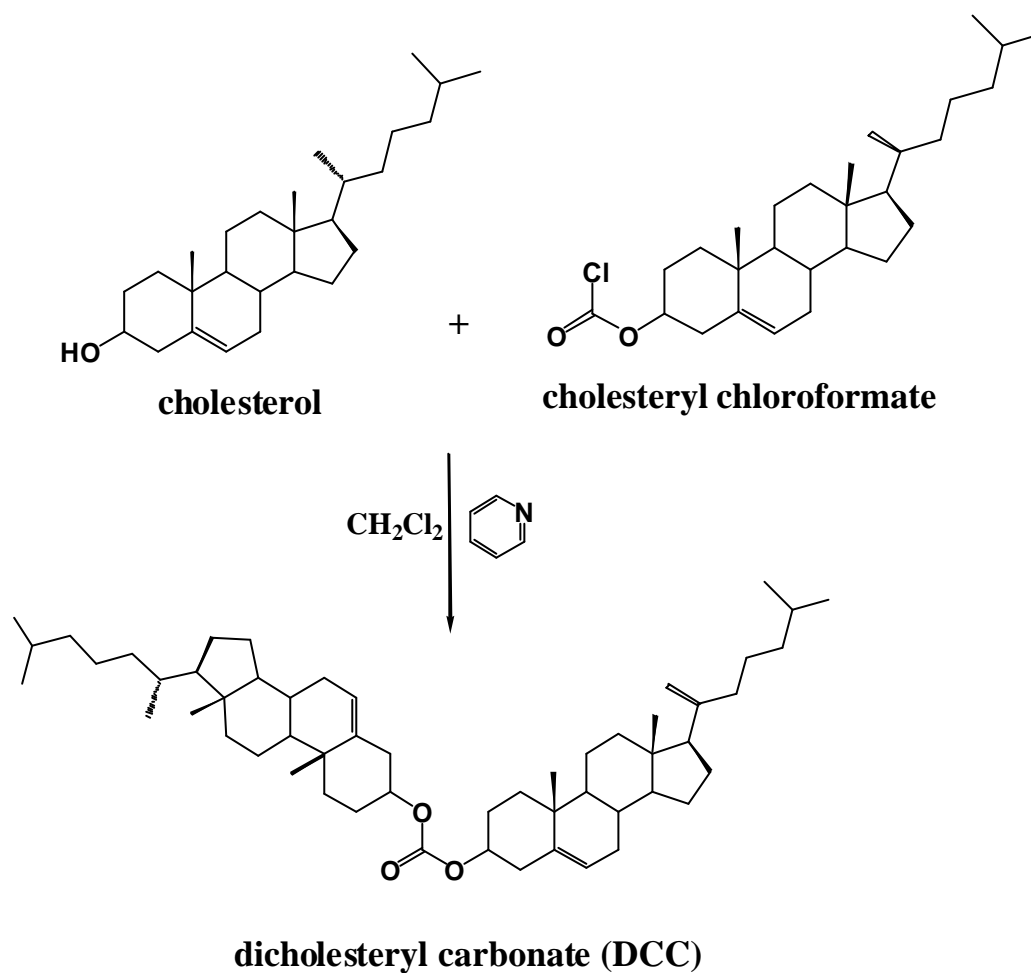


**Figure 3.3** Synthesis route of dicholesteryl carbonate (DCC)

### 3.2.2 Characterization of cholesteryl carbonate esters

#### A) Fourier Transforms Infrared Spectroscopy (FTIR)

The functional group of cholesteryl carbonate esters were recorded by using PerkinElmer precisely (PerkinElmer Inc., Hercules, CA, USA) in the frequency range  $4000\text{-}450\text{ cm}^{-1}$ . A small amount of sample was sealed into KBr pellets by a hydraulic press prior to measurement at ambient temperature.

#### B) Nuclear Magnetic Resonance Spectroscopy (NMR)

The  $^1\text{H}$ -NMR and  $^{13}\text{C}$ -NMR spectra were performed on Varian Unity Inova 500 spectrometer at 500 MHz (Varian, Germany). All the NMR spectra were recorded at 298 K using deuteriochloroform ( $\text{CDCl}_3$ ) as solvent.  $^1\text{H}$ -NMR chemical shifts were referenced to internal standard TMS; for  $^{13}\text{C}$ -NMR spectra resonance line of  $\text{CDCl}_3$  at 77.00 ppm was taken as reference line.

#### C) Mass Spectroscopy (MS)

The electrospray ionization (negative mode) mass spectra were obtained from a Micromass LCT mass spectrometer (Bruker, Bremen, Germany).

#### D) Differential Scanning Calorimetry (DSC)

A modulated differential scanning calorimeter (DSC) (model 2920, TA Instruments, New Castle, DE) was used to determine the thermal phase transitions. Generally, samples (5 mg) were enclosed within aluminum hermetically sealed pans and subjected to a heating rate of  $5^\circ\text{C}/\text{min}$ . After cooling to  $0^\circ\text{C}$ , the heating and

cooling process was repeated. Aside from a slightly more narrow transition, no significant differences were observed between the first and second scan unless specifically noted. Transition temperatures were determined as the intersection of the extrapolated, tangential line of the most rapidly rising part of the peak with the horizontal baseline. The enthalpy change was simultaneously obtained as the integrated area under the curve. The entropy change was calculated from the change in enthalpy and the transition temperature.

#### **E) Video-enhanced Microscope (VEM)**

Crystals of each cholesterol carbonate ester were observed under a video-enhanced microscope (VEM) (Nikon Optiphot-Pol, Tokyo, Japan) equipped with the Metamorph Imaging System software (Universal Imaging Co., West Chester, PA). Samples were heated using a heating rate 10 °C/min and cooled at the same rate to room temperature (25 °C).

#### **F) X-ray Diffraction**

The X-ray diffraction measurements were performed on a focusing camera in a 12kW rotating anode X-ray generator (Rigaku RU200, Rigaku Corp., Tokyo, Japan) with  $CuK\alpha$  (Ni filter,  $\lambda = 1.5418 \text{ \AA}$ ) radiation at 40 kV and 60 mA. X-ray diffraction data were collected by using a Siemens Hi-star multi-wire area detector. A double focusing Frank's mirror was used to provide a highly focus beam. Samples were sealed in 1 mm-thick flat Kapton windows, perpendicular to the X-ray beam, placed in a copper sample holder with an attached temperature control unit (Neslab RTE-221, Thermo Neslab Inc., Newington, NH). The sample to detector distance was 0.30 meter.

Each sample was also run at a longer distance to detect the existence of a long *d*-spacing, although none was found.

### 3.3 Results and discussions

Sodium cholesteryl carbonate (SCC), cholesteryl palmityl carbonate (CPC) and dicholesteryl carbonate (DCC) were obtained from the reaction in the presence of triethylamine or pyridine as a base. The chemical structure Figure 3.1, 3.2 and 3.3 associated with the compounds was investigated by using infrared spectral analysis, NMR techniques, mass spectrometry and elemental analysis. The thermal properties of compounds were studied as compared with COC and CM.

Sodium cholesteryl carbonate, the title compound was obtained in 40% yield as white plate crystals,  $R_f = 0.84$  (chloroform/hexane 1:4). The molecular structure of SCC was analyzed in the conventional 1D  $^1\text{H-NMR}$  and  $^{13}\text{C-NMR}$  (see appendix).  $^1\text{H-NMR}$  ( $\text{CDCl}_3$ ) : 5.35 (t, 1H, H-6), 4.52 (m, 1H, H-3), 1.97 (m, 2H, H-7), 2.38-1.02 (m, 26H), 0.88 (s, 3H,  $\text{CH}_3$ -19), 0.89 (s, 3H,  $\text{CH}_3$ -21), 0.85 (d, 3H,  $\text{CH}_3$ -26 or  $\text{CH}_3$ -27), 0.86 (d, 3H,  $\text{CH}_3$ -26 or  $\text{CH}_3$ -27), 0.67 (s, 3H,  $\text{CH}_3$ -18);  $^{13}\text{C-NMR}$  ( $\text{CDCl}_3$ ): 155.54 (C=O), 140.01(C-5), 122.27 (CH, C-6), 74.24 (CH, C-3), 56.64 (CH, C-14 or C-17), 56.07 (CH, C-14 or C-17), 49.95 (CH, C-9), 42.27 (C-13), 39.70 ( $\text{CH}_2$ , C-4), 39.48 ( $\text{CH}_2$ , C-12), 38.69 ( $\text{CH}_2$ , C-24), 37.02 ( $\text{CH}_2$ , C-1), 36.56 (C-10), 36.14 ( $\text{CH}_2$ , C-22), 35.78 (CH, C-20), 31.85/31.89 ( $\text{CH}_2/\text{CH}$ , C-7/C-8), 28.29 ( $\text{CH}_2$ , C-2), 28.22 ( $\text{CH}_2$ , C-16), 27.99 (CH, C-25), 24.27 ( $\text{CH}_2$ , C-23), 23.80 ( $\text{CH}_2$ , C-15), 22.81 ( $\text{CH}_3$ , C-26 or C-27), 22.54 ( $\text{CH}_3$ , C-26 or C-27), 21.01 ( $\text{CH}_2$ , C-11), 19.37 ( $\text{CH}_3$ , C-19), 18.68 ( $\text{CH}_3$ , C-21), 11.83 ( $\text{CH}_3$ , C-18). Mass Spectrometry [MS; Electrospray ionization (ESI) negative mode]:  $m/z$  487.4  $[\text{M}+\text{Cl}]^-$ , calculated for  $\text{C}_{28}\text{H}_{45}\text{O}_3\text{Na}$ . Elemental analysis: Calculated

for SCC ( $C_{28}H_{45}NaO_3$ , 452.33): C, 74.30; H, 10.20; Na, 5.08; O, 10.60. Found: C, 73.94; H, 9.96; O, 10.54.

Cholesteryl palmityl carbonate was obtained in 80% yield as white plate crystals with  $R_f$  of 0.89 (chloroform/hexane 1:4). The molecular structure of CPC was analyzed in the conventional 1D  $^1H$ -NMR and  $^{13}C$ -NMR (see appendix).  $^1H$ -NMR ( $CDCl_3$ ): 5.37 (t, 1H, H-6), 4.45 (m, 1H, H-3), 4.09 (m, 2H, H-a);  $^{13}C$ -NMR ( $CDCl_3$ ): 154.67 (C=O), 139.39 (C-5), 122.86 (CH, C-6), 77.59 (CH, C-3), 56.66 (CH, C-14 or C-17), 56.09 (CH, C-14 or C-17), 49.96 (CH, C-9), 42.28 (C-13), 39.69 (CH<sub>2</sub>, C-4), 39.49 (CH<sub>2</sub>, C-12), 38.03 (CH<sub>2</sub>, C-24), 36.84 (CH<sub>2</sub>, C-1), 36.51 (C-10), 36.15 (CH<sub>2</sub>, C-22), 35.77 (CH, C-20), 31.88/31.92 (CH<sub>2</sub>/CH, C-7/C-8), 28.66 (CH<sub>2</sub>, C-2), 28.21 (CH<sub>2</sub>, C-16), 27.99 (CH, C-25), 24.26 (CH<sub>2</sub>, C-23), 23.80 (CH<sub>2</sub>, C-15), 22.81 (CH<sub>3</sub>, C-26 or C-27), 22.55 (CH<sub>3</sub>, C-26 or C-27), 21.01 (CH<sub>2</sub>, C-11), 19.25 (CH<sub>3</sub>, C-19), 18.69 (CH<sub>3</sub>, C-21), 11.83 (CH<sub>3</sub>, C-18); alkyl chain: 67.89 (CH<sub>2</sub>, C-a), 31.81 (CH<sub>2</sub>, C-n), 29.36-29.69 (CH<sub>2</sub>, C-d to C-l), 29.22 (CH<sub>2</sub>, C-d/C-m), 27.68 (CH<sub>2</sub>, C-b), 25.71 (CH<sub>2</sub>, C-c), 22.69 (CH<sub>2</sub>, C-o), 14.12 (CH<sub>3</sub>, C-p). Mass Spectrometry [MS; EI and FAB]:  $m/z$  368.5 [Cholesterol]<sup>+</sup> calculated for cholesterol fragment from ( $C_{44}H_{78}O_3$ ). Elemental analysis: Calculated for CPC ( $C_{44}H_{78}O_3$ , 654.60): C, 80.67; H, 12.00; O, 7.33. Found: C, 79.45; H, 11.60; O, 8.90.

Dicholesteryl carbonate, the title compound was obtained in 80% yield as white plate crystals,  $R_f = 0.89$  (chloroform/hexane 1:4). The molecular structure of DCC was analyzed in the conventional 1D  $^1H$ -NMR and  $^{13}C$ -NMR (see appendix).  $^1H$ -NMR ( $CDCl_3$ ): 5.36 (t, 1H, H-6), 4.44 (m, 1H, H-3);  $^{13}C$ -NMR ( $CDCl_3$ ): 153.87 (C=O), 139.42 (C-5), 122.84 (CH, C-6), 77.46 (CH, C-3), 56.67 (CH, C-14 or C-17), 56.10 (CH, C-14 or C-17), 49.96 (CH, C-9), 42.28 (C-13), 39.69 (CH<sub>2</sub>, C-4), 39.50

(CH<sub>2</sub>, C-12), 38.04 (CH<sub>2</sub>, C-24), 36.85 (CH<sub>2</sub>, C-1), 36.52 (C-10), 36.16 (CH<sub>2</sub>, C-22), 35.78 (CH, C-20), 31.81/31.88 (CH<sub>2</sub>/CH, C-7/C-8), 28.21 (CH<sub>2</sub>, C-2), 28.00 (CH<sub>2</sub>, C-16), 27.70 (CH, C-25), 24.26 (CH<sub>2</sub>, C-23), 23.81 (CH<sub>2</sub>, C-15), 22.81 (CH<sub>3</sub>, C-26 or C-27), 22.55 (CH<sub>3</sub>, C-26 or C-27), 21.02 (CH<sub>2</sub>, C-11), 19.25 (CH<sub>3</sub>, C-19), 18.69 (CH<sub>3</sub>, C-21), 11.84 (CH<sub>3</sub>, C-18). Mass Spectrometry [MS; EI and FAB]: *m/z* 368.5 [Cholesterol]<sup>+</sup> calculated for cholesterol fragment from (C<sub>55</sub>H<sub>90</sub>O<sub>3</sub>). Elemental analysis: Calculated for DCC (C<sub>55</sub>H<sub>90</sub>O<sub>3</sub>, 798.69): C, 82.65; H, 11.35; O, 6.01. Found: C, 81.79; H, 12.03; O, 6.20.

**Table 3.1** Specific characteristics of SCC, CPC and DCC as compared with cholesterol and COC from IR spectra.

Compounds	Assignments			
	$\nu_{\text{C-H}}$ stretching	$\nu_{\text{C=O}}$	$\nu_{\text{O-C-O}}$	$\nu_{\text{O-H}}$
Cholesterol	2934, 2901, 2866	-	-	3391
SCC	2932, 2853	1705	1276	-
CPC	2919, 2850	1736	1270	-
DCC	2948, 2865	1743	1262	-
COC	2928, 2853	1742	1252	-

The IR spectra of compounds and selected data are shown Table 3.1. The most prominent vibrations observed for SCC, CPC, DCC and cholesteryl oleyl carbonate (COC) were the carbonyl group vibration at 1705-1743 cm<sup>-1</sup> (strong). The presences of alkyl groups are located at 2963-2868 cm<sup>-1</sup>. The band with medium



intensities observed for all compounds at  $1464\text{-}1474\text{ cm}^{-1}$  may be due to the methylene groups of cholesterol fragment. A strong band occurred at  $1250\text{-}1276\text{ cm}^{-1}$  in IR spectra of SCC, CPC, DCC and COC can be attributed to the stretching of O-C-O.

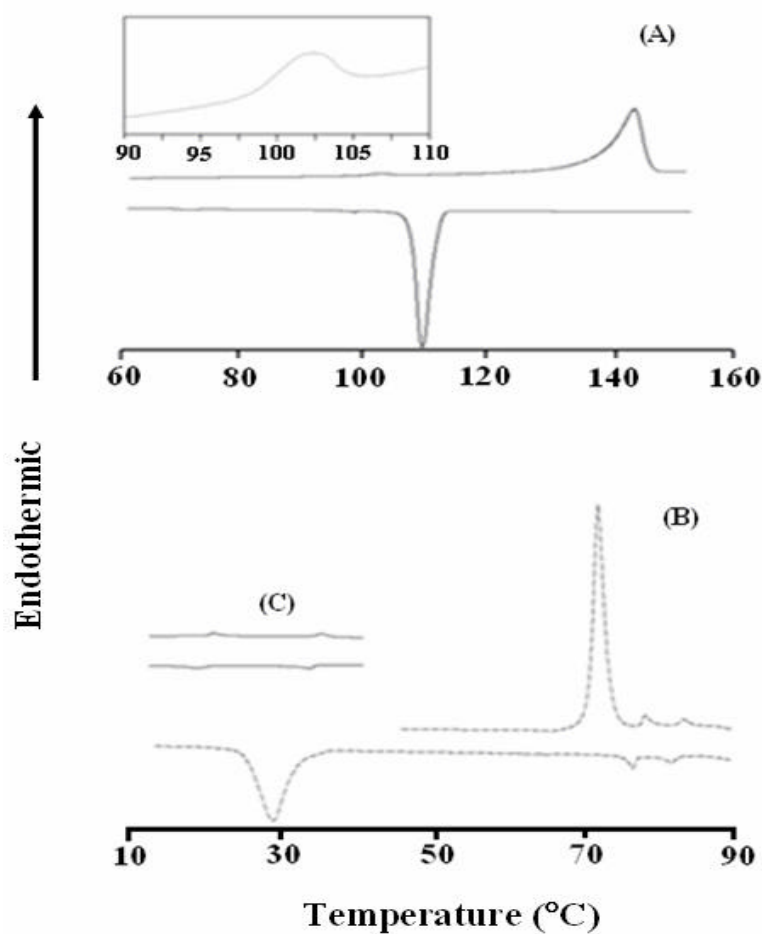


**Figure 3.4** A plot of the excess heat capacity as a function of temperature for heating (upper curves) and cooling (lower curves) for (A) SCC (—), (B) CM (---) and (C) COC (—). Inset shows expanded region

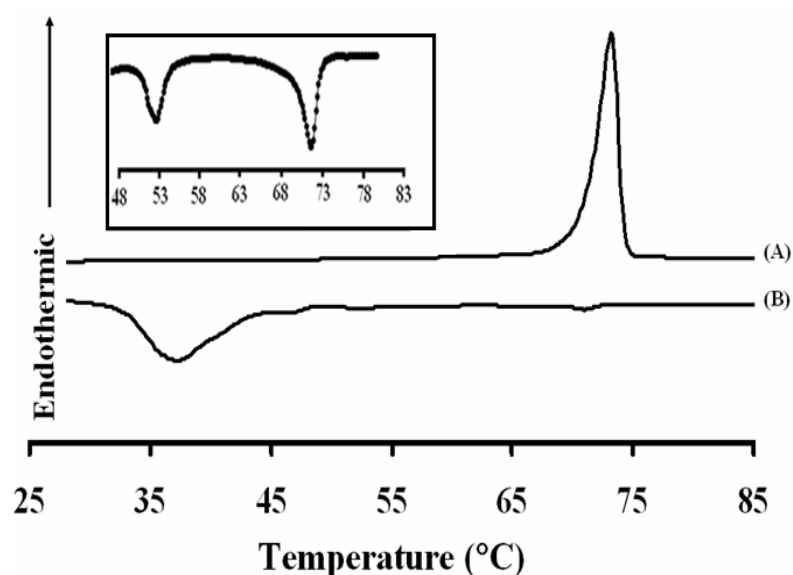
In Figure 3.4 (A), the DSC thermogram of SCC is given. A main transition was observed just above  $140\text{ }^{\circ}\text{C}$  for SCC. In addition, a minor endothermic transition was seen at  $102\text{ }^{\circ}\text{C}$ , which is shown with an expanded scale in the inset of

Figure 3.4 (A). Placing the samples in open pans under high vacuum ( $< 50$  microTorr) overnight and in the presence of phosphorus pentoxide prior to sealing did not result in the elimination of this small endothermic transition. However, the addition of excess water resulted in a very large endothermic transition in the samples that had a leading edge at about  $60$  °C and was not complete until the temperature exceeded  $100$  °C (data not shown). With cooling, a broad exothermic peak was seen between  $105$  and  $115$  °C.

DSC was also carried out with CM and COC, since these lipids were reported to form smectic and cholesteric liquid crystalline phases. For CM (Figure. 3.4 (B)), a large endothermic peak was observed just above  $72$  °C, which was followed by two smaller peaks near  $78$  and  $85$  °C. With cooling, the small exothermic peaks were observed at slightly lower temperatures than the endothermic transitions. However, a large, exothermic transition that presumably reverses the large endothermic transition did not take place until the temperature fell below  $30$  °C. For COC (Figure 3.4 (C)), no large, endothermic peaks were observed but rather two small endothermic peaks occurred at about  $20$  and  $35$  °C. With cooling, small exothermic peaks were observed at similar temperatures. The peaks were analyzed, and the transition temperatures and calculated enthalpy and entropy changes are given in Table 3.2. The main transition temperature for inorganic cholesteryl carbonate ester fell within  $142.8$  °C. The changes in enthalpy and entropy changes for SCC were  $4.55$  kcal/mole and  $10.16$  cal/mole-K, respectively. The small endothermic peak observed near  $102$  °C could not be reliably integrated, but the estimated enthalpy change was less than  $0.07$  kcal/mole. With cooling, the absolute value of the enthalpy and entropy change occurring near  $108$  °C was observed near  $140$  °C during heating.

For CM, the main endothermic peak had a transition temperature of 71.5 °C and an associated enthalpy change of 10.01 kcal/mole (Table 3.2). The transition temperatures of the smaller endotherms were 78.2 and 84.5 °C, and the enthalpy changes were 0.20 and 0.15 kcal/mole. For COC, the transition temperatures were 20 and 36 °C, and enthalpy changes were 0.13 and 0.11 kcal/mole, respectively.

For CPC (Figure 3.5), a large endothermic peak was observed about 72.8 °C. The changes in enthalpy and entropy changes for CPC were 12.55 kcal/mole and 36.30 cal/mole-K, respectively. While cooling down process, the main transition temperature was obtained at 37.1 °C and following with two small exothermic peaks at 52.5 and 71.0 °C (expanded scale in the set of Figure 3.5). The associated enthalpy changes and entropy changes of CPC were 9.25, 0.16, 0.28 kcal/mole and 26.74, 0.50, 0.88 cal/mole-K, respectively. The result shows that CPC is monotropic liquid crystal.



**Figure 3.5** A plot of the excess heat capacity as a function of temperature of CPC for heating (A) and cooling (B). Inset shows expanded region

In Figure 3.6, the DSC thermogram of DCC was obtained. The two main endothermic peaks had transition temperatures at 169.5 and 175.2 °C. The enthalpy changes of endothermic peak associated to 3.32 and 2.02 kcal/mole, respectively. In addition, the entropy changes of endothermic peaks were observed of 7.50 and 4.52 cal/mole-K. With cooling, a large and broadened exothermic peak can be observed at slightly lower temperature than the endothermic transitions. In spite of an enthalpy and entropy change of endothermic peaks, an exothermic peak given enthalpy and entropy changes slightly larger than endothermic peaks as shown in Table 3.2. However, the exothermic peak of DCC exhibits a broadening peak which may be consisted of two exothermic peaks. The results correlated with those obtained from polarized light microscope. It indicates that DCC is enantiotropic liquid crystal.

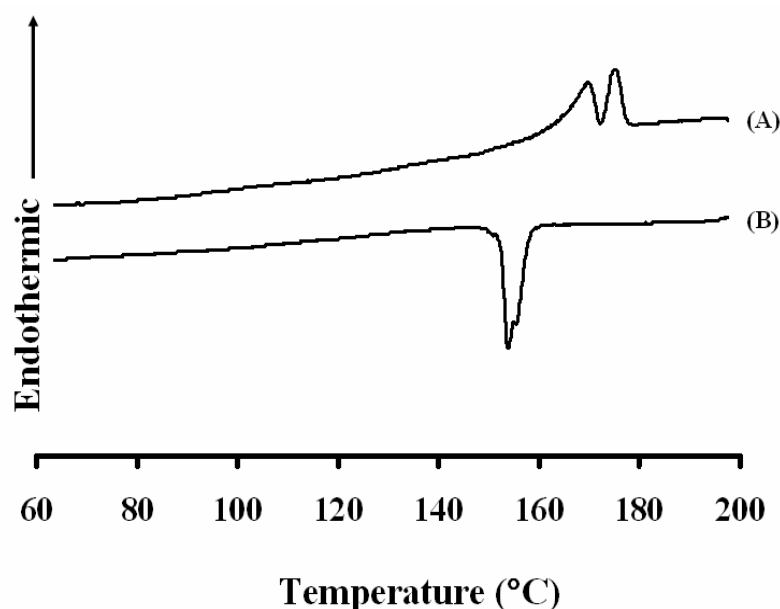


**Figure 3.6** A plot of the excess heat capacity as a function of temperature of DCC for heating (A) and cooling (B)

**Table 3.2** Thermotropic phase transition temperatures,  $T_p$  ( $^{\circ}\text{C}$ ), associated enthalpy change,  $\Delta H$  (kcal/mole) and entropy change,  $\Delta S$  (cal/mole-K) with heating and cooling at  $5^{\circ}\text{C}/\text{min}$  for SCC, CPC, DCC, COC and CM.

Compound	Heating process			Cooling process		
	$T_p$	DH	DS	$T_p$	DH	DS
SCC	102.3	0.07	0.18	71.2	0.07	0.18
	142.8	4.22	10.16	108.9	4.45	11.66
CPC	72.8	12.55	36.30	37.1	9.25	26.74
				52.5	0.16	0.50
				71.0	0.28	0.88
DCC	169.5	3.32	7.50	153.8	5.93	13.91
	175.2	2.02	4.52			
COC	20.0	0.13	0.44	19.3	0.11	0.37
	36.0	0.11	0.34	33.6	0.08	0.26
CM	71.5	10.01	29.05	28.9	7.29	24.15
	78.2	0.2	0.58	76.1	0.34	0.98
	84.5	0.15	0.43	81.2	0.17	0.48

In Figure 3.7, the results obtained with video-enhanced microscopy are shown for SCC, which is representative of the inorganic cholesteryl carbonate esters. As can be seen, the sample appears birefringent at  $25^{\circ}\text{C}$  characteristic of a crystalline solid. This remains visually unchanged until the temperature was increased past the small endothermic transition at  $102^{\circ}\text{C}$ . A smectic phase was formed at temperature over 102 to  $145^{\circ}\text{C}$ . At  $165^{\circ}\text{C}$ , the sample had liquefied, which resulted in a loss of birefringence, and with cooling to  $25^{\circ}\text{C}$  the sample again appeared crystalline.

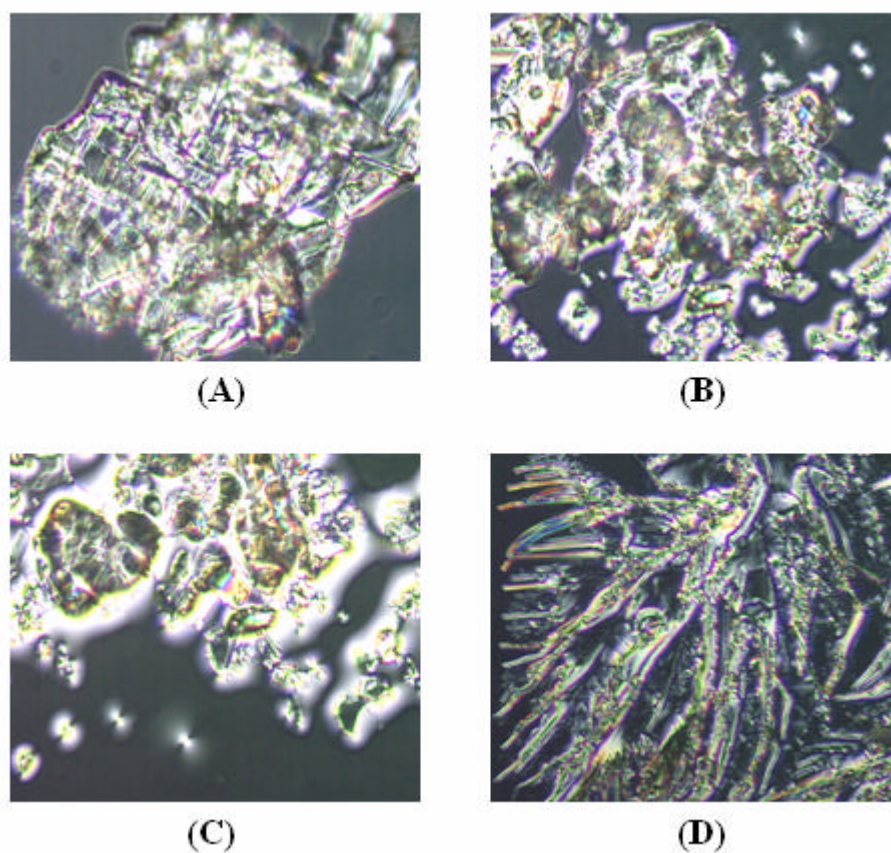


**Figure 3.7** Photographs of SCC crystals using polarizing lenses at temperatures of 25 °C (A), 110 °C (B), 140 °C (C), and after cooling to 25°C (D) (200x)

Figure 3.8 presents the micrographs of CPC which observed under polarized light microscope. The solid crystal of CPC was obtained with less of birefringent at 25 °C. This characteristic remains visually unchanged until the temperature was increased over an endothermic transition at ~73 °C and the sample was liquefied (non-birefringent). When the temperature was cooled down under 71 °C, the cholesteric-smectic phase was obtained at 52.5 °C and the smectic-solid crystal phase was observed at 37 °C, respectively. The brilliantly birefringent of spherulite crystals

was observed until cooling down to 25 °C (Figure 3.8 (B)). Therefore, the heating and cooling process affected an order of crystal in CPC molecules.

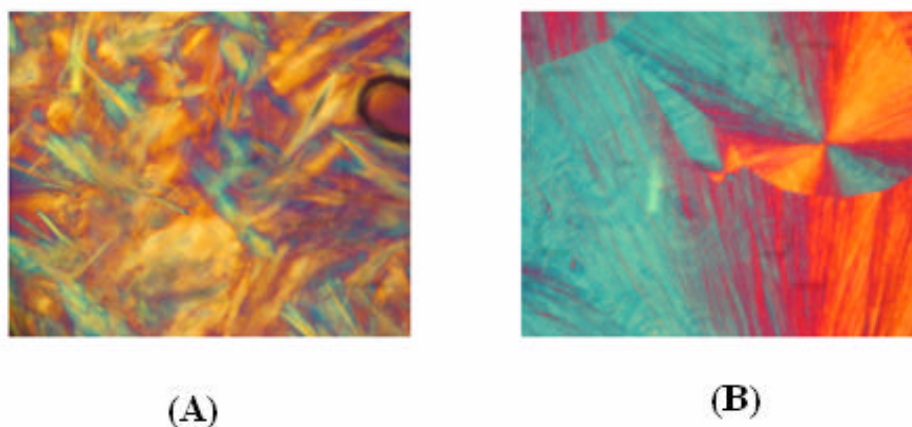


**Figure 3.8** Photographs of CPC using polarizing lenses at temperatures of (A) 25 °C and (B) after cooling to 25 °C (200x)

For DCC (Figure 3.9), the sample appeared birefringent characteristic of the solid crystalline phase from 25 to 170 °C. With an increase in the temperature, solid-smectic phase transition at 170 °C and smectic-isotropic liquid phase transition at ~175 °C. The sample was isotropic liquid with further increase temperature over 175 °C. Upon cooling down process, the liquid-smectic phase transition was obtained at 153 °C and smectic-solid crystal phase transition appeared around 149 °C when the temperature was decreased back to 25 °C, the banana-shaped crystal was observed with highly birefringent.

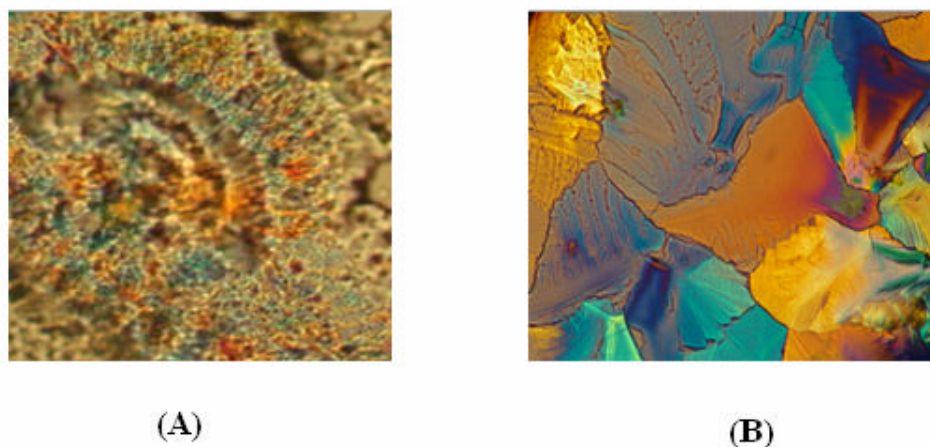


**Figure 3.9** Photographs of DCC using polarizing lenses at temperatures of (A) 25 °C and (B) after cooling to 25 °C (200x)

The corresponding VEM results for COC are given in Figure 3.10. At 17°C, the sample appeared birefringent characteristic of the smectic liquid crystalline phase. With an increase in the temperature to 25 °C, the sample became brilliantly birefringent. With further heating to 37 °C, the sample was liquefied and when the temperature was cooled down to 25 °C, solid crystal occurred with highly birefringent.

In this chapter, SAXD technique was used to characterize SCC as compared with COC and CM. The X-ray diffraction pattern for SCC is shown in Figure 3.11. The broad peak centered at  $0.4 \text{ \AA}^{-1}$  arises from the background of the sample holder. SCC compound yielded an intense Bragg reflection peak at about  $0.65 \text{ \AA}^{-1}$ . In addition, a weak reflection was observed between  $0.55 \text{ \AA}^{-1}$ . At low scattering angles, there is a diffuse reflection at  $0.27 \text{ \AA}^{-1}$ . The details of the diffraction pattern are better seen in Figures 3.12, 3.13 (A) and 3.13 (B), which have expanded scales and are in terms of  $d$ -spacing.



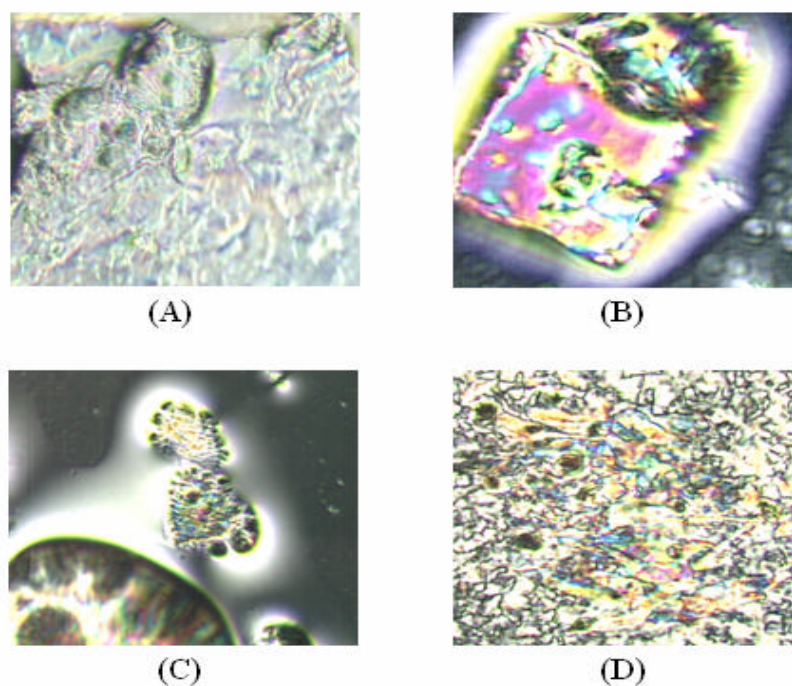


**Figure 3.10** Photographs of COC using polarizing lenses at temperatures of 17 °C (A), 25 °C (B), 37 °C (C) and after cooling to 25 °C (D) (200x)

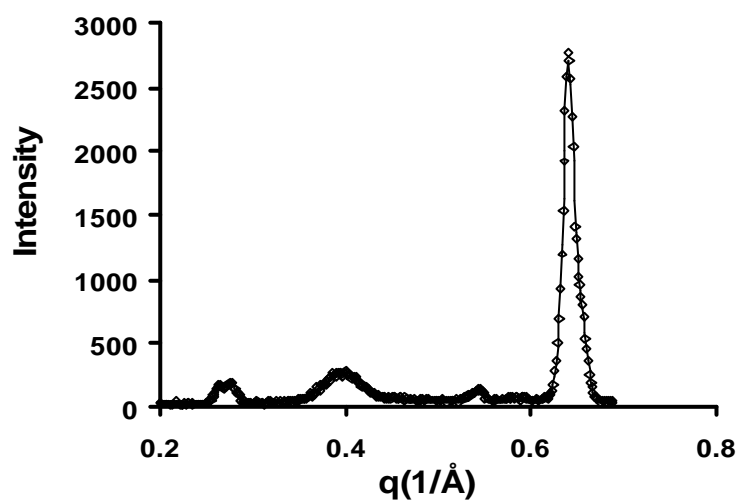


**Figure 3.11** A plot of the X-ray diffractometry intensity as a function of  $q$  ( $1/\text{\AA}$ ) obtained at 25 °C for SCC

In Figure 3.12 (A), the reflection at large angle is seen to be bimodal for SCC, near 9.6 and 9.8 Å. The low intensity diffraction peaks between 10.9 and 12.5 Å are given in Figure 3.12 (B) and appear relatively uniform among the carbonate esters. In Figure 3.12 (C), the reflections occurring between 20 and 25 Å are shown. In this case, SCC had profiles consisting of two broad reflections that were merged and were centered at 22.5 and 23.5 Å. All profiles were analyzed by fitting the data as summed Lorentzian peaks, the fitted Bragg reflections and full widths at half heights as well as the fitting error are given in Table 3.3.

In Figure 3.13 (A) and (B), the observed Bragg reflections for SCC obtained as a function of temperature are shown. For the reflections at low spacing (Figure 3.13 (A)), the bimodal profile at 25 °C is given as described above. As the temperature was measured at 60 °C, there was a loss in intensity as reflected in a reduction of FWHM value. The profile obtained at 102 °C was notably shifted to larger spacing such that the peaks occurred at 9.7 and 10 Å. With a further increase in temperature to 110 °C, the peaks were broadened, and finally at 150 °C there was almost a complete loss of the reflections. In Figure 3.13 (B), the reflections occurring between 20 and 25 Å are shown. A similar broadening occurred with increasing temperature, but the shift occurring at 102 °C was to a shorter spacing.

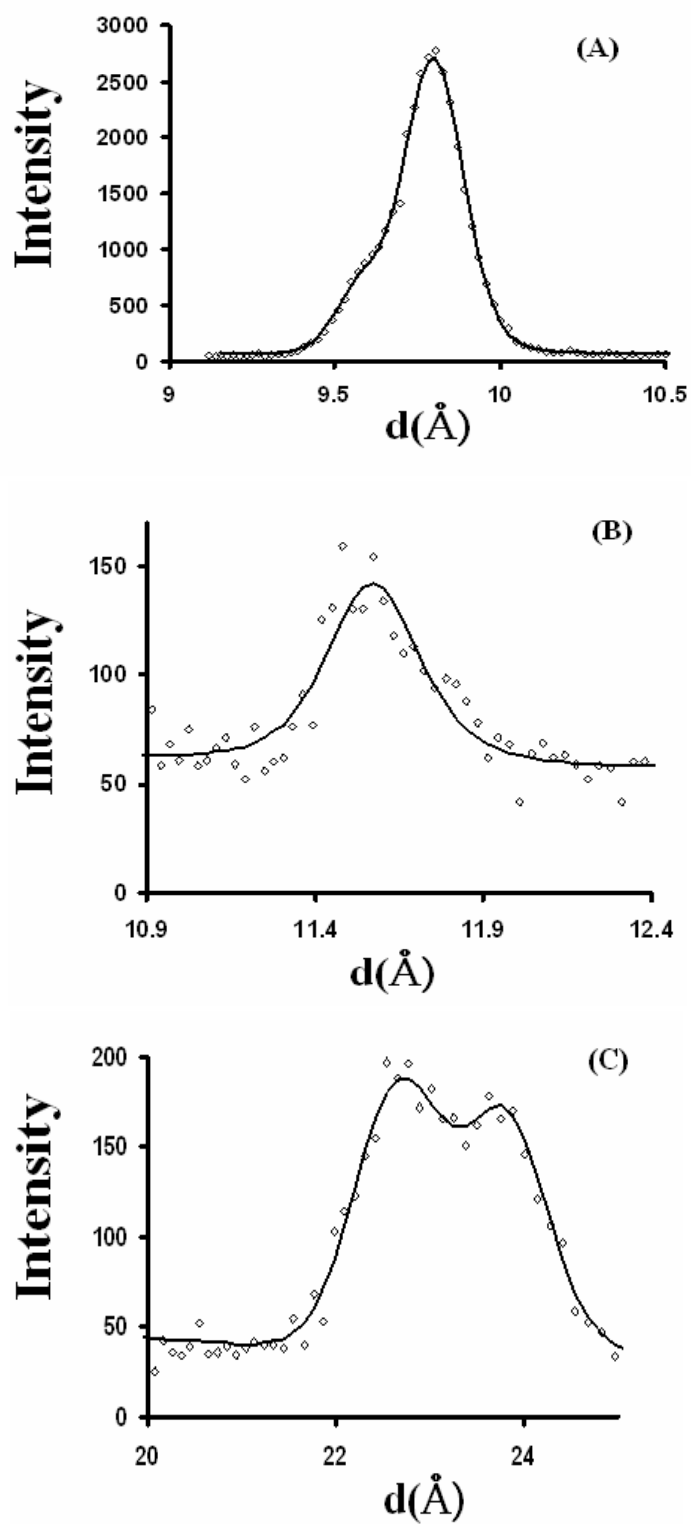


**Figure 3.12** A plot of the X-ray diffractometry intensity as a function of  $d$  (Å) obtained at 25 °C for SCC

**Table 3.3** Spacing of X-ray diffraction peaks (SE of fit) and associated full widths at half maximum (FWHM) of SCC, CM and COC obtained at the indicated temperatures.

Compounds	SCC		CM			COC	
	Temperature(°C)		Temperature(°C)			Temperature(°C)	
Spacing	25	25	76	82	17	25	32
d(Å)	9.68 (0.01)	9.31 (0.03)	9.37 (0.04)				
FWHM	0.27 (0.01)	0.28 (0.03)	0.30 (0.04)				
d(Å)	10.69 (0.05)	10.32 (0.06)	10.37 (0.08)			13 (0.06)	13.05 (0.1)
FWHM	0.16 (0.05)	0.27 (0.04)	0.25 (0.06)			0.24 (0.03)	0.35 (0.07)
d(Å)	11.63 (0.02)					18.93 (0.02)	18.8 (0.09)
FWHM	0.26 (0.02)					0.16 (0.01)	0.3 (0.03)
d(Å)	22.97 (0.24)	25.62 (0.10)	25.69 (0.10)				
FWHM	0.21 (0.07)	0.26 (0.01)	0.25 (0.01)				
d(Å)	23.06 (0.32)						
FWHM	0.35 (0.14)						
d(Å)			33.34 (0.32)	30.62 (0.86)	38.33 (0.28)	32.50 (0.01)	30.44 (0.83)
FWHM			0.26 (0.02)	0.88 (0.07)	0.26 (0.01)	0.95 (0.14)	1.53 (0.08)
d(Å)		51.01 (0.68)	51.09 (0.64)				
FWHM		0.27 (0.02)	0.25 (0.02)				

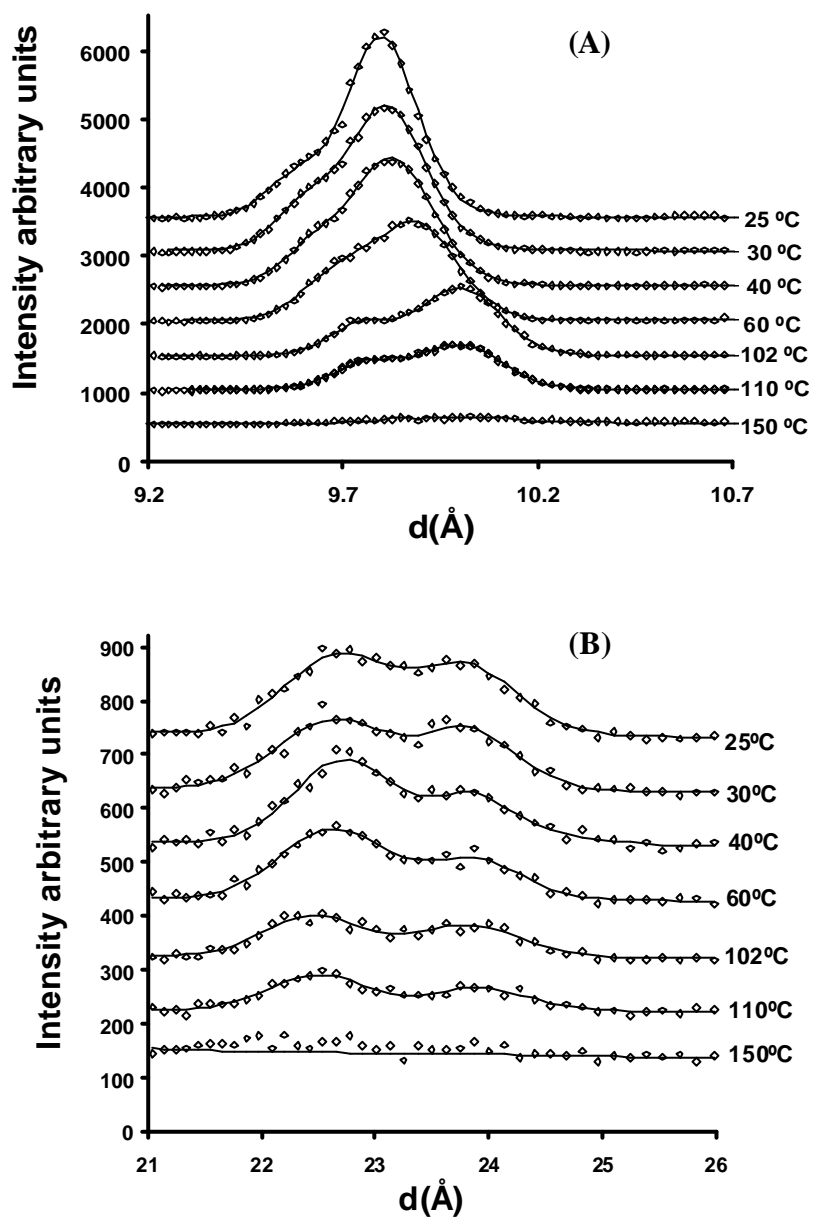


**Figure 3.13** A plot of the X-ray diffractometry intensity as a function of  $d$  (Å) for SCC at indicated temperatures: observed at  $d$ -spacings 9.2-10.7 Å (A) and 21-26 Å (B), experimental ( $\diamond$ ), and Lorentzian function fitting (—)

In Figure 3.14, the X-ray diffraction profiles for CM at 25 and 76 °C are given. At 25 °C, three main reflections were observed, and the fitted data are given in

Table 3.3. One is a bimodal peak with individual reflections at 9.31 and 10.32 Å, the second is at 25.62 Å and the third is at 51.1 Å. At 76 °C, an additional reflection was observed at 33.34 Å. For COC, the diffraction profile is given in Figure 3.15, and the corresponding fitted parameters are also given in Table 3.3. At 17 °C, only two narrow spacing reflections were observed at 13 and 18.8 Å. With an increase in temperature to 25 °C, a relatively broad peak emerged with a spacing of 38 Å.

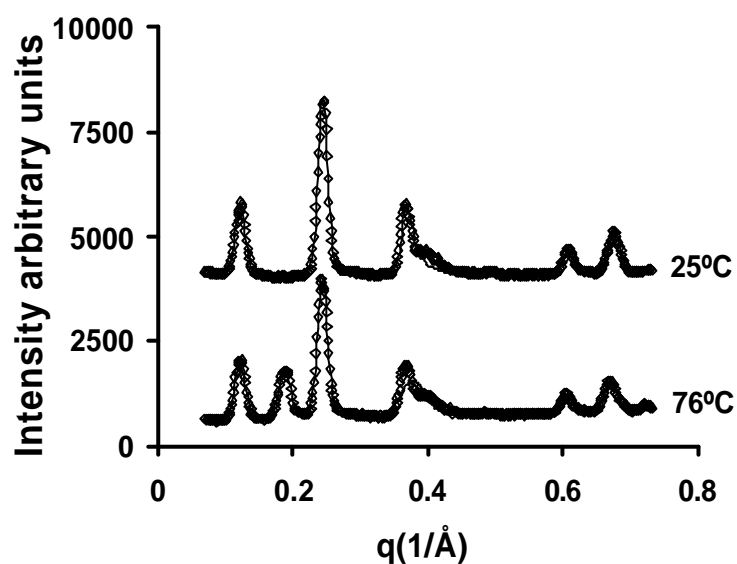


**Figure 3.14** A plot of the X-ray diffraction intensity as a function of  $q(1/\text{\AA})$  for CM at the indicated temperature: experimental ( $\diamond$ ), and Lorentzian function fitting (—)

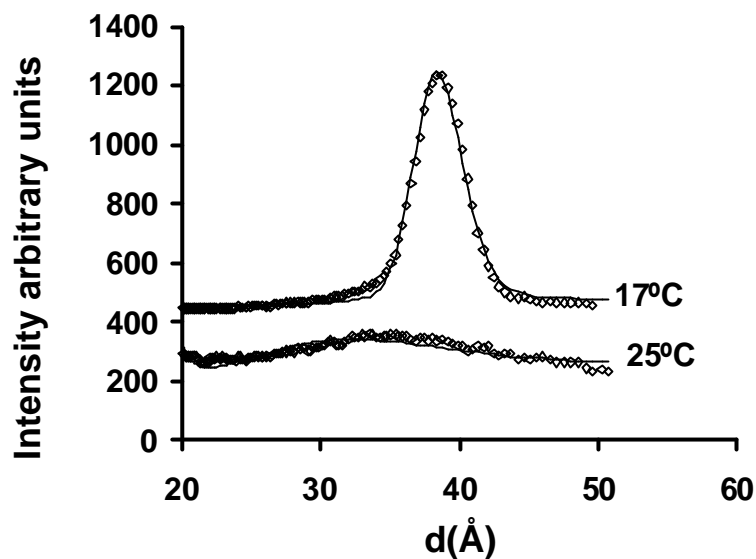


**Figure 3.15** A plot of the x-ray diffractometry intensity as a function of  $d$  (Å) for COC at the indicated temperatures: experimental ( $\diamond$ ), and Lorentzian function fitting (—)

While CCEs have many desirable properties in terms of providing chemical stability and a hydrophobic environment for solubilizing water insoluble drugs, there do not appear to be any systematic studies of their properties. In contrast, there are many studies and excellent reviews for CEs (cf. Ginsberg *et al.*), which differ from CCEs by having one less oxygen. As such, it was expected that the properties of these two series of compounds may also coincide. This was further suggested by the early X-ray diffraction work with cholesterol hexyl carbonate (CHC) that indicated that the crystalline state could be interpreted based on the crystal structure studies with CE's (Suh *et al.*, 1988). However, as shown in this work, the sodium salt of CCE exhibits liquid crystalline behavior over a wide temperature range and under anhydrous conditions.

CCE, with special emphasis on SCC was studied. For chemical properties, changing the linkage from ester to carbonate ester affected the chemical shifts in NMR. The most notable changes were the carbonyl resonance. The carbonate carbonyl resonance is 155.5 ppm, which was shifted about 20 ppm upfield from the ester carbonyl (Croll *et al.*, 1987). These results indicated the inductive effect of 2 oxygen atoms flanking carbonyl group. In addition, from FTIR spectrum of the carbonyl group in the sodium salt of cholesteryl carbonate molecule is located at 1705  $\text{cm}^{-1}$ , which is lower than other carbonate esters by 31-38  $\text{cm}^{-1}$ . This may be a result of the proximity of the carbonyl carboxylate group, which is normally lower than typical CCE by 30-50  $\text{cm}^{-1}$ .

This study contrasts the phase behavior of cholesteryl ester derivatives. In this case, the change to organic alkyl chain decreases the phase transition, especially with the introduction of an unsaturated chain as in COC. In comparison to the cholesteryl ring (DCC) and SCC, all phase transitions occur well above body temperature. While the transition at 102 °C observed with the SCC had a low enthalpy characteristic of liquid crystalline transition, it appears to be a solid-liquid crystal transition. A number of factors and experiments were examined to rule out the existence of a hydrate. First, the transition had a relatively low enthalpy, which is not characteristic of hydrate formation. In addition, the compounds were subjected to drying under high vacuum and in the presence of phosphorus pentoxide. This treatment had no effect on the thermal behavior. The addition of excess water to the carbonate ester resulted in thermal behavior consisting of broad endotherms, which were more characteristic of the presence of adsorbed moisture than the formation of distinct phase. Finally, the temperature dependence of the X-ray diffraction pattern of SCC indicate



there is only a minor rearrangement of the packing, since the 9.6 and 9.8 Å were shifted to longer spacing, but the 22-24 Å reflections were shifted to slightly more narrow spacing.

SCC undergoes a liquid crystal to isotropic liquid transition at temperatures between 142 and 144 °C. Previous work has shown that CHC forms a monoclinic crystal that corresponds to the type II monolayer packing described for the cholesterol esters, octanoate and oleate (Suh *et al.*, 1988). The structure of CHC forms a  $P2_1$  space group and a unit cell with  $a=12.728(2)$ ,  $b=9.184(1)$  and  $c=13.991(2)$  Å and  $\beta=92.93^\circ$  (1). The cholesterol and carbonate groups were found to have typical bond lengths and valence angles, but the hexyl group had a high thermal vibration causing shortened bond lengths. The C17 cholesterol side chain was found to be almost fully extended. Cholesterol esters can also exist in the monolayer type I (*MLI*) (nonanoate, decanoate, laurate, palmitoleate, and nervonate) and a bilayer (*BL*) arrangement (CM) (Ginsburg, 1984). It is noteworthy that with the cholesterol ester, the enthalpy of transition and  $d_{001}$  spacing were correlated with chain length. Specifically, the change in enthalpy increased with increasing chain length within predictable ranges of 5-12 kcal/mole for the melting of *MLI* and monolayer type II (*MLII*), but 10-30 kcal/mole for esters with a *BL* structure. The  $d_{001}$  spacing ranged from 13.5 to 16 Å (*MLII*), 28-36 Å (*MLI*) and 50-64 Å (*BL*) for the CEs.

The enthalpy changes for the SCC was about 4.5 kcal/mol, which would be consistent with either a *MLI* or *MLII* crystalline structure (Ginsburg, 1984). This value is not greatly different from some of the short chain esters or carbonate esters, indicating that ring-ring interactions may affect significantly in this case. The longest  $d$ -spacing observed for SCC was less than 24 Å. This is intermediate between the *MLI* and

*MLII* structures. The carbonate-oxygen bond should extend the length of the cholesterol group by 1.1 Å assuming normal bond lengths (1.33 Å) and valence angle (O-C-O, 110 °) in comparison to an ester linkage (Suh *et al.*, 1988). This would be insufficient to extend the spacing to the *MLII* range of 13.5-16 Å. On the other hand, the background peak may obscure a broad *d*-spacing in the 13-16 Å range, although the intensities and peak position of the background was high reproducible among the samples. The change in the relatively complex and overlapping peaks observed with SCC as a function of temperature may indicate disorder and subtle changes in the packing. SAXD of CPC will be further studied in chapter 4. DCC was not carried out with SAXD due to its high transition temperature (170-175 °C). Also, such high temperature may cause AmB degradation.

### 3.4 Conclusions

In summary, the saturated CCEs form stable crystals over wide range of temperatures and water content. Moreover, the inherent high chemical stability of the covalent linkages of the carbonate esters coupled with the hydrophobic character provide a desirable feature for their use in drug delivery systems.

# CHAPTER 4

## INTERACTION OF AMPHOTERICIN B WITH CHOLESTERYL CARBONATE ESTERS

### 4.1 Introduction

Cholesteryl carbonates are structurally composed of three parts; steroid planar nucleus, various hydrocarbons chains and a carbonate linkage between the steroid ring and hydrocarbon chain. These molecules have the ability to form thermotropic liquid crystals. As such, there is an interest in developing cholesteryl carbonates for drug delivery to the lungs. However, few investigations of cholesterol carbonate analogues have been carried despite the plethora of studies for cholesteryl esters, which are molecules consisting of a cyclopentaphenanthrene ring linked via an ester bond at the C3-position to an aliphatic hydrocarbon. Many of physical properties of pure cholesteryl esters have been determined (Small, 1970; Ginsburg *et al.*, 1985; Small, 1986), and the phase behavior including a thermotropic mesophase has been identified (Ginsburg, 1984). Cholesteryl esters typically form nematic liquid crystals that are twisted into a helical arrangement forming a pseudo-layered structure.

The drug investigated in this study is amphotericin B (AmB), an antifungal agent that is the most potent and is the drug of choice in the treatment of serious fungal infections (Walsh and Pizzo, 1990). The major limitation to its use is toxicity, mainly nephrotoxicity. However, the toxicity can be reduced by incorporating AmB into various lipids (Metha *et al.*, 1984).

In this study, AmB was incorporated into three different cholesteryl carbonate esters, CPC, DCC and SCC as compared with cholesterol (the chemical structure of compounds are given in Figure 4.1). The interaction of AmB and cholesteryl carbonate ester was investigated by using various techniques.

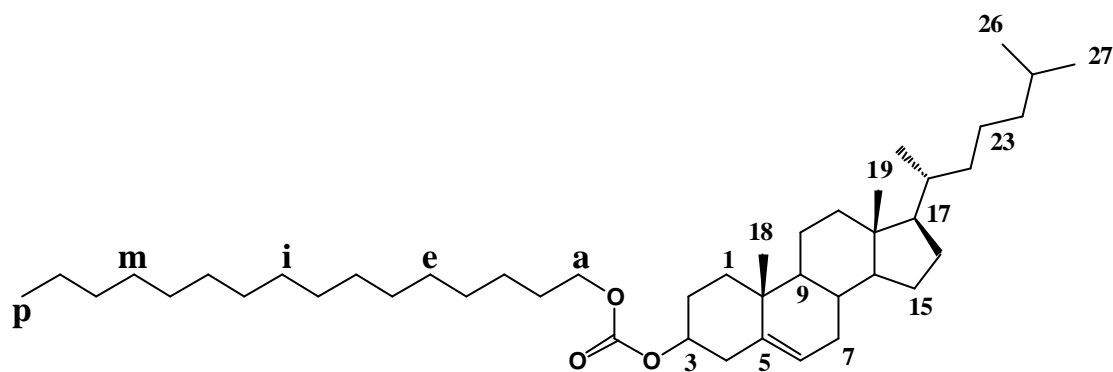
## **4.2 Materials and methods**

### **4.2.1 Materials**

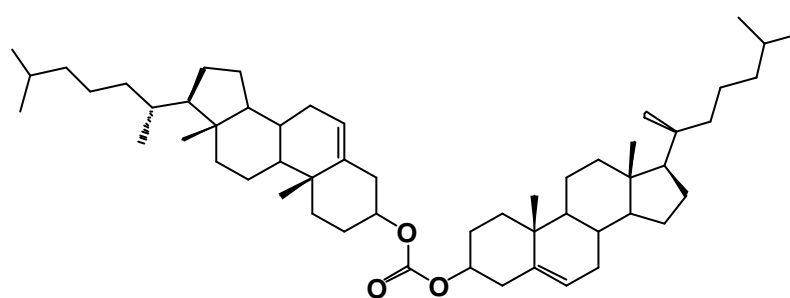
CPC, DCC and SCC were synthesized as described in section 3.2.1. The chemical structures of each compound along with cholesterol are shown in Figure 4.1. AmB was obtained from Ambalal Sarabhai Enterprises Ltd. (Vadodara, India). All other reagents and chemicals are analytical grade.

### **4.2.2 Sample preparation**

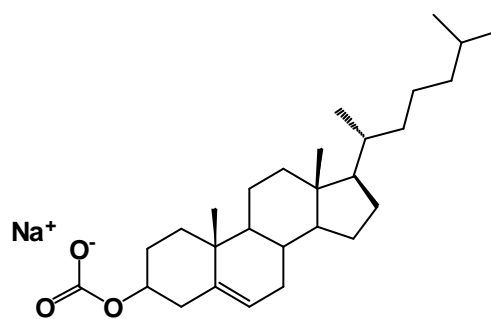
Samples were prepared by solvent evaporation. Briefly, a differently weighed amount of CPC, DCC or SCC was dissolved in 100 mL methanol-chloroform (1:1, v/v). Appropriate amount of AmB (0.27 mM) was slowly added into the liquid crystal solution to yield varying mole ratios (1:0, 1:1, 1:2, 1:3, 1:6, 1:12 and 0:1, mole ratios, respectively), and mixture was stirred for 20 h until a clear solution was obtained. The organic solvent was evaporated under vacuum (200 mbar) at 40-45 °C in rotary evaporator (Eyela, Tokyo Rikakikai Co., LTD., Japan). The resulting dry powder of AmB in cholesteryl carbonate was stored at 2-8 °C.



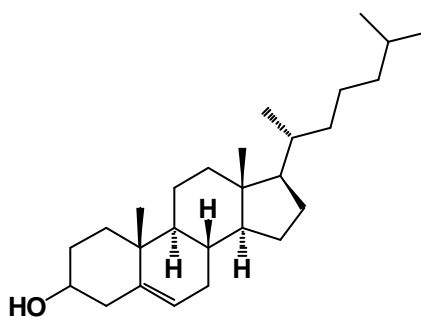
(A), MW=654



(B), MW=798



(C), MW=452



(D), MW=386

**Figure 4.1** Chemical structures of CPC (A), DCC (B), SCC (C) and cholesterol (D)

#### **4.2.3 Differential Scanning Calorimetry (DSC)**

A differential scanning calorimeter (DSC, Perkin-Elmer) was employed to determine the thermal properties of the liquid crystals. Approximately 4-5 mg samples were accurately weighed and placed into standard aluminum pans, which were hermetically sealed. An empty pan was used as a reference. The heating rate was 10°C/min from 25 to 200°C with a close pan system under the stream of N<sub>2</sub> gas flow, after which the system was cooled down at the same rate from 200 to 25°C. Transition temperatures were determined as the intersection of the extrapolated, tangential line of the most rapidly rising part of the peak with the horizontal baseline. The enthalpy change was simultaneously obtained as the integrated area under the curve. The entropy change was calculated from the change in enthalpy over the transition temperature (Martin *et al.*, 1993).

#### **4.2.4 Transmission Electron Microscopy (TEM)**

The dry powder was dispersed into distilled water with the aids of ultrasonication for 15 min. The sample was then dropped onto a 200 mesh copper grid. The dried sample was kept in a desiccator overnight before examination by TEM (JEOL JEM-2010, Japan).

#### **4.2.5 Polarized Light Microscope (PLM)**

An Olympus polarizing optical microscope (POM) was used to observe the morphology of crystalline shape and the birefringence during melting and recrystallization process of AmB-liquid crystal mixtures.

#### 4.2.6 Small Angle X-ray Diffractometry (SAXD)

Samples for the SAXD experiments were irradiated with copper Ka radiation (wavelength  $\lambda = 1.54 \text{ \AA}$ ) generated by a Rigaku Ultrex 18 kW generator with Osmic cross-coupled multi-layer parallel optics. Data were collected with a Bruker HI-STAR multiwire area detector and corrected for detector response.

#### 4.2.7 solid state Nuclear Magnetic Resonance Spectroscopy (ssNMR)

All NMR measurements were performed on an AVANCE 300 MHz digital NMR Spectrometer (Bruker Biopsin, DPX-300) (7.05 T, corresponding to 75 MHz for  $^{13}\text{C}$ ) equipped with a BL-7 magic angle spinning probe and a high power amplifier unit. Neat samples were placed in a 7-mm  $\text{ZrO}_2$  rotor (~400  $\mu\text{L}$  sample volume). Sample spinning rates were 5 kHz. The spectral parameter used as 1,600 number of scans (NS), relaxation delay of 4 s and spectral size 2 K with 4 K time domain size (adapted from Guo and Hamilton, 1993).

### 4.3 Results and discussions

#### 4.3.1 Differential Scanning Calorimetry Studies

DSC heating and cooling scans of pure CPC and AmB in CPC mixture are given in Figures 4.2 and 4.3. For pure CPC (curve *a*), a large endothermic transition was observed at 73.2 °C. The calorimetric enthalpy of the heating was 12.8 kcal/mole. While the three exotherms were obtained at 71.0, 52.5 and 37.1 °C with enthalpy changes of 0.3, 0.2 and 9.8 kcal/mole, respectively. The thermogram indicates that pure

CPC exhibited monotropic liquid crystalline behavior. The phase transition of the solid crystal to isotropic liquid was observed around 73.2 °C whereas a liquid crystal phase could be obtained only with cooling the isotropic liquid phase. The isotropic liquid to cholesteric phase transition was at 71.0 °C, cholesteric to smectic at 52.5 °C and smectic to crystal was 37.1 °C.

The addition of AmB into CPC in the range of 1:1 to 1:12 mole ratio did not appreciably affect endothermic phase transition temperature of CPC but a smaller enthalpy was observed. Despite correcting the enthalpy change for the mass of AmB (Figure 4.2 (A)), the experimental enthalpy of AmB in CPC mixture was less than theoretical enthalpy by about 1 kcal/mole. The second endothermic peak of AmB in CPC mixture was slightly shifted from 169.0 °C to 176.2 °C and was also narrower than pure AmB (Figure 4.2 (B)).

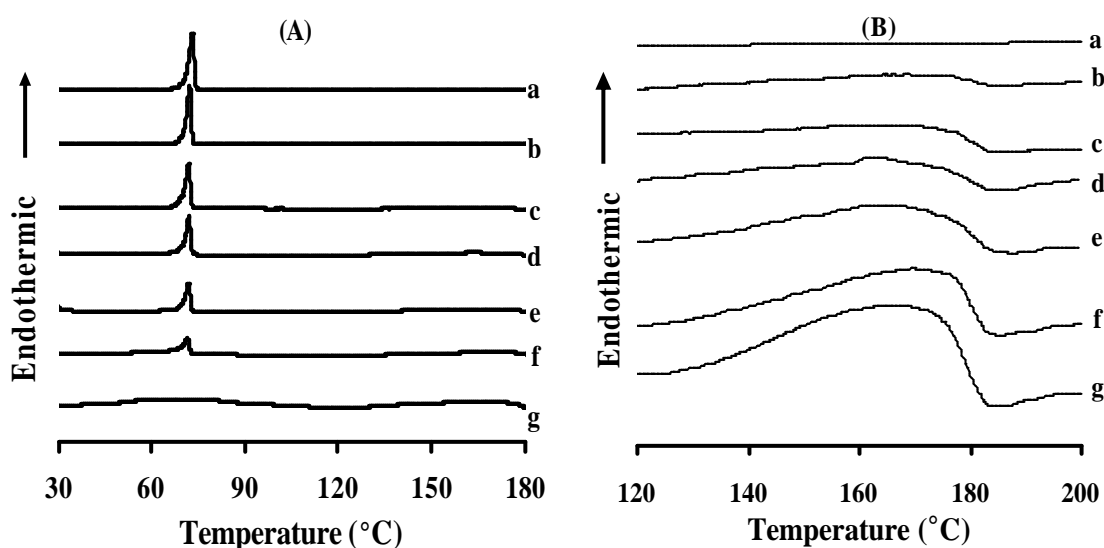


**Figure 4.2** (A) A plot of the excess heat capacity as a function of temperature (heating process) for AmB in CPC at mole ratios; 0:1 (a), 1:12 (b), 1:6 (c), 1:3 (d), 1:2 (e), 1:1 (f)



and 1:0 (g) and (B) is the expansion scale

Figure 4.3 (A), the smectic to crystal phase transition of AmB in CPC mixture on cooling process was slightly shifted to higher transition temperature when the amount of AmB increased. Whereas, the transition temperature of isotropic to cholesteric phase was shifted to lower temperature since the amount of AmB was increased. The addition of AmB into CPC may depress the isotropic-cholesteric phase transition of mixture (Figure 4.3 (B)).

Figures 4.4 and 4.5 illustrate the thermograms for pure DCC and a binary mixture of AmB and DCC. For pure DCC (Figure 4.4 (curve *a*)), two peaks at 169.5 and 175.2 °C were evident and were associated with the solid-smectic transition and smectic-isotropic liquid transitions, respectively. The endothermic enthalpy changes of pure DCC were 3.3 and 2.0 kcal/mole, respectively. On cooling (Figure 4.5 (B)), a broad exothermic peak (curve *a*) was observed around 153-155 °C, which had a total enthalpy change of 5.9 kcal/mole.

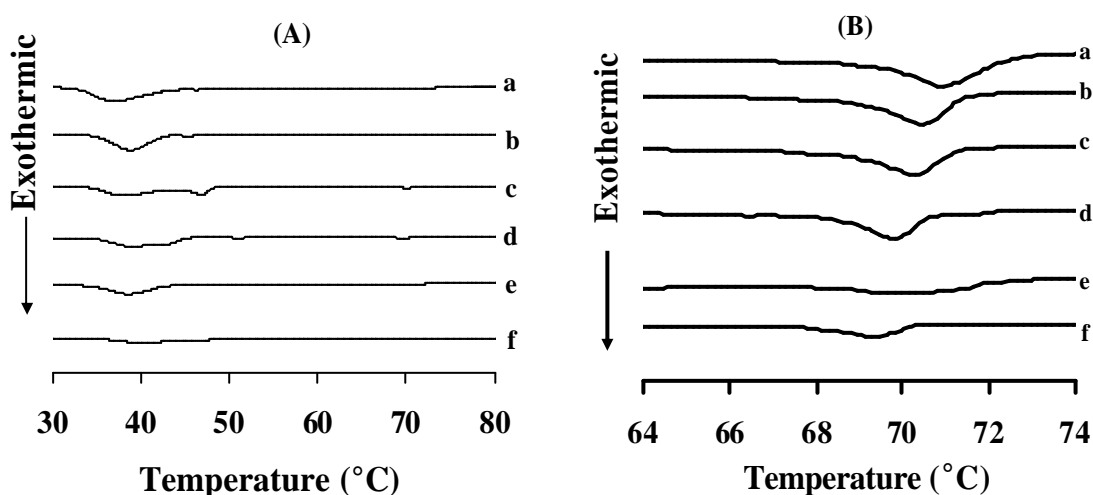


**Figure 4.3** (A) A plot of the excess heat capacity as a function of temperature (cooling process) for AmB in CPC at mole ratios; 0:1 (a), 1:12 (b), 1:6 (c), 1:3 (d), 1:2 (e)

and 1:1 (f) and (B) is the expansion scale

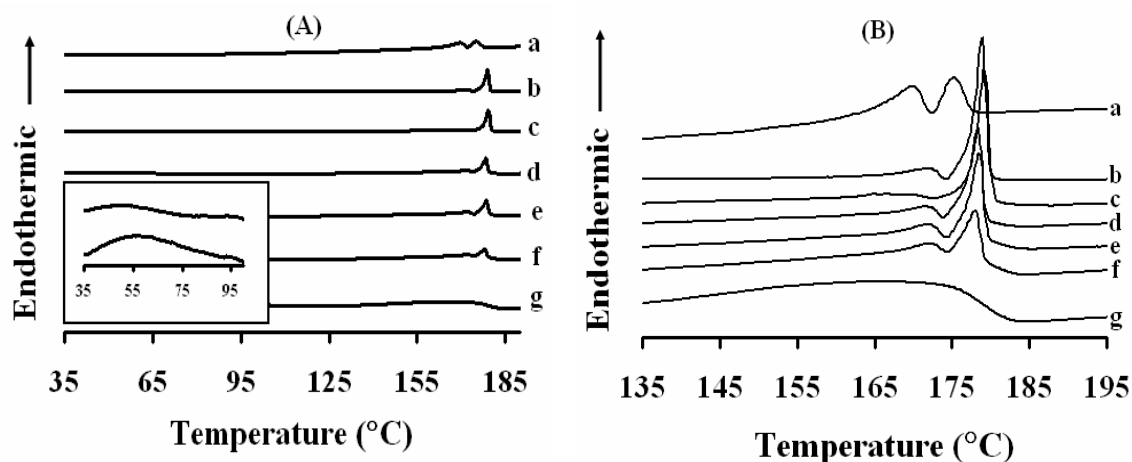


**Figure 4.4** (A) A plot of the excess heat capacity as a function of temperature (heating process) for AmB in DCC at mole ratios; 0:1 (a), 1:12 (b), 1:6 (c), 1:3 (d), 1:2 (e), 1:1 (f) and 1:0 (g) and (B) is the expansion scale

With incorporation of AmB into DCC (Figure 4.4), the first peak transition was broadened but did not disappear and was slightly shifted to a higher temperature (from 169.5 to 172.2 °C, except 1:6 mole ratio,) while the second endothermic was also shifted to a higher temperature (~4 °C, from 175.2 to 179.2 °C). In case of AmB in DCC at 1:6 mole ratio, (Figure 4.4 (B) curve *c*) a solid-liquid crystal phase transition could be observed at the lowest temperature about 166.5 °C. This result strongly suggests that there may be complex formation of AmB with DCC. The total enthalpy of the endothermic peak slightly increased (from 5.3 to 7.2 kcal/mole) when the amount of DCC was decreased from 100 to 60% in the mixture. However, when the content of DCC was decreased to less than 50%, the total enthalpy of AmB-DCC mixture was dramatically increased. In another word, the addition of AmB into DCC from 1:12 (10% AmB) to 1:3 (30% AmB) mole ratios may slightly affected phase

transition and lattice orientation of AmB-DCC mixture. When the AmB was at 40% (1:2 mole ratio) or higher (1:1 mole ratio), the lowest phase transition temperature increased with the content of AmB. Perhaps some free AmB may not interact with DCC.

In the case of pure AmB, two endothermic peaks were observed at 69.2 and 169.0 °C, and the associated with enthalpy changes were 34.8 and 28.9 kcal/mole, respectively. The first endotherm of AmB was shifted to a lower temperature (56.7 and 53.6 °C for mole ratios of 1:1 and 1:2) and the endotherm was no longer visible at mole ratios of AmB in DCC  $\geq$  1:3 (Figure 4.4 (A) inset curve). On the other hand, the endothermic peaks at 169.0 °C were shifted to higher temperature (from 169.0 to 179.2 °C); however, the mixture of AmB-DCC exhibited a higher second transition temperature than pure AmB and pure DCC.

Exothermic transitions of AmB in DCC mixture are shown in Figure 4.5. The phase transition of the binary mixture was shifted to a higher temperature (from 153.8 to 162.5 °C). With an increase in the amount of AmB, the transition temperature tended to increase. However, in the case of lower content of DCC in AmB-DCC mixture, the transition was slightly shifted to lower transition temperature and a broad should become evident. The changes in the thermodynamic properties are consistent with AmB interacting specifically with DCC resulting in changes in the molecular orientation or crystallinity (Lin *et al.*, 2000; Kuntsche *et al.*, 2004).

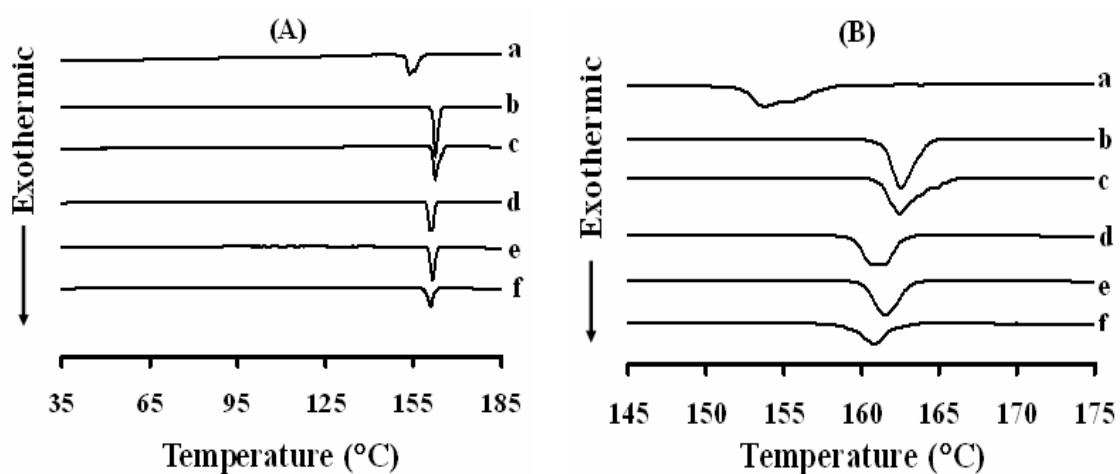


**Figure 4.5** (A) A plot of the excess heat capacity as a function of temperature (cooling process) for AmB in DCC at mole ratios; 0:1 (a), 1:12 (b), 1:6 (c), 1:3 (d), 1:2 (e) and 1:1 (f) and (B) is the expansion scale

In Figures 4.6 and 4.7, the thermotropic transitions of pure SCC and binary mixtures of AmB and SCC are given. The pre-transition endothermic peak which is observed near 102 °C is not visible but is likely related to the sample preparation method of solvent evaporation, which leaves the sample in a metastable state. However, a small shoulder can still be observed at 98.0 °C. The lower temperature and apparent lower enthalpy change are consistent with molecular re-orientation and/or a higher energetic state. The endothermic peak was observed at 142.8 °C and the associated enthalpy change was 4.2 kcal/mole, and the peak of exothermic was exhibited at 108.9 °C. The calorimetric enthalpy value was 4.45 kcal/mole.

For the binary mixture of AmB and SCC, three endotherms were observed as follows: the first peak was shifted to a lower temperature (~54.8 °C), and the second peak was slightly shifted to higher temperature (~143.5 °C) as was the third peak (~175.0 °C). The disappearance of 175.0 °C peak for AmB in SCC at 1:12 mole

ratio indicates that AmB was completely incorporated into SCC at a 1:12 mole ratio. AmB was either in a solid solution or amorphous form in SCC. However, the total calorimetric enthalpies were increased as the amount of AmB was increased sequentially (4.2, 7.2, 12.7, 18.6, 23.2, 26.4 and 63.7 kcal/mole for pure SCC, AmB in SCC at 1:12, 1:6, 1:3, 1:2, 1:1, mole ratio and pure AmB, respectively).

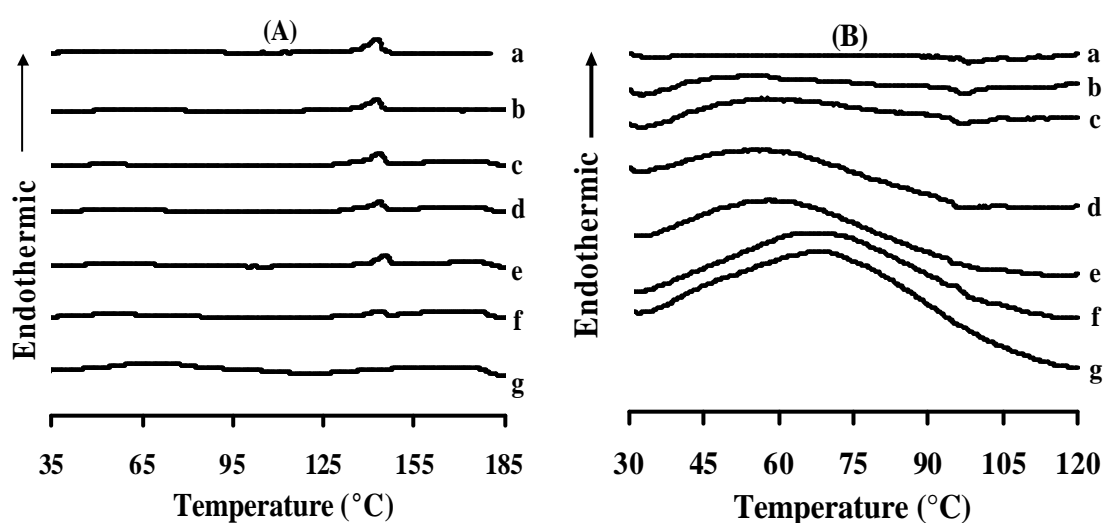


**Figure 4.6** (A) A plot of the excess heat capacity as a function of temperature (heating process) for AmB in SCC at mole ratios of 0:1 (a), 1:12 (b), 1:6 (c), 1:3 (d), 1:2 (e), 1:1 (f) and 1:0 (g) and (B) is the expansion scale

The thermogram of AmB-SCC is shown Figure 4.7. The exothermic peak of AmB in the SCC mixture is decreased, broadened and shifted to a lower temperature (from 107.3-99.8 °C). In addition, a small exothermic peak was obtained at 110 °C, which also had a smaller enthalpy change  $\sim 0.20$  kcal/mole. The altered phase behavior of AmB-SCC indicates minimal AmB-SCC interaction.

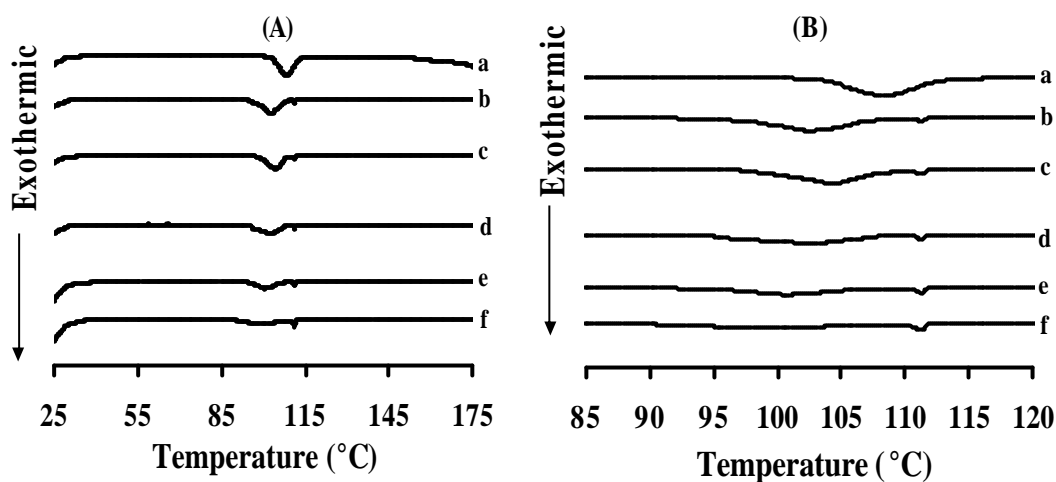


**Figure 4.7** (A) A plot of the excess heat capacity as a function of temperature (cooling process) for AmB in SCC at mole ratios of 0:1 (a), 1:12 (b), 1:6 (c), 1:3 (d), 1:2 (e) and 1:1 (f) and (B) is the expanded scale

Overall, the DSC can be a useful tool in studying drug-excipient interaction based on the shift of the phase transition temperature (Ali *et al.*, 2000; Kuntsche *et al.*, 2004; Hsueh *et al.*, 2005).

#### 4.3.2 Transmission Electron Micrographs

TEMs of pure DCC and AmB in DCC are shown in Figure 4.8, where at least three different structures can be distinguished. For pure DCC, only spherical particles were observed. Whereas with addition of AmB into DCC, cylindrical and hexagonal shapes were also evident; however, as more AmB was loaded into DCC, irregular shaped particles appeared. This may be due to the incomplete incorporation of AmB into DCC crystal lattice, which resulted in particles of pure AmB appearing. AmB loaded in CPC or SCC could not be observed under TEM, due to low transition

temperature of CPC and SCC. Specifically, pure CPC, pure SCC, and AmB loaded into CPC or SCC were instantly melted during the TEM operation. If these experiments are to be pursued in the future, cryo-TEM will be necessary to visualize these samples.

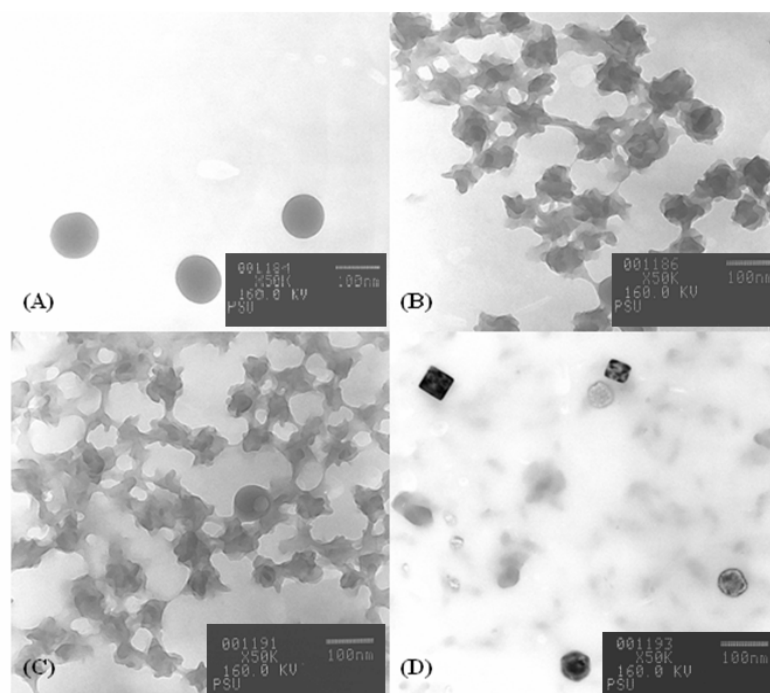


**Figure 4.8** TEM micrographs of AmB in DCC with different mole ratios; pure DCC (A), 1:3 (B), 1:6 (C) and 1:12 (D) (bars = 100 nm)

### 4.3.3 Polarized Light Microscopic Studies

Polarized light micrographs of pure CPC, DCC, SCC, AmB loaded in CPC, DCC and SCC are shown in Figure 4.9. All compounds exhibited colorful birefringence both as pure liquid crystals and as liquid crystals mixtures. The optical textures for these liquid crystals and AmB loaded in liquid crystals, which appear as focal conic domains remain essentially unchanged after isotropic liquid cooled down to

the room temperature. The results indicate that incorporation of AmB into liquid crystals (CPC, DCC and SCC) by solvent evaporation did not cause a change in the optical textures of these compounds, despite the shift in the phase transition temperatures.

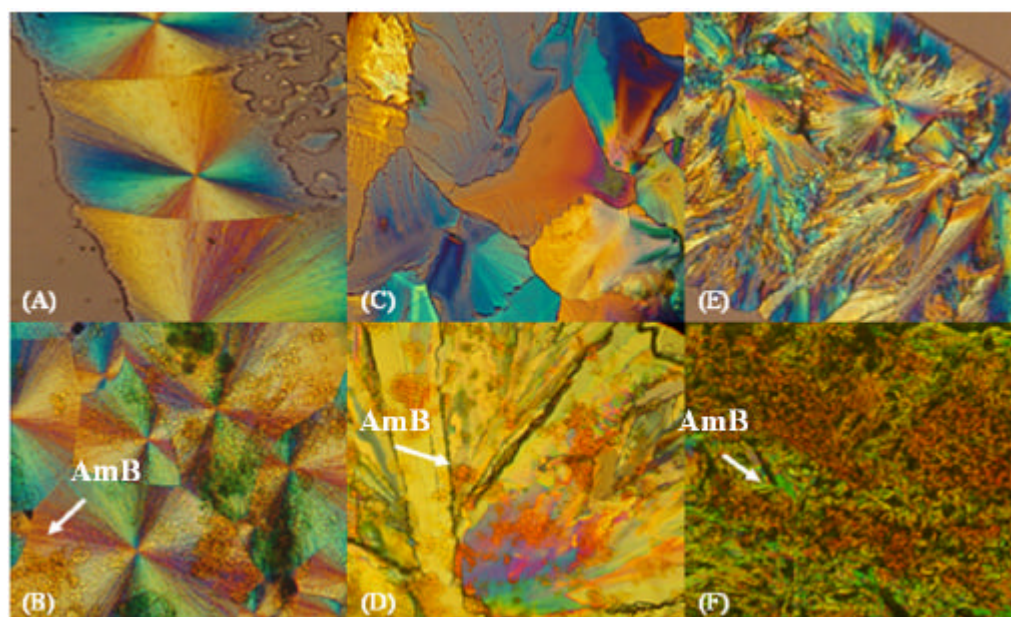


**Figure 4.9** PLM micrographs of pure CPC (A), AmB in CPC, 1:3 mole ratio (B), pure DCC (C), AmB in DCC, 1:3 mole ratio (D), pure SCC (E) and AmB in SCC, 1:3 mole ratio (F) (observed at 25 °C after cooling down from molten state, x 400)

#### 4.3.4 State diagram analysis



The state diagrams of AmB–CPC during heating process are shown in Figure 4.10 (A), at temperature less than 73 °C, solid crystals can be observed for the whole concentration range of CPC. While isotropic liquid and solid phases were obtained between 73 and 175 °C when content of AmB was 40% or higher in the mixture.

On the other hand, liquid crystal phases occurred with decreasing temperature. When the concentration of CPC in AmB-CPC mixture is lower than 80%, two domains are clearly observed under an optical microscope even though a partial isotropic liquid state remained. As the temperature decreased, two domains co-existed (isotropic liquid and solid states) over 70 °C, while others exhibited cholesteric-solid phase between 52-70 °C, smectic-solid phase below 52 °C and subsequently complete crystallization below 40 °C as shown in Figure 4.10 (B). These results indicate that the two domains corresponding to a CPC/AmB-rich phase containing less than 80% of CPC and a CPC-single phase. The binary mixture of AmB and CPC is partially miscible over all weight ratios in this study depend upon the observed temperature. However, homogeneous isotropic liquid and homogeneous liquid crystal (cholesteric and smectic) were observed when concentration of CPC is 80% or higher and temperature was higher than 45 °C. After cooling down to temperature less than 45 °C, the exothermic peaks were detected for smectic and solid phases. The result suggests that crystallization of CPC occurs in the mixture.

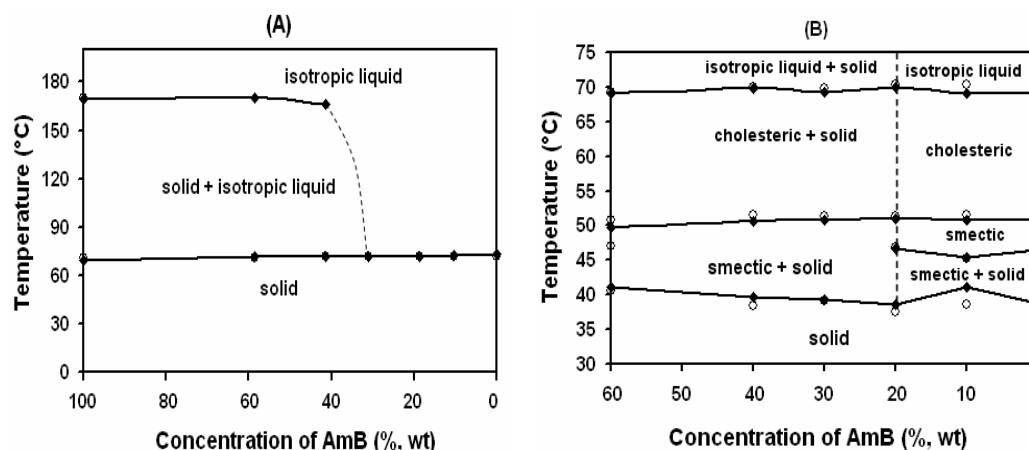


**Figure 4.10** State diagram of binary mixture of AmB in CPC (1:0, 1:1, 1:2, 1:3, 1:6, 1:12 and 0:1, mole ratio) during heating up process (A) and during cooling down process (B); (♦) 1<sup>st</sup> run and (o) 2<sup>nd</sup> run

The state diagram for the binary mixture of AmB and DCC is depicted in Figure 4.11. As can be seen, the solid-smectic phase transition continuously decreased from 60 to 42 °C at all concentrations of DCC. The coexisting phases (smectic + solid crystal) remained as the temperature increase from 169 °C up to 172 °C with concentration of DCC less than 80%, but transition temperature was depressed to 167 °C for concentration of DCC ~80% and was 175 °C for pure DCC. The diagram for the homogeneous liquid crystal and homogeneous isotropic liquid is shown in Figure 4.11 (A). As the concentration of DCC increase, the isotropic liquid transition temperature was increased from 170 °C to 178 °C. It was found that phase separation of binary mixture AmB and DCC occurred at temperatures higher than 65 °C but lower than 167 °C. This is probably due to incorporation of AmB into DCC, which was responsible for increasing the transition temperature of DCC. Upon cooling, isotropic liquid phase was

obtained at temperature over 150 °C for pure DCC, while two phases of smectic and solid crystal were observed from 154-160 °C, transition phase temperature increased when the concentration of AmB in AmB-DCC mixture increased (Figure 4.11 (B)). Solid crystal phase was observed during cooling process at temperature lower than 154 °C for pure DCC and slightly shifted to higher temperature when increased content of AmB in binary mixture.

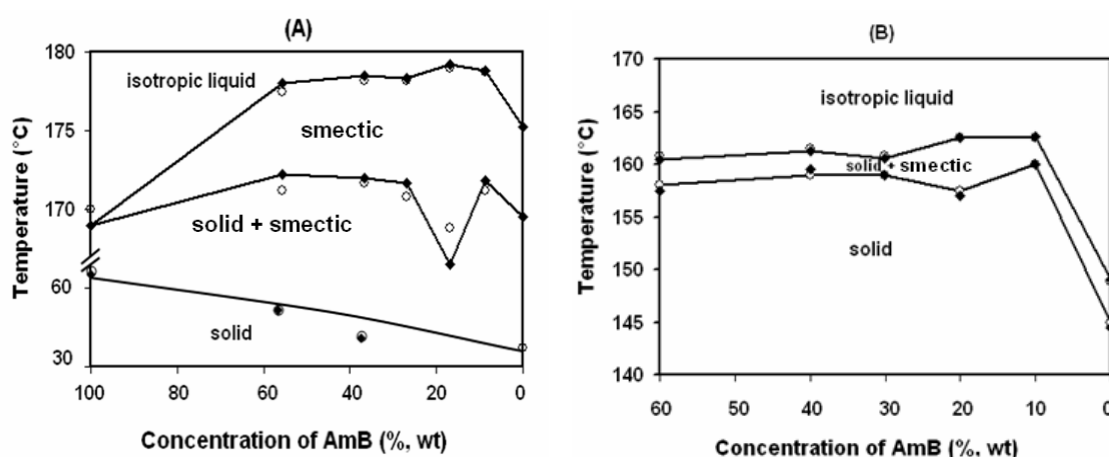


**Figure 4.11** State diagram of binary mixture of AmB in DCC (1:0, 1:1, 1:2, 1:3, 1:6, 1:12 and 0:1, mole ratio) during heating up process (A) and during cooling down process; (♦) 1<sup>st</sup> run and (o) 2<sup>nd</sup> run

Figure 4.12 shows the state diagram of binary mixtures of AmB and SCC. On heating, solid crystalline phase was obtained at temperature less than 75 °C for content of AmB greater than 20% and the transition temperatures of solid to two phases of smectic and solid are rising up to 100 °C when SCC content increased higher than 80%. The coexisting phases of solid and smectic were observed. The transition from solid crystal to smectic + solid crystal was significantly increased as

can be seen in Figure 4.12 (A). However, those transition temperatures are lower than that SCC content which higher than 80%. When the concentration of AmB was increased from 40 to 70%, the isotropic liquid and solid crystal phases were obtained at temperatures higher than 145 °C. This result suggests that the addition of AmB into SCC increases the phase transition temperature of the mixture, and thus the mixture remains as solid state until 70 °C. After cooling down, the smectic + solid crystal phases was obtained when temperature was lower than 109 °C for pure SCC whereas phase transition was slightly shifted to higher temperature when increased AmB concentration in AmB-SCC mixture (Figure 4.12 (B)). Furthermore, the two domains of solid crystal of AmB and SCC occurred at temperatures lower than 100 °C.

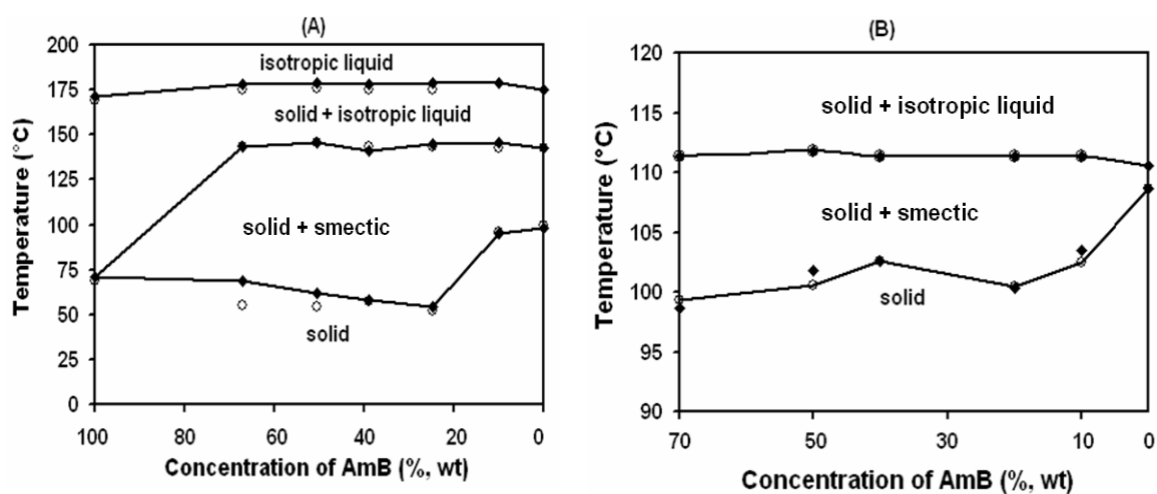


**Figure 4.12** State diagram of binary mixture AmB in SCC (1:0, 1:1, 1:2, 1:3, 1:6, 1:12 and 0:1, mole ratio) during heating up process (A) and during cooling down process (B); (◆) 1<sup>st</sup> run and (○) 2<sup>nd</sup> run

### 4.3.5 Small Angle X-ray Diffraction Patterns

From DSC and microscopy techniques, the phase transition temperature of pure liquid crystal and binary mixture of AmB and liquid crystal were obtained. The results suggest that pure CPC and the binary mixture of AmB and CPC had the lowest phase transition temperature, which were suitable to investigate by using SAXD and ssNMR techniques.

The X-ray diffraction pattern of pure CPC is shown in Figure 4.13. From Bragg's equation (equation 2.2, chapter 2), the interlayer spacing ( $d$ ) is inversely proportional to the angle of reflection ( $\theta$ ). At 25 °C (Figure 4.13 (A)), two broad peaks were observed ( $2\theta$ ) at 1.5 and 3.0° which corresponds to a  $d$ -spacing of 58.74 and 29.25 Å, respectively. The results show that pure CPC exhibited lattice spacing typical of a crystal at the room temperature. With the crystal to isotropic liquid phase transition at 75 °C, the structural of pure CPC disordered as can be seen with broadened and diffused diffraction in Figure 4.13 (B). After cooling down the isotropic phase transition to 65 °C, broad peaks were obtained with  $d$ -spacings of 58.93, 54.02, 29.00 and 27.72 Å (Figure 4.14 (A)). The results suggest that the structural order of pure CPC is largely recovered.

The changes of  $d$ -spacing value and diffraction pattern reflect the transition phase behavior of thermotropic liquid crystals (Duarte *et al.*, 2002). In the case of pure CPC, the cholesteric phase was obtained at 65 °C, which is characterized by a very broad bimodal peak with weak X-ray diffraction intensity. Figure 4.14 (B), at ~45 °C, the X-ray diffraction of a smectic phase exhibited greater intensity than that of cholesteric phase. The  $d$ -spacings were 58.63, 53.86, 28.95 and 27.65 Å, which

represents smaller spacings. Therefore, the smectic phase of CPC molecules maintains orientational order. In smectic phases, the motions are restricted within the planes and the separated planes. In addition, at this temperature, the structural order of pure CPC was investigated after cooling from isotropic temperature to RT. The smallest  $d$ -spacings were observed about of 57.61, 53.54, 28.91 and 27.61 Å. These values were decreased from those observed at RT with a broader peak. The results indicate that the molecules of CPC were not completely re-crystallized. This may be due to the rearrangement of crystal molecules for pure CPC were slow.

The SAXD patterns are in agreement with those results obtained from state diagram analysis. Short  $d$ -spacing obtained from SAXD diffraction correlated with ordered and restricted molecules at temperature less than 40 °C during cooling process. The longer  $d$ -spacing could also obtain in liquid crystal phase and isotropic liquid phase which molecules were disordered at temperature higher than 42 and 70 °C, respectively.

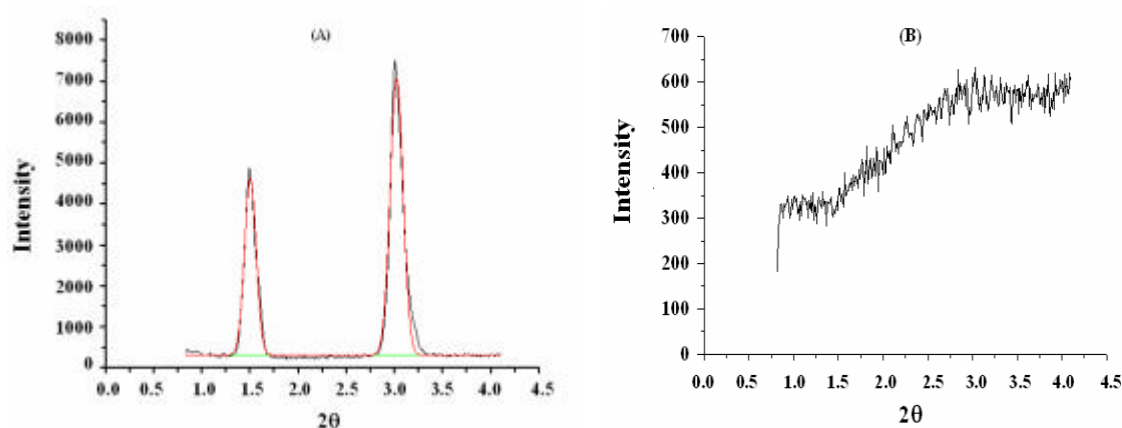


**Figure 4.13** A plot of the X-ray diffractometry intensity as a function of  $2\theta$  for pure CPC; at 25 °C (A) and 75 °C (B): experimental (—) and Lorentzian function fitting (---)

The mixture of AmB in CPC (1:3, mole ratio) was investigated as a function of temperature. At 25 °C, two main peaks centered at  $2\theta$  of 1.5 and 3.1° were

observed that correspond to  $d$ -spacing values of 58.69 and 29.14 Å (Figure 4.15 (A)). With heating the sample to 75 °C, only a diffuse peak was seen (Figure 4.15 (B)). The results indicate that the ordered structure of binary mixture of AmB and CPC (1:3, mole ratio) was destroyed upon reaching 75 °C.

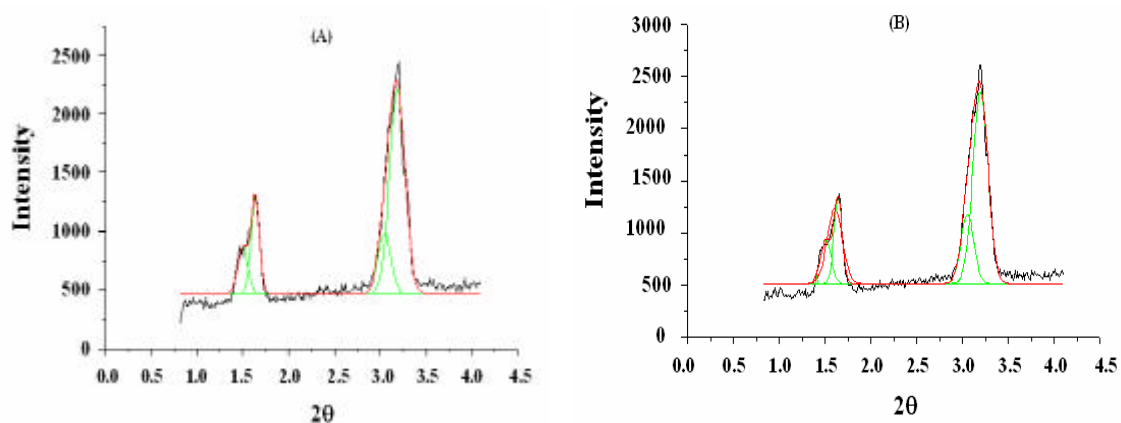


**Figure 4.14** A plot of the X-ray diffractometry intensity as a function of  $2\theta$  for pure CPC during cooling down process; at 65 °C (A), 45 °C (B); experimental (—), and Lorentzian function fitting (—)

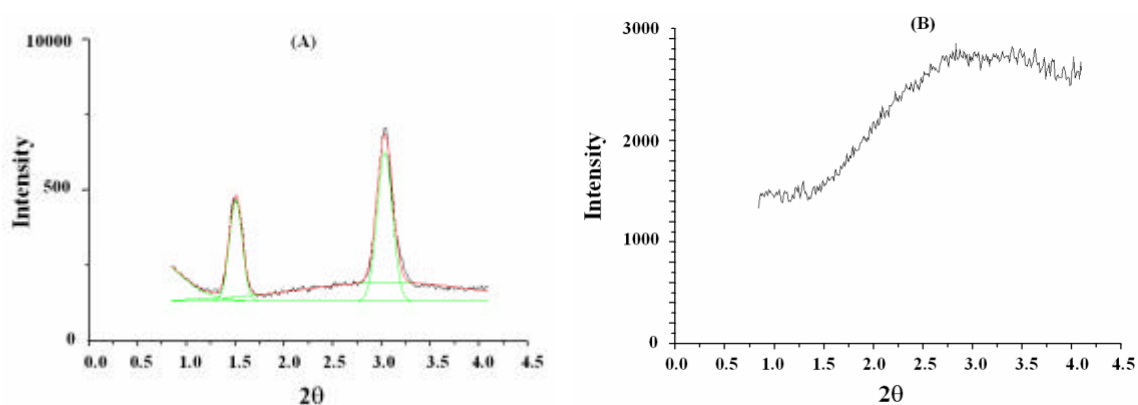


**Figure 4.15** A plot of the X-ray diffractometry intensity as a function of  $2\theta$  for binary mixture of AmB in CPC (1:3, mole ratio) at 25 °C (A) and 75 °C (B); experimental (—), and Lorentzian function fitting (—)

Upon cooling, the  $d$ -spacing values of AmB in CPC (1:3, mole ratio) were slightly shifted to lower spacing but the intensity increased (Figure 4.16). Diffraction patterns of AmB in CPC mixture following cooling were quite distinct from pure CPC. AmB molecules evidently affect the structure of CPC. Thus binary mixture of AmB and CPC exhibited higher ordered structure than CPC. However, AmB incorporated into CPC did not change optical texture (section 4.3.3 (Figure 4.9)).

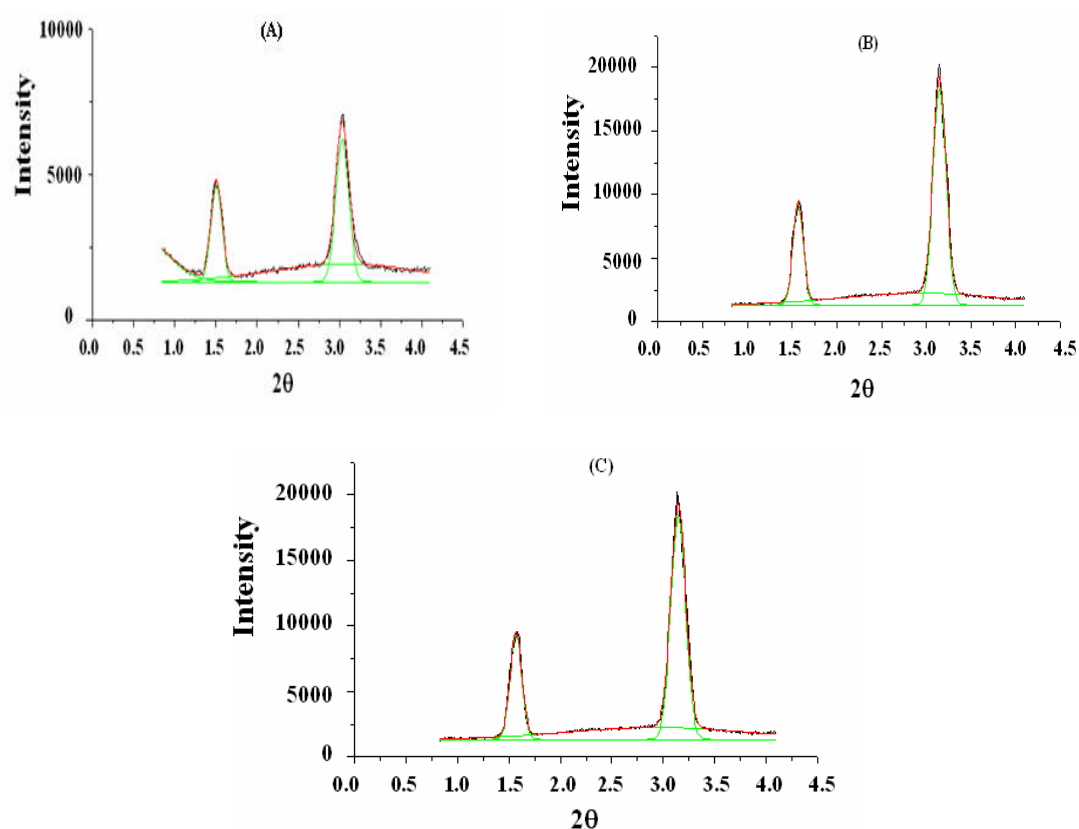


**Figure 4.16** A plot of the X-ray diffractometry intensity as a function of  $2\theta$  for AmB in CPC (1:3, mole ratio) during cooling down process; at 65 °C (A), 45 °C (B) and 25 °C (C): experimental (—), and Lorentzian function fitting (—)



#### 4.3.6 solid state Nuclear Magnetic Resonance (ssNMR) Spectra

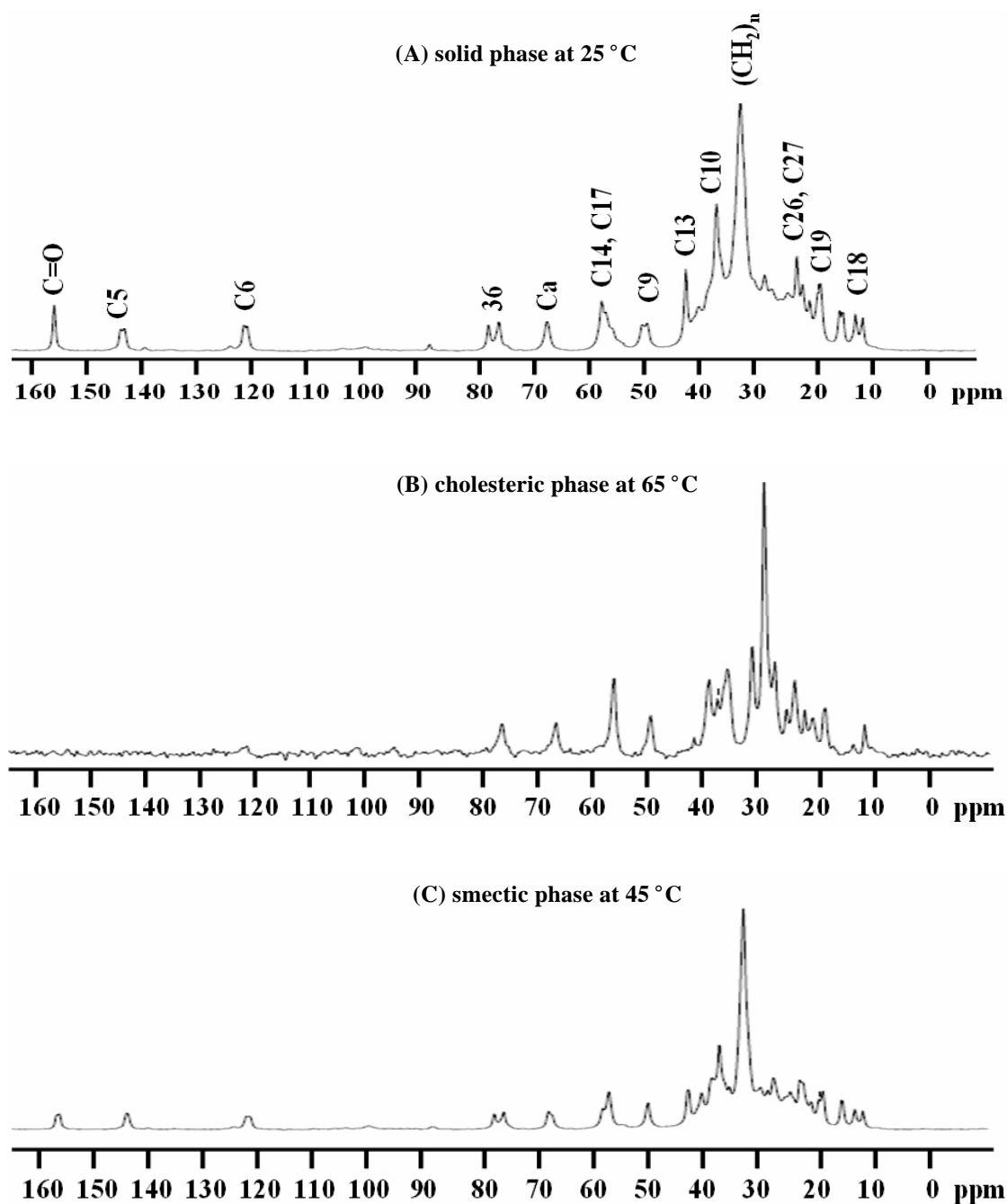
Chemical shifts for pure CPC and AmB in CPC (1:3, mole ratio) are listed in Table 4.1. The  $^{13}\text{C}$  MASNMR spectrum at 25 °C of pure CPC (Figure 4.17 (A)) shows signals for the C=O, the nonprotonated carbons C5, C13 and C10, the angular methyls C18 and C19, the side chain methyls C26 and C27 and several alkyl chain carbons. The resonances from protonated carbons of the steroid ring are significantly broader than resonances for nonprotonated ring carbons and carbons of the acyl side chain. High resolution  $^{13}\text{C}$  spectra of crystalline cholesteryl carbonate esters were also obtained by MASNMR with cross-polarization transfer.

Craven (1986) studied the three crystallographic types of cholesteryl esters (monolayer type I, *MLI*; monolayer type II, *MLII* and bilayer, *BL*) that can be distinguished by unique chemical shifts. Specifically, *MLI* and *BL* forms are characterized by twin signals for certain carbons, such as C5, C6, C18, C13, C10, C19, C=O and  $\omega\text{CH}_3$  in the *BL* form, and C=O, C5, C6, C9 and C18 and in the *MLI* form, reflecting the two crystallographically inequivalent molecules. While cholesteryl esters in the *MLII* forms were characterized by a single peak for each carbon therefore all molecules are equivalent in this crystalline structure (Guo and Hamilton, 1993). In case of cholesteryl carbonate, CPC, peaks assignments are shown in Table 4.1, the two sets of peaks for C5, C6, C3, C9 and C18 were observed. These separations due to the two sets of peaks are attributed to the nonequivalent A and B molecules in the *MLI* crystal lattice as compared with cholesteryl esters. The isotropic liquid was obtained during increased temperature up to 75 °C.

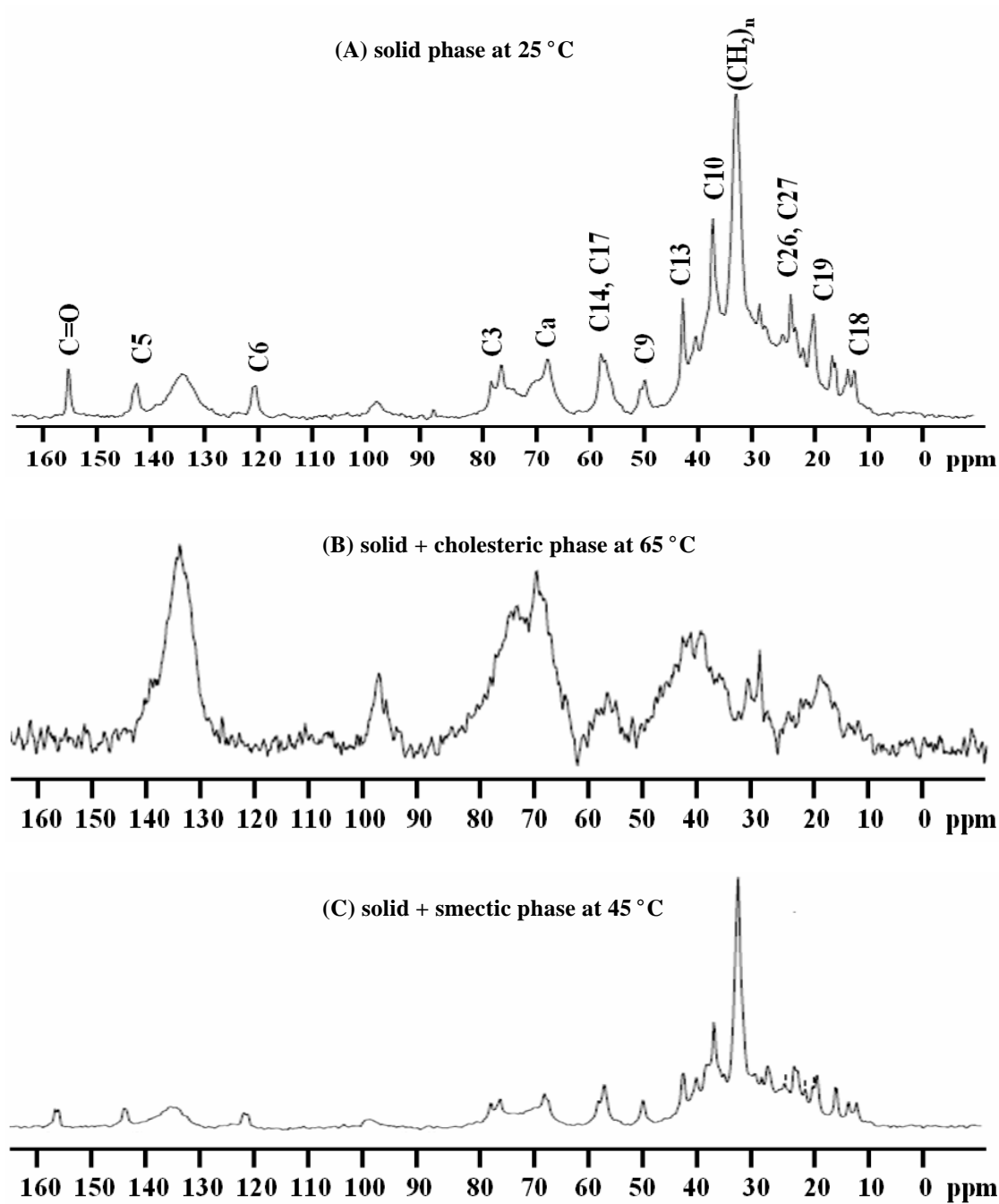
In liquid crystal phases, smectic or cholesteric phase can be differentiated by  $^{13}\text{C}$ MASNMR during cooling. Crystalline phases can be detected effectively only by MASNMR with cross-polarization transfer, whereas liquid crystalline can be detected with or without cross-polarization transfer due to the higher mobility. In the case of cholesteric phases (Figure 4.17 (B)), the most broadened and diffuse signals, particularly for carbons were observed with a large chemical shift anisotropy, such as C5, C6 and C=O. These broad line widths are not significantly affected by decoupling power, temperature or spinning rate and are standard features for the recognition of the cholesteric phase (Guo and Hamilton, 1993). They attributed this line broadening to a broad chemical shift distribution caused by motional modulation of the shielding environment. The biaxial nature of the cholesteric phase might also contribute to such line broadening. Whereas, smectic phase (Figure 4.17 (C)), a broader signal was observed in comparison to the solid state spectrum (Figure 4.17 (A)).

Figure 4.18 shows the  $^{13}\text{C}$ MASNMR spectra of binary mixture of AmB and CPC (1:3, mole ratio). The chemical shifts of carbons in CPC were slightly shifted as compared with pure CPC (Table 4.1). Upon heating, the solid crystalline AmB in CPC melted into the crystal-isotropic liquid at 75 °C and gave a  $^{13}\text{C}$ MASNMR spectrum of AmB-CPC mixture rougher than pure AmB (data not shown). Following cooling to 65 °C, the  $^{13}\text{C}$ MASNMR spectrum of AmB in CPC mixture exhibited a similar spectrum to that obtained at 75 °C. Thus  $^{13}\text{C}$ MASNMR spectra obtained at 65 °C still showed a similarly diffuse spectrum to that observed at 75 °C. This may be due to the incorporation of AmB into CPC molecule, which may have affected the structural order and increased time needed for re-orientation of molecules in binary mixture of

AmB and CPC. It should be borne in mind that the crystallization temperature depends on the cooling rate and increases at lower scan rate (Kuntsche *et al.*, 2004).

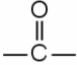


**Figure 4.17**  $^{13}\text{C}$  MAS NMR spectra of pure CPC: at 25 °C (A) and during cooling down to 65 °C (B) and 45 °C (C)



**Figure 4.18**  $^{13}\text{C}$  MAS NMR spectra of binary mixture of AmB in CPC (1:3, mole ratio) : at 25 °C (A) and during cooling down to 65 °C (B) and 45 °C (C)

**Table 4.1** The  $^{13}\text{C}$  chemical shift (ppm) of pure CPC and binary mixture of AmB and CPC (1:3, mole ratio) at various physical states.

Peak assignment	Pure CPC			AmB in CPC (1:3, mole ratio)		
	Solid (25 °C)	Liquid crystal cool down (45 °C)	Solid cool down (25 °C)	Solid (25 °C)	Liquid crystal cool down (45 °C)	Solid cool down (25 °C)
C24	37.61	37.72	38.91	37.64	37.78	37.65
C4	40.72	40.86	40.77	40.73	40.90	40.84
C13	43.02	43.24	43.11	43.07	43.27	43.13
C9	49.89/50.70	50.36	50.17	49.98	50.43	50.28
C14 or C17	57.19	57.25	57.09	57.89	57.31	57.14
C14 or C17	57.86	58.31	58.19/57.09	57.89	58.34	57.14
Ca	67.54	67.92	67.90	67.64	67.98	67.97
C3	76.07/77.88	75.87/77.52	75.80/77.28	76.05/77.86	75.87/77.50	75.81/77.28
C6	120.55/121.06	120.81/121.33	120.89	120.71	121.48	120.93
C5	142.22/142.32	142.47	142.32	142.31	142.73	142.47
	154.68	154.53/154.87	154.45	154.68	154.56/155.07	155.07

Both SAXD and ssNMR techniques are complimentary to DSC and PLM in investigation of molecular orientation. However in this study, AmB-SCC and AmB-DCC have high state transition temperature ( $> 100\text{ }^{\circ}\text{C}$ ). Thus, only AmB-CPC mixture was chosen to study in details. The SAXD and ssNMR results indicate that molecular orientation of AmB-CPC mixture related well with state diagram obtained from thermotropic behavior.

#### **4.4 Conclusions**

The phase behavior of binary mixtures AmB and liquid crystals, CPC, DCC and SCC, was studied by DSC, PLM, TEM, SAXD and ssNMR. From the results it can be concluded that AmB was incorporated into CPC when it exhibited liquid crystal behavior. This property was only evident by cooling CPC from a temperature that exceeded the isotropic phase transition (i.e., melting point). In the case of AmB with DCC, the liquid crystal phase remained only on heating process and with increase AmB concentration, there was a progressively increase effect on the liquid crystal property of DCC. Despite AmB incorporated into SCC, the liquid crystal phase was observed both with heating and cooling.

The results suggest that AmB can be incorporated into liquid crystals by using the solvent evaporation technique; however, the amount of AmB loaded into liquid crystal was limited. The mixture of AmB in liquid crystal did not produce a new complex, but rather, the addition of AmB affected the orientation order and the motional aspects of liquid crystal molecule. Thus, the physical properties of binary mixtures AmB and liquid crystal changed.

# CHAPTER 5

## AMPHOTERICIN B IN LIQUID CRYSTALS

### AS DRY POWDER AEROSOLS

#### 5.1 Introduction

Liquid crystals are phases of matter defined as having less than three dimensional orders. Therefore, liquid crystalline phases possess properties of both liquid and solid phases. The liquid phase is has no long range order, which imparts the ability of flow whereas crystalline solids have long range order, inhibits flow (Kelker and Hatz, 1980). The liquid crystalline phases, also called mesophases, exhibit intermediate properties those are. The mesophase is reached either by adding a solvent (lyotropic liquid crystal) or by increasing the temperature (thermotropic liquid crystal).

A few reports of pharmaceutical applications appeared in the literature, which used thermotropic liquid crystals as drug carrier. Kuntsche and coworkers (2004) used a dispersion of supercooled smectic nanoparticles prepared from naturally occurring, cholesteryl myristate (CM), as potential novel carrier system for lipophilic drugs (ibuprofen, miconazole, etomidate and progesterone). CM remained in a smectic phase for 1 year at 23°C. A cholesteryl carbonate ester, cholesteryl oleyl carbonate (COC), was developed as a thermo-responsive agent embedded within a cellulose nitrate membrane (Lin *et al.*, 1996). They found that enhancers (ethanol, propylene glycol and Azone<sup>®</sup>) improved solubility of COC (Lin *et al.*, 2000), which is useful

information in topical dosage form. However, COC is perhaps not the best choice from the standpoint of chemical stability due to the presence of unsaturated hydrocarbons. Nevertheless, it was proposed that such a mixture could then be used for drug delivery applications to the skin where the surface temperature is slightly lower than the normal 37 °C body temperature. Moreover, the room temperature liquid crystalline phase would provide enhanced chemical stability in comparison to the isotropic liquid phase.

In our studies, SCC, CPC and DCC were found to have quite distinct properties in comparison to COC. The melting temperatures of SCC, CPC and DCC are higher than that of COC, and they also can be prepared as dry powders at room temperature. This is due to the contribution of the saturated hydrocarbon chain in the molecule, which will impart greater chemical stability to cholesteryl carbonate.

AmB is a drug of choice in systemic fungal infections and is also used in lung fungal infections (Walsh and Pizzo, 1990; Sarosi, 1990; Denning and Stevens, 1990). However, AmB has a narrow therapeutic index and a host of undesirable side effects. The purpose of this effort was to identify and develop chemically stable systems that can be used for inhalation drug delivery of AmB. Therefore, an alternative carrier system containing a saturated hydrocarbon chain covalently bonded with cholesterol was introduced as a thermotropic liquid crystal. SCC, CPC and DCC were chosen for this study, since they are solid materials with ordered structures from which dry powders can be prepared with greater chemical stability. They also form mobile, thermotropic mesophases, which was postulated to increase drug loading capacity and decrease immobilization potential for AmB molecules.



## **5.2 Materials and methods**

### **5.2.1 Validation of HPLC method for determination of AmB**

To ensure that the analytical method is precise and reliable for the determination of AmB, it was validated prior to formulation and development of the dry powder aerosol. High performance liquid chromatography (HPLC) was employed as a tool for drug analysis.

#### **A) Materials**

AmB was obtained from Ambalal Sarabhai Enterprises Ltd. (Vadodara, India). Acetonitrile and methanol were purchased from Labscan Asia, Bangkok, Thailand. Dimethylsulfoxide was obtained from Riedel-de Haëan, Germany. Polyamide membrane pore size 0.45  $\mu\text{m}$  was purchased from Satorius, Germany. All reagents were analytical grade.

#### **B) Equipment**

The HPLC system (Thermo Electron Corporation, California, USA) was equipped with AS 3000 autosampler, P 1000 pump and UV 2000 detector. The microbondapak C18 column (Phenomenex, USA) (250 $\times$ 4 mm i.d., 10  $\mu\text{m}$ ) was used in this study.

#### **C) Chromatographic conditions**

The mobile phases consisted of 20 mM acetate buffer pH 7.2: acetonitrile (60:40 v/v). The mobile phase was delivered at a flow rate of 1 mL/min at

ambient temperature. The UV/VIS detector was operated at wavelength 407 nm. The injection volume was 50  $\mu\text{L}$  (adapted from Tiyaboonchai *et al.*, 2001).

#### **D) Method validation of AmB**

A stock solution was prepared as follow. Ten milligrams of AmB were weighed and placed in a 100 mL volumetric flask, which was filled with DMSO. Working standard solutions were prepared as needed by diluting the stock solution with methanol to yield final concentrations of 2.0, 4.0, 6.0, 8.0 and 10.0  $\mu\text{g/mL}$ . The standard curve was constructed using the area under the response curve as a function of concentration of AmB.

The intra-day precision was determined by performing five repeated analyses of a preparation on the same day. The inter-day precision was determined by analyzing freshly prepared samples on five separate days over a period of 1 week. The precision was determined by calculating the analyte peak area over the mean peak area presented as a percentage of the relative standard deviation (%RSD).

The accuracy of the analysis was determined by the systemic error, which was calculated as the recovery of the analyte by a standard addition method at concentration between 2.0–10.0  $\mu\text{g/mL}$  for AmB. Recovery was evaluated by comparing the theoretical and measured concentration of a spike analyte.

The linearity of the response of analytical method was determined by analyzing the corresponding reference standards three times for each concentration in the range of 2.0–10.0  $\mu\text{g/mL}$  of AmB. The correlation coefficient value ( $r^2$ ), generated by plotting the analyte peak area versus the concentration of the drug was determined.

### **E) Calibration curve for standard AmB**

Stock solutions of AmB were prepared by dissolving 10 mg of standard AmB in 100 mL DMSO. The stock solution was kept at -20 °C, protected from light until use.

The stock solution of AmB was diluted stepwise with methanol to give final drug concentrations of 2.0, 4.0, 6.0, 8.0 and 10.0 µg/mL. The standard solution of AmB was determined by HPLC as described in section 5.2.1 B and 5.2.1 C. Calibration curve of standard AmB was generated by plotting the peak area of the drug as a function of concentrations.

### **5.2.2 Preparations of AmB in cholesteryl carbonate esters dry powder**

The dry powder was prepared by solvent evaporation. Briefly, a certain accurately weighed amount of SCC, CPC, DCC or cholesterol was dissolved in 100 mL methanol-chloroform (1:1, v/v). AmB (0.27 mM) was slowly added into the liquid crystal solution to generate different ratios of AmB to liquid crystal (1:3, 1:6 and 1:12, mole ratios) and stirred for 20 h until a clear solution was obtained. The organic solvent was evaporated under vacuum (200 mbar) at 40-45 °C in rotary evaporator (Eyela, Tokyo Rikakikia Co., LTD., Japan). The resulting AmB in liquid crystal was stored at 2-8 °C.

### **5.2.3 Content uniformity of AmB in cholesteryl carbonate esters dry powders**

AmB in cholesteryl carbonate esters powder (10 mg) was randomly sampled and weighed. A total of 10 doses were collected, three doses at top, four in the middle and three at the bottom of the bottle containing formulation. The powder was

suspended in 5 mL of DMSO to dissolve AmB. Methanol was used to adjust to the volume of 25 mL following by sonication to obtain a clear solution. AmB content from the clear solution was analyzed by HPLC as described in sections 5.2.1 B and 5.2.1 C.

#### **5.2.4 Solubility studies of AmB in cholesteryl carbonate esters**

An excess amount of pure AmB or AmB formulation (10 mg) was added to 10 mL of 0.25% w/v sodium dodecyl sulfate (SDS) in phosphate buffered saline (PBS) pH 7.4. The solubility of AmB was measured at  $37 \pm 0.5$  °C in a shaking bath (oscillating at 200 rpm) and in the dark. One milliliters of sample was collected at 6, 12, 24 and 48 h. Samples were centrifuged at 10,000 rpm for 30 min, and filtered through a 0.2  $\mu$ m membrane. The supernatant was diluted with 0.25% w/v SDS in PBS solution to yield an appropriate concentration for assay. The concentration of AmB was determined by HPLC (section 5.2.1 B and 5.2.1 C) in triplicate.

#### **5.2.5 Dissolution studies of AmB in cholesteryl carbonate esters**

AmB has very poor aqueous solubility. Thus, 0.25% w/v SDS in PBS pH 7.4 was used as a dissolution medium. The drug release profile of AmB formulations was studied at  $37 \pm 0.5$  °C. Ten milligrams of AmB formulations were placed into 200 mL of the 0.25% w/v SDS in PBS dissolution medium and stirred at 200 rpm in the dark. An aliquot (2 mL) was taken at time interval of 0.25, 0.5, 1, 2, 4, 8, 16 and 24 h. Samples were filtered through a 0.2  $\mu$ m membrane. The amount of AmB release was determined by HPLC as described in section 5.2.1 B and 5.2.1 C. Dissolution studies were performed in triplicate.

### **5.2.6 *In vitro* deposition of AmB in cholesteryl carbonate esters dry powder by Andersen Cascade Impactor (ACI)**

Aerosolization parameters of the AmB dry powder formulation, including mass median aerodynamic diameter (MMAD), %fine particle fraction (FPF) and %emitted dose (%ED), were evaluated by the Andersen cascade impactor (ACI), (Atlanta, GA, USA). Dry powder formulation was subdivided into each dose (30 mg) and delivered by an inhaler device made in house (Srichana *et al.*, 2003) before directing the particles into the ACI. The eight stages of the ACI separates the samples aerosol into nine size intervals when used with a backup filter after the last impaction stage (Stein and Olson, 1997). Each stage of an ACI has multi-orifices that display progressively smaller diameters from top to bottom (Figure 5.1). The ACI was applied with a vacuum pump under flow rate of 60 L/min for 10 s. AmB depositing on each stage was rinsed with 10% DMSO in methanol and quantified by HPLC. The cumulative percentage of drug deposition was transformed to the Z-value and plotted against log cut-off diameter of each stage. MMAD was obtained from the particle diameter at the Z-value of zero (Srichana *et al.*, 1998). Emitted dose is an amount of drug propelled from delivery device whereas fine particle fraction (FPF) was defined as the mass fraction of particles smaller than 5  $\mu\text{m}$  (Srichana *et al.*, 2003) which is the percentage of drug deposited on stages 1-7. Each experiment was run five times.

### **5.2.7 Statistical analysis**

Data, when applicable, are presented as mean  $\pm$  standard deviation (SD) from at least three separated experiments unless otherwise indicated. The data and all aerosol parameters of each AmB formulation were compared using analysis of variance

(ANOVA). All statistical comparisons were calculated using the SPSS software version 11.5 (SPSS, Inc., Chicago, IL). A significance level of  $p$ -value  $< 0.05$  was considered statistically significant.

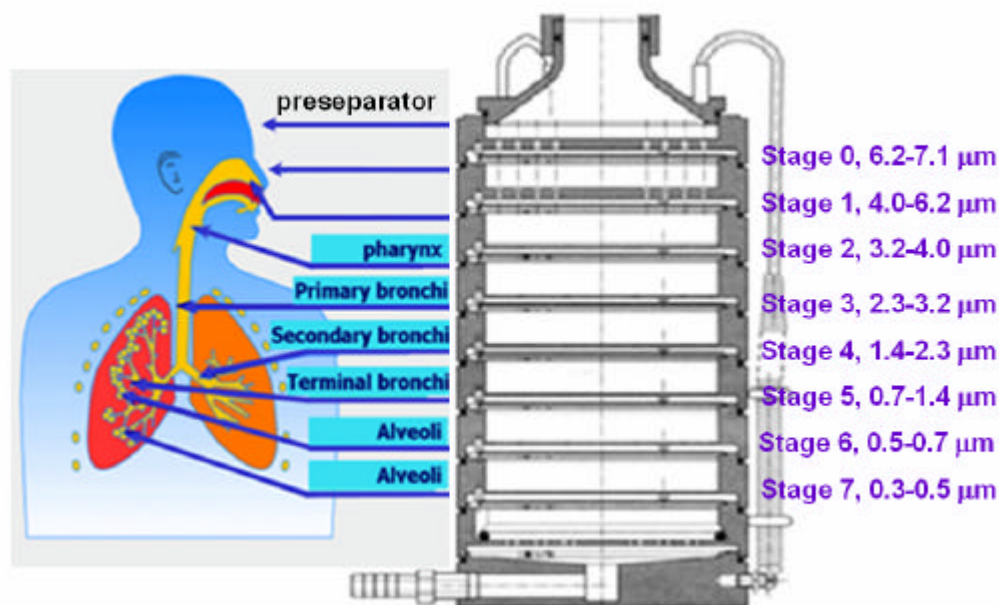


**Figure 5.1** Andersen cascade impactor and respiratory airways (BP, 2007)

## 5.3 Results and discussions

### 5.3.1 Method validation of AmB

The procedure for validating the analytical determination of AmB followed the guidance for industry: validation of analytical procedure (ICH, 1996). Figure 5.2 shows the intra-day and inter-day precision of AmB. The %RSD of AmB was less than 2% in all concentrations in this study. The results show that the analytical

method was acceptable for analysis of sample in the same day and inter-day within 1 week.

Table 5.1 shows that AmB determination have good linearity with the correlation coefficient ( $r^2 \geq 0.999$ ) in concentration range between 2.0–10.0  $\mu\text{g/mL}$  of AmB. Thus, this range of concentrations was acceptable for preparing the standard solution and samples for analysis.

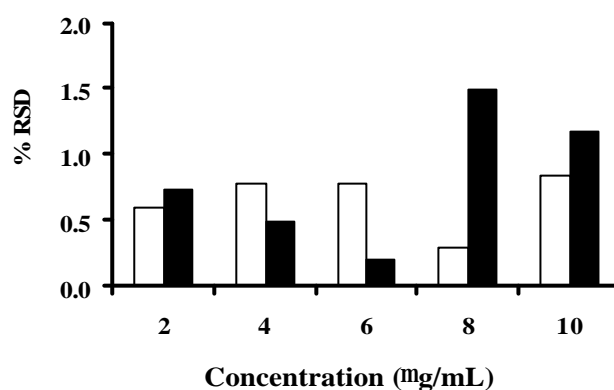


**Figure 5.2** Precision of AmB analysis; intra-day (□) and inter-day (■)

**Table 5.1** Linearity of AmB standard curve determination by HPLC.

No.	intercept	slope	$r^2$
1	6595.9	57029	0.9993
2	9479.3	56448	0.9995
3	6190.7	56962	0.9993
4	4515.5	57697	0.9984
5	6624.4	56737	0.9995

Table 5.2 shows that AmB has high accuracy. The percent recovery of AmB gave over than 98% in all concentration from 2.0–10.0  $\mu\text{g/mL}$ . The results

suggest that the analytical method of AmB is accurate. Limit of detection (LOD) and limit of quantification (LOQ) of this method were 0.2 and 0.8  $\mu\text{g/mL}$ , respectively.

**Table 5.2** Accuracy of AmB standard curve determination by HPLC.

No.	Theoretical concentration ( $\mu\text{g/mL}$ )	Measured concentration ( $\mu\text{g/mL}$ )	%Recovery
1	2.0	2.085	104.28
2	4.0	3.927	98.18
3	6.0	5.963	99.40
4	8.0	7.948	99.35
5	10.0	10.075	100.75

### 5.3.2 Calibration curve for standard AmB

A representative standard curve of AmB is shown in Figure 5.3. The calibration curve was prepared with freshly prepared samples. The correlation coefficients are above 0.999 in the concentration range of 2-10  $\mu\text{g/mL}$ .

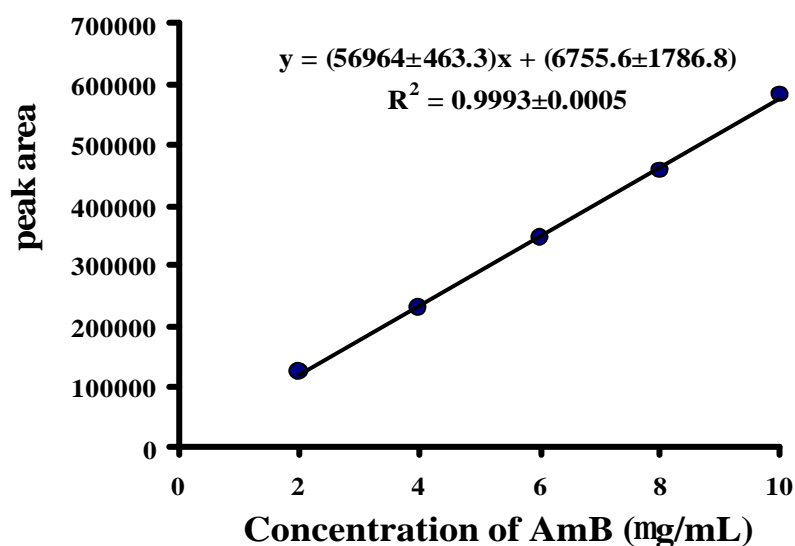


**Figure 5.3** Standard curve of AmB (mean  $\pm$  SD,  $n = 5$ , error bars are smaller than the figure legends)



### 5.3.3 Stability of AmB in cholesteryl carbonate esters formulations

**Table 5.3** Composition and %drug content of AmB in cholesteryl carbonate ester dry powder as compared with AmB in cholesterol (Chol) (n = 10, mean  $\pm$  SD).

Formulation No.	Composition (mole ratio)	% drug content	
		Initial	6 months
1	AmB:CPC (1:3)	95.0 $\pm$ 3.2	96.7 $\pm$ 6.1
2	AmB:CPC (1:6)	108.4 $\pm$ 4.4	101.1 $\pm$ 7.4
3	AmB:CPC (1:12)	105.7 $\pm$ 2.7	96.9 $\pm$ 5.8
4	AmB:DCC (1:3)	102.0 $\pm$ 9.6	99.6 $\pm$ 7.2
5	AmB:DCC (1:6)	103.5 $\pm$ 9.0	98.0 $\pm$ 7.2
6	AmB:DCC (1:12)	102.4 $\pm$ 7.8	95.8 $\pm$ 4.1
7	AmB:SCC (1:3)	97.5 $\pm$ 1.7	103.5 $\pm$ 4.8
8	AmB:SCC (1:6)	105.9 $\pm$ 7.6	98.9 $\pm$ 6.0
9	AmB:SCC (1:12)	103.1 $\pm$ 5.2	101.1 $\pm$ 4.8
10	AmB:Chol (1:3)	98.5 $\pm$ 6.3	102.4 $\pm$ 7.4
11	AmB:Chol (1:6)	111.6 $\pm$ 6.3	109.4 $\pm$ 9.6
12	AmB:Chol (1:12)	112.3 $\pm$ 5.4	100.1 $\pm$ 1.7

Dry powders composed of AmB in various CCEs (CPC, DCC and SCC) were prepared by the solvent evaporation method. AmB content in dry powder formulations were determined by HPLC. Content uniformity of AmB formulations ranged between 95.0  $\pm$  3.2 to 112.3  $\pm$  5.4%. The results indicate that the solvent evaporation method is accurate and reproducible, and uniform mixing was achieved by employing this procedure. The composition and percent drug content uniformity are shown in Table 5.3. The percent drug remaining was measured in the formulations stored at a refrigerated temperature (2-8 °C). AmB content was maintained over 95%

for at least 6 months. In addition, physical properties of dry power formulation remained unaltered. Thus, AmB formulations in dry powder state are likely to be stable. However, these AmB formulations could be further developed to obtain the good physicochemical properties of dry powder inhaler (Sanna *et al.*, 2003).

### 5.3.4 Solubility of AmB formulations

The solubility of pure AmB in 0.25% SDS in PBS was  $152.8 \pm 3.3$   $\mu\text{g/mL}$ . Whereas, AmB in liquid crystals (CPC, DCC, SCC or cholesterol) at mole ratio 1:12 had a solubility of  $90.5 \pm 4.5$  to  $112.5 \pm 8.7$   $\mu\text{g/mL}$  (Table 5.4). Pure AmB gave a higher soluble than AmB formulations (*p-value* < 0.01). In addition, the approximated partition coefficients of AmB (liquid crystals, CPC, DCC, SCC and cholesterol/buffer solution phase) were calculated to be 824.1, 682.6, 742.0 and 848.7, respectively. The results indicate that AmB molecules were partitioned into liquid crystal phase higher than that into aqueous phase. This will directly affect solubility of AmB in binary system (liquid crystals-aqueous phase) resulting in lower concentration of AmB in aqueous phase (90-100  $\mu\text{g/mL}$ ).

**Table 5.4** Solubility of AmB and AmB formulations in 0.25% w/v SDS in phosphate buffer saline pH 7.4 at 37 °C (mean  $\pm$  SD, n = 3).

Composition (mole ratio)	Solubility (mg/mL)	Partition coefficient ( $K_{LC/w}$ )
AmB	$152.8 \pm 3.3$	
AmB:CPC (1:12)	$93.2 \pm 7.8$	824.1
AmB:DCC (1:12)	$112.5 \pm 8.7$	682.6
AmB:SCC (1:12)	$103.5 \pm 7.3$	742.0
AmB:Chol (1:12)	$90.5 \pm 4.5$	848.7

$K_{LC/w}$ : partition coefficient of AmB between liquid crystals and aqueous phase.

### 5.3.5 Dissolution profiles of AmB in cholesteryl carbonate esters

Figures 5.4 to 5.7 show cumulative drug release of AmB from dry powder formulations in the presence of 0.25% w/v SDS. The results show that dry powder formulations provide rapid release, with most of AmB released from particles within 30 min (2,700  $\mu\text{g}$ ,  $\geq 80\%$ ). The extent of drug release from all formulations, which were composed of AmB in liquid crystals at mole ratio of 1:3, was 90% ( $\sim 3,000$   $\mu\text{g}$ ) within 2 h and rising up to 100% ( $\sim 3,400$   $\mu\text{g}$ ) in 4 h, in cases of AmB-CPC and AmB-SCC. While drug release decreased to lower than that in the mixture of AmB-DCC and AmB-cholesterol of similar ratio around 3,000 and 2,800  $\mu\text{g}$ , respectively. This may be due to AmB was not completely incorporated into microparticle. In contrast, the formulations containing high content of liquid crystal (mole ratios of 1:6 and 1:12), AmB releases were 2,900  $\mu\text{g}$  and 2,500  $\mu\text{g}$  or 85 and 75%, respectively. It can be seen that AmB in CPC, DCC and SCC of 1:6 mole ratios had higher AmB release ( $\sim 80\%$ ) than AmB-cholesterol ( $\sim 70\%$ ). However at 1:12 mole ratio drug release profiles are quite similar in different types of liquid crystals 1,800-2,500  $\mu\text{g}$  (55-70%). The release profiles of AmB in liquid crystal formulation are related with the solubility and the partition coefficient in section 5.3.4. High concentration of liquid crystal in AmB formulation leads to give a low soluble of AmB in aqueous phase. Taking this into account of the fact that AmB molecule is quite hydrophobic, it can be considered that AmB molecules would prefer to be in liquid crystal phase rather than aqueous phase. Lower release of AmB is observed when higher liquid crystal containing in the formulation. In another word, high content of liquid crystal retards the release of AmB. It appears that the hydrophobic properties of thermotropic liquid crystal dissolved AmB

in the lipid crystalline matrix resulting in a slow release. Also, it seems to have a partitioning effect and equilibrium between the aqueous solution and the liquid crystalline phase. In this case, a complete release occurred at 4 h and it seems to be equilibrium. Although, percent release of AmB in liquid crystals at 1:6 and 1:12 did not reach 100 from the effect of partition. In order to achieve 100% release the AmB content in formulation is expected to be at 1:3 or higher. As AmB is insoluble in water the release rate of AmB *in vivo* should be lower than that seen *in vitro* studies, which in turn will return the maximum concentration in plasma and thereby avoid toxic effects (Tiyaboonhai and Limpeanchai, 2007). In our case we achieved AmB concentration at lowest about 9  $\mu\text{g/mL}$  which is high enough to inhibit the fungi growth.

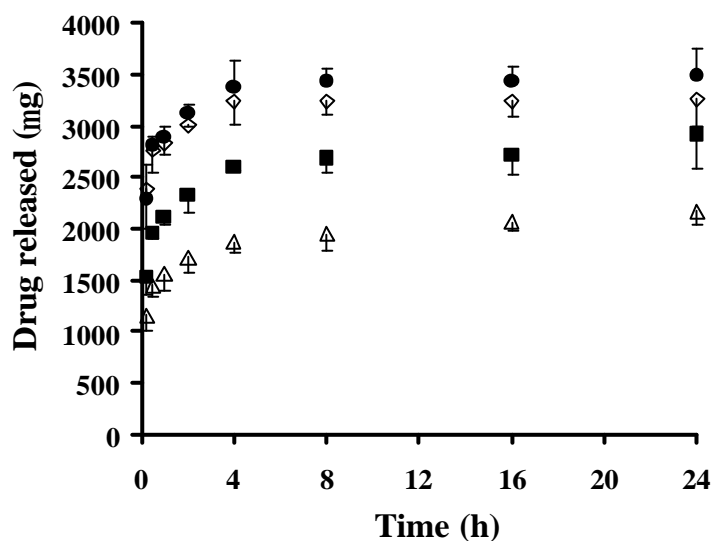


**Figure 5.4** *In vitro* release of AmB in CPC at various mole ratios; pure AmB (●), 1:3 (◇), 1:6(■) and 1:12(△) in phosphate buffer saline pH 7.4 containing 0.25% w/v SDS (mean  $\pm$  SD, n = 3)

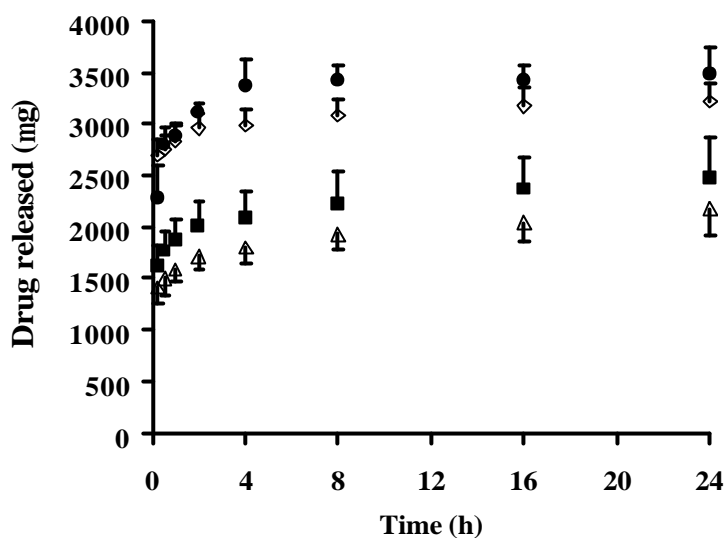


**Figure 5.5** *In vitro* release of AmB in DCC at various mole ratios; pure AmB (●), 1:3 (◇), 1:6(■) and 1:12(△)in phosphate buffer saline pH 7.4 containing 0.25% w/v SDS (mean  $\pm$  SD, n = 3)

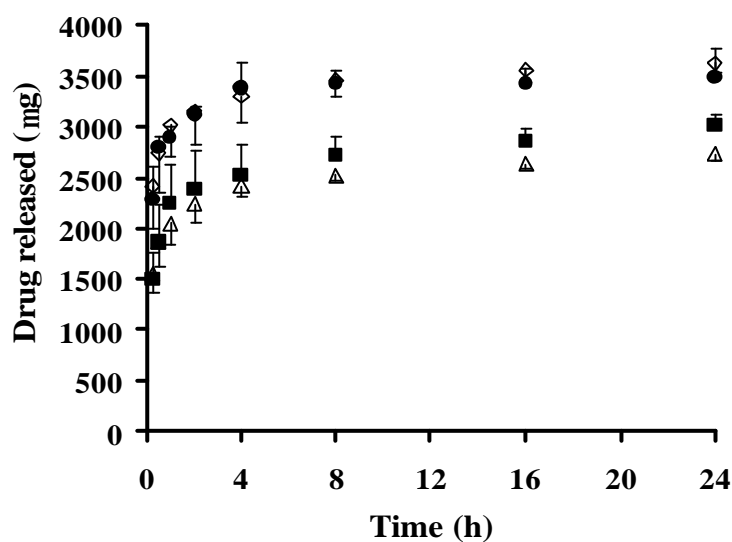


**Figure 5.6** *In vitro* release of AmB in SCC at various mole ratios; pure AmB (●), 1:3 (◇), 1:6(■) and 1:12(△)in phosphate buffer saline pH 7.4 containing 0.25% w/v SDS (mean  $\pm$  SD, n = 3)

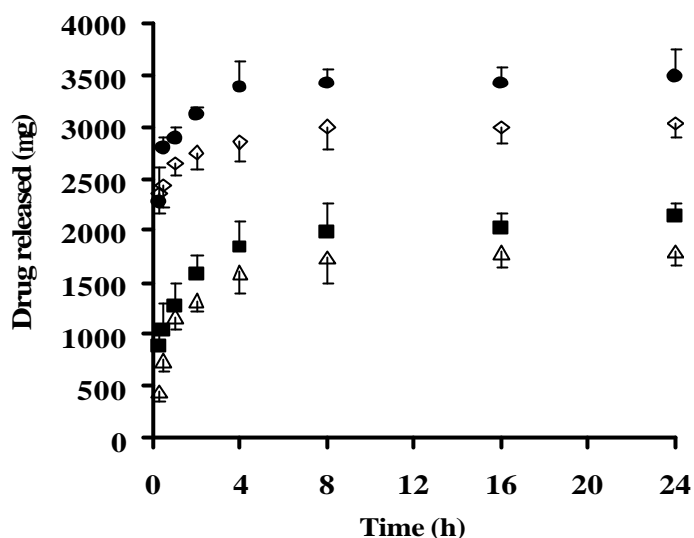


**Figure 5.7** *In vitro* release of AmB in cholesterol various mole ratios; pure AmB (●), 1:3 (◇), 1:6(■) and 1:12(△) in phosphate buffer saline pH 7.4 containing 0.25% w/v SDS (mean  $\pm$  SD, n = 3)

### 5.3.6 Aerosolization of AmB in cholesteryl carbonate esters dry powder

The aerosol formulations offer the potential for needle-free, systemic delivery of low molecular weight drugs. The lungs are an efficient port of entry to the bloodstream because: (i) the tremendous surface area of the alveoli (100 m<sup>2</sup>), immediately accessible to drug; (ii) a low metabolic activity locally, as well as a low of first-pass hepatic metabolism; and (iii) the elevated blood flow (5 L/min) which rapidly distributes drug throughout the body (Wall, 1995; Adjei and Gupta, 1997).

Dry powder inhalers present several advantages for the delivery of drug to the lung. They are propellant-free, portable, easy to operate and low cost devices. Moreover, the formulations generally have improved stability of the active ingredient since it is present in the dry state (Prim *et al.*, 1997).

Figures 5.8 and 5.9 show the weight fraction as a function of aerodynamic size for various AmB formulations which are composed of different types and ratios of liquid crystals.

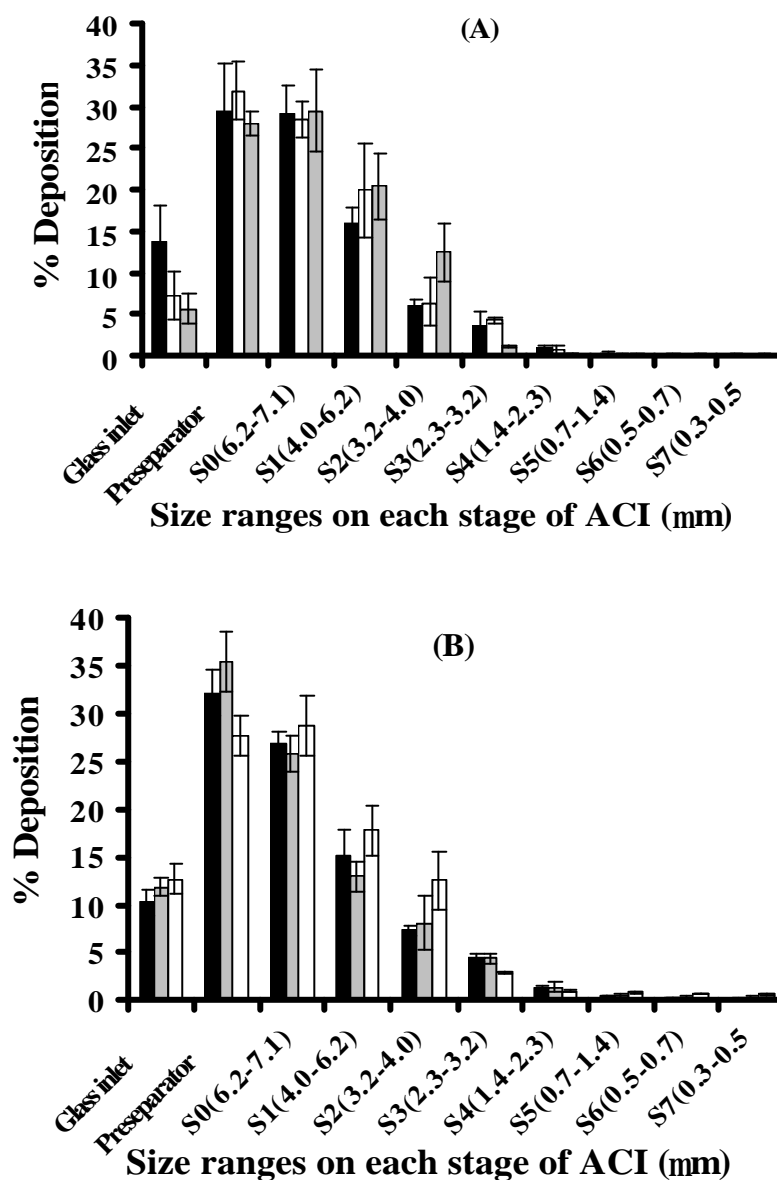


**Figure 5.8** Size distribution of AmB in CPC (A) and AmB in DCC (B) dry powder formulations at various mole ratios; 1:3 (■), 1:6 (■) and 1:12 (□) on each stage of the ACI as aerosolized at a flow rate of 60 L/min (mean  $\pm$  SD, n = 5)

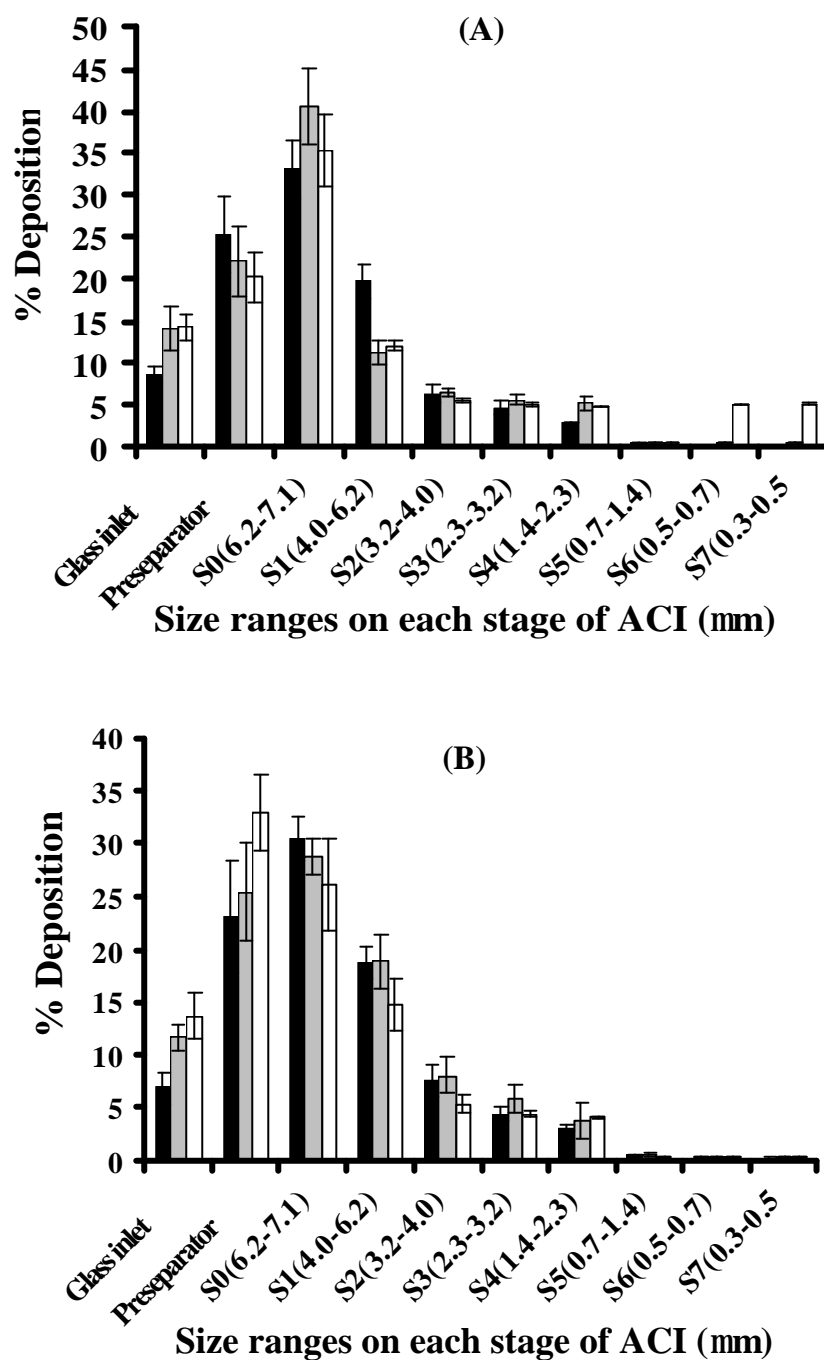


**Figure 5.9** Size distribution of AmB in SCC (A) and AmB in cholesterol (B) dry powder formulations at various mole ratios; 1:3 (■), 1:6 (▣) and 1:12 (□) on each stage of the ACI as aerosolized at a flow rate of 60 L/min (mean  $\pm$  SD, n = 5)



The aerodynamic behavior of all formulations was evaluated with ACI, which provides the *in vitro* deposition profile. The effect of liquid crystal and drug on mass median aerodynamic diameter (MMAD) and % fine particle fraction (FPF) are shown in Table 5.5. Dry powder of AmB in CPC gave a large MMAD of  $8.1 \pm 0.6$ ,  $6.4 \pm 0.4$  and  $6.5 \pm 1.3$   $\mu\text{m}$  for Formulations 1, 2 and 3, respectively. The MMAD of AmB in DCC formulations were smaller at  $5.8 \pm 0.4$ ,  $6.2 \pm 0.4$  and  $4.9 \pm 2.0$   $\mu\text{m}$  for Formulations 4, 5 and 6. In the case of AmB in SCC, the MMAD were  $5.6 \pm 0.1$ ,  $6.0 \pm 1.1$  and  $3.8 \pm 0.7$   $\mu\text{m}$  for Formulations 7, 8 and 9, and the MMADs of AmB in Chol were  $5.4 \pm 0.0$ ,  $4.8 \pm 0.9$  and  $5.0 \pm 0.1$   $\mu\text{m}$  (Formulation No 10, 11 and 12), respectively. Different type and ratio of liquid crystal gave significant effect on MMAD (Formulations No 1 and 9,  $p\text{-value} = 0.004$ ).

The emitted dose (ED) of all types and all ratios of liquid crystal was  $87.7 \pm 4.8$ - $94.1 \pm 3.9\%$  ( $p\text{-value} = 0.50$ ). The ED was substantially lower than the theoretical dose. This may be due to the deposition of drug in glass device. The FPF fell in the range of  $26.3 \pm 1.7$  to  $38.0 \pm 1.3\%$  ( $p\text{-value} = 0.33$ ), none of which is significantly different from the others (Table 5.5). The low FPF correlated with large MMAD ( $> 5$   $\mu\text{m}$ ). The results indicate that the higher content of liquid crystal in AmB formulation led to a decrease in the MMAD and improve %FPF. These may be a result of their physical properties which is in a solid state at room temperature. Moreover, these materials can be used as a carrier in dry powder formulation. Nevertheless, MMADs of formulations No 1, 2, 3, 4, 5, 7, 8 and 10 were larger than 5  $\mu\text{m}$ , which is not suitable for inhalation. Liquid crystals themselves have low density ( $< 0.25$  g/mL). Large

MMAD of AmB in liquid crystal particles may result from high density of AmB and powder aggregation that affected flowability of dry powders. These aggregates were presumably responsible for the large fractions of these particles depositing in the preseparator and the higher stage of the ACI. Particle aggregation occur secondary to moisture sorption and electrostatic attractive forces. However, different strategies have been developed to improve the flowability of dry powders (French *et al.*, 1996). These include mixing the drug particles with carriers such as a sugar, trehalose, or a polyol, mannitol and lactose. In addition, the preparation of large and porous particles reduces the inter-particle cohesiveness (Edwards *et al.*, 1997). All of formulations gave GSD values above 1.25, and therefore were characterized as polydispersed (Suarez and Hickey, 2000).

**Table 5.5** The aerodynamic characteristics of AmB in cholesteryl carbonate ester dry powder (mean  $\pm$  SD, n = 5).

<b>Formulation No.</b>	<b>Composition (mole ratio)</b>	<b>MMAD (mm)</b>	<b>ED (%)</b>	<b>FPF (%)</b>	<b>GSD</b>
1	AmB:CPC (1:3)	8.1 $\pm$ 0.6	87.7 $\pm$ 4.8	27.6 $\pm$ 4.8	2.72 $\pm$ 0.35
2	AmB:CPC (1:6)	6.4 $\pm$ 0.4	92.5 $\pm$ 2.3	32.1 $\pm$ 3.7	2.45 $\pm$ 0.15
3	AmB:CPC (1:12)	6.5 $\pm$ 1.3	94.1 $\pm$ 3.9	34.1 $\pm$ 0.6	2.40 $\pm$ 0.23
4	AmB:DCC (1:3)	5.8 $\pm$ 0.4	89.6 $\pm$ 2.1	30.3 $\pm$ 0.2	2.62 $\pm$ 0.05
5	AmB:DCC (1:6)	6.2 $\pm$ 0.4	90.5 $\pm$ 2.8	26.3 $\pm$ 1.7	2.82 $\pm$ 0.33
6	AmB:DCC (1:12)	4.9 $\pm$ 2.0	89.0 $\pm$ 2.1	32.5 $\pm$ 1.5	2.82 $\pm$ 0.54
7	AmB:SCC (1:3)	5.6 $\pm$ 0.1	90.8 $\pm$ 1.2	36.6 $\pm$ 3.6	2.48 $\pm$ 0.04
8	AmB:SCC (1:6)	6.0 $\pm$ 1.1	88.5 $\pm$ 2.7	29.6 $\pm$ 0.7	2.82 $\pm$ 0.06
9	AmB:SCC (1:12)	3.8 $\pm$ 0.7	87.9 $\pm$ 1.3	38.0 $\pm$ 1.3	3.02 $\pm$ 0.62
10	AmB:Chol (1:3)	5.4 $\pm$ 0.1	93.8 $\pm$ 1.0	36.0 $\pm$ 2.6	2.48 $\pm$ 0.03
11	AmB:Chol (1:6)	4.8 $\pm$ 0.9	89.6 $\pm$ 1.0	37.0 $\pm$ 0.4	2.52 $\pm$ 0.70
12	AmB:Chol (1:12)	5.0 $\pm$ 0.1	88.9 $\pm$ 2.2	31.2 $\pm$ 2.3	2.61 $\pm$ 0.04

MMAD: mass median aerodynamic diameter, %FPF: % fine particle fraction, %ED: %emitted dose,  
GSD: geometric standard deviation

#### **5.4 Conclusions**

In conclusions, AmB dry powders were successfully prepared by using a solvent evaporation technique. AmB formulations in dry powders were uniform and stable at least 6 months. Cholesteryl carbonate esters (CPC, DCC and SCC) can be used as a carrier to produce dry powder aerosols. However, the particle size varied with MMAD ranging from 4 to 8  $\mu\text{m}$ , where a higher content of liquid crystal in the AmB formulation resulted in a smaller MMAD. This was consistent with the visual appearance of the liquid crystals as being light and free flowing at room temperature. The properties of the aerosols may be further enhanced by combining the drug/liquid crystalline mixtures with inert carriers such as sugar. In addition, there is a possibility of preparing the lipid based system as porous particles.

# CHAPTER 6

## BIOACTIVITY AND TOXICITY STUDIES OF AMPHOTERICIN B INCORPORATED IN LIQUID CRYSTALS

### 6.1 Introduction

The epidemiology of fungal infections has undergone radical changes in the last decade. Specifically, these diseases now represent a significant cause of morbidity and mortality in patients, particularly those who are immunocompromised (Baum and Rhodes, 1998; Kauffman, 2006). AmB has been effective in the treatment of a number of fungal infections occurring in the respiratory tract arising from cryptococcosis, candidiasis, histoplasmosis, and invasive aspergillosis (Bryskier, 2005). However, AmB is unstable in aqueous solution and is also sensitive to light and high temperature, which represent a challenge for wide spread distribution and use. In addition, AmB gives rise to a number of serious side effects that appear to be related to the method of delivery.

An ideal drug delivery systems would provide targeted therapy that will allow effective concentrations of drug to reach the disease site without exposing other tissues to toxic levels of the drug. AmB has been under investigation for a long time in its conventional dosage form (Fungizone<sup>®</sup>) of mixed micelles of AmB with sodium deoxycholate. It has severe side effects such as fever, chills, hemolysis, vomiting and

nephrotoxicity (Gallis *et al.*, 1990).

Lipid-based formulations of AmB have been developed. After many attempts to decrease the toxicity of AmB by using liposomes, emulsions and other systems; three lipid formulations of AmB (AmBisome<sup>®</sup>, Amphocil<sup>®</sup>, Abelcet<sup>™</sup>) were made commercially available. The toxicity, especially nephrotoxicity, of AmB can be reduced by incorporating it into liposomes or by complexing it to various lipids. Due to the reduced toxicity, lipid AmB formulations can be administered in higher doses which provide greater efficacy. However, these lipid formulations showed low rate of elimination and the increased doses of AmB administration may accumulate in the body (Atkinson and Bennett, 1978). In addition, ingredients of lipid AmB formulations are more expensive and the high costs are a major limitation in clinical practice (Persson *et al.*, 1992).

To solve these problems, cholesteryl carbonate esters (CPC, DCC and SCC) were developed for use as AmB carriers for pulmonary infections. It was hypothesized that the thermotropic liquid crystal formation would improve the drug efficiency and safety. The efficacy was monitored by measuring the bioactivity of AmB in liquid crystal in comparison with pure AmB. The safety of AmB in cholesteryl carbonate esters reaching to the airways was determined to ensure that products did not induce the release of any inflammatory substance in the airways and did not induce the cytotoxicity of respiratory associated cells.

## **6.2 Materials and methods**

### **6.2.1 Potency of AmB in cholesteryl carbonate esters**

The activity (potency) of antibiotics may be demonstrated under suitable conditions by their inhibitory effect on microorganisms (USP29-NF24, 2006). Two general methods are employed: the cylinder-plate or “plate” assay and the turbidimetric or “tube” assay. The cylinder plate method and broth microdilution were employed for microbial assay of AmB in cholesteryl carbonate esters. The cylinder plate method performs the relative potency by determining the clear zone of AmB formulation in the inoculum medium as compared with a clear zone of AmB standard. Broth microdilution method can be used to measure the minimum inhibitory concentrations (MIC). The MIC is that concentration of antifungal agent which inhibits the growth of a fungus under standardized test conditions. The MIC value is based upon a predetermined endpoint, which may be interpreted as an absence of visible growth in a broth containing known concentrations of AmB (adapted from McGinnis and Rinaldi, 1991).

### **6.2.2 Evaluation of AmB formulations potency**

#### **A) Preparation of inoculum and inoculated medium**

The cylinder plate method depends upon diffusion of antibiotic from a vertical cylinder through a solidified agar layer in a petri dish or plate to an extent such that growth of the added microorganism is prevented entirely in a circular area or “zone” around the cylinder containing a solution of the antibiotic. Potency of AmB and AmB formulation were screened by the cylinder plate method with *Saccharomyces*

*cerevisiae* (ATCC 9763, Rockville, MD, USA) approximately  $10^8$  CFU/mL. The *S. cerevisiae* was grown at 29-31 °C on Sabouraud dextrose agar (SDA) (Difco, NJ, USA) for 48 h. The *S. cerevisiae* inoculum was prepared by adjusting to 25 % transmittance at 580 nm with sterile normal saline. Sterile antibiotic medium 19 was used as an inoculated medium. The inoculum (1mL) was mixed with 100 mL of sterile antibiotic medium 19 at 50 °C. Inoculated medium was poured into sterile plate, 8 mL/plate. The medium was left to cool down then put the plate at room temperature. The six cylinder cups were slightly put on the surface of each plate by using a mechanical guide (UPS29-NF24, 2006).

#### **B) Preparation of standard solution and sample solution**

Standard AmB 10 mg was weighed and adjusted with DMSO to 10 mL and used as stock solution. AmB stock solution (1,000 µg/mL) further diluted with DMSO to give concentrations of 12.8, 16, 20, 25, 31.2 µg/mL. Five milliliters of each concentration was pipetted and adjusted with buffer No.10 to 100 mL. The final concentrations of standard AmB ( $S_1$ - $S_5$ ) were 0.64, 0.8, 1.0, 1.25, 1.56 µg/mL, respectively. A sample of AmB formulation was prepared as described in standard AmB preparation to give a final concentration of 1.0 µg/mL ( $U_3$ ).

#### **C) Preparation of buffer No. 10 (0.2 M, pH 10.5)**

Dibasic potassium phosphate 35 g (Fluka, Switzerland) was dissolved in 1000 mL of distilled water and 2 mL of 10 N potassium hydroxide was added into buffer No.10. Buffer No.10 was adjusted by either 18 N of phosphoric acid or 10 N of potassium hydroxide to obtain pH 10.5.

#### **D) Cylinder plate analysis**

For the 1-level assay with a standard curve, dilutions were prepared representing five test levels of the standard ( $S_1$ - $S_5$ ) and a single test level of the unknown ( $U_3$ ) corresponding to  $S_3$  of the standard curve, as defined under preparation of the standard and preparation of the sample. For deriving the standard curve, alternate cylinders were filled on each of three plates with the mean test dilution ( $S_3$ ) of the standard and each of the remaining nine cylinders with one of the other four dilutions of the standard. The process was repeated for the three dilutions of the standard. For each unknown of AmB in CCEs (CPC, DCC, SCC and Chol), alternate cylinders were filled on each of three plates with the median test dilution of the standard ( $S_3$ ), and the remaining nine cylinders with the corresponding test dilution ( $U_3$ ) of the samples. All of plates were incubated at 29-31°C for 16-18 h. These experiments were carried out triplicate. The inhibition zones diameters were measured and calculated the concentration of AmB from standard curve (adapted from UPS29-NF24, 2006).

### **6.2.3 Broth microdilution for antifungal susceptibility testing**

#### **A) Preparation of inoculum**

*C. neoformans* and *C. albicans* were gifts from the Department of Pathology, Faculty of Medicine, Songklanagarind Hospital, PSU, Thailand. *S. cerevisiae* ATCC 9763 was obtained from ATCC (Rockville, MD, USA). Before testing, all yeasts were subcultured on Sabouraud dextrose agar (SDA) (Difco, NJ, USA) at 35 °C for 24-48 h to ensure optimal growth characteristics. Stock suspensions were prepared in sterile 0.85% saline solution and adjusted to give a final concentration



of  $1 \times 10^6$ – $5 \times 10^6$  colony-forming units (CFU)/mL (90% transmittance, 530 nm) (adapted from McGinnis and Rinaldi, 1991).

#### **B) Assay media**

Antibiotic medium 3 was obtained from Merck (Darmstadt, Germany). Broth medium was prepared from 17.5 g of antibiotic medium 3 in 1 L distilled water. Sterilized broth was performed by autoclaving at 121 °C, 15 psi for a minimum of 15 min.

#### **C) Preparation of standard solution and sample solution**

Standard AmB and AmB formulations were dissolved in DMSO at a concentration of 5,000 µg/mL. Stock solutions were stored at -70 °C until use. Subsequently, the stock solutions were diluted with antibiotic medium 3 broth (Merck, Darmstadt, Germany) to concentration of 0.005-10 µg/mL.

#### **D) Broth microdilution analysis**

The microdilution method was adapted from McGinnis and Rinaldi, 1991. Minimum inhibitory concentrations (MICs) were determined in a microtitre assay. Five microliters of inoculum was added in 96-well plate with two-fold serials 100 µL of standard AmB or AmB in liquid crystal (CPC, DCC, SCC and cholesterol) at concentration 0.005-10 µg/mL. The sterile medium was used as a negative control (sterility of medium). Whereas, sterile medium added inoculum was used as positive control (growth promotion of inoculum). The plate was incubated at 30 °C for 48 h and UV absorption was recorded at wavelength 570 nm. The MIC endpoint was defined as

the lowest drug concentration exhibiting of AmB which completely inhibited fungal growth. The last drug dilution showing no growth and all of the other dilutions showing no growth are streaked on SDA. Agitate each well to be tested and remove a sample from the well with a sterile 0.01 mm calibrated loop. Streak the inoculum in a label pie-shaped area on a SDA plate and incubated the plates at 30 °C for 48 h. The minimum lethal concentration (MLC) or minimum fungicidal concentration (MFC) was defined as the last dilution with three or fewer colonies present from two of three wells. All experiments were done in triplicate.

#### **6.2.4 Hemolysis of pure AmB and AmB in cholesteryl carbonate esters**

The human red blood cells lysis was evaluated as described by Metha *et al.* (1984). Briefly, erythrocytes (Blood Bank, Department of Pathology, Faculty of Medicine, Songklanagarind Hospital, PSU, Thailand) were isolated from fresh human blood, washed three times with phosphate buffer saline solution (PBS) and centrifuge at 1500 rpm for 5 min. The standard AmB and AmB formulations were added to the suspended erythrocytes and the suspension diluted with PBS to give final AmB concentrations in the range of 1-8 µg/mL and a final hematocrit of 1%. The solutions were incubated at 37 °C in water bath and sampling at 0.5, 3, 6 and 24 h. The unlysed cells were removed by centrifugation at 3000 rpm for 5 min and hemoglobin in supernatant was determined by its absorbance at 541 nm. Control samples showing no lysis (PBS without AmB; negative control) and 100% lysis with 1% Triton X-100 (Sigma-Aldrich, Steinheim, Germany, positive control) was used in all experiments. According to Equation 6.1, % hemolysis can be calculated:

$$\% \text{Hemolysis} = \left( \frac{\text{Abs} - \text{Abs}_0}{\text{Abs}_{100} - \text{Abs}_0} \right) \times 100 \quad \text{Equation.....6.1}$$

Where: Abs is the absorbance of sample

: Abs<sub>0</sub> is the absorbance of negative control

: Abs<sub>100</sub> is the absorbance of positive control

### **6.2.5 Cytotoxicity and determination of cytokines and nitric oxide production**

#### **A) Small airway epithelial cell (SAEC)**

Small airway epithelial cells (SAEC) were cultured in the clonetics media and its supplement (SAGM bullet kit<sup>®</sup>) provided by Lonza Group Ltd. (Walkerville, MD, USA). The cell was cultured following the Lonza recommended protocol. Briefly, the cell was seeded density was 2,500 cells/cm<sup>2</sup> and incubated under 37 °C, 5% CO<sub>2</sub> and 95% humidity incubator. For subculturing, when the cells are 60 - 80% confluent the cells are rinsed with HEPES buffered saline solution (HEPES-BSS) to wash remaining complex protein which may neutralize trypsin activity. HEPES-BSS is aspirated and the cells are covered with 2 mL of 0.05% trypsin/EDTA solution. After cell released, the trypsin/EDTA activity was neutralized with trypsin neutralizing solution, centrifuged at 1200 rpm for 7 min. Pallet cells were resuspended and then transferred to new culture flask (incubated media at least 30 min before subculture). The cells were used in early passage numbers, since clonetics SAEC cryopreserved cultures are assured for experimental use for fifteen population doubling. All solutions (reagent

pack) used for maintenance and culture of SAEC were from Lonza Group Ltd (Walkerville, MD, USA).

## **B) Alveolar macrophage cell line**

A rat alveolar macrophage cell line NR 8383 (ATCC CRL-2192, Rockville, MD, USA) was established from normal rat lung lavage. The cell exhibit characteristics of macrophage cell: phagocytosis of zymosan, and *Pseudomonas aeruginosa*, non specific esterase activity, Fc receptors, oxidative burst, IL-1 $\beta$ , TNF- $\alpha$  and IL-6 secretion, and replicative response to exogenous growth factors. The cells respond to appropriate microbial, particulate or soluble stimuli with phagocytosis and killing. The NR 8383 cell line provides a homogenous source of highly responsive alveolar macrophages, which can be used *in vitro* to study macrophage related activities (<http://www.atcc.org>). The cell was cultured in F12 Kaighn's cell culture medium with 2 mM L-glutamine adjusted to contain 1.5 g/L sodium bicarbonate (Gibco, Grand Island, NY, USA) supplemented with 15% (v/v) heat inactivated fetal bovine serum, 50 units/mL penicillin, 50  $\mu$ g/mL of streptomycin (Gibco, Grand Island, NY, USA) and incubated under 37 °C, 5% CO<sub>2</sub> and 95% humidity incubator. Cultures were maintained by transferring floating cells to additional flasks. Adherent cells were harvested by scraping. Upon reseeded, about one half of the cells were found to re-attach. The fresh medium was replaced two or three times weekly.

**C) Determination of cytotoxicity of AmB in cholesteryl carbonate esters formulations**

Viabilities of SAEC and AMs were determined by using the MTT assay to detect functioning mitochondria. Live mitochondria transform 3-(4,5-dimethylthiazole-2-yl)-2 diphenyltetrazolium bromide or MTT (Sigma Chemicals, St. Louis, MO, USA) to formazan, which was measured with a spectrophotometer. Briefly, 100  $\mu$ L of  $1 \times 10^5$  cells/mL was cultured in each well of 96-well plate and allowed to adhere and grow overnight in an incubator at 37 °C, under 5% CO<sub>2</sub> and 95% humidity. The following day, the media (100  $\mu$ L) was replaced and 100  $\mu$ L of cell culture media containing either standard AmB or AmB formulations or free AmB solution was added. The plate was then incubated for 24 h. The supernatant from each well of AMs culture was removed and the level of generated inflammatory cytokine by ELISA method or nitric oxide by Griess reagent as described in section 6.2.5 D was assessed. The remaining cell number was measured and compared with the untreated control by MTT assay. Filtered sterilized stock MTT solution (50  $\mu$ L of 5 mg/mL in Dulbecco's phosphate buffer saline, DPBS, Gibco, Grand Island, NY, USA) was added to each well containing 150  $\mu$ L fresh media, which were then incubated for 4 h at 37 °C. After that, the supernatant was carefully removed, and the resulting formazan crystal was dissolved by adding 200  $\mu$ L of DMSO (Riedel-de Haën, Seelze, Germany) and mixed thoroughly. The absorbance was recorded at 570 nm with the microplate reader (Biohit BP 800, Helsinki, Finland). The proportion of viable cells in treated well was compared to the untreated well (Huttunen *et al.*, 2000; Punturee *et al.*, 2004).

**D) Determination of alveolar macrophage response to AmB in cholesteryl carbonate esters formulations**

- *Production of inflammatory cytokines*

The inflammatory cytokines level of TNF- $\alpha$  and IL-1 $\beta$  generated from AMs responding to standard AmB, liquid crystal free AmB, AmB formulations or lipopolysaccharide (LPS) from *E.coli* (positive control) was measured by enzyme linked immunosorbent assay (ELISA) method. Commercial ELISA kits (Quantikine<sup>®</sup> RTA00 and Quantikine<sup>®</sup> RLB00 for rat TNF- $\alpha$  and IL-1 $\beta$ , respectively, R&D systems Inc., MN, USA) were used as described in the product assay procedures. The detectable dose of both TNF- $\alpha$  and IL-1 $\beta$  is less than 5 pg/mL. The assay employs the quantitative sandwich enzyme immunoassay technique (Figure 6.1). A monoclonal antibody specific for rat TNF- $\alpha$  or IL-1 $\beta$  was pre-coated on a microplate (Step 1). Standards, controls and samples were pipetted into the wells and any rat TNF- $\alpha$  or IL-1 $\beta$  present was bound by the immobilized antibody (Step 2). After washing away any unbound substances (Step 3), an enzyme-linked polyclonal antibody specific for rat TNF- $\alpha$  or IL-1 $\beta$  was added in to the wells (Step 4). Following a wash to remove any unbound antibody-enzyme reagent (Step 5), a substrate solution was added to the wells (Step 6). The enzyme reaction yielded a blue product that turned yellow when the stop solution was added (Step 6). The intensity of the color measured was in proportion to the amount of rat TNF- $\alpha$  or IL-1 $\beta$  bound in the initial step. The sample values were then read off the standard curve.

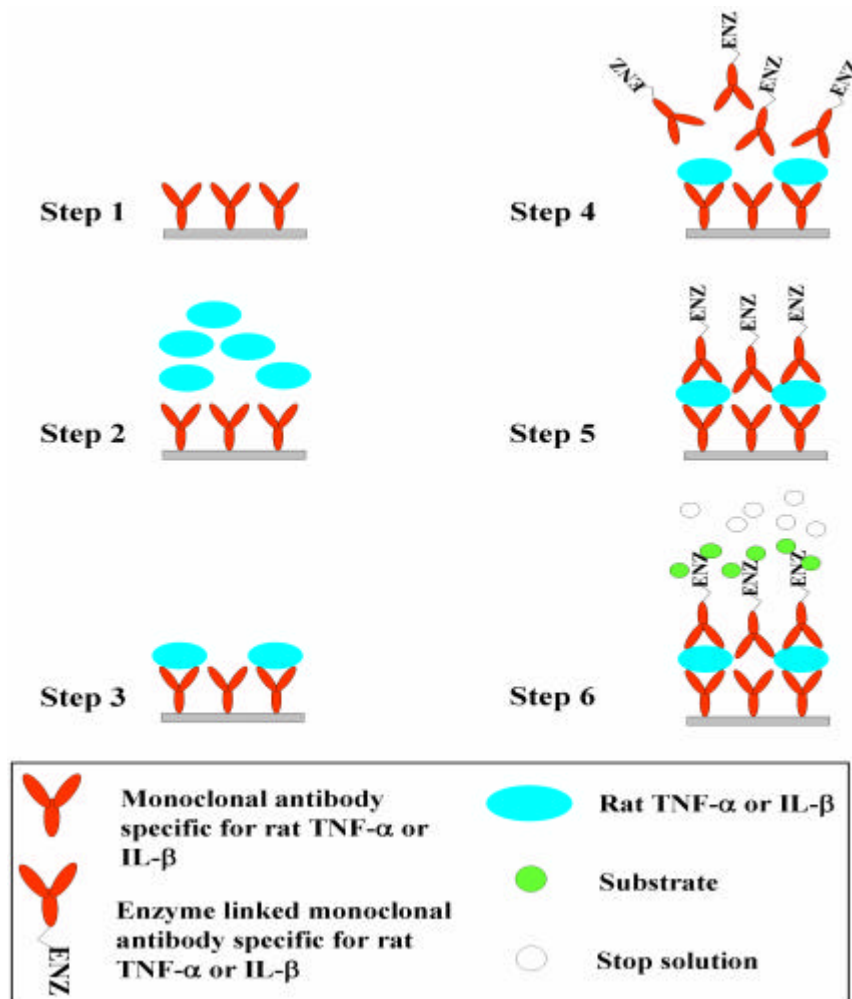


**Figure 6.1** Sandwich enzyme linked immunosorbent assay (adapted from Crowther, 1995).

· *Nitric oxide*

This method was used to investigate nitric oxide in the form of nitrite ( $\text{NO}_2^-$ ), which is one of two primary, stable and nonvolatile breakdown product of NO. This measurement relies on a diazotization reaction of the Griess reagent as shown in

Figure 5.4. Griess reagent was prepared by mixing of 1% sulfanilamide (Sigma Chemicals, St. Louis, MO, USA), 0.1% N-(1-naphthyl)-ethylenediamine dihydrochloride (NED, Sigma Chemicals, St. Louis, MO, USA) and 2.5% phosphoric acid in water. Equal volumes of cell supernatant (100  $\mu$ L) and Griess reagent (100  $\mu$ L) were mixed. The absorbance was determined using a microplate reader (Biohit BP800, Helsinki, Finland) 10 minutes after mixing at 450 nm. The nitrite concentration was calculated from sodium nitrite standard curve (Huttunen *et al.*, 2000; Punturee *et al.*, 2004).

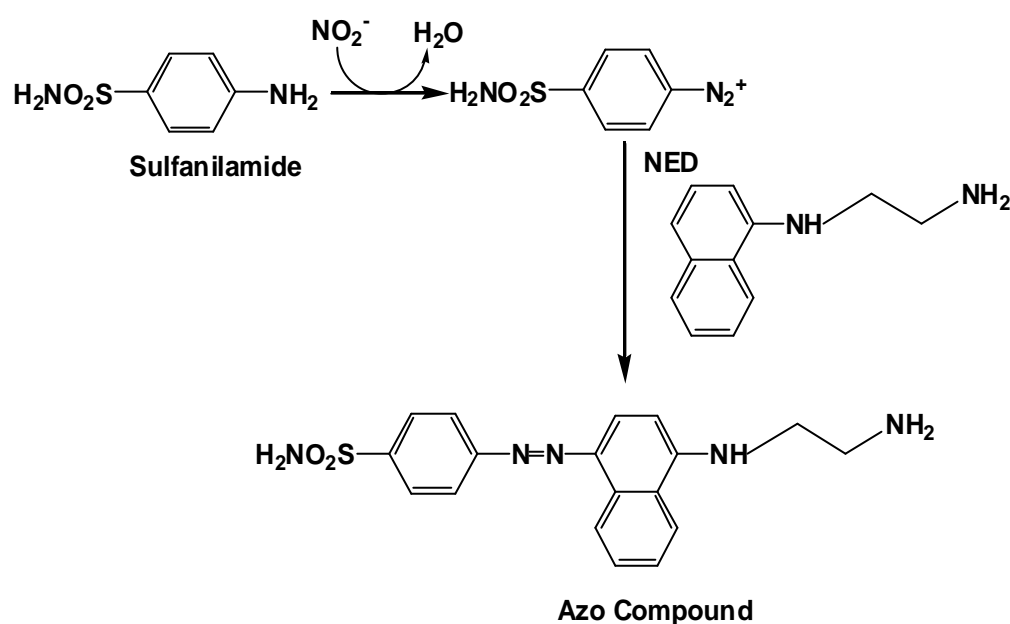


**Figure 6.2** Griess reaction (Promega, 1995)

### 6.2.6 Statistical analysis

Data, when applicable, are presented as mean  $\pm$  SD from at least three separated experiments unless otherwise indicated. The data and all aerosol parameters of each AmB formulation were compared using ANOVA. All statistical comparisons



were calculated using the SPSS software version 11.5 (SPSS, Inc., Chicago, IL). A significance level of  $p$ -value  $< 0.05$  was considered statistically significant.

### **6.3 Results and discussions**

#### **6.3.1 Activity of AmB in cholesteryl carbonate ester dry powder against fungal cells**

In Table 6.1, the potency of pure AmB and AmB in cholesteryl carbonate formulations were carried out by using two methods as explained in sections 6.2.2 and 6.2.3. The potencies with respect to their corresponding percent label amounts of AmB in CPC were 162.8, 163.1 and 178.6 % for Formulations No 1, 2 and 3, respectively. AmB in DCC (Formulations No 4, 5 and 6) gave 129.2, 144.0 and 132.3%. Formulations No 7, 8 and 9 (AmB in SCC) were 152.9, 165.2 and 144.9%, respectively. Whereas, percent label amount (%LA) of AmB in cholesterol (Formulations No 10, 11 and 12) revealed 113.3, 119.7 and 126.5, respectively. In contrast, the pure liquid crystals, CPC, DCC, SCC and cholesterol, did not inhibit the growth of yeasts (data not shown). All of AmB in liquid crystal formulations had higher potency than that of standard AmB ( $p$ -value,  $< 0.05$ ) AmB in CPC and AmB in SCC showed the highest potency, which differed significantly from standard AmB, AmB in DCC and AmB in cholesterol ( $p$ -value,  $< 0.05$ ). The results indicate that liquid crystal may play a role in enhancing the potency of AmB. This remarkable finding may be related to the specific structural properties of the liquid crystal that contains a cholesterol ring. As we know that the fungal membrane contains ergosterol which is structural related to cholesterol, this may enhance AmB transport into fungus cells

and/or greater penetration into the fungus membrane. As a result, the potency of AmB in liquid crystal formulation is higher than that of pure AmB.

Table 6.1 summarizes all susceptibility testings of AmB and AmB in various liquid crystals. In this study, pure AmB against *C. neoformans*, MICs and MFCs ranged from 0.08-0.3 and 0.3-0.6  $\mu\text{g/mL}$ , respectively. For *C. albicans*, MICs were from 0.08 to 0.15  $\mu\text{g/mL}$ ; the corresponding MFC value ranged from 0.3 to 1.25  $\mu\text{g/mL}$ . The AmB in liquid crystals gave lower MICs and MFCs than pure AmB (2-4 times). The MICs of AmB against *C. neoformans* were previously reported 0.06-0.5  $\mu\text{g/mL}$  (Aller *et al.*, 2000), 0.5-2  $\mu\text{g/mL}$  (Archibald *et al.*, 2004), 0.03-0.5  $\mu\text{g/mL}$  (Lopez-Jodra *et al.*, 2000) and 0.0625-2  $\mu\text{g/mL}$  (Lozano-Chiu *et al.*, 1998). Whereas, MICs of AmB against *C. albicans* were reported at 0.03-0.5  $\mu\text{g/mL}$  (Van Eldere *et al.*, 1996) and 0.015-0.25  $\mu\text{g/mL}$  (Park *et al.*, 2006). The results suggest that liquid crystals provided a synergistic effect of AmB to inhibit fungus growth. This may be due to the association of the liquid crystal with the fungal membrane that facilitates transfer or perhaps induces the formation of ionophores (Umegawa, 2007). AmB may transport into fungal cells together with liquid crystal molecules. This still needs to prove the statement.

**Table 6.1** Potency, minimum inhibitory concentration (MIC) and minimum fungicidal concentration (MFC) of AmB in cholesteryl carbonate ester dry powder (n = 3).

Formulation	Composition	Potency	<i>S. cerevisiae</i> ATCC 9763		<i>C. albicans</i>		<i>C. neoformans</i>	
No.	(mole ratio)	(%)	MIC (mg/mL)	MFC (mg/mL)	MIC (mg/mL)	MFC (mg/mL)	MIC (mg/mL)	MFC (mg/mL)
Pure AmB	AmB	100	0.08-0.3	0.3-2.5	0.08-0.3	0.3-1.25	0.08-0.3	0.3-0.6
1	AmB:CPC (1:3)	162.8	0.08-0.15	0.08-0.15	0.08-0.15	0.08-0.15	0.08-0.15	0.08-0.3
2	AmB:CPC (1:6)	163.1	0.08-0.15	0.08-0.15	0.08-0.15	0.08-0.15	0.08-0.15	0.08-0.3
3	AmB:CPC (1:12)	178.6	0.08-0.15	0.08-0.15	0.08-0.15	0.08-0.15	0.08-0.15	0.08-0.3
4	AmB:DCC (1:3)	129.2	0.08-0.15	0.15-0.3	0.08-0.15	0.15-0.3	0.08-0.15	0.15-0.6
5	AmB:DCC (1:6)	144.0	0.08-0.15	0.15-0.3	0.08-0.15	0.15-0.15	0.08-0.15	0.08-0.3
6	AmB:DCC (1:12)	132.3	0.08-0.15	0.15-0.3	0.08-0.15	0.15-0.3	0.08-0.15	0.15-0.3
7	AmB:SCC (1:3)	152.9	0.08-0.15	0.15	0.08-0.15	0.08-0.15	0.08-0.15	0.08-0.3
8	AmB:SCC (1:6)	165.2	0.08-0.15	0.08-0.15	0.08-0.15	0.08-0.15	0.08-0.15	0.08-0.3
9	AmB:SCC (1:12)	155.9	0.08-0.15	0.08-0.15	0.08-0.15	0.08-0.15	0.08-0.15	0.08-0.3
10	AmB:Chol (1:3)	113.3	0.08-0.15	0.15-0.6	0.08-0.15	0.15-0.6	0.08-0.15	0.15-0.6
11	AmB:Chol (1:6)	119.7	0.08-0.15	0.15-0.6	0.08-0.15	0.15-0.6	0.08-0.15	0.15-0.6
12	AmB:Chol (1:12)	126.5	0.08-0.15	0.15-0.6	0.08-0.15	0.15-0.3	0.08-0.15	0.15-0.6

### 6.3.2 Hemolysis of AmB in cholesteryl carbonate ester

Figure 6.3 (A, B, C, D and E) shows the resulting hemolysis from pure CPC, DCC, SCC, cholesterol and AmB, which was carried out at various concentrations and times interval. The hemolysis of pure liquid crystals was less than 5% (at concentration 80  $\mu\text{g/mL}$ , 24 h incubation time), which is in contrast to pure AmB that gave the highest erythrocyte lysis (up to 32%, 24 h). For AmB in liquid crystal formulations, RBC lysis was observed in a concentration of AmB 8, 4, 2 and 1  $\mu\text{g/mL}$  at various incubation times (0.5, 3, 6 and 24 h). The hemolysis from AmB in liquid crystal at low concentration ( $\leq 2\mu\text{g/mL}$ ) and short incubated time gave the lowest erythrocyte lysis ( $< 1\%$ ) at 30 min. However, higher hemolysis was obtained when concentration of AmB  $\geq 8\mu\text{g/mL}$  and long incubation time (24 h). AmB-DCC and AmB-cholesterol exhibited toxicity to human RBC ( $\sim 10\%$  hemolysis) when AmB concentration increased to  $8\mu\text{g/mL}$ . In addition, AmB-liquid crystals at 1:3 mole ratio caused the highest erythrolysis when compared to other two mole ratios (1:6 and 1:12). These results correlated with the drug release profile which percent release of AmB from AmB-liquid crystal reached toxic concentrations ( $17\mu\text{g/mL}$ , 100% released). Moreover, AmB-SCC formulations showed more erythrolysis (up to 15%) than other three liquid crystals. This may be due to an inorganic sodium salt in SCC molecule.

The results indicate that AmB in liquid crystal formulations had less toxicity to human RBC, whereas pure AmB caused high hemolysis in a comparison of concentration of AmB  $\geq 2\mu\text{g/mL}$  and incubation time longer than 0.5 h. This may be due to the stabilizing effect of the liquid crystal (CPC, DCC, SCC and cholesterol) that limited transfer of AmB to the RBC. In particular, Forster *et al.* (1988) reported that

lecithin-stabilized emulsion showed very low toxicity. They speculated that the low toxicity of liposome and lecithin-stabilized emulsion was from the strong AmB-phospholipid interaction by binding, consistent with their binding studies (Bolard *et al.* 1980; Witzke and Bittman, 1984; Jullien *et al.*, 1990). Moreover, Fukui and coworkers (2003) used lecithin as the stabilizer in lipid nano-sphere (LNS)-AmB. LNS-AmB showed no erythrocyte lysis. Thus, the liquid crystals used in this study may be operating by a similar mechanism.

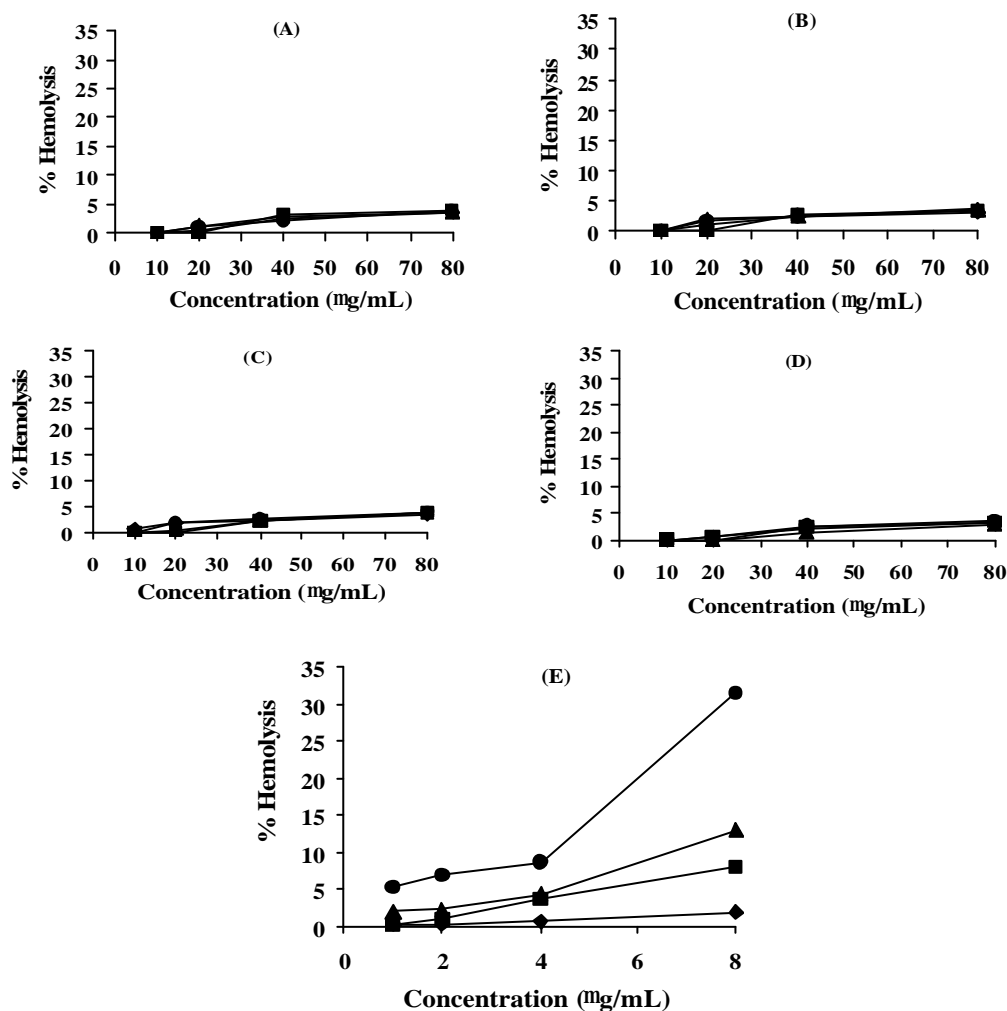


**Figure 6.3** *In vitro* hemolysis after incubation with pure CPC (A), pure DCC (B), pure SCC (C), pure cholesterol (D) and pure AmB (E) at various times; 0.5 h (◆), 3 h (■), 6 h (▲) and 24 h (●) (mean  $\pm$  SD, n = 3)

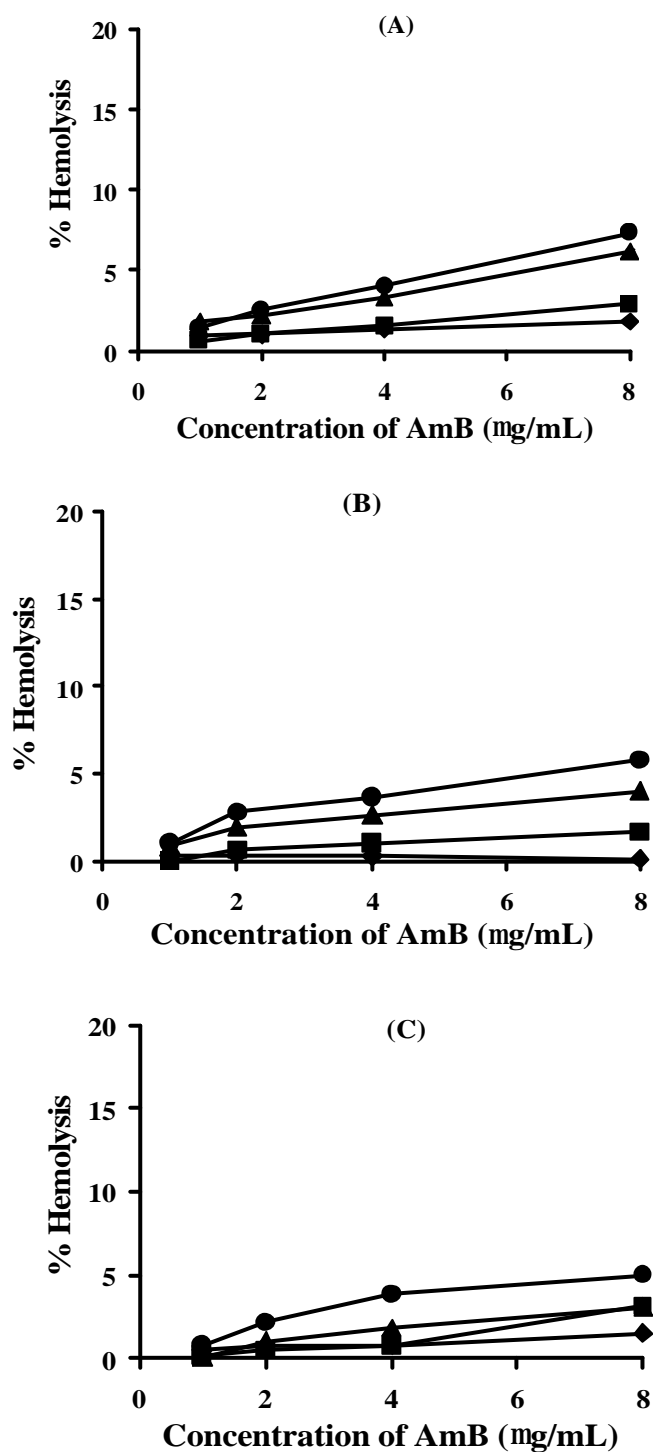


**Figure 6.4** *In vitro* hemolysis after incubation with AmB in CPC; mole ratios 1:3 (A), 1:6 (B) and 1:12 (C) at various times; 0.5 h (◆), 3 h (■), 6 h (▲) and 24 h (●) (mean  $\pm$  SD, n = 3)

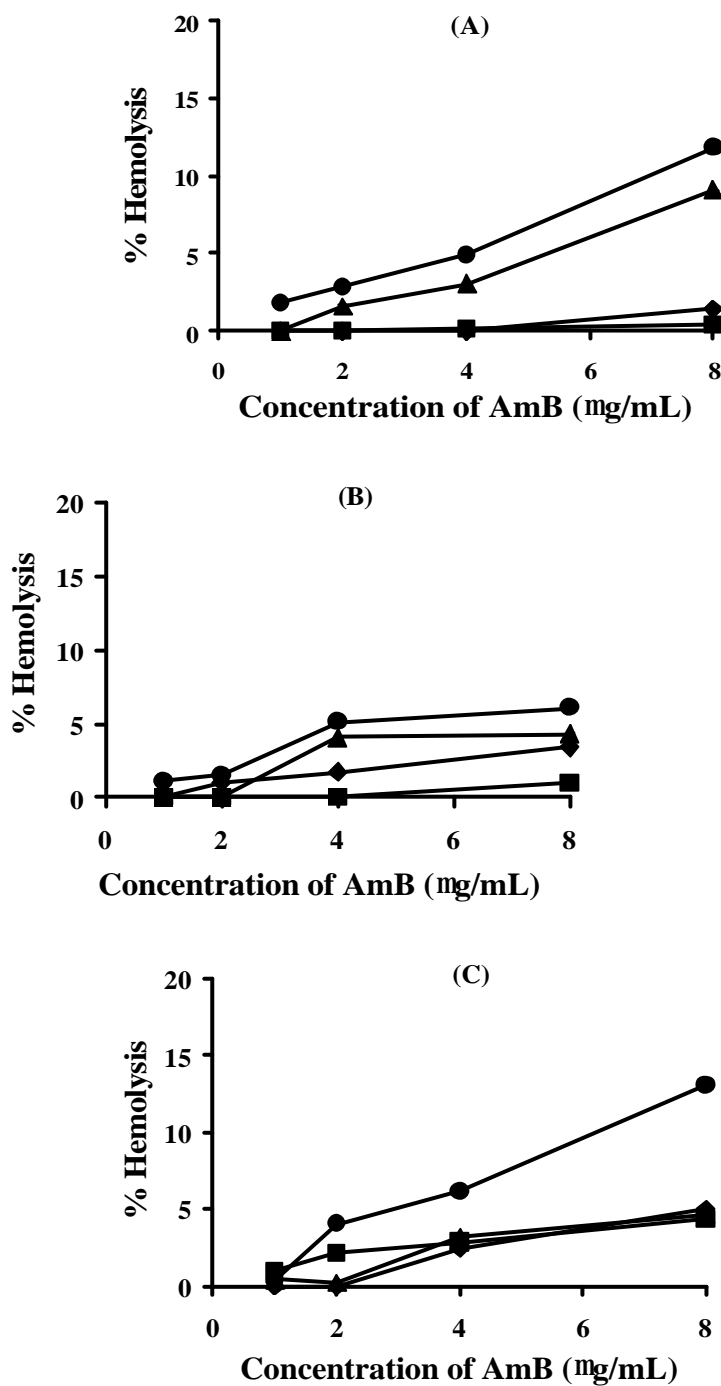


**Figure 6.5** *In vitro* hemolysis after incubation with AmB in DCC; mole ratios 1:3 (A), 1:6 (B) and 1:12 (C) at various times; 0.5 h (◆), 3 h (■), 6 h (▲) and 24 h (●) (mean  $\pm$  SD, n = 3)

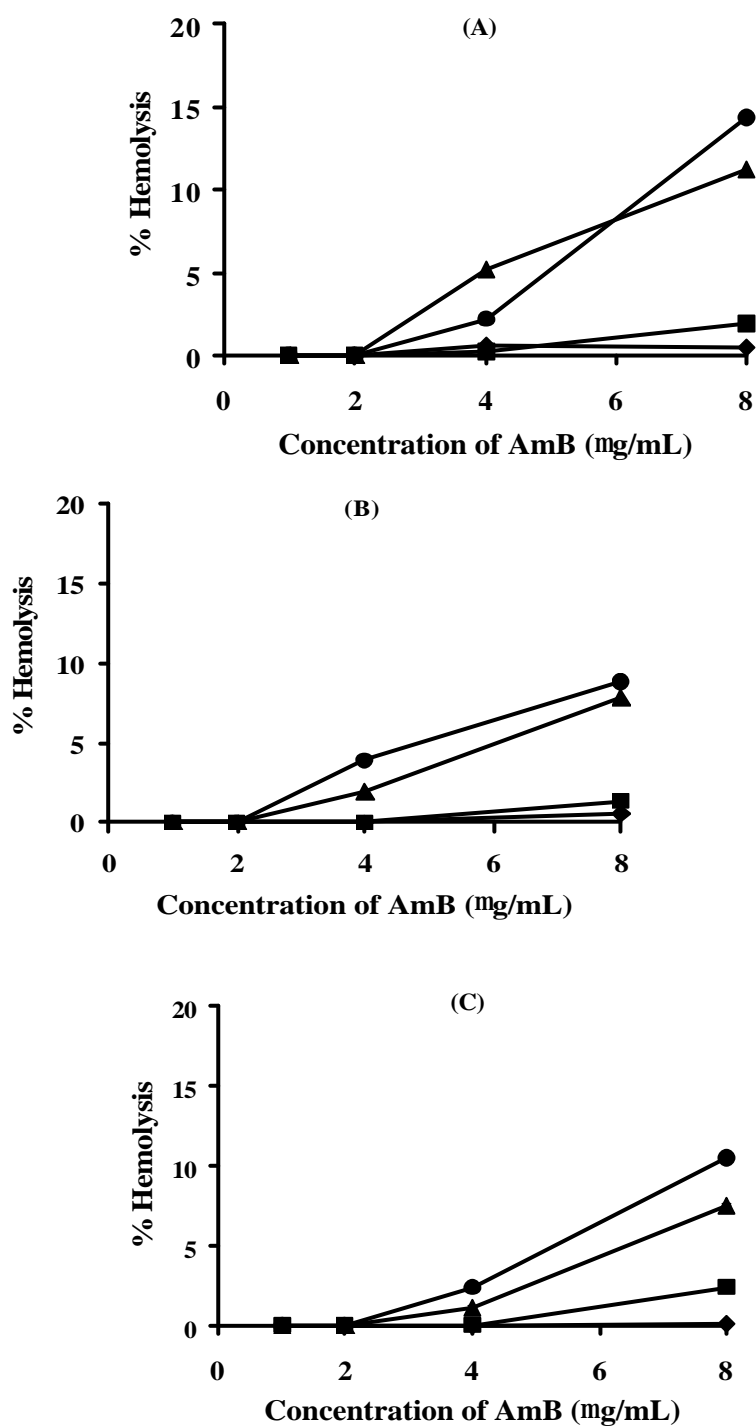


**Figure 6.6** *In vitro* hemolysis after incubation with AmB in SCC; mole ratios 1:3 (A), 1:6 (B) and 1:12 (C) at various times; 0.5 h (◆), 3 h (■), 6 h (▲) and 24 h (●) (mean  $\pm$  SD, n = 3)



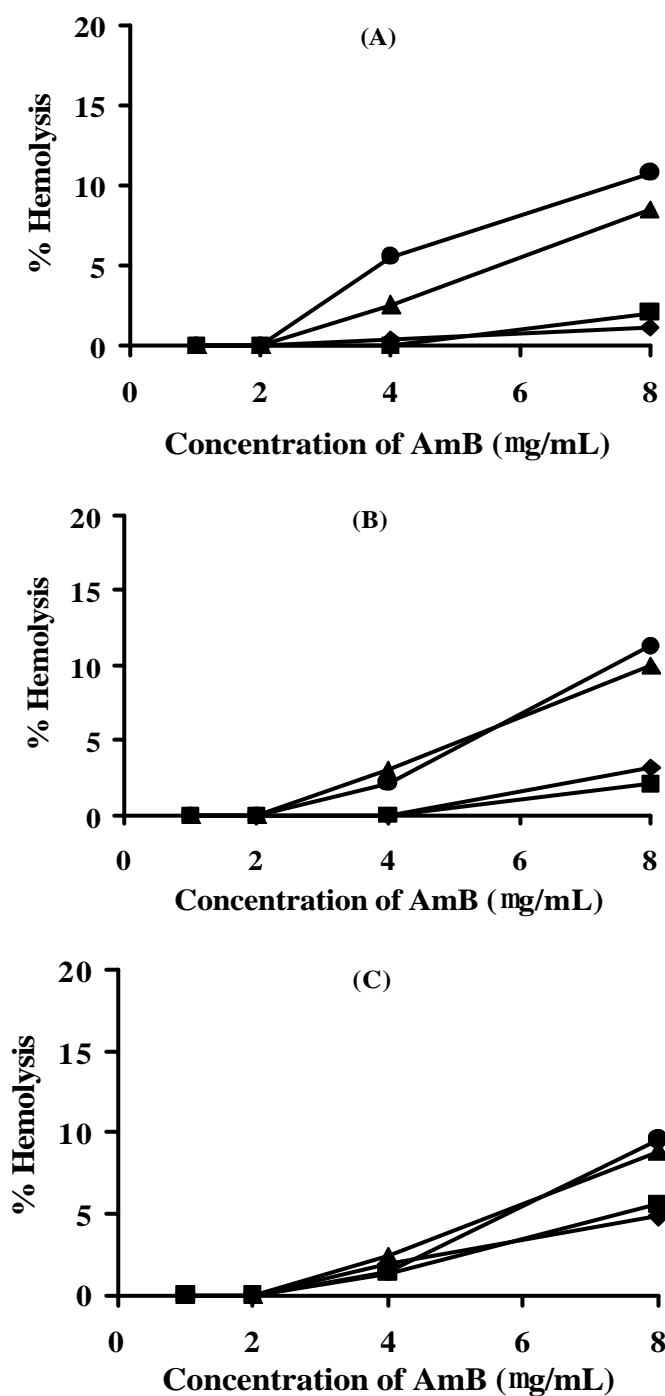


**Figure 6.7** *In vitro* hemolysis after incubation with AmB in cholesterol; mole ratios 1:3 (A), 1:6 (B) and 1:12 (C) at various times; 0.5 h (◆), 3 h (■), 6 h (▲) and 24 h (●) (mean  $\pm$  SD, n = 3)

### 6.3.3 Cytotoxicity of AmB in cholesteryl carbonate ester to the respiratory tract cell lines

The viability of SAEC and AMs was estimated after challenging the cultures with pure liquid crystals (CPC, DCC, SCC and cholesterol) at different concentrations from 10-80  $\mu\text{g/mL}$ . All pure liquid crystals are likely to be safe for respiratory cell lines (Figure 6.8), since almost at least 90% SAEC and AMs remained viable. In the case of pure AmB, viability of SAEC cell was decreased from 80, 75 and 65% when high concentrations were 8, 16 and 32  $\mu\text{g/mL}$  in respectively order. Similarly, the AMs viability with pure AmB was rapidly decreased from 90 to 40% with an increased in concentration of AmB from 1 to 32  $\mu\text{g/mL}$ . These results are in agreement with dissolution and hemolysis studies obtained with pure AmB.

In the presence of pure AmB, the viability of AMs was less than that seen with SAEC cell ( $p\text{-value} < 0.05$ ). The results suggest that AMs are more sensitive to AmB than SAEC cell lines. AMs are phagocytic cells that play an important role in early pulmonary defense against inhaled substances (Hocking and Glode, 1979). It can be envisaged that free AmB has to be encapsulated to prevent its toxicity to AM. AmB in CPC (Formulations No 1, 2 and 3) were likely to be safe for both respiratory cell lines (SAEC and AMs). The viability of SAEC and AMs was maintained over 80% with all formulations at concentrations ranges 1-32  $\mu\text{g/mL}$  (Figure 6.9).

The viability of cells incubated with AmB in DCC (Formulations No 4, 5 and 6) is shown in Figure 6.10. A concentration of AmB  $\geq 8 \mu\text{g/mL}$  induced toxicity, with gave the viability of SAEC cell less than 80%. However, AMs cell showed a smaller toxic response to AmB in DCC. The viability of both cell types with AmB in SCC (Formulations No 7, 8 and 9) was dramatically reduced (80 to 55%) when the

concentration was increased from 8 to 32  $\mu\text{g/mL}$ . Whereas, the viability of SAEC and AMs cells could be maintained over 80% when the concentration of AmB was decreased lower than 4  $\mu\text{g/mL}$  (Figure 6.11).

Figure 6.12 shows the viability of SAEC and AMs cells after incubation with AmB in cholesterol. The viable of SAEC cells was about 100% in Formulation No 10 while the viability of AMs cells was decreased to 75% (at AmB concentration 32  $\mu\text{g/mL}$ ). Formulations No 11 and 12 expressed highly toxic in both SAEC and AMs cells. However, this toxic concentration ( $> 4 \mu\text{g/mL}$ ), which is unlikely to occur in the respiratory tract following inhalation administration. This is 20 times higher than the MIC of AmB against the fungal cells. Hence, this dose need not happen in the real life application.

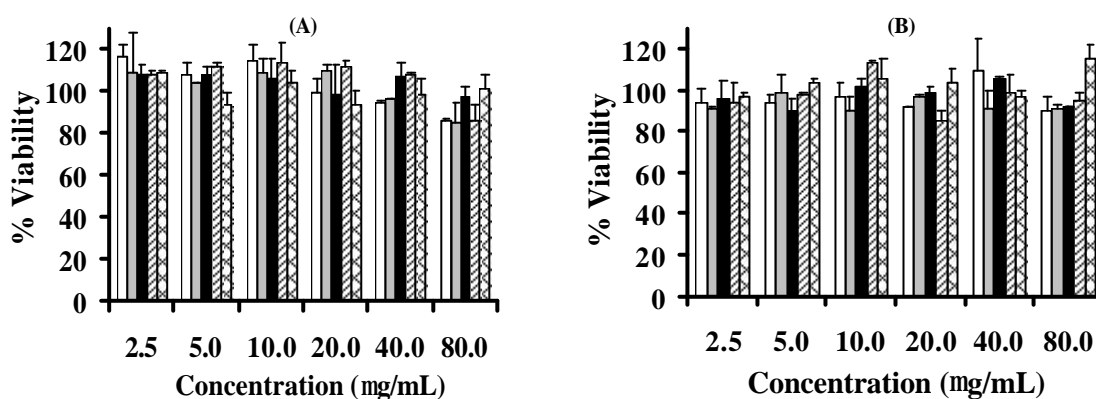


**Figure 6.8** Viability of SAEC (A) and AMs (B) after they have been incubated with pure CPC (□), pure DCC (■), pure SCC (■), pure Chol (▨) and untreated cell line (⊠) (mean  $\pm$  SD, n=3)

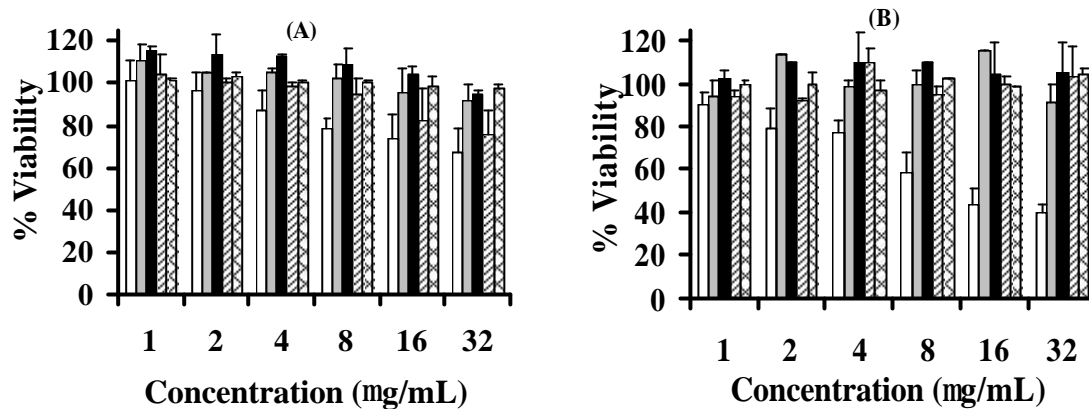


**Figure 6.9** Viability of SAEC (A) and AMs (B) after they have been incubated with pure AmB (□), AmB in CPC; Formulation No 1 (■), Formulation No 2 (■), Formulation No 3 (▨) and untreated cell line (▨)(mean  $\pm$  SD, n = 4)

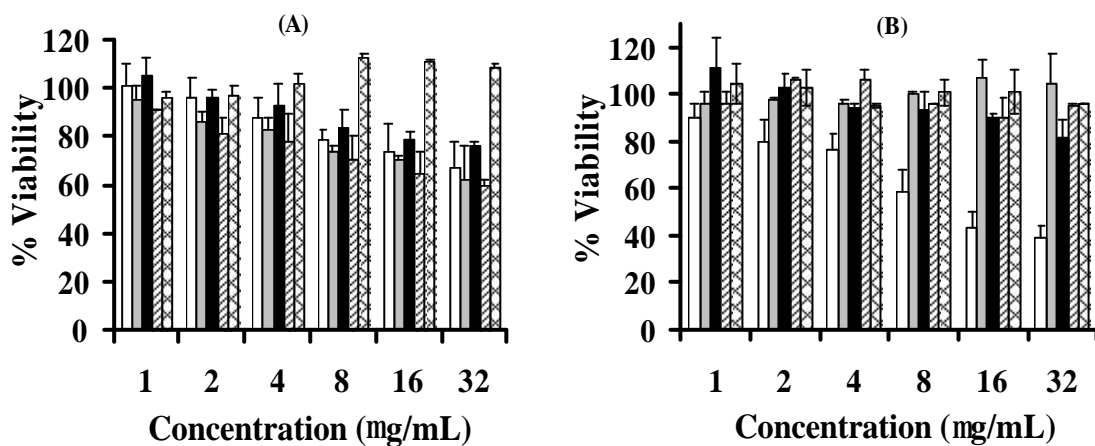


**Figure 6.10** Viability of SAEC (A) and AMs (B) after they have been incubated with pure AmB (□), AmB in DCC; Formulation No 4 (■), Formulation No 5 (■),

Formulation No 6 (▨) and untreated cell line (▩)(mean  $\pm$  SD, n = 4)

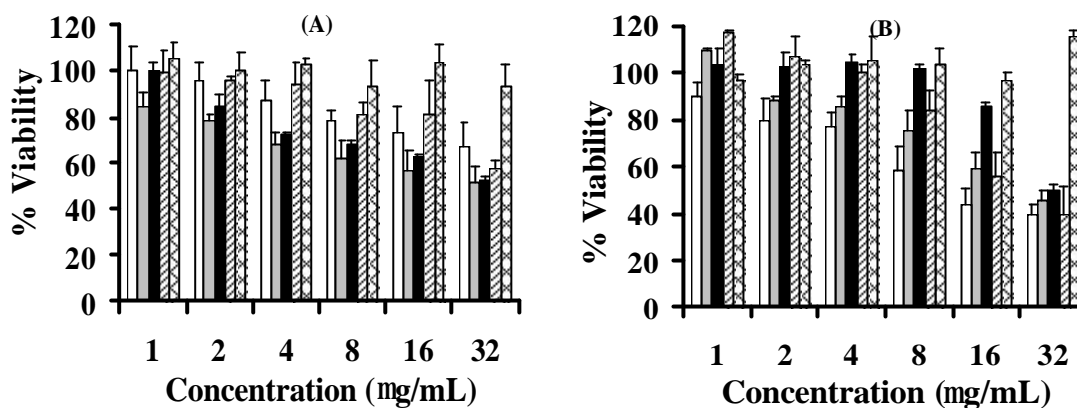


**Figure 6.11** Viability of SAEC (A) and AMs (B) after they have been incubated with pure AmB (□), AmB in SCC; Formulation No 7 (■), Formulation No 8 (■), Formulation No 9 (▨) and untreated cell line (▩)(mean  $\pm$  SD, n = 4)

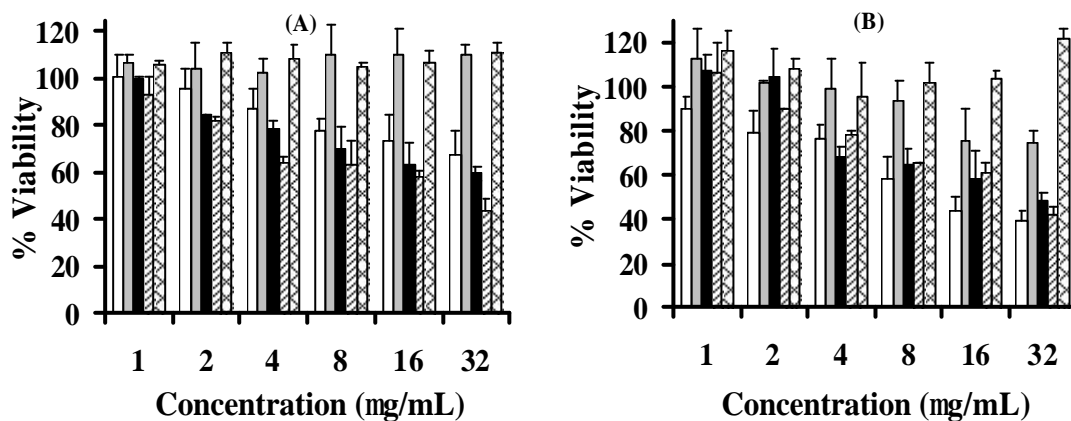


**Figure 6.12** Viability of SAEC (A) and AMs (B) after they have been incubated with pure AmB (□), AmB in cholesterol; Formulation No 10 (■), Formulation No 11 (■),

Formulation No 12 (▨) and untreated cell line (▨)(mean ± SD, n = 4)

#### **6.3.4 Immunological response of AMs to AmB in cholesteryl carbonate ester dry powder formulations**

AMs are phagocytic cells and play an important role in pulmonary defense and are known to undergo increased oxidative metabolism (Fantone and Ward, 1982) and release of inflammatory cytokines (IL-1 $\beta$  or TNF- $\alpha$ ) (Driscoll and Maurer, 1991) following their activation by phagocytosis of particulates. Accordingly, the response of AmB to liquid crystal formulations may reflect the potential safety/toxicity of such formulations when delivered to the peripheral airways. Thus, the induction of an oxidative burst and release of cytokines (IL-1 $\beta$  and TNF- $\alpha$ ) of AMs cell was assessed in an *in vitro* experiment.

Despite the potential concern, AMs did not produce IL-1 $\beta$ , TNF- $\alpha$  and nitric oxide responding to AmB in liquid crystal formulation, pure liquid crystal, compared to LPS from *E. coli*. After AMs were incubated with different concentrations of AmB for 24 h, IL-1 $\beta$ , TNF- $\alpha$  and nitric oxide from the cell culture supernatant are shown in Figures 6.13–6.16, respectively. The concentration of LPS to stimulate AMs to produce the immunological response was less than the concentration of AmB formulation sample for 1,000 times. LPS activated AMs to produce inflammatory cytokines significantly higher than AmB formulation ( $p$ -value < 0.05). Production of IL-1 $\beta$ , TNF - $\alpha$  and nitric oxide by AMs were detected at very low level, while very high level of IL-1 $\beta$ , TNF- $\alpha$  and nitric oxide was generated from AMs exposed to LPS. AmB-CPC and AmB-DCC mixtures stimulated AMs cells to produce proinflammatory cytokines less than those of AmB-SCC and AmB-cholesterol. However, these levels of cytokines are much lower than the reported toxic levels (Meldrum *et al.*, 2009). When concentration of AmB in liquid crystals less than 8

$\mu\text{g/mL}$ , the exposed AMs produced nitric oxide at a similar level as that in the control except the AmB-SCC. However, AMs produced a high concentration of nitric oxide when they were incubated with AmB  $\geq 8 \mu\text{g/mL}$  (2-6  $\mu\text{M}$ ). Thus, AmB in liquid crystal (CPC, DCC, SCC and cholesterol) did not cause the AMs to produce the toxic cytokines and NO at a level that cascade to other inflammatory mediators. This result correlated with the hemolysis and cytotoxicity testing.

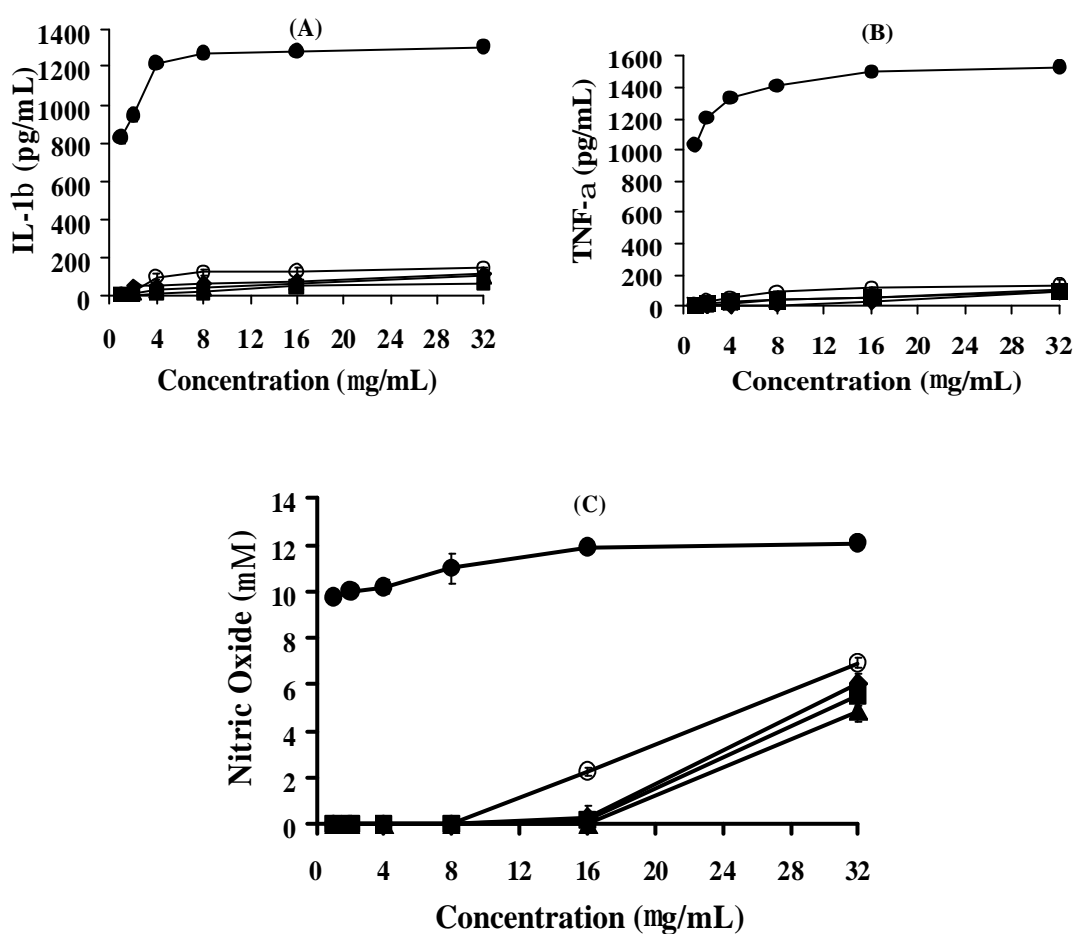


**Figure 6.13** The level of inflammatory cytokine (A): IL-1 $\beta$ , (B): TNF- $\alpha$  and (C): nitric oxide produced from AMs after exposure with pure AmB(○), AmB in CPC Formulation No 1(◆), 2 (■), 3 (▲) and LPS from *E. coli* (●) for 24 h (mean  $\pm$  SD, n = 4)



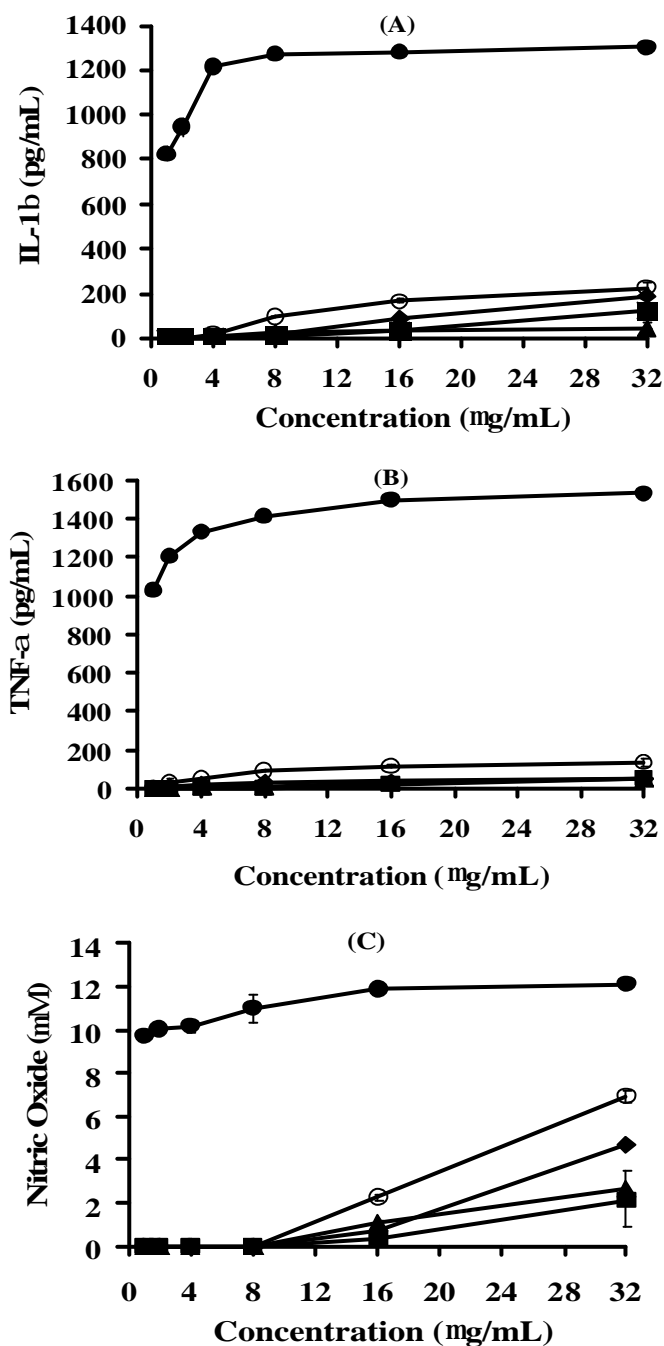


**Figure 6.14** The level of inflammatory cytokine (A): IL-1 $\beta$ , (B): TNF- $\alpha$  and (C): nitric oxide produced from AMs after exposure with pure AmB(○), AmB in DCC Formulation No 4 (◆), 5 (■), 6 (▲) and LPS from *E. coli* (●) for 24 h (mean  $\pm$  SD, n = 4)

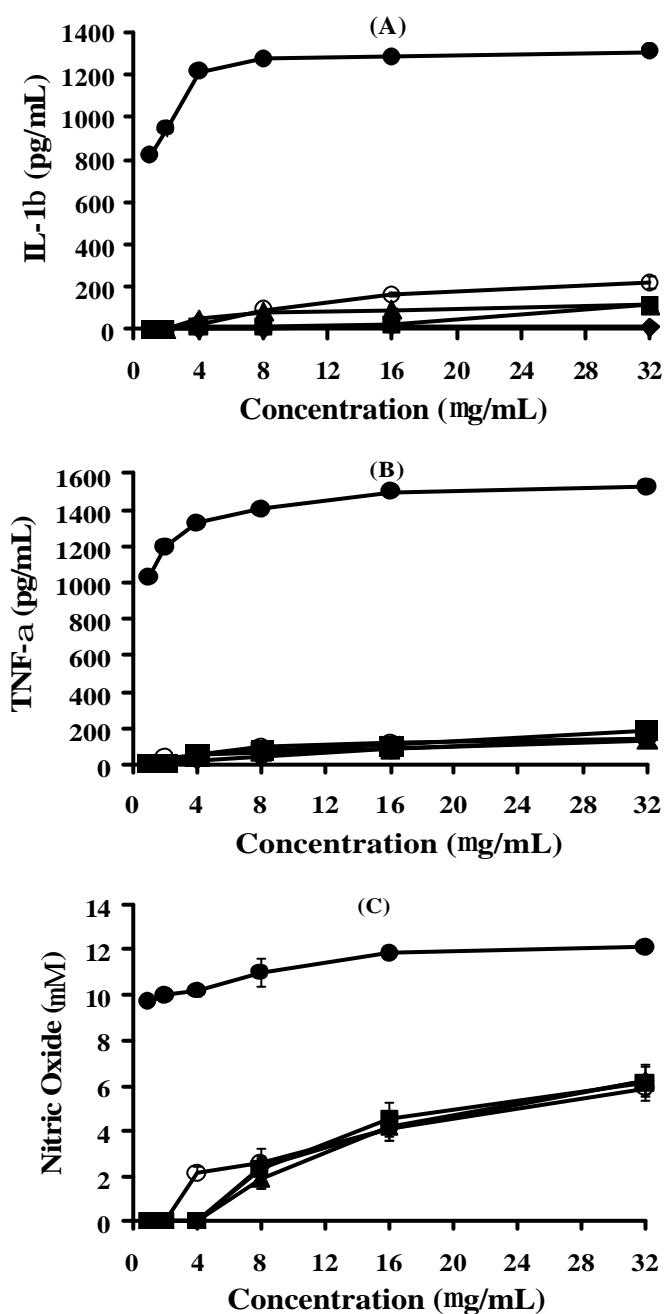


**Figure 6.15** The level of inflammatory cytokine (A): IL-1 $\beta$ , (B): TNF- $\alpha$  and (C): nitric oxide produced from AMs after exposure with pure AmB(○), AmB in SCC Formulation No 7 (◆), 8 (■), 9 (▲) and LPS from *E. coli* (●) for 24 h (mean  $\pm$  SD, n = 4)

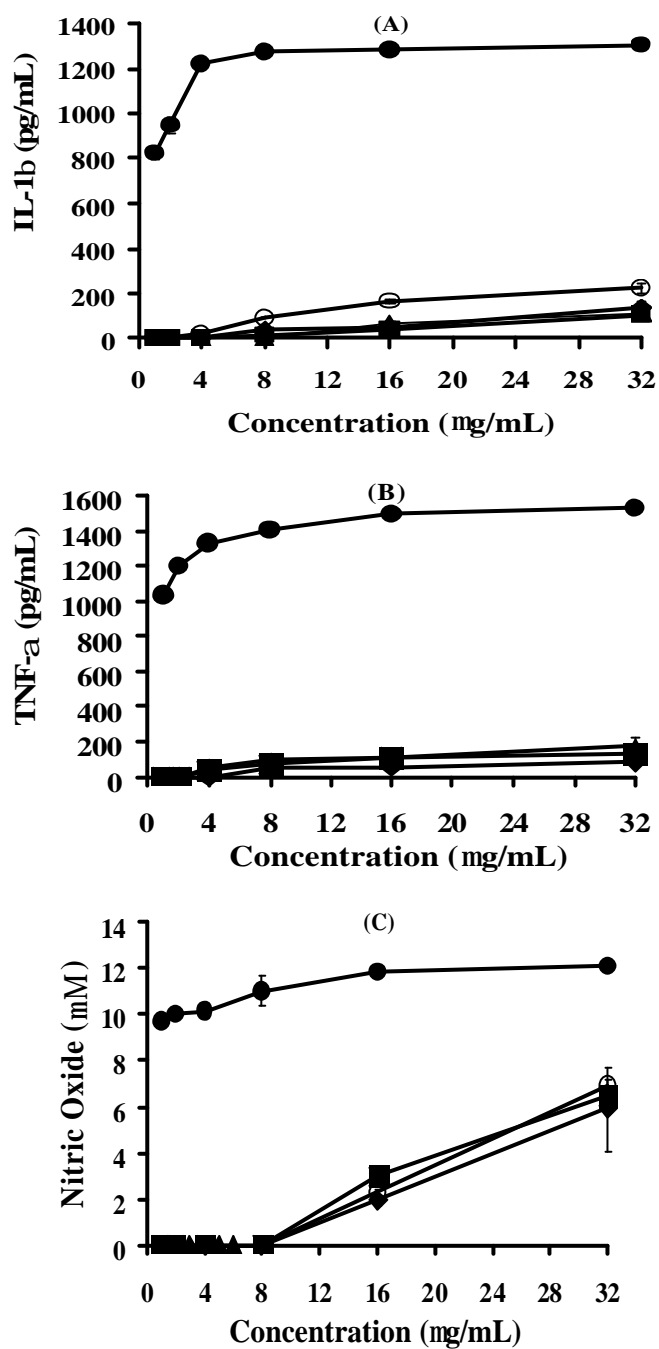


**Figure 6.16** The level of inflammatory cytokine (A): IL-1 $\beta$ , (B): TNF- $\alpha$  and (C): nitric oxide produced from AMs after exposure with pure AmB(○), AmB in cholesterol Formulation No 10 (◆), 11 (■), 12 (▲) and LPS from *E. coli* (●) for 24 h (mean  $\pm$  SD, n = 4)

## 6.4 Conclusions

In this study, we have evaluated the efficacy and toxicity of cholesteryl carbonate ester formulations of AmB. AmB formulations retained the potent activity against fungal cells. In fact, incorporation of AmB into cholesteryl carbonate esters (CPC, DCC and SCC) has been shown to enhance antimicrobial activity when compared to free drug. The human hemolysis in AmB formulations was significantly less than that observed with pure AmB, and only high concentrations (far in excess of the MIC) coupled with long incubation times were able to illicit a toxic response. In addition, AmB in cholesteryl carbonate formulations were less toxic to respiratory associated cells, since they did not induce the toxicity to the cells and did not activate AMs to produce the inflammatory cytokines and nitric oxide whereas free AmB induced cytotoxicity at the equivalent concentration. Therefore, cholesteryl carbonate ester formulations were shown to have enhanced efficacy and reduced toxicity in comparison with free AmB, and thereby may provide a more favorable means to eradicate pulmonary fungal infections.

## CHAPTER 7

### CONCLUSIONS

Cholesteryl carbonate esters, cholesteryl palmityl carbonate (CPC), dicholesteryl carbonate (DCC) and sodium cholesteryl carbonate (SCC), were synthesized and characterized as thermotropic liquid crystals. The phase behavior of three thermotropic liquid crystals are quite different, due to their molecular structure composition; CPC consists of cholesterol ring conjugated with alkyl chain via carbonate ester, DCC composes of two cholesterol rings conjugated by carbonate ester and SCC contains of cholesterol ring conjugate by carbonate ester together with inorganic sodium salt. Nevertheless, liquid crystal compounds are more stable and non labile in solid state at RT. Moreover, cholesteryl carbonate liquid crystals were evidently to be non toxic to human RBC and respiratory cell lines. Thus, they might be suitable to develop as drug carrier system in aerosol formulations.

Dry powder of AmB in thermotropic liquid crystals was successfully prepared by solvent evaporating method. However, it is still needed to further improve the aerosolized characteristics to decrease its MMAD and obtain high FPF. Both AmB in liquid crystals formulations have been shown to have physical and chemical study over a period of this study. From the potency and susceptibility testing against yeasts, *S. cerevisiae*, *C. neoformans* and *C. albicans*, the MICs of AmB in cholesteryl carbonate liquid crystals are 2 - 4 times lower than that of standard AmB. The cholesteryl carbonate in these formulations improved the efficacy of AmB. The cytotoxicity

examinations of respiratory associated cells and human hemolysis show higher viability when they were exposed to AmB in liquid crystals formulations as compared with pure AmB. In addition, alveolar macrophage cell lines were not stimulated to produce inflammatory cytokines when incubation with liquid crystal or AmB in liquid crystal. These are supporting evidences of the potential to develop AmB in cholesteryl carbonate liquid crystals dry powder as an alternative antifungal systemic treatment. Finally, the success in pre-clinical study of AmB in liquid crystal dry powder inhaler will bring further into clinical studies in systemic fungal infectious patients. This has to be compare with a conventional treatment.

## BIBLIOGRAPHY

- Abu-Salah, K.M. 1996. Amphotericin B: an update. *Br. J. Biomed Sci.* 53, 122 – 133.
- Adjei, A.L. and Gupta, P.K. 1997. Inhalation delivery of therapeutic peptides and proteins. New York: Marcel Dekker Inc.
- Adler-Moore, J.P. and Proffitt, R.T. 1993. Development, characterization, efficacy and mode of action of AmBisome, a unilamellar liposomal formulation of amphotericin B. *J. Liposome Res.* 3, 429-450.
- Adler-Moore, J.P., and Proffitt, R.T. 1998. AmBisome: Long circulating liposomal formulation of amphotericin B. In: Woodle, M.C. and Storm G. (Eds), Long circulating liposomes: Old drugs, new therapeutics. New York: Springer-Verlag, pp 185-206.
- Ali, S., Minchey, S., Janoff, A. and Mayhew, E. 2000. A differential scanning calorimetry study of phosphocholines mixed with paclitaxel and its bromoacylated taxanes. *Biophys. J.* 78, 246-256.
- Allen, S.D., Sorensen, K.N., Nejdil, M.J., Durrant, C. and Proffit, R.T. 1994. Prophylactic efficacy of aerosolized liposomal (AmBisome) and non-liposomal (Fungizone) amphotericin B in murine pulmonary aspergillosis. *J. Antimicrob. Chemother.* 34, 1001-1013.
- Aller, A.I., Martin-Mazuelos, E., Gutierrez, M.J., Bernal, S., Chavez, M. and Recio, F.J. 2000. Comparison of the E-test and microdilution method for antifungal susceptibility testing of *Cryptococcus neoformans* to four antifungal agents. *J. Antimicrob. Chemother.* 46, 997-1000.
- AmBisome<sup>®</sup> : drug description (<http://www.rxlist.com/ambisome-drug.htm>)

American Type Cell Culture Collection 2008. [http:// www.atcc.org](http://www.atcc.org)

Antoniadou, A. and Dupont, B. 2005. Lipid formulations of AmB: where are we today?

*J. Med. Mycol.* 15, 230-238.

Archibald, L.K., Tuohy, J., Wilson, D.A., Nwanyanwu O., Kazembe, P.N.,

Tansuphasawadikul, S., Eampokalap, B., Chaovavanich, A., Reller, L.B., Jarvis,

W.R., Hall, G.S. and Procop, G.W. 2004. Antifungal susceptibility of

*Cryptococcus neoformans*. *Emerg. Infect. Dis.* 10, 143-145.

Ashurst, I., Malton, A., Prime, D. and Sumbly, B. 2000. Latest advances in the

development of dry powder inhalers. *Pharm. Sci. Technol. Today.* 3, 246-256.

Atkinson, A.J. And Bennett, J.E. 1978. Amphotericin B pharmacokinetics in humans.

*Antimicrob. Chemother.* 13, 271-276.

Baginski, M., Resat, H. and Borowski, E. 2002. Comparative molecular dynamics

simulations of amphotericin B-cholesterol/ergosterol membrane channels.

*Biochim. Biophys. Acta.* 1567, 63-78.

Baum, G.L. and Rhodes, J. 1998. In: Pulmonary fungal infections. Baum, G.L. Crapo,

J.D., Celli, B.R., Karlinsky, J.B. (Ed). 6<sup>th</sup> Ed., Textbook of pulmonary disease.

Philadelphia: Lippincott-Raven Publisher.

Beaucage, G. 1995. Approximations leading to a unified exponential/power-law approach

to small-angle scattering. *J. Appl. Cryst.* 28(6), 717-728.

Beaucage, G. 1996. Small angle scattering from polymeric mass fractals of arbitrary mass

fractal dimension. *J. Appl. Cryst.* 29, 134-146.

Bekersky, I., Fielding, R. M., Buell, D. and Lawrence, I. 1999. Lipid-based amphotericin

B formulations: from animals to man. *J. Pharm. Sci.* 2, 230-236.



- Bennett, J.E. 2001. Antimicrobial agents, In: Hardman, J.G., Limbird, L.E. and Molinoff P.B. (Eds), Goodman & Gilman, The pharmacological basis of therapeutics 10<sup>th</sup> Ed. New York: McGraw-Hill. pp 1295-1312.
- Bennett, W.D., Brown, J.S., Zeman, K.L., Hu, S.C., Scheuch, G. and Sommerer, K. 2002. Targeting delivery of aerosols to different lung regions. *J. Aerosol. Med.* 15, 179–188.
- Beyer, J., Barzen, G., Risse, R., Weyer, C., Miksits, K., Dullenkopf, K., Huhn, D. and Siegert, W. 1993. Aerosol amphotericin B for prevention of invasive pulmonary aspergillosis. *Antimicrob. Chemother.* 37, 1367-1369.
- Binnemans, K. 2005. Ionic liquid crystal. *Chem. Rev.* 105, 4148-4204.
- Bolard, J. Seigneuret, M. and Boudet, G. 1980. Interaction between phospholipids bilayer membranes and the polyene antibiotic amphotericin B: lipid state and cholesterol content dependence. *Biochim. Biophys. Acta.* 599, 280-293.
- Bragg, W.L. 1913. The diffraction of short electromagnetic waves by a crystal. *Proceedings of the Cambridge Philosophical Society.* 17, 43–57. Retrieved from "[http://en.wikipedia.org/wiki/Bragg%27s\\_law](http://en.wikipedia.org/wiki/Bragg%27s_law)"
- Brajtburg, J., Powderly, G.W., Kobayashi, S.G. and Medoff, G. 1990. Amphotericin B: current understanding of mechanism of action. *Antimicrob. Agent Chemother.* 34, 183-188.
- British Pharmacopoeia. 2007. Aerodynamic assessment of fine particle-fine particle dose and particle. Her Majesty's Stationery Office, Appendix XII F.
- Brykier, A. 2005. Antifungal targets and research into antifungal agents. In: Brykier, A. (Ed), Antimicrobial agent: antibacterials and antifungals. Washington DC: ASM Press. pp 1288-1319.

- Carver, P.L. 1999. Invasive Fungal infection. In: Dipiro J., Beltz, L., Neira, D., Axtell, C. and Iverson, S. (Eds), *Pharmacotherapy: a pathophysiological approach* (4<sup>th</sup> Ed). Stamford: Appleton & Lange. pp 2059-2081.
- Chandrasekhar, S., Sadashiva, B. K. and Suresh K. A. 1977. Liquid crystals of disk-like molecules. *Pramana*. 9, 471–480.
- Clements, J.S. and Peacock, J.E. 1990. Amphotericin B revisited: reassessment of toxicity. *Am. J. Med.* 88, 5-22N-27N.
- Conneally, E., Cafferkey, M.T., Daly, P.A., Keane, C.T. and McCann, S.R. 1990. Nebulized amphotericin B as prophylaxis against invasive aspergillosis in granulocytopenic patients. *Bone Marrow Transplant*. 5, 403 – 406.
- Cotero, V.B., Rebolledo, A.S. and Ortega, B. I. 1998. On the role of sterol in the formation of the amphotericin B channel. *Biochim. Biophys. Acta*. 1375, 43-51.
- Craven, B. M. 1986. Cholesterol crystal structures: adducts and esters. In: Small, D. M. (Ed), *Handbook of Lipid Research*. Vol. 4, New York: Plenum. pp 149-152.
- Crissey, J.T., Ferguson, J.L. and Bettenhausen, J.M. 1965. Cutaneous thermography with liquid crystals. *J. Invest. Dermatol.* 45, 329-333.
- Croll, D.H., Small, D.M. and Hamilton, J.A. 1986. Temperature-dependent molecular motions of saturated acyl cholesteryl esters: a <sup>13</sup>C NMR study. *J. Chem. Phys.* 85, 7380-7387.
- Croll, D.H., Sripada, P.K. Small and Hamilton, J.A. 1987. Temperature-dependent molecular motions and phase behavior of cholesteryl ester analogues. *J. Lipid Res.* 28, 1444-1454.
- Crowder, T.M., Rosati, J.A., Schroeter, J.D., Hickey, A.J. and Martonen, T.B. 2002. Fundamental effects of particle morphology on lung delivery: prediction of stokes'

- law and the particular relevance to dry powder inhaler formulation and development. *Pharm. Res.* 19, 239-245.
- Crowther, J.R. 1995. Systems in ELISA, Method in molecular biology. Vol 19, The ELISA guidebook. New Jersey: Humana Press.
- De Marie, S., Janknegt, R. and Bakker-Woudenberg, I.A.J.M. 1994. Clinical use of liposomal and lipid-complexed amphotericin B. *J. Antimicrob. Chemother.* 33, 907-916.
- Demus, D. and Richter, L. 1978. Textures of liquid crystals. Weinheim: Verlag Chemie
- Denning, D.W. and Stevens, D.A. 1990. Antifungal and surgical treatment of invasive fungal aspergillosis: review of 2121 published cases. *Rev. Infect. Dis.* 12, 1147-1210.
- Deray, G. 2002. Amphotericin B nephrotoxicity. *J. Antimicrob. Chemother.* 49 (Suppl.1), 37-41.
- Dolovich, M.B. and Ramsdale, E.H. 1990. Replacing CFC aerosols with powders [letter]. *Can. Med. Assoc. J.* 142, 1036.
- Driscoll, K.E. and Maurer, J.K. 1991. Cytokine and growth factor release by alveolar macrophages: potential biomarkers of pulmonary toxicity. *Toxicol. Pathol.* 19, 398-405.
- Duarte, E.L., Itri, R., Sampaio, A.R., Simoes, M. and Palangana, A.J. 2002. Smectic A-cholesteric phase transition investigated by small angle X-ray diffraction and viscosity measurements. *Braz. J. Phys.*, 32(2B), 495-500.
- Edwards, D.A., Hanes, J., Caponetti, G., Hrkach, J., Ben-Jebria, A., Eskew, M.L., Mintzes, J.D., Deaver, D., Lotan, N. and Langer, R. 1997. Large porous particles for pulmonary drug delivery. *Science.* 276, 1868-1871.

- Elser, W. and Ennular, R.D. 1976. In: Brow, G.H. (Ed), *Advances in liquid crystals*. New York: Academic Press.
- Fairhurst, C. E., Fuller, S., Gray, J., Holmes, M. C. and Tiddy, G. J. T. 1998. *Liquid crystals handbook*. Vol. 3, Weinheim, Germany: Wiley-VCH. pp 341-392.
- Fantone, J.C. and Ward, P.A. 1982. Role of oxygen-derived free radicals and metabolites in leukocyte-dependent inflammatory reactions. *Am. J. Pathol.* 107, 397-418.
- Fielding, R.M., Singer, A. W., Wang, L. H., Babbar, S. and Guo, L. S. 1992. Relationship of pharmacokinetics and drug distribution in tissue to increased safety of amphotericin B colloidal dispersion in dogs. *J. Antimicrob. Chemother.* 36, 299-307.
- Fontell, K., 1974. X-ray diffraction by liquid crystals–amphiphilic systems. In: Gray, G.W., Winsor, P.A. (Eds.), *Liquid Crystals and Plastic Crystals. Physico-Chemical Properties and Methods of Investigation*. Vol. 2, New York: Wiley. pp 81–109.
- Fontell, K., Mandell, I. and Ekwall, P. 1968. Some isotropic mesophases in systems containing amphiphilic compounds. *Acta Chem. Scand.* 22, 3209–3232.
- Forster, D., Washington, C. and Davis, S.S. 1988. Toxicity of solubilized and colloidal amphotericin B formulations to human erythrocytes. *J. Pharm. Pharmacol.* 40, 325-328.
- Fournier, I., Barwicz, J. and Tancredi, P. 1998. The structuring effects of AmB on pure and ergosterol or cholesterol-containing dipalmitoylphosphatidylcholine bilayer: a differential scanning calorimetry study. *Biochim. Biophys. Acta.* 1373, 76-86.
- Fraser, V.J., Jones, M., Dunkel, J., Storfer, S., Medoff, G. and Dunagan, W.C. 1992. Candidemia in a tertiary care hospital: epidemiology, risk factors, and predictors of mortality. *Clin. Infect. Dis.* 15, 414-421.

- French, D.L., Edwards, D.A. and Niven, R.W. 1996. The influence of formulation on emission, deaggregation and deposition of dry powders for inhalation. *J. Aerosol Sci.* 27, 769-783.
- Friberg, S. 2000. Phase of liquid crystal. <http://plc.cwru.edu/tutorial/enhanced/files/lc/phase/phase.htm>
- Fukui, H., Koike, T., Saheki, A., Sonoke, S., Tomii, Y. and Seki, J. 2003. Evaluation of the efficacy and toxicity of amphotericin B incorporated in lipid nano-sphere (LNS<sup>®</sup>). *Int. J. Pharm.* 263, 51-60.
- Gallis, H.A., Drew, R.H. and Pickard, W.W. 1990. Amphotericin B 30 years of clinical experience. *Rev. Infect. Dis.* 12 (2), 308 – 329.
- Gilbert, B.E., Wyde, P.R., and Wilson, S.Z. 1992. Aerosolized liposomal amphotericin B for treatment of pulmonary and systemic *Cryptococcus neoformans* infections in mice. *Antimicrob. Agents Chemother.* 36, 1466-1471.
- Ginsburg, G.S. 1984. Lipid-lipid and lipid-protein interactions in model systems of low density lipoprotein. Ph.D. Dissertation. Boston University.
- Ginsburg, G.S., Atkinson, D. and Small, D.M. 1985. Physical properties of cholesteryl esters. *Prog. Lipid Res.* 23, 135-167.
- Ginsburg, G.S., Small, D.M. and Hamilton, J.A. 1982. Temperature-dependent molecular motions of cholesterol esters: carbon-13 nuclear magnetic resonance study. *Biochemistry.* 21, 6857-6867.
- Gonda, I. 1992. Targeting by deposition. In: Hickey, A.J. (Ed), *Pharmaceutical inhalation aerosol technology*. New York: Marcel Dekker, Inc. pp 60-82.

- Guo, L.S.S., Fielding, R.M., Lasic, D.D., Hamilton, R.L. and Mufson, D. 1991. Novel antifungal drug delivery: stable amphotericin B-cholesteryl sulfate discs. *Int. J. Pharm.* 75, 45-54.
- Guo, L. S. S., and Working, P. K. 1993. Complexes of amphotericin B and cholesteryl sulfate. *J. Liposome Res.* 3, 473-490.
- Guo, W. and Hamilton, J.A. 1993. Molecular organization and motions of cholesterol esters in crystalline and liquid crystalline phases: a  $^{13}\text{C}$  and  $^1\text{H}$  magic angle spinning NMR study. *Biochemistry.* 32, 9038-9052.
- Hamilton, J.A., Oppenheimer, N. and Cordes, E.H. 1977. Carbon-13 NMR studies of cholesteryl esters and cholesteryl ester/triglyceride mixtures. *J. Biol. Chem.* 252, 8071-8080.
- Hartsel, S. and Bolard, J. 1996. Amphotericin B: new life for an old drug. *Trends Pharmacol. Sci.* 17, 445-449.
- Harvey, R.L. and Myers, J.P. 1987. Nosocomial fungemia in a large community teaching hospital. *Arch. Intern. Med.* 147, 2117-2120.
- Hay, R.J. 1999. Science and clinical practice lipid amphotericin B combination. *J. Infect.* 39, 16-20.
- Henderson, V.J. and Hirvela, E.R. 1996. Emerging and reemerging microbial threats: nosocomial fungal infections. *Arch. Surg.* 131, 330-337.
- Hickey, A.J., Gonda, I., Irwin, W.J. and Fildes, F.J.T. 1990. Factors influencing the dispersion of dry powders as aerosols. *J. Pharm. Sci.* 79, 1009-1014.
- Hickey, A.J. and Jones, L.T.D. 2000. Particle-size analysis of pharmaceutical aerosols. *Pharm. Technol.* 9, 48-58.

- Hickey, A.J. and Thompson, D.C. 1992. Physiology of the airways. In: Hickey, A.J. (Ed),  
Pharmaceutical inhalation aerosol Technology. New York: Marcel Dekker, Inc. pp  
1-27.
- Hiemenz, J.W. and Walsh, T.J. 1998. Lipid formulations of amphotericin B. *J. Liposome  
Res.* 8, 443-467.
- Hinds, W.C. 1982. Adhesion of particle. In: Hinds, W.C. (Ed), Aerosol technology:  
properties, behavior and measurement of airborne particles. New York: Wiley. pp  
127-132.
- Hocking, W.G. and Glode, D.W. 1979. The pulmonary-alveolar macrophage. *New Engl.  
J. Med.* 301, 580-587.
- Horn, R., Wong, B., Kiehn, T.E. and Armstrong, D. 1985. Fungemia in a cancer hospital:  
changing frequency, earlier onset, and results of therapy. *Rev. Infect. Dis.* 131,  
330-337.
- Hsueh, Y., Gilbert, K., Trandum, C, Zuckermann and Thewalt, J. 2005. The effect of  
ergosterol on dipalmitoylphosphatidylcholine bilayer: a deuterium NMR and  
calorimetric study. *Biophys. J.* 88, 1799-1808.
- Huttunen, K., Ruotsalainen, M., Iivanainen, E., Torkko, P., Katila, M-L. and Hirvonen,  
M-R. 2000. Inflammatory responses in RAW 264.7 macrophages caused by  
mycobacteria isolated from moldy houses. *Environ. Toxicol. Pharmacol.* 8, 237-  
244.
- Hwang, J.J., Iyer, S.N., Li, L.S., Claussen, R., Harrington, D.A. and Stupp, S.I. 2002.  
Self-assembling biomaterials: Liquid crystal phases of cholesteryl oligo(L-lactic  
acid) and their interactions with cells. *Proc. Natl. Acad. Sci.* 99(15), 9662-9667.
- ICH. 1996. Guidance for industry Q2B validation of analytical procedures: methodology.  
Center for drug evaluation and research (CDER), Rockville, MD, USA.

- Janknegt, R., de Marie, S. and Bakker-Woudenberg, I.A.J.M. 1992. Liposomal and lipid formulations of amphotericin B. *Clin. Pharmacokin.* 23, 279-291.
- Janoff, A.S., Perkins, W.R., Saletan, S.L., and Swenson, C.E. 1993. Amphotericin B lipid complex (ABLC™): a molecular rationale for the attenuation of amphotericin B related toxicities. *J. Liposome Res.* 3:451-471.
- Jenning, V. and Gohla, S.H. 2001. Encapsulation of retinoids in solid lipid nanoparticles (SLN). *J. Microencapsul.* 18, 149-158.
- Jenning, V., Schäfer-Korting, M. and Gohla, S.H. 2000. Vitamin A loaded solid lipid nanoparticles for topical application: drug release properties. *J. Controlled Release.* 66, 115-126.
- Jullien, S., Brajtborg, J. and Bolard, J. 1990. Affinity of amphotericin B for phosphatidylcholine vesicles as a determinant of the in vitro cellular toxicity of liposomal preparations. *Biochim. Biophys. Acta.* 1021, 39-45.
- Kauffman, C.A. 2006. Fungal infection. *Proc. Am. Thorac. Soc.* 3, 35-50.
- Kelker, H. and Hatz, R. 1980. Handbook of Liquid Crystals. Weinheim: Wiley-VCH Verlag GmbH. pp 656. doi.10.1002/anie.198006561.
- Koizumi, T., Kubo, K., Kaneki, T., Hanaoka, M., Hayano, T., Miyahara, T., Okada, K., Fujimoto, K., Yamamoto, H., Kobayashi, T. and Sekiguchi, M. 1998. Pharmacokinetic evaluation of amphotericin B in lung tissue: lung lymph distribution after intravenous injection and airspace distribution after aerosolization and inhalation of amphotericin B. *Antimicrob. Agent Chemother.* 42, 1597-1600.
- Koning, J.P. 2001. Chapter 1: Dry powder inhalation: Technical and physiological aspect prescribing and use. pp 1-25. <http://dissertations.ub.rug.nl/FILES/>



[faculties/science/2001/j.p.de.koning/c1.pdf](http://faculties/science/2001/j.p.de.koning/c1.pdf)

- Kuntsche, J., Westesen, K., Drechsler, M., Koch, M. H. J. and Bunjes, H. 2004. Supercooled smectic nanoparticles: A potential novel carrier system for poorly water soluble drugs. *Pharm. Res.* 21, 1834-1843.
- Lin, Y.Y., Chen, K.S. and Lin, S.Y. 1995. Thermophysical properties of cholesteryl oleyl carbonate determined with microscopic FTIR/DSC system. *J. Chinese Chem. Soc. (Taipei)*. 42(5), 865-868.
- Lin, Y.Y., Chen, K.S. and Lin, S.Y. 1996. Development and investigation of a thermoresponsive cholesteryl oleyl carbonate-embedded membrane. *J. Controlled Release.* 41, 163-170.
- Lin, S.Y., Li, M.J. and Lin, H.L. 2000. Effect of skin penetration enhancers on the thermo-physical properties of cholesteryl oleyl carbonate embedded in a thermo-responsive membrane. *J. Mat. Sci. Med.* 11, 701-704.
- Lopez-Berestein, G., Mehta, R., Hopffer, R., Millis, K., Kasi, L., Mehta, K., Fainstein, V., Luna, M., Harsh, E.N. and Juliano, R. 1983. Treatment and prophylaxis of disseminated infections due to *Candida albicans* in mice with liposomal encapsulated amphotericin B. *J. Infect. Dis.* 147, 939-945.
- Lopez-Jodra, O., Torres-Rodriguez, J.M., Mendez-Vasquez, R., Ribas-Forcadell, E., Morere-Lopez, Y., Baro-Tomas, T. and Alia-Aponte, C. 2000. *In vitro* susceptibility of *Cryptococcus neoformans* isolates to five antifungal drugs using a colorimetric system and the reference microbroth method. *J. Antimicrob. Chemother.* 45, 645-649.
- Lozano-Chiu, M., Paetznick, V.L., Ghannoum, M.A. and Rex, J.H. 1998. Detection of resistance to amphotericin B among *Cryptococcus neoformans* clinical isolates: performances of three different media assessed by using Etest and National

- Committee for Clinical Laboratory Standards M27-A methodologies. *J. Clinical Microb.* 36(10), 2817-2822.
- Luzzati, V., Mustacchi, H., Skoulios, A. and Husson, F. 1960. La structure des colloïdes d'association, I. Les phases liquide-cristalline des systemes amphiphile-eau. *Acta Crystallogr.* 13, 660–677.
- Madhusudana, N.V. 2001. Recent advances in thermotropic liquid crystals. *Current Science*, 80, 1018-1025.
- Martin, A., Bustamante, P. and Chun, A.H.C. 1993. Physical pharmacy. 4<sup>th</sup> ed., Marvern Philadelphia: Lea & Febiger.
- Mcginnis, M.R. and Rinaldi, G.M. 1991. Antifungal drugs: Mechanisms of action, drug resistance, susceptibility testing, and assays of activity in biological fluids. In: Lorian V. (Ed), Antibiotics in laboratory medicine. 3<sup>rd</sup> ed., Baltimore: Williams & Wilkins.
- Meldrum, D.R., Shames, B.D., Meng, X, Fullerton, D.A., McIntyre, R.C., Grover, F.L. and Harken, A.H. 2009. Nitric oxide downregulates lung macrophage inflammatory cytokine production. *Ann. Thorac. Surg.* 66, 313-317.
- Metha, R., Lopeze-Berestein, G., Hoper, R. Mills, K. and Juliano, R.L.1984. Liposomal amphotericin B is toxic to fungal cells but not to mammalian cells. *Biochem. Biophys. Acta.* 770, 230–234.
- Meyerhoff, A. 1999. US food and drug administration approval of AmBisome (liposomal amphotericin B) for treatment to visceral leishmaniasis. *Clin. Infect. Dis.* 28, 42–8.
- Mitchell, J.P. and Nagel, M.W. 2004. Particles size analysis of aerosol from medicinal inhalers. *KONA.* 22, 32-64.

- Moncton, D.E. and Pindak, R. 1979. Long-range order in two- and three-dimensional Smectic-*B* sliquid-crystal films. *Phys. Rev. Letter.* 43, 701-704.
- Monforte, V., Roman, A., Gavalda, J., Bravo, C., Tenorio, L., Ferrer, A., Maestre, J. and Morell, F. 2001. Nebulized amphotericin B prophylaxis for *Aspergillus* infection in lung transplantation: study of risk factor. *J. Heart and Lung Transplant.* 20(12), 1274–1281.
- Mouritsen, O. G. and Bloom, M. 1984. Modeling the phase equilibrium in two component membranes of phospholipids with different acyl-chain lengths. *J. Biophys.* 46, 141-153.
- Mueller-Goymann, C.C. 2001. Liquid crystals in drug delivery. In: Swabrick, J., Boyland, J.C. (Eds), *Encyclopedia of Pharmaceutical Technology*, New York: Marcel Dekker. pp 117-146.
- Muller-Goymann, C.C. 2004. Physicochemical characterization of colloidal drug delivery systems such as reverse micelles, vesicle, liquid crystals and nanoparticles for topical administration. *Eur. J. Pharm. Biopharm.* 58, 343-356.
- Notter, R. H. 2000. *Lung surfactants: basic science and clinical applications*. New York: Marcel Dekker. pp 120.
- Nucleus Communications, Inc. (<http://www.nucleusinc.com>)
- Park, B.J., Arthington-Skaggs, B.A., Hajjeh, R.A., Iqbal, N., Ciblak, M.A., Lee-Yang, Wendy, Hairston, M.D., Phelan, M., Plikaytis, B.D., Sofair, A.N., Harrison, L.H., Fridkin, S.K. and Warnock. 2006. Evaluation of amphotericin B interpretive breakpoints for *Candida* bloodstream isolates by correlation with therapeutic outcome. *Antimicrob. Agents Chemother.* 50, 1287-1292.
- Persson, U., Tennvall, G.R., Anderson, S., Tyden, G. and Wettermark, B. 1992. Cost-

effectiveness analysis of treatment with liposomal amphotericin B versus conventional amphotericin B in organ or bone marrow transplant recipients with systemic mycoses. *PharmacoEconomics*. 2, 500-508.

Plotnick, A.M. 2000. Lipid-based formulations of amphotericin B. *J. Am. Vet. Med. Assoc.* 216, 838-841.

Prime, D., Atkins, P.J., Slater, A. and Sumby, B.1997. Review of dry powder inhalers. *Adv. Drug Deliv. Rev.* 26, 51-58.

Promega, Corporation. 1995. Griess Reagent System. Promega Corporation (Ed), Technical Bulletin. Madison: Promega ([www.promega.com](http://www.promega.com)).

Punturee, K., Wild, C.P. and Vinitketkumneun, U. 2004. Thai medicinal plants modulate nitric oxide and tumor necrosis factor in J774.2 mouse macrophage. *J. Ethnopharmacol.* 95, 183-189.

Reinitzer, F. 1888. Cholesterin. *Monatsh. Chem.* 2, 421-441.

Ringden, O., Meunier, F., Tollemar, J., Ricci, P., Tura, S., Kuse, E., Viviani, M. A., Gorin, N. C., Klastersky, J., Fenoux, P., Prentice, H. G. and Ksionski, G. 1991. Efficacy of amphotericin B incorporated in liposomes (AmBisome) in the treatment of invasive fungal infections in immunocompromised patients. *Antimicrob. Agent Chemother.* 28 (suppl B), 73-82.

Robinson, R.F. and Nahata, M. 1999. A comparative review of conventional and lipid formulations of AmB. *Clin. Pharmacol. Ther.* 24, 249-257.

Ruijgrok, E.J., Vulto, A.G. and Van Etten, E.W.M. 2001. Efficacy of aerosolized amphotericin B desoxycholate and liposomal amphotericin B in the treatment of invasive pulmonary aspergillosis in severely immunocompromised rats. *J. Antimicrob. Chemother.* 48, 89-95.

Russell, E. 2007. Antifungal pharmacology. ([http://www. Doctorfungus.org/thedrugs](http://www.Doctorfungus.org/thedrugs))

[/antif\\_pharm.html](#)).

- Saeva, F.D. 1979. Liquid crystals: The fourth state of matter. New Jersey: Marcel Dekker. pp 286-300.
- Sanders, S.W., Buchi, K. N., Goddard, M. S., Lang, J. K. and Tolman, K. G. 1991. Single-dose pharmacokinetics and tolerance of a cholesteryl sulfate complex of amphotericin B administered to healthy volunteers. *Antimicrob. Agents Chemother.* 35, 1029-1034.
- Sanna, V., Kirschvink, N., Gustin, P., Gavini, E, Roland, I., Delattre, L. and Evrard, B. 2003. Preparation and in vivo toxicity study of solid lipid microparticles as carrier for pulmonary administration. *AAPS. Pharm. Sci. Tech.* 5 (2), 1-7.
- Santangelo, R., Paderu, P., Delmas, G., Chen, Zi-Wei, Mannino, R., Zarif, L. and Perlin, D.S. 2000. Efficacy of oral coxlate-amphotericin B in a mouse model of systemic candidiasis. *Antimicrob. Agents Chemother.* 44, 2356-2360.
- Sarosi, G.A 1990. Amphotericin B: still the 'gold standard' for antifungal therapy. *Postgrad. Med.* 88, 151-152, 155-161, 165-166.
- Sawaya, B.P., Briggs, J.P. and Schnermann, J. 1995. Amphotericin B nephrotoxicity: the adverse consequences of altered membrane properties. *J. Am. Soc. Nephrol.* 6, 154-164.
- Schaffner, A. and Roland, W. 2000. Antifungal drugs. In: Dukes M.N.G. and Aronson, J.K., Meyler's side effects of drugs. 14<sup>th</sup> Ed, Elsevier. pp 922-926.
- Shah, S.P. and Misra, A. 2004. Development of liposomal amphotericin B dry powder inhaler formulation. *Drug Delivery.* 11, 247-253.
- Shin, S., Kumar, S., Finotello, D., Keast, S. and Neubert, M. 1992. High-precision heat capacity study of phase transitions in a lyotropic liquid crystal. *J. Am. Phys. Soc.* 45, 8683-8692.

- Small, D.M. 1970. The physical state of lipids in biological importance: cholesteryl esters, cholesterol, triglyceride. *Adv. Exp. Med. Biol.* 7, 55-83.
- Small, D.M. 1986. The physical chemistry of lipids. New York: Plenum. pp 395-473.
- Sorensen, K.N., Allen, S.D., Nejdil, M.J. and Profitt, R.T. 1993. Aerosolization of Liposomal (AmBisome) and non-liposomal (Fungizone) amphotericin B as a treatment for pulmonary fungal infections. pp 187. In: Proceedings of the Sixth International Symposium on Recent Advances in Drug Delivery Systems Abstracts. University of Utah, Salt Lake City.
- Srichana, T., Martin, G.P. and Marriott, C. 1998. On the relationship between drug and carrier deposition from dry powder inhalers *in vitro*. *Int. J. Pharm.* 167, 13–23.
- Srichana, T., Suedee, R. and Srisudjai, P. 2003. Application of spectrofluorometry for evaluation of dry powder inhalers *in vitro*. *Pharmazie*. 58, 125-129.
- Stein, S.W. and Olson, B.A. 1997. Variability in Size distribution measurement obtained using multiple Andersen Mark II cascade impactors. *Pharm. Res.* 14, 1718-1725.
- Storm, G. and van Etten, E. 1997. Biopharmaceutical aspects of lipid formulations of Amphotericin B. *Eur. J. Clin. Microbiol. Infect. Dis.* 16, 64-73.
- Suarez, S. and Hickey, A. 2000. Drug properties affecting aerosol behavior. *Respir. Res.* 45, 652-666.
- Suh, I-H., Ko, T.S., Park, Y.J. Yoon, Y.K. and Saenger, W. 1988. Structure of cholesterol *n*-hexyl carbonate. *Acta Cryst.* C44, 2163-2167.
- Szoka, F.C., and Tang, M. 1993. Amphotericin B formulated in liposomes and lipid based systems: a review. *J. Liposome Res.* 3, 363-375.
- Taylor, K. 2002. Pulmonary drug delivery. In: Aulton, M.E. (Ed), *Pharmaceutics: The science of dosage form design*. Spain: Churchill Livingstone. pp 473-488.

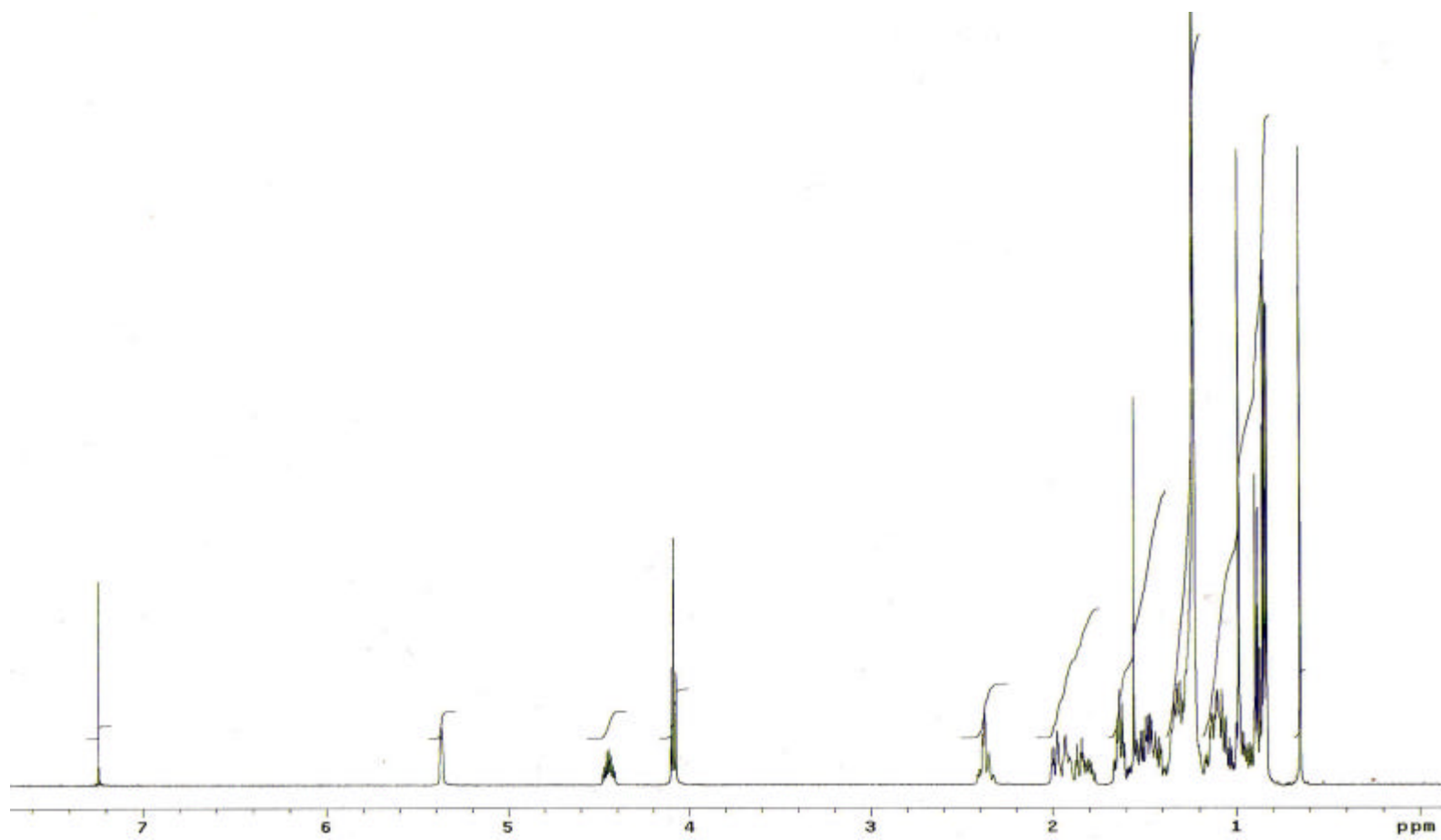
- Timsina, M.P., Martin, G.P., Marriott, C., Ganderton, D. and Yianneskis, M. 1994. Drug delivery to the respiratory tract using dry powder inhalers. *Int. J. Pharm.* 101, 1-13.
- Tiyaboonchai, W. and Limpeanchob, N. 2007. Formulation and characterization of amphotericin B-chitosan-dextran sulfate nanoparticles. *Int. J. Pharm.* 329, 142-149.
- Tiyaboonchai, W., Woiszwilllo, J. and Middaugh, R.C. 2001. Formulation and characterization of amphotericin B-polyethylenimine-dextran sulfate nanoparticles. *J. Pharm. Sci.* 90 (7), 902-914.
- Tyle, P. 1988. Liquid crystals and their applications in drug delivery. In: Controlled release of drugs: polymers and aggregate systems. New York: VCH Publisher, Inc.
- Umegawa, Y., Matsumori, N., Oishi, T. and Murata, M. 2007. Amphotericin B covalent dimers with carbonyl-amino linkage: a new probe for investigating ion channel assemblies. *Tetrahedron lett.* 48, 3393-3396.
- US Pharmacopeia, 29, NF, 24. 2006. Guideline No. 66: Antibiotics-microbial assays. Rockville, MD: US Pharmacopeial Convention, Inc.
- US Pharmacopeia 30, NF, 25. 2007. Guideline No. 905: Uniformity of dosage units. Rockville, MD: US Pharmacopeial Convention, Inc.
- Van Eldere, J., Joosten, L., Verhaeghe, A. and Surmont, I. 1996. Fluconazole and amphotericin B antifungal susceptibility testing by National Committee for Clinical Laboratory Standards broth macrodilution method compared with E-test and semiautomated broth microdilution test. *J. Clin. Microbiol.* 34(4), 842-847.
- Vyas, S.P., Quraishi, S., Gupta, S. and Jaganathan, K.S. 2005. Aerosolized liposome-based delivery of amphotericin B to alveolar macrophages. *Int. J. Pharm.* 296, 12-25.

- Wall, D.A. 1995. Pulmonary absorption of peptides and proteins. *Drug Delivery*. 2, 1-20.
- Walsh, T.J. and Pezzo, A. 1988. Treatment of systemic fungal infections: recent progress and current problems. *Eur. J. Clin. Microbiol. Infect. Dis.* 7, 460-475.
- Wang, L.H., Fielding, R.M., Smith, P.C. and Guo, L.S.S. 1995. Comparative tissue distribution and elimination of amphotericin B colloidal dispersion (Amphocil) and Fungizone after repeated dosing in rats. *Pharm. Res.* 12, 275-283.
- Witzke, N.M. and Bittman, R. 1984. Dissociation kinetics and equilibrium binding properties of polyene antibiotics complexes with phosphatidylcholine/sterol vesicles. *Biochemistry*. 23, 1668-1674.
- Yu, B.G., Okano, T., Kataoka, K. and Kwon, G. 1998. Polymeric micelles for drug delivery: solubilization and haemolytic activity of AmB. *J. Controlled Release*. 53, 131-136.

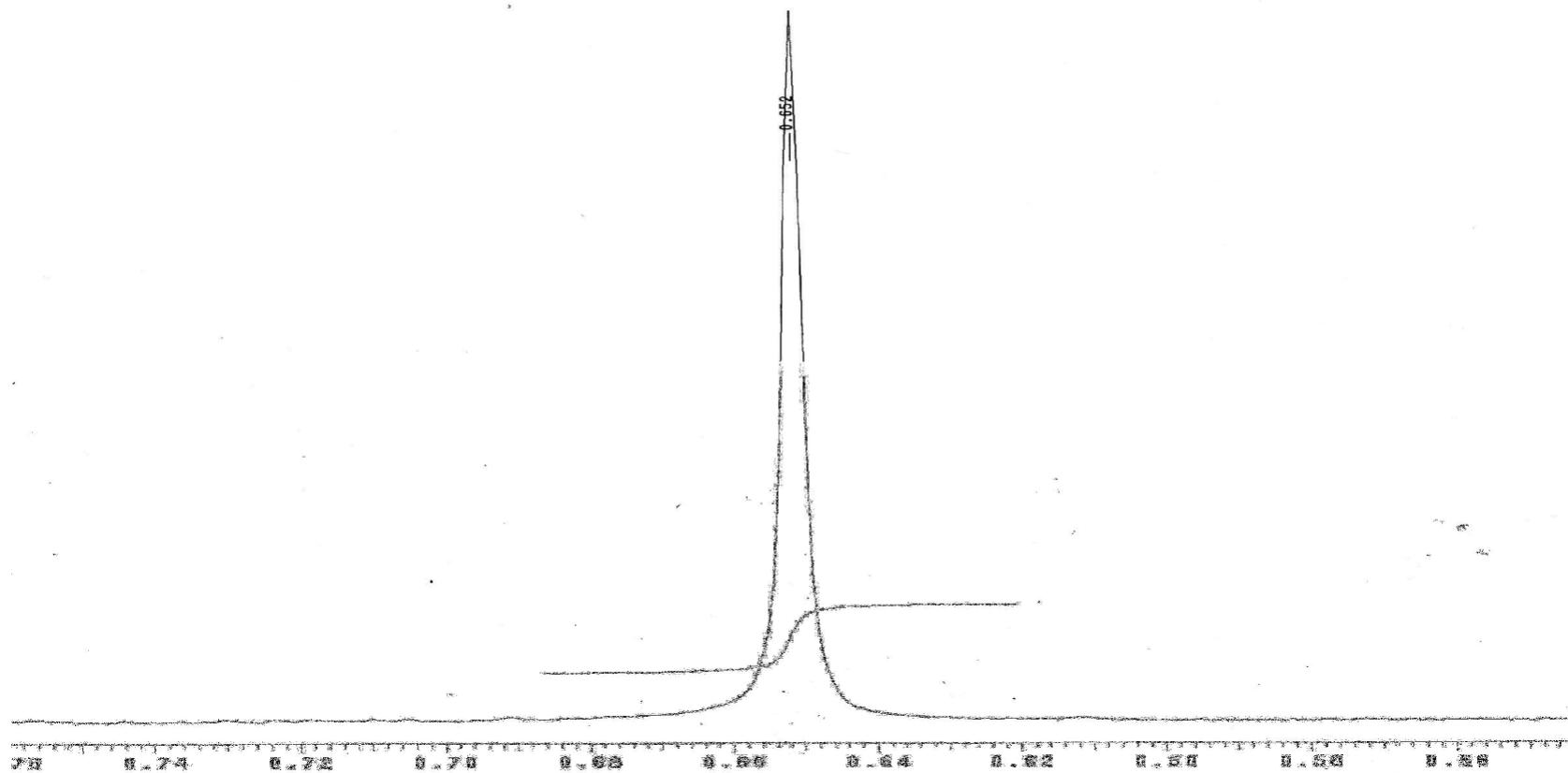


## APPENDICES

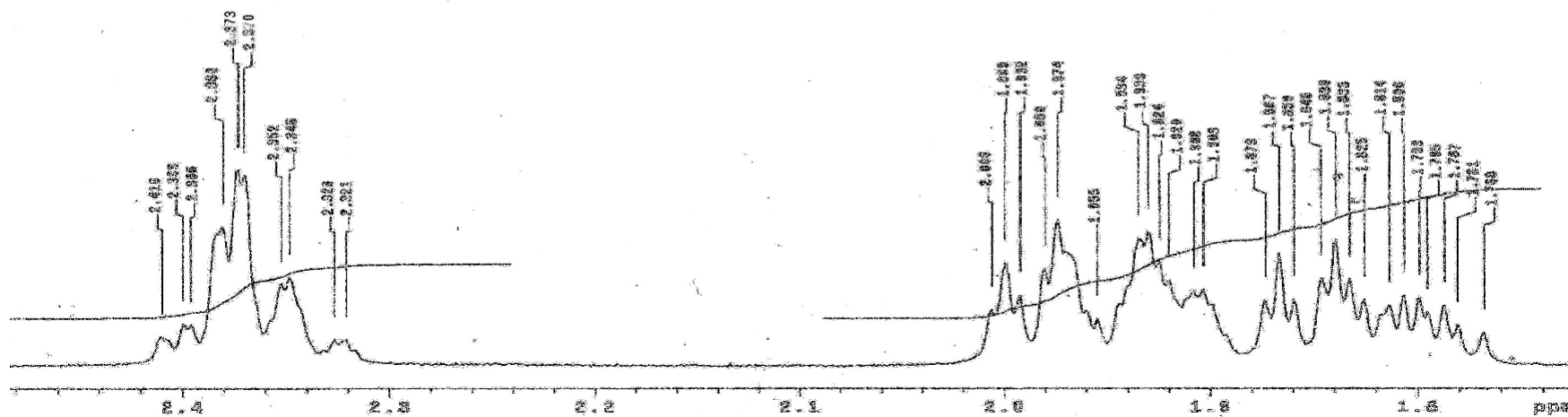
### <sup>1</sup>H-NMR AND <sup>13</sup>C-NMR SPECTRA



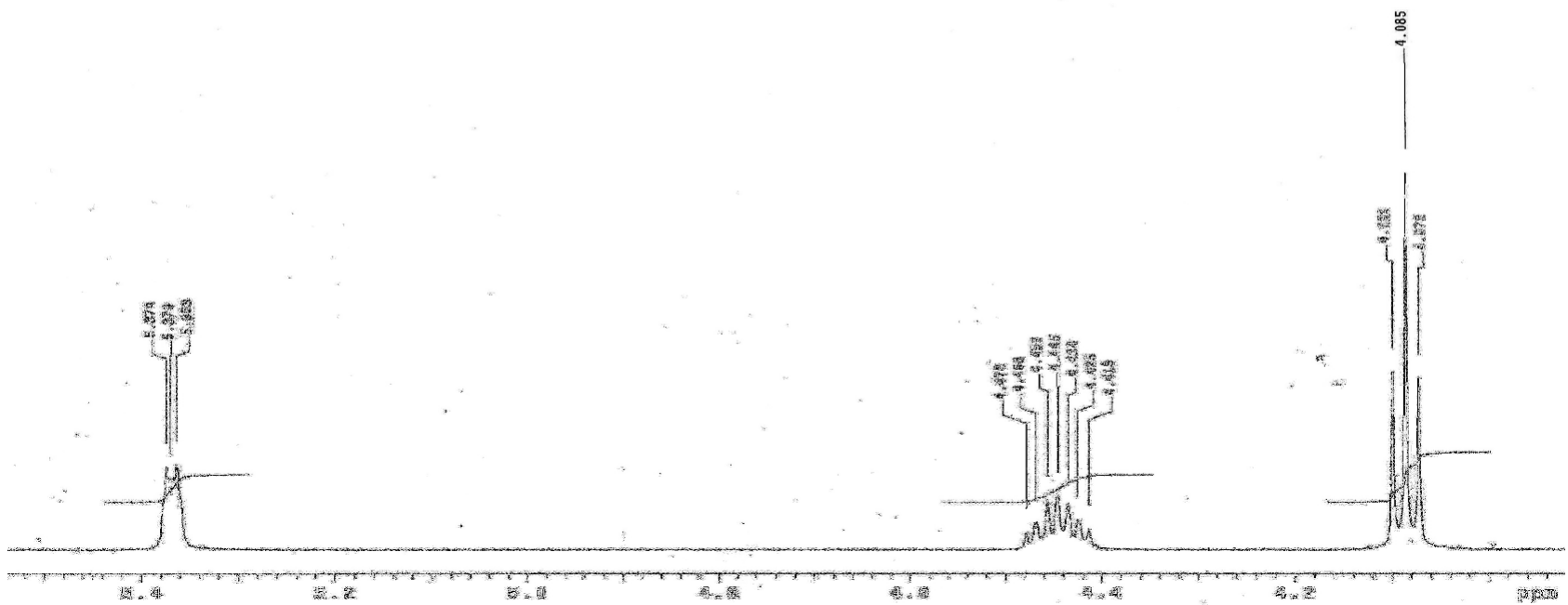
<sup>1</sup>H-NMR spectra of cholesteryl palmityl carbonate (CPC)



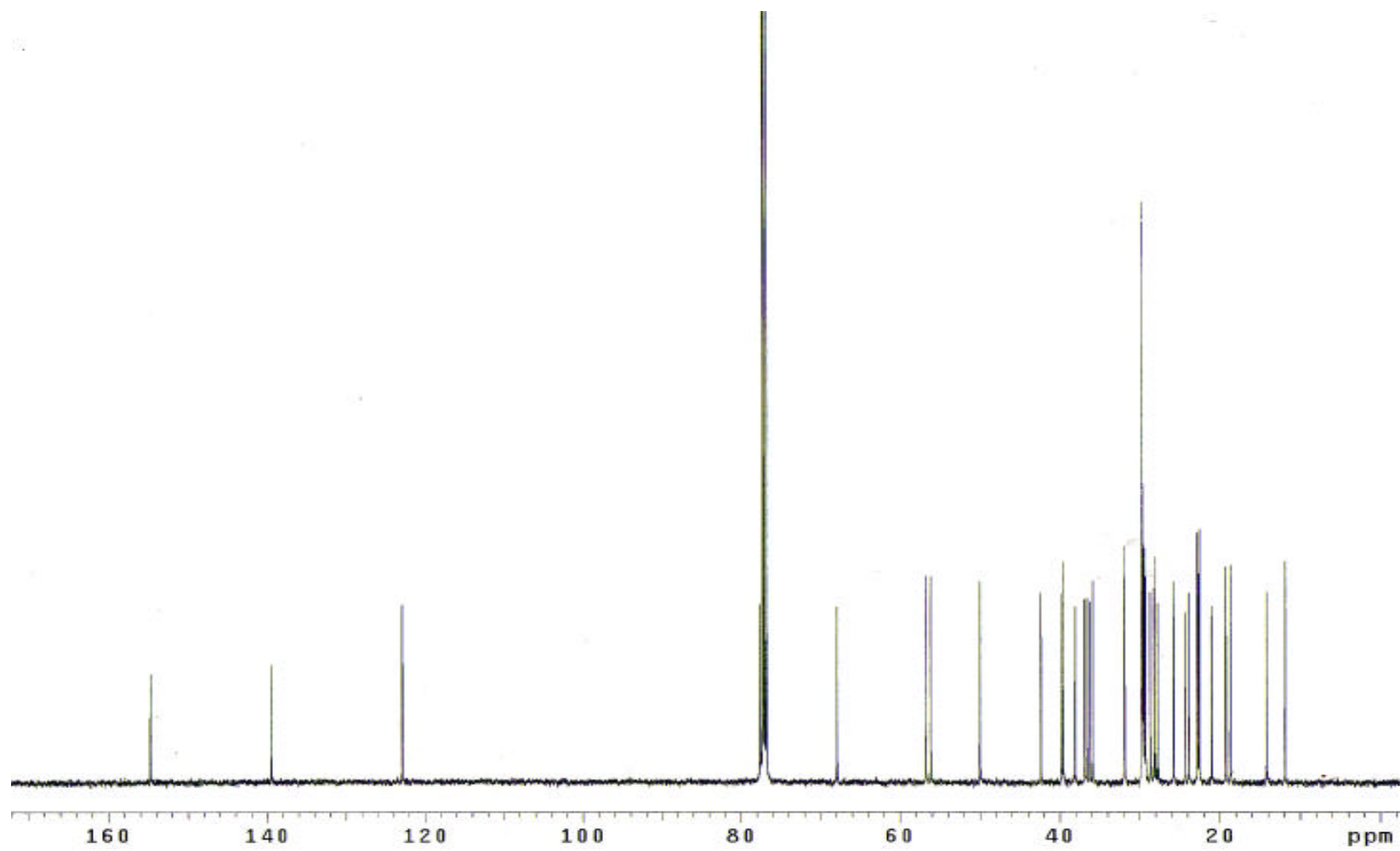
<sup>1</sup>H-NMR spectra of cholesteryl palmityl carbonate (CPC)



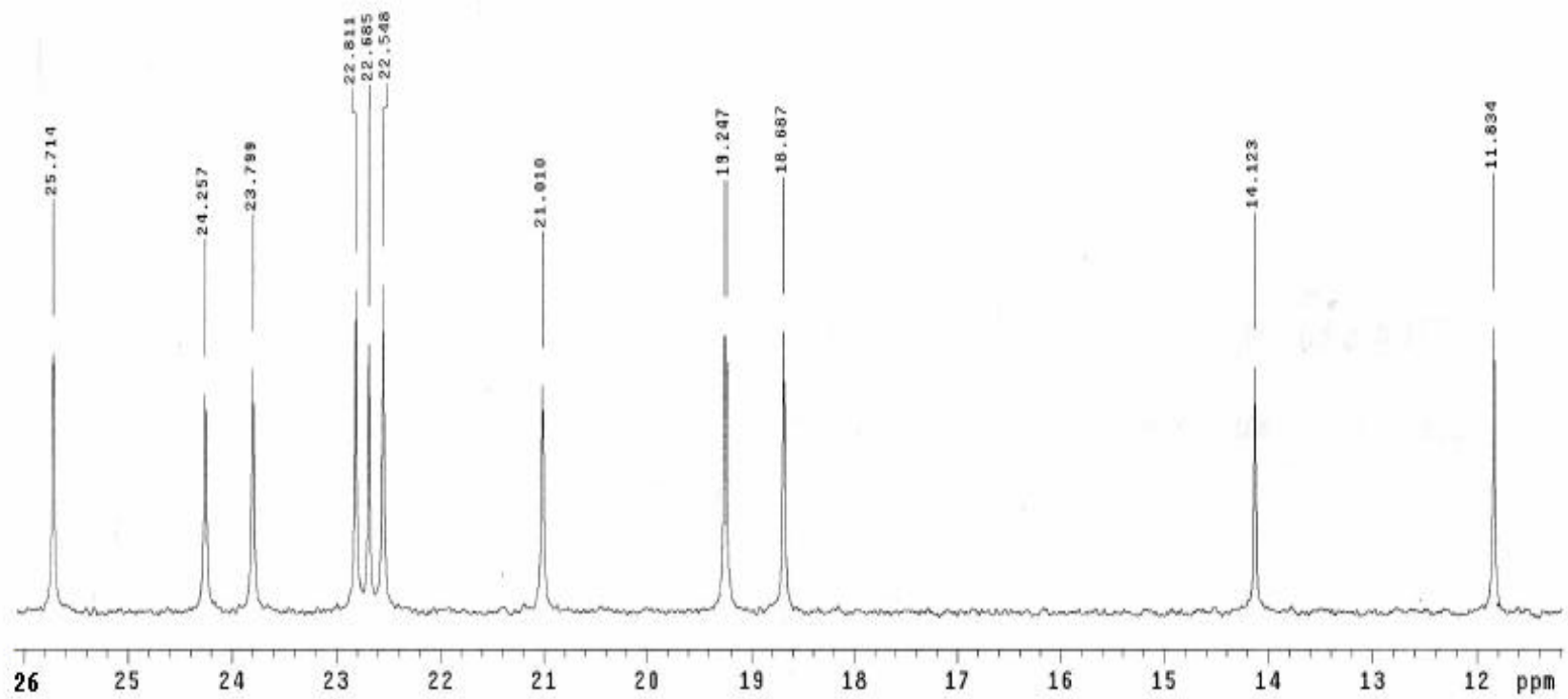
<sup>1</sup>H-NMR spectra of cholesteryl palmitate (CPC)



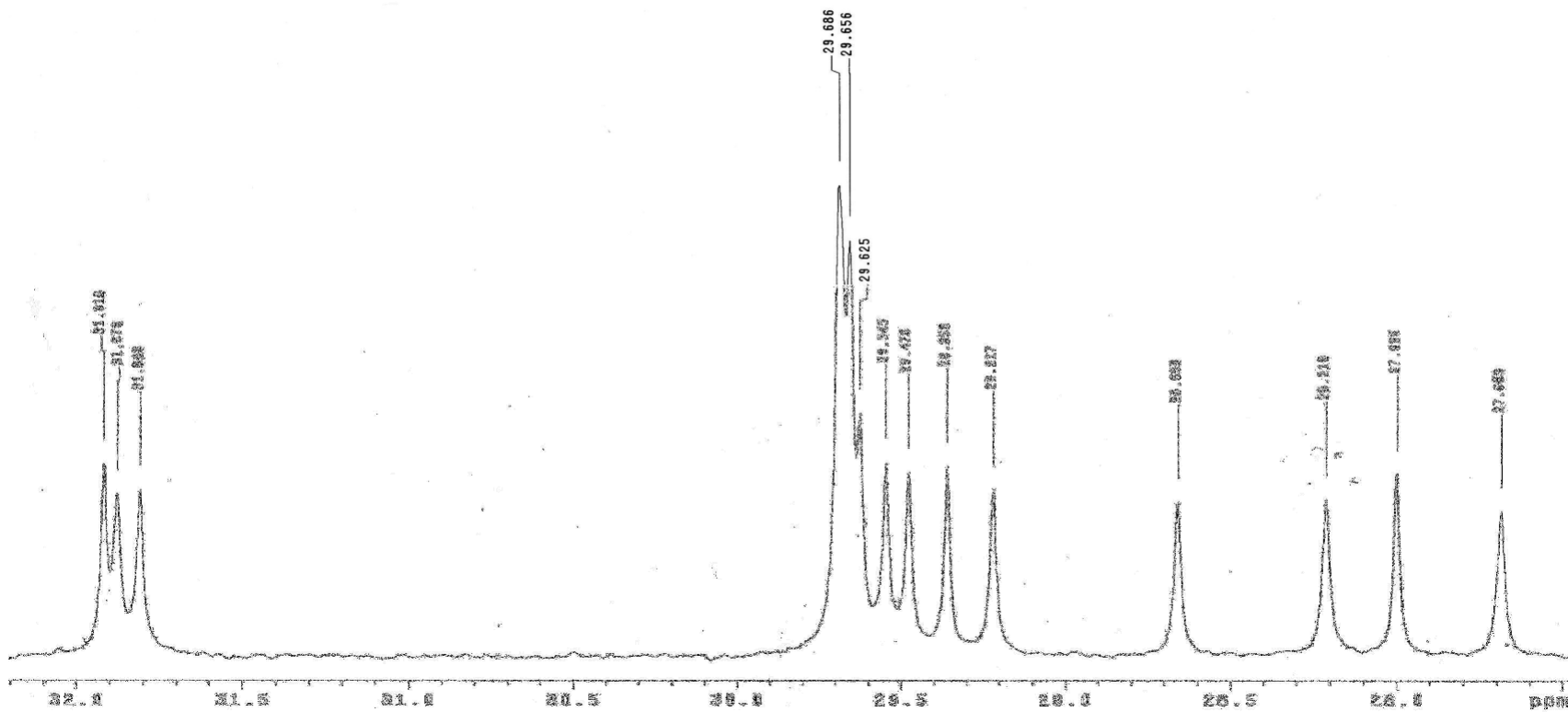
<sup>1</sup>H-NMR spectra of cholesteryl palmityl carbonate (CPC)



$^{13}\text{C}$ -NMR spectra of cholesteryl palmityl carbonate (CPC)

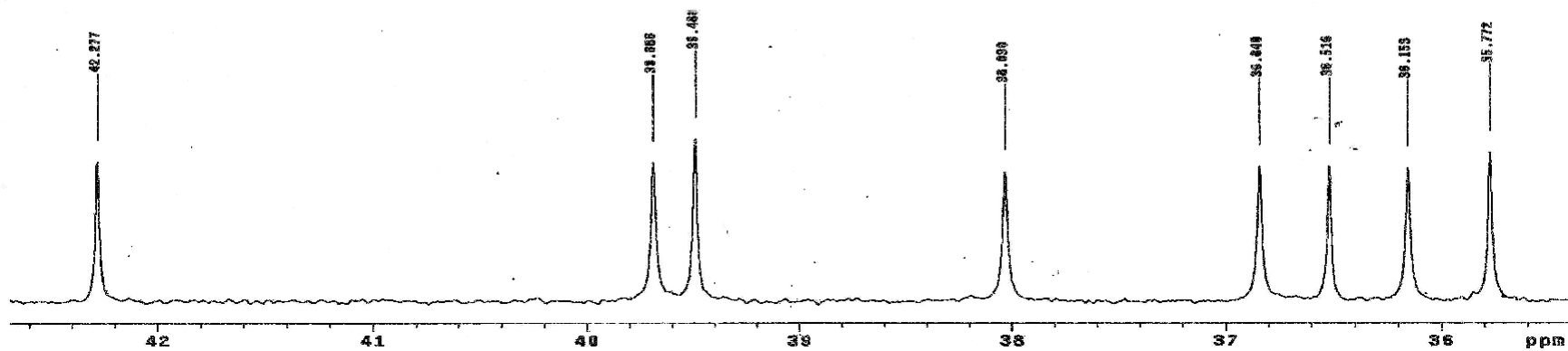


$^{13}\text{C}$ -NMR spectra of cholesteryl palmityl carbonate (CPC)

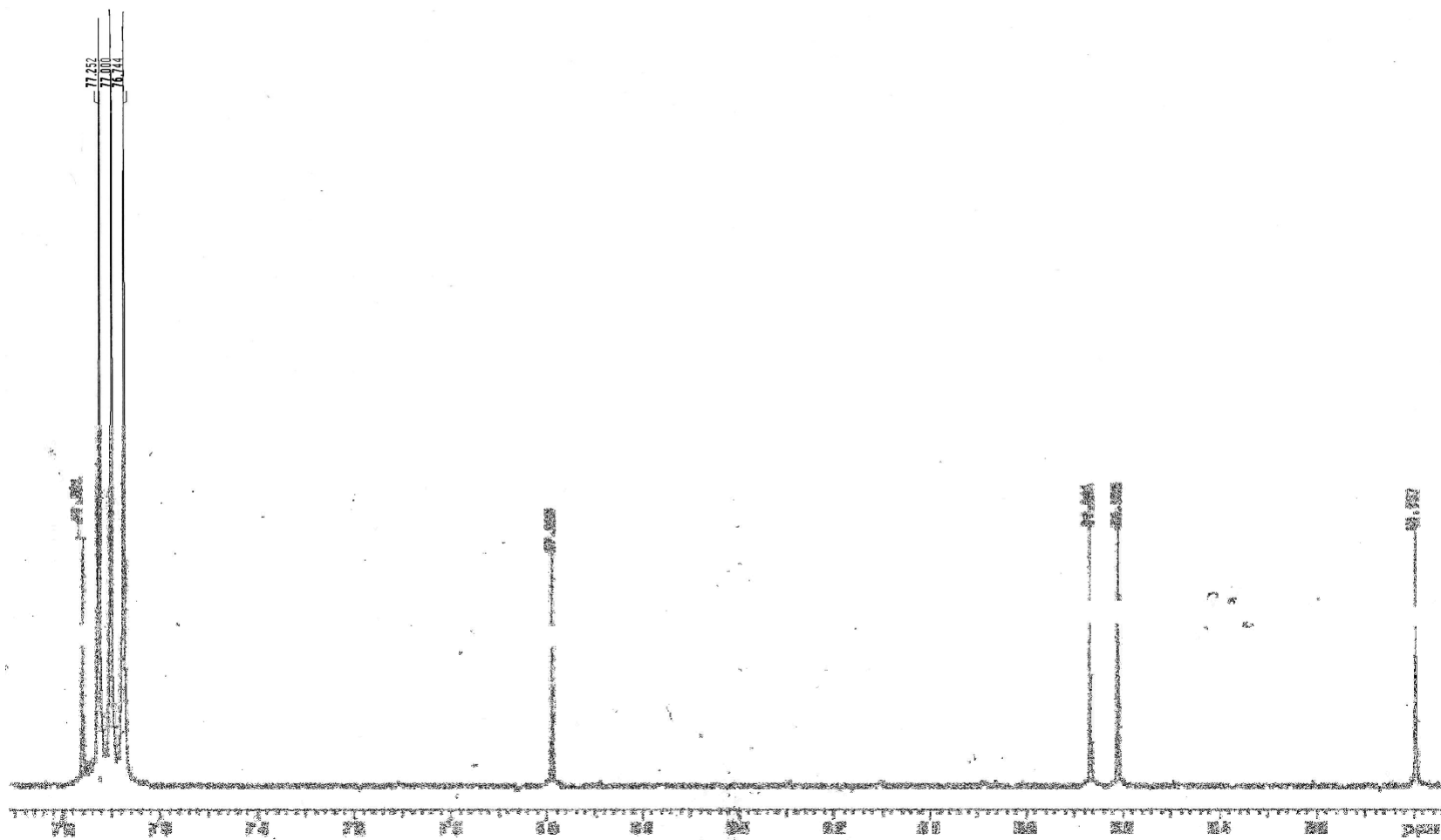


$^{13}\text{C}$ -NMR spectra of cholesteryl palmityl carbonate (CPC)

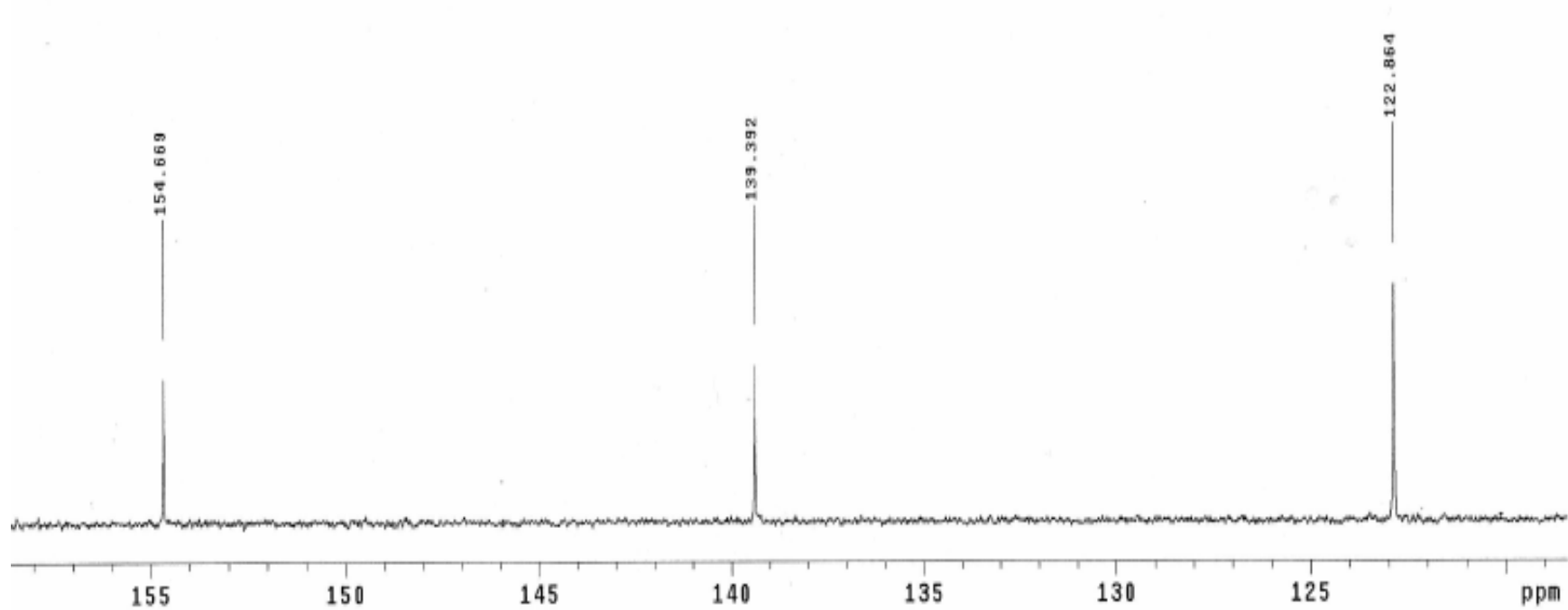




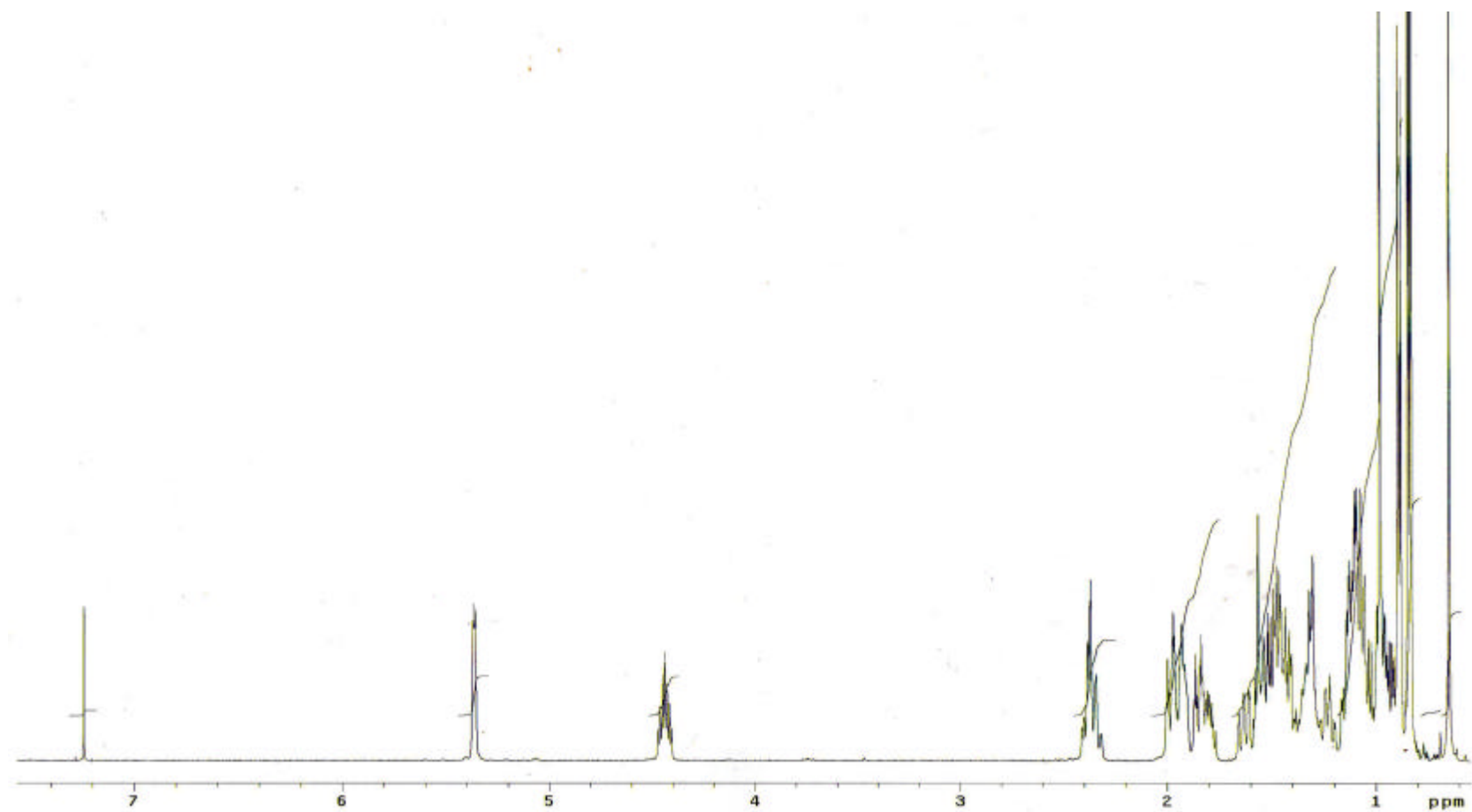
$^{13}\text{C}$ -NMR spectra of cholesteryl palmityl carbonate (CPC)



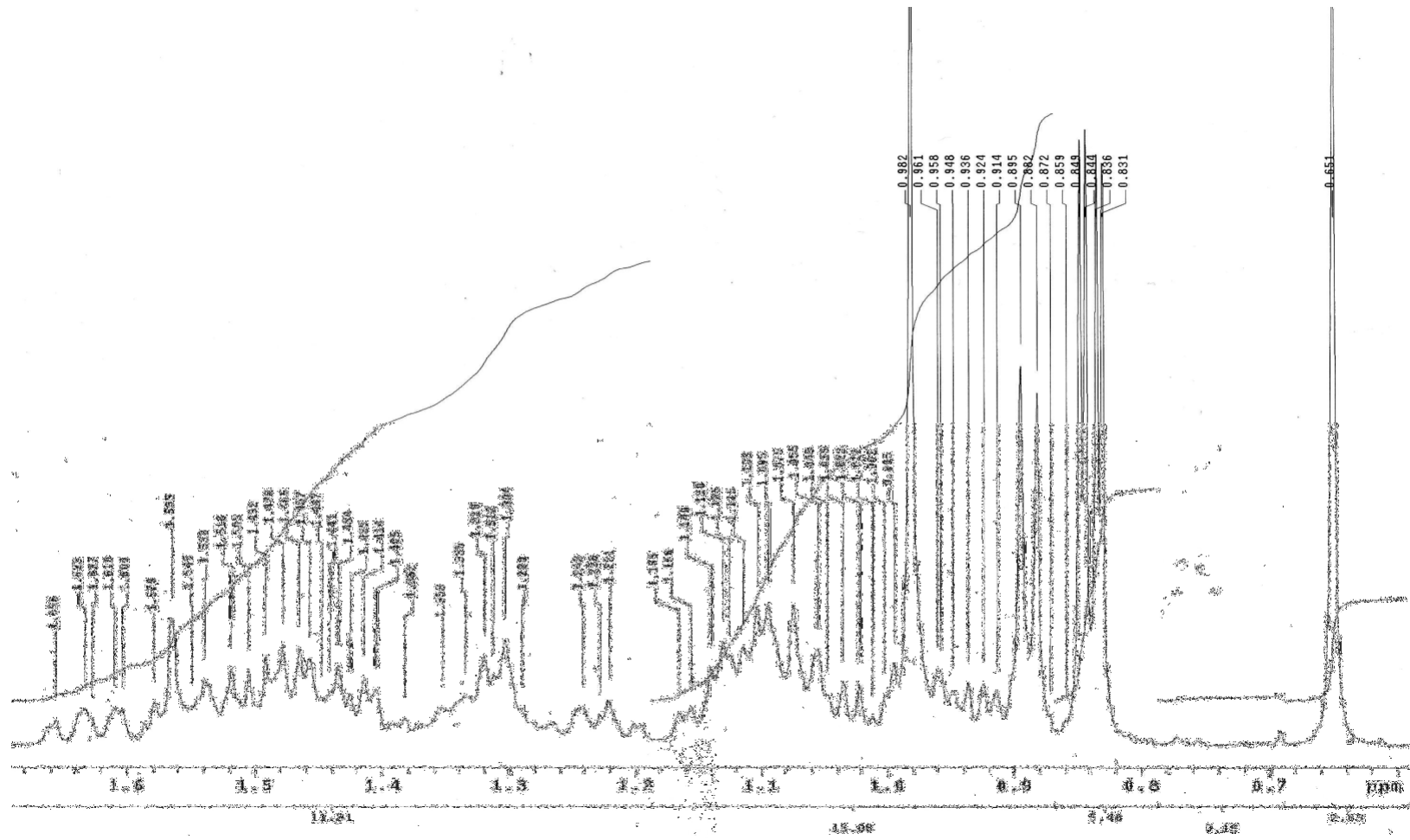
$^{13}\text{C}$ -NMR spectra of cholesteryl palmityl carbonate (CPC)



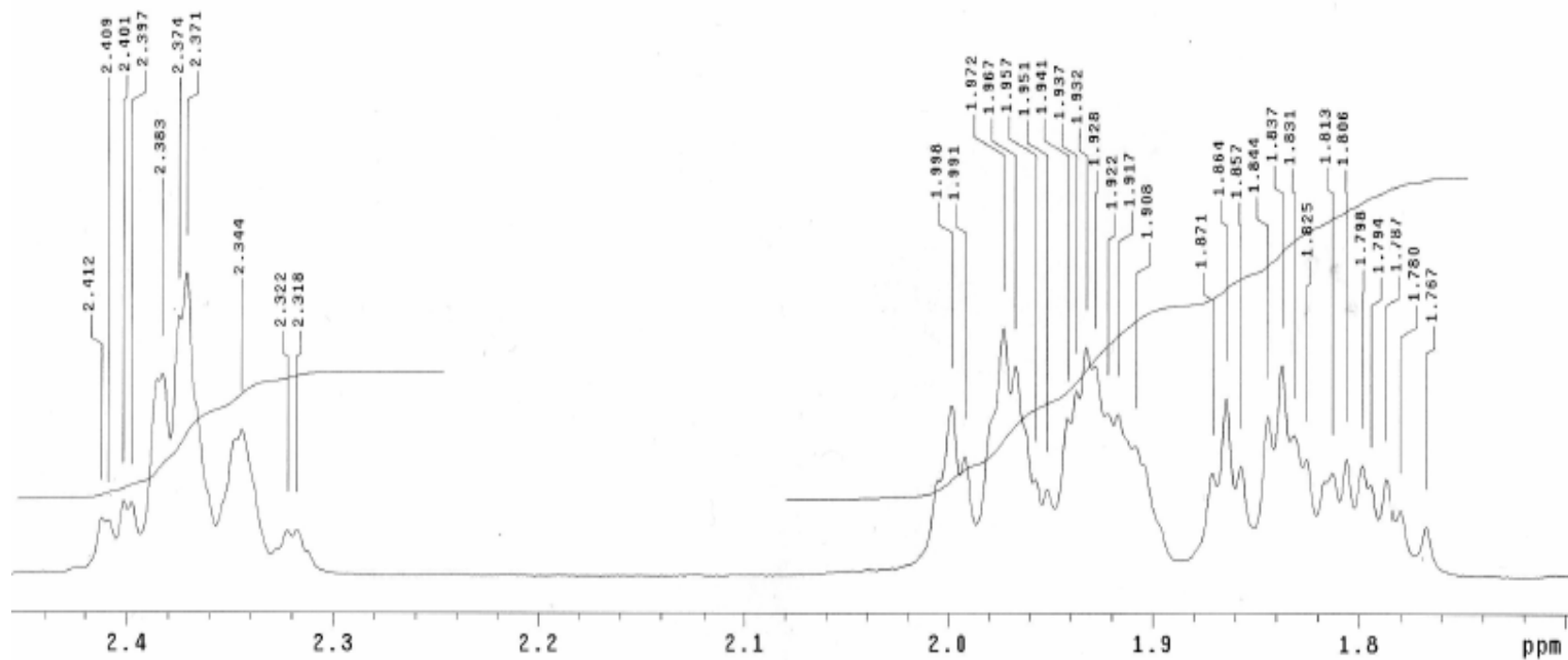
$^{13}\text{C}$ -NMR spectra of cholesteryl palmityl carbonate (CPC)



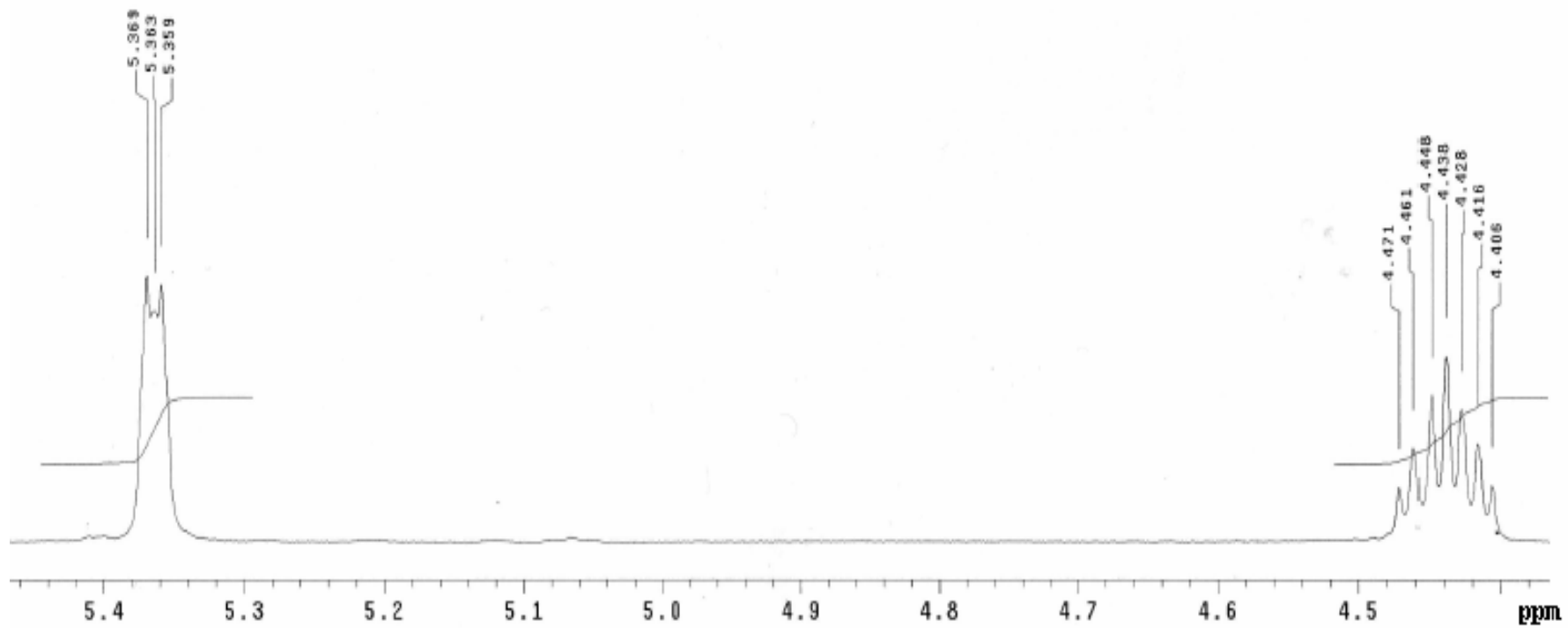
$^1\text{H-NMR}$  spectra of dicholesteryl carbonate (DCC)



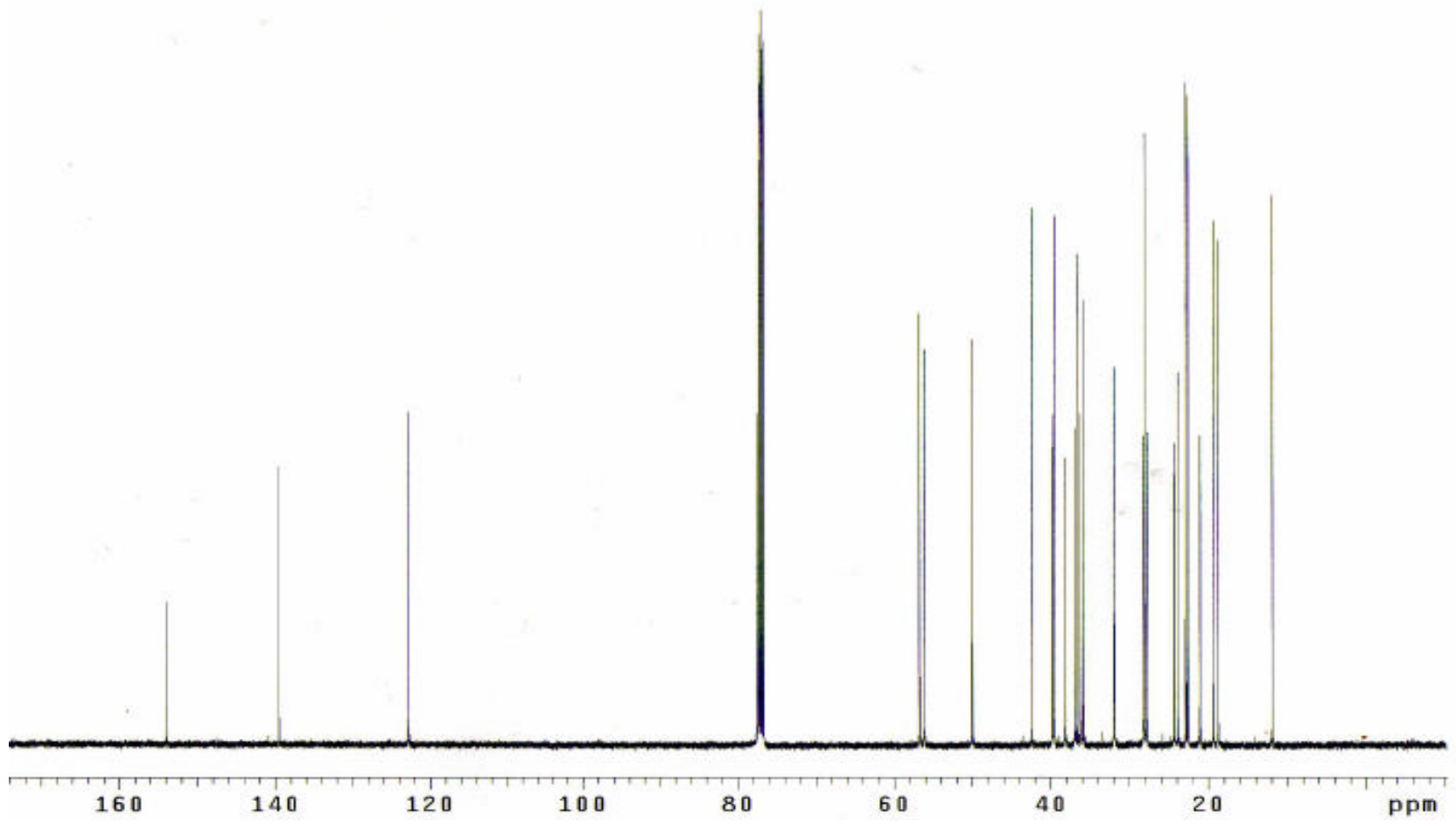
<sup>1</sup>H-NMR spectra of dicholesteryl carbonate (DCC)



<sup>1</sup>H-NMR spectra of dicholesteryl carbonate (DCC)

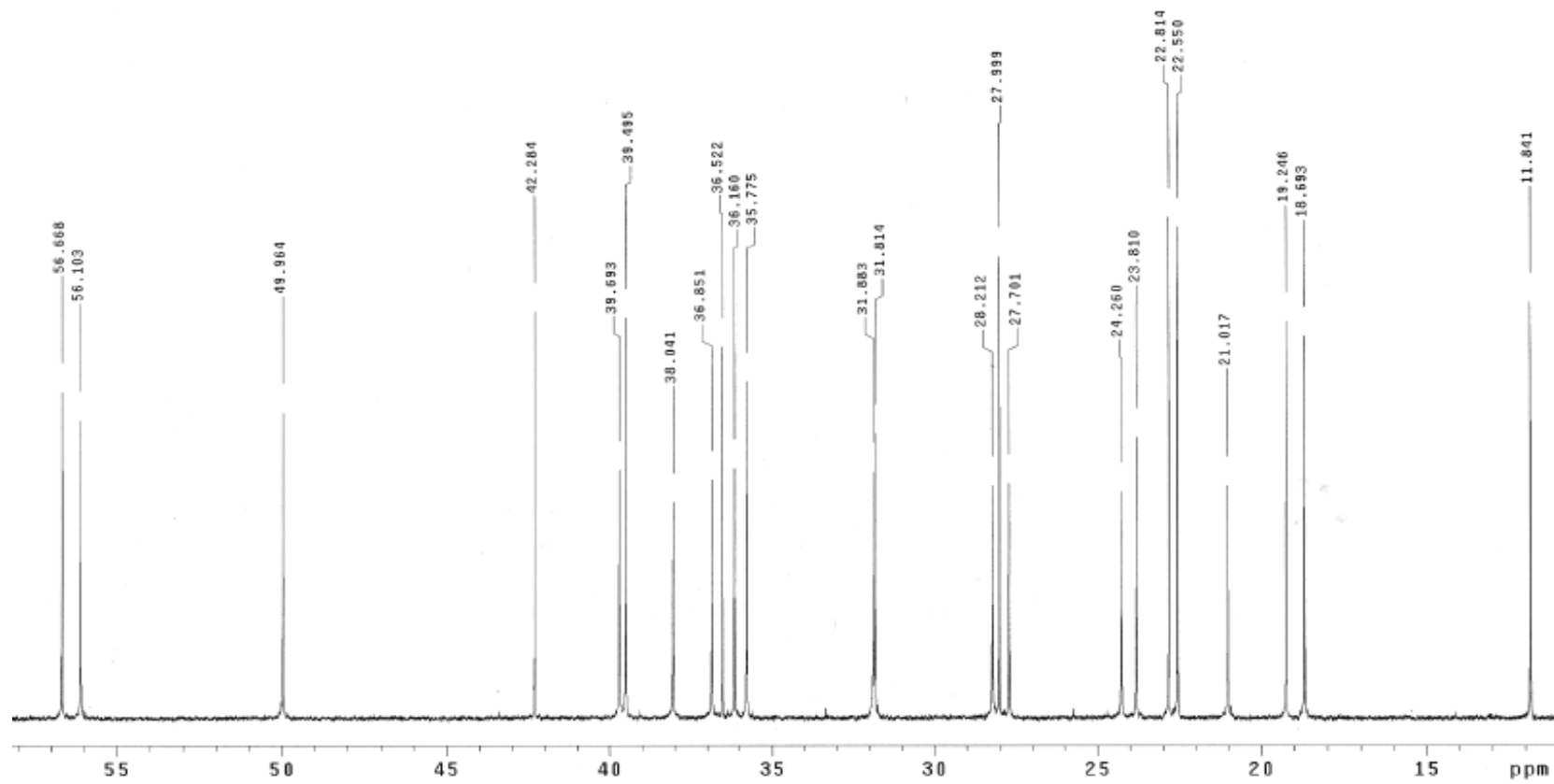


<sup>1</sup>H-NMR spectra of dicholesteryl carbonate (DCC)

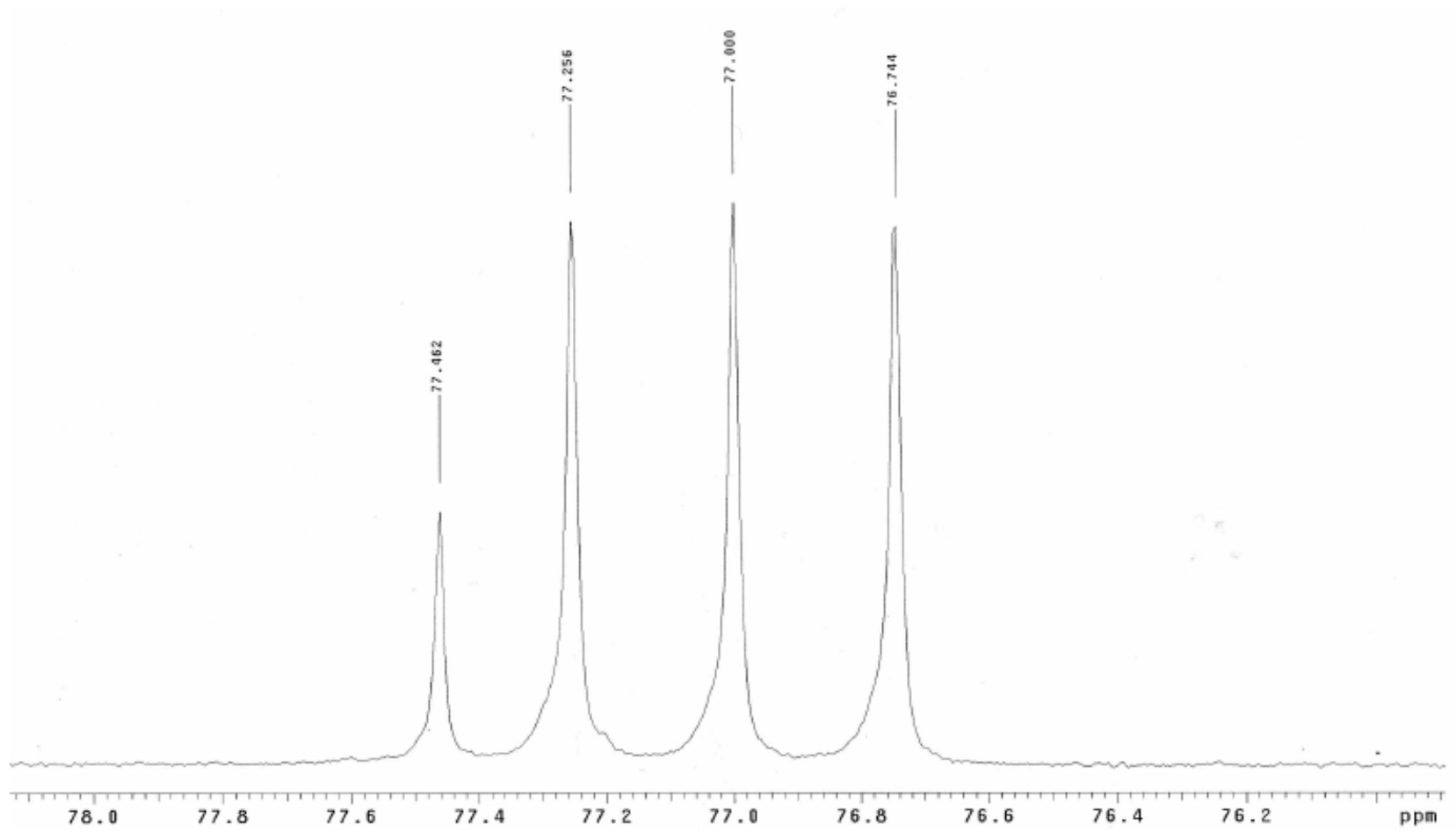


$^{13}\text{C}$ -NMR spectra of dicholesteryl carbonate (DCC)

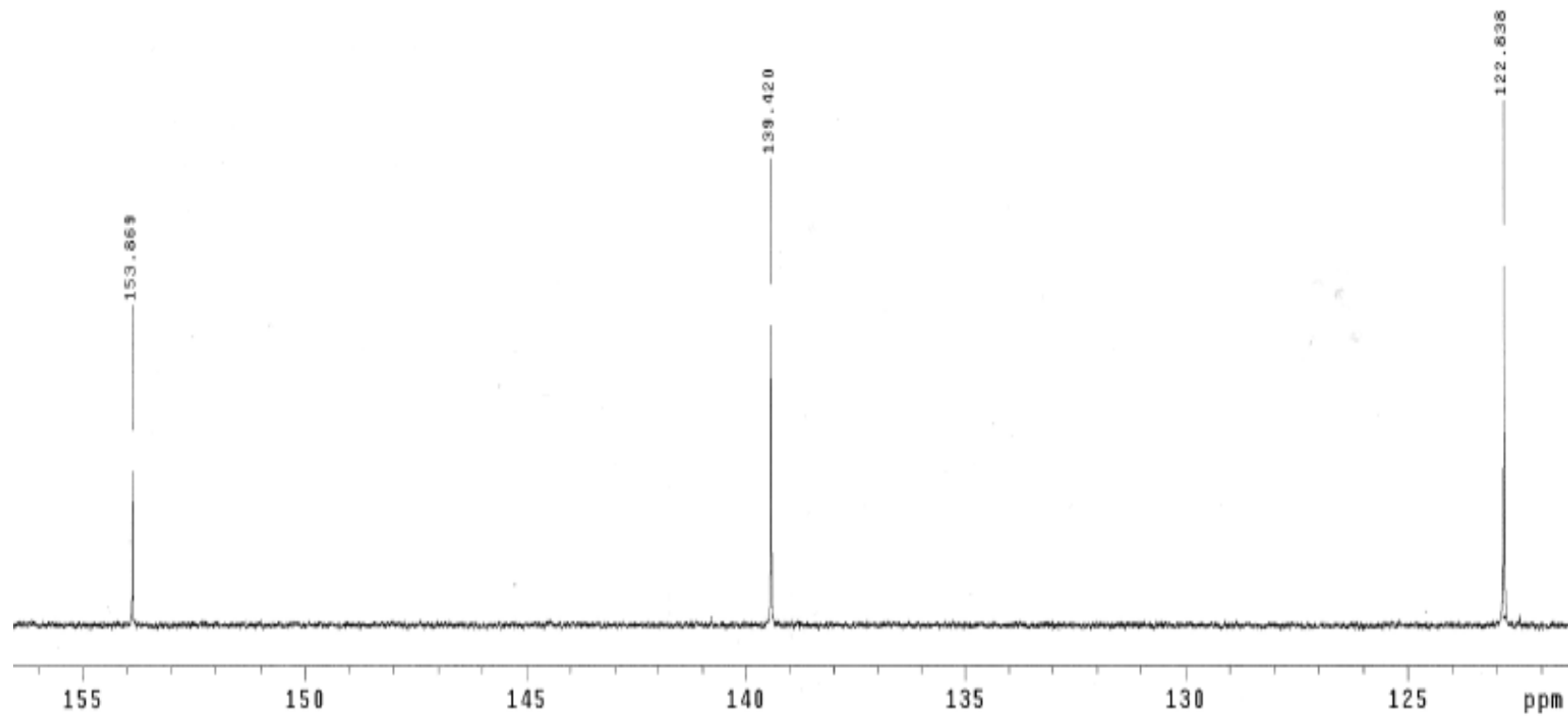




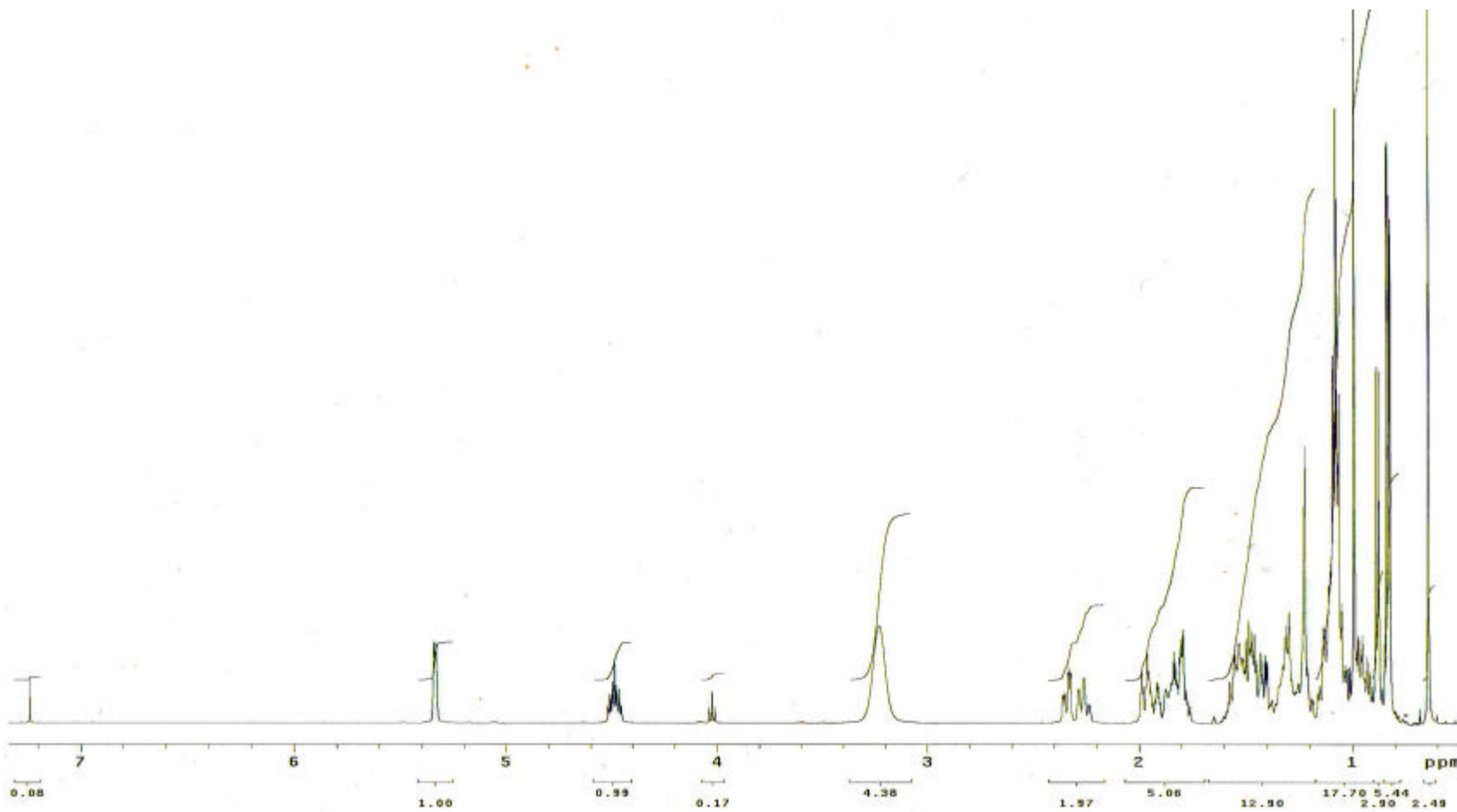
$^{13}\text{C}$ -NMR spectra of dicholesteryl carbonate (DCC)



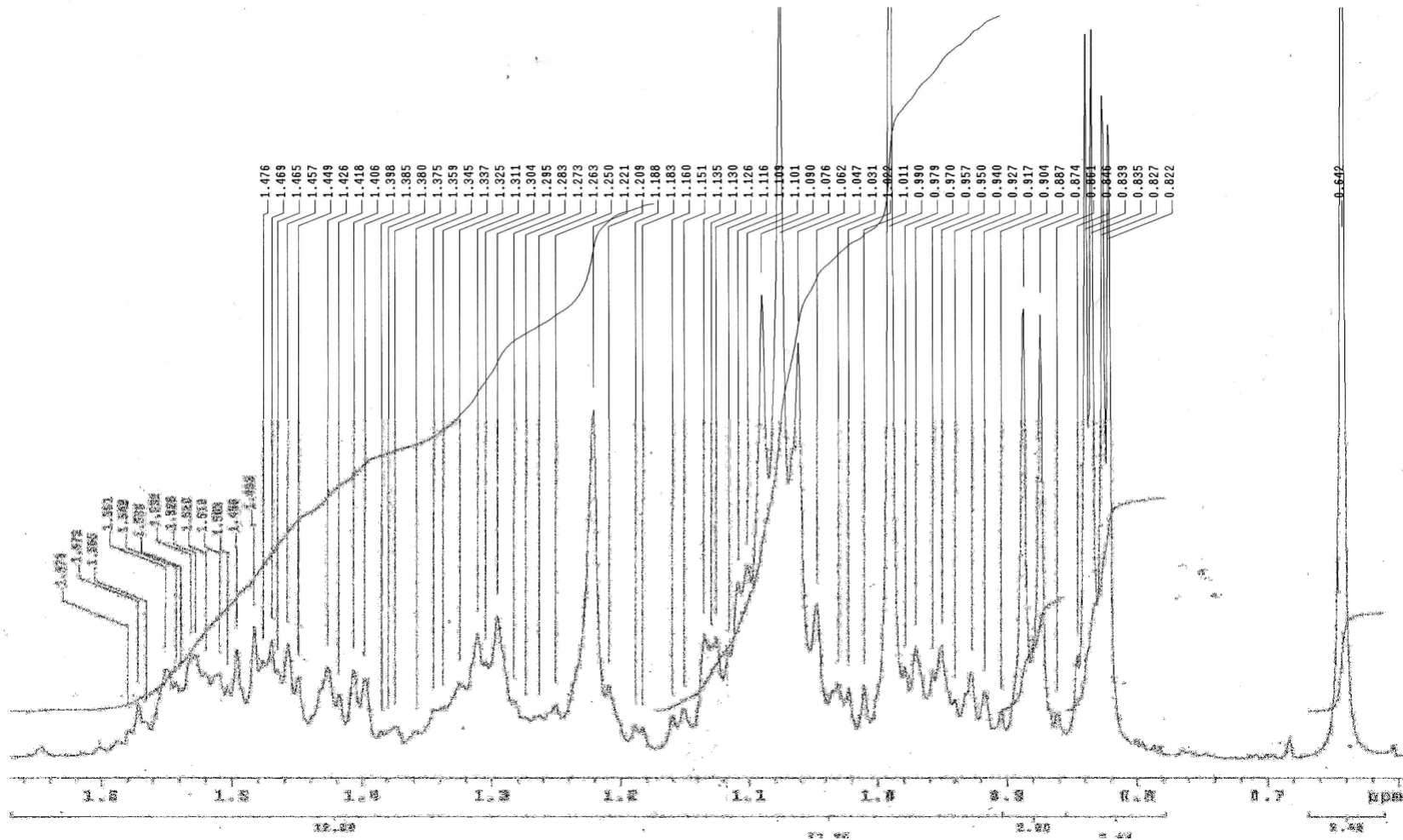
$^{13}\text{C}$ -NMR spectra of dicholesteryl carbonate (DCC)



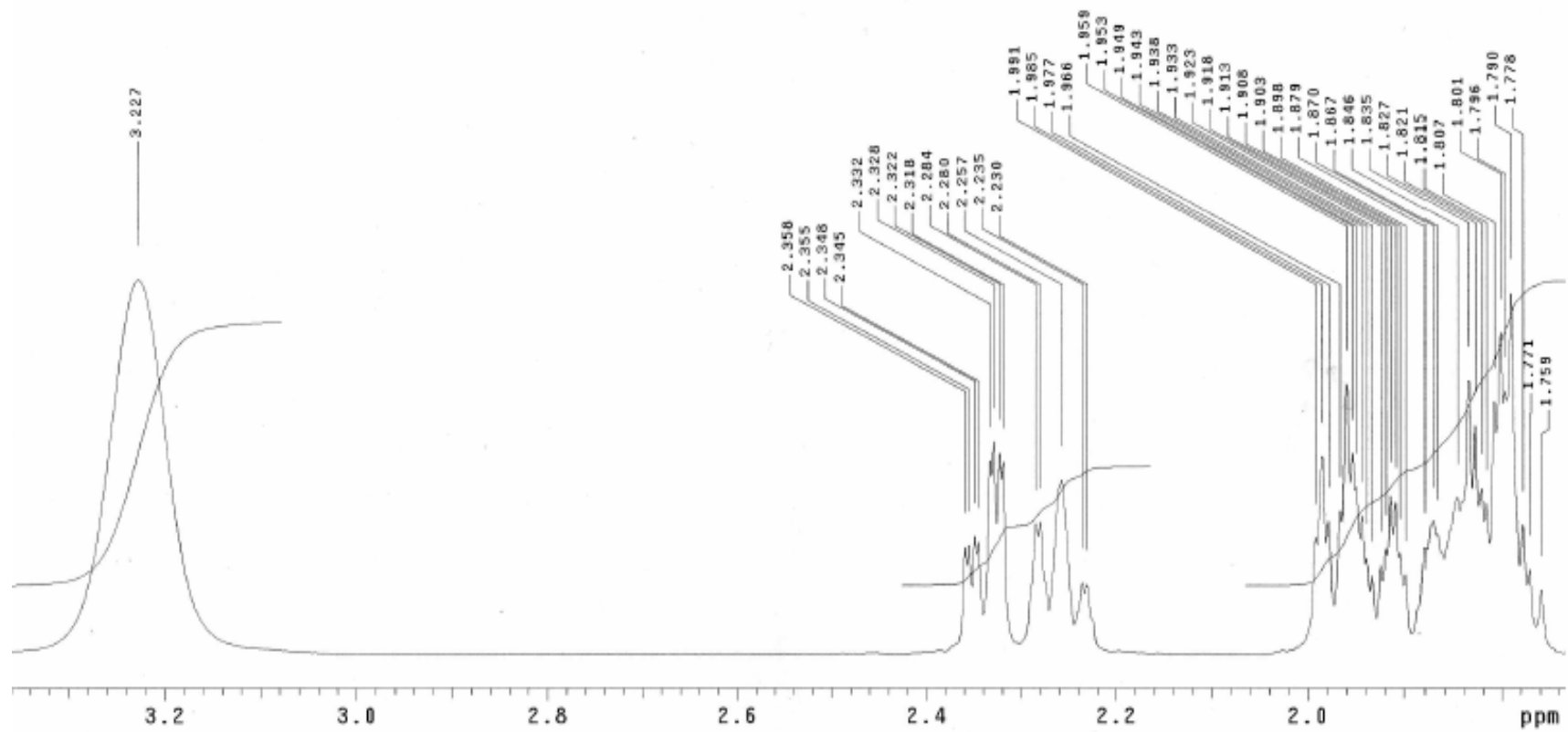
$^{13}\text{C}$ -NMR of dicholesteryl carbonate (DCC)



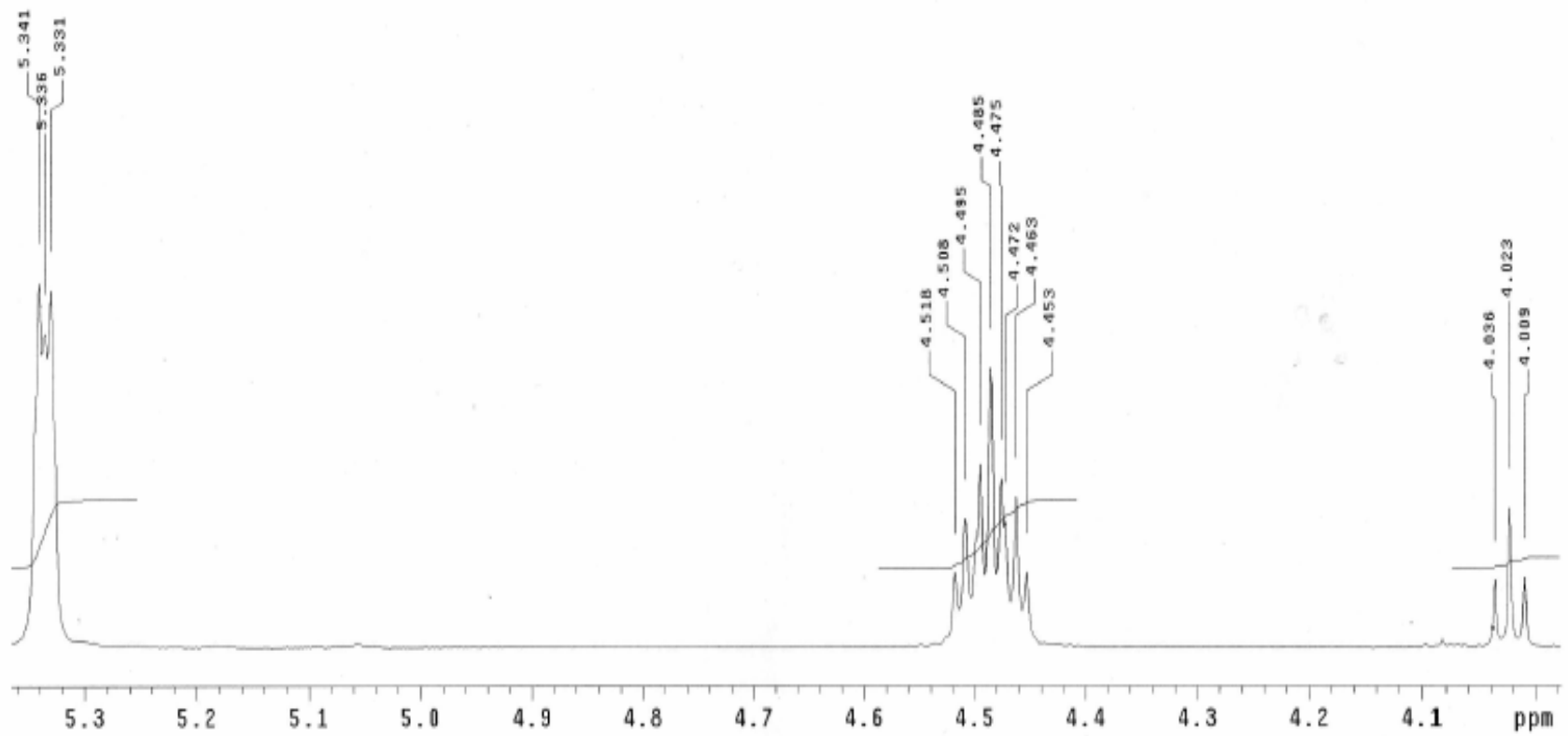
<sup>1</sup>H-NMR spectra of sodium cholesteryl carbonate (SCC)



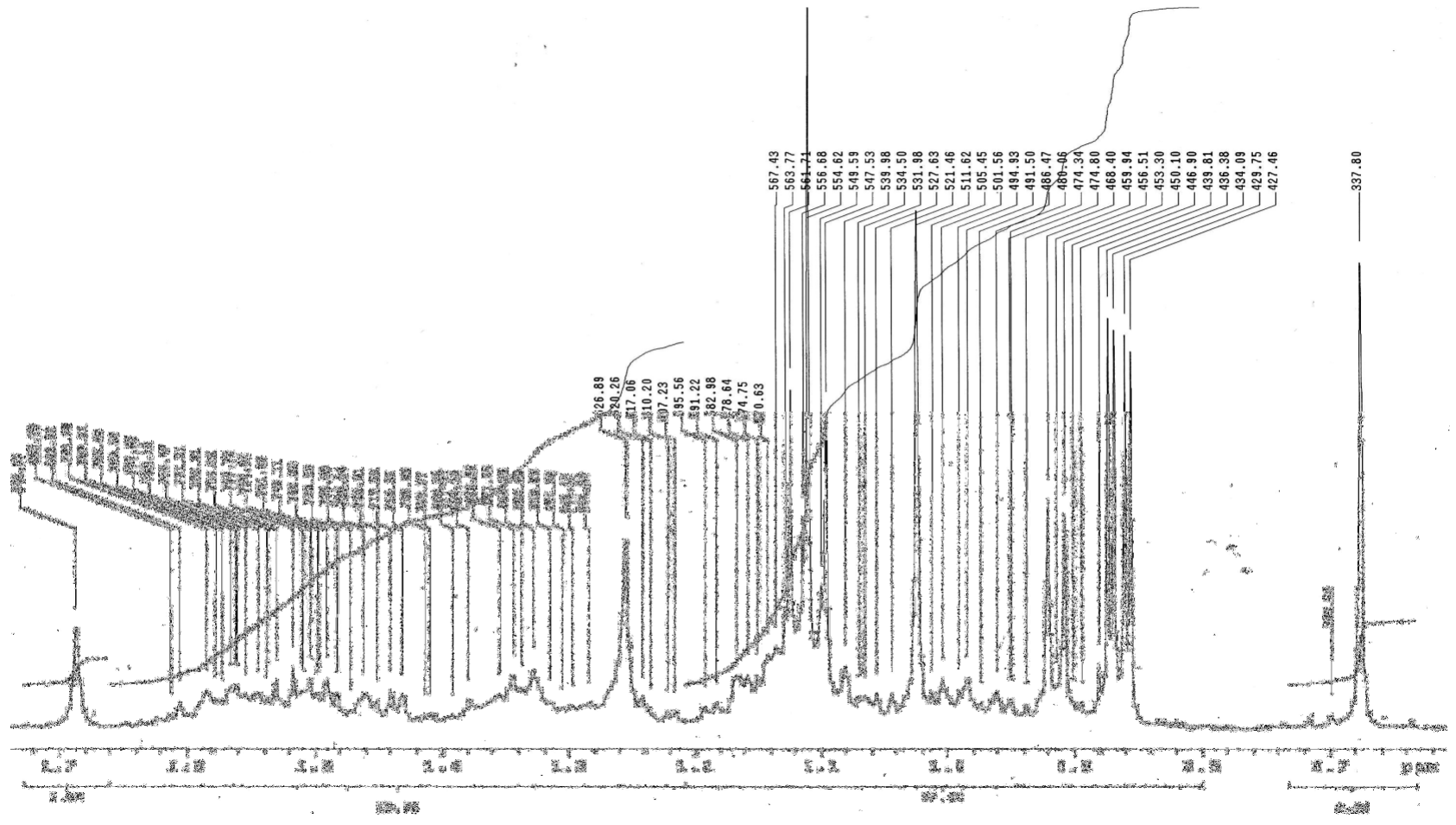
$^1\text{H-NMR}$  spectra of sodium cholesteryl carbonate (SCC)



$^1\text{H-NMR}$  spectra of sodium cholesteryl carbonate (SCC)

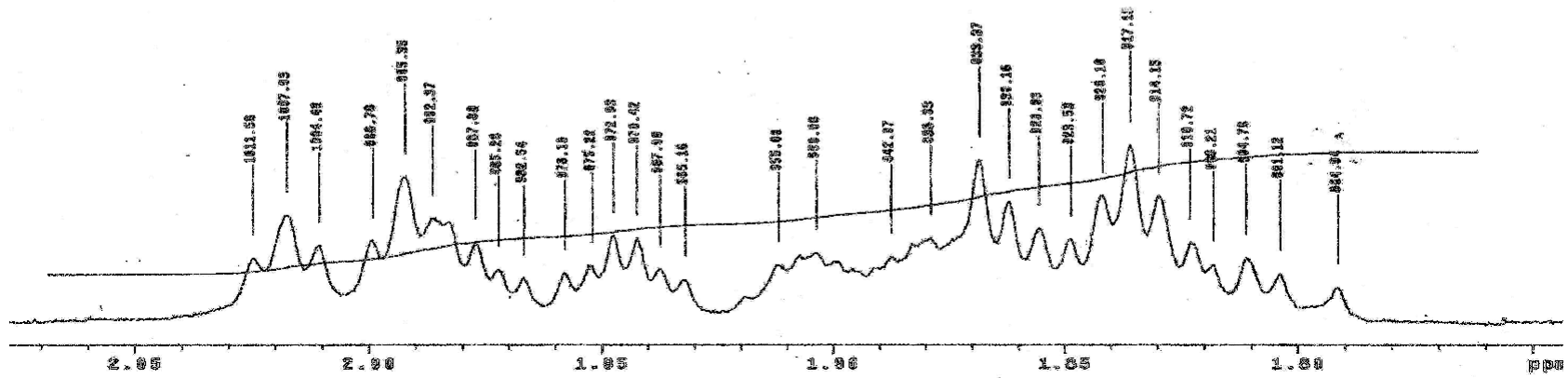


<sup>1</sup>H-NMR spectra of sodium cholesteryl carbonate (SCC)

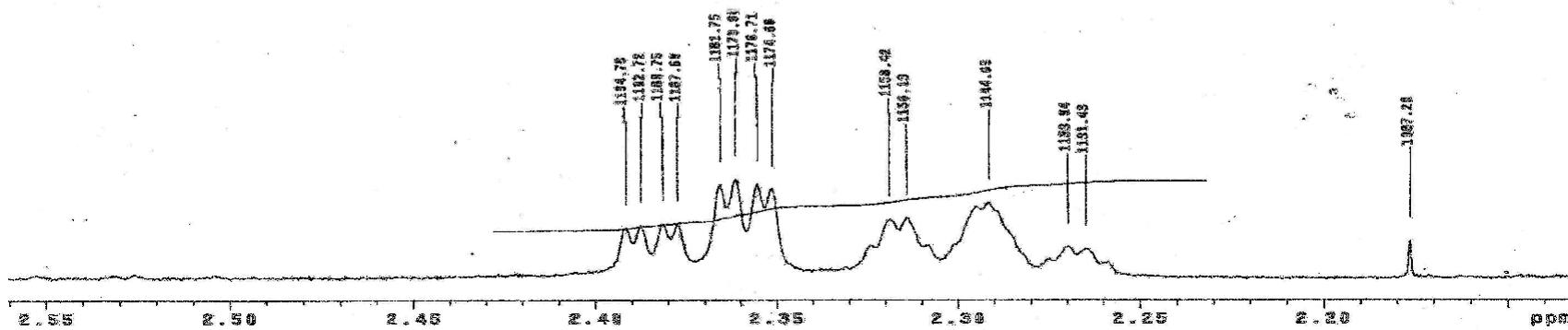


<sup>1</sup>H-NMR spectra of sodium cholesteryl carbonate (SCC)

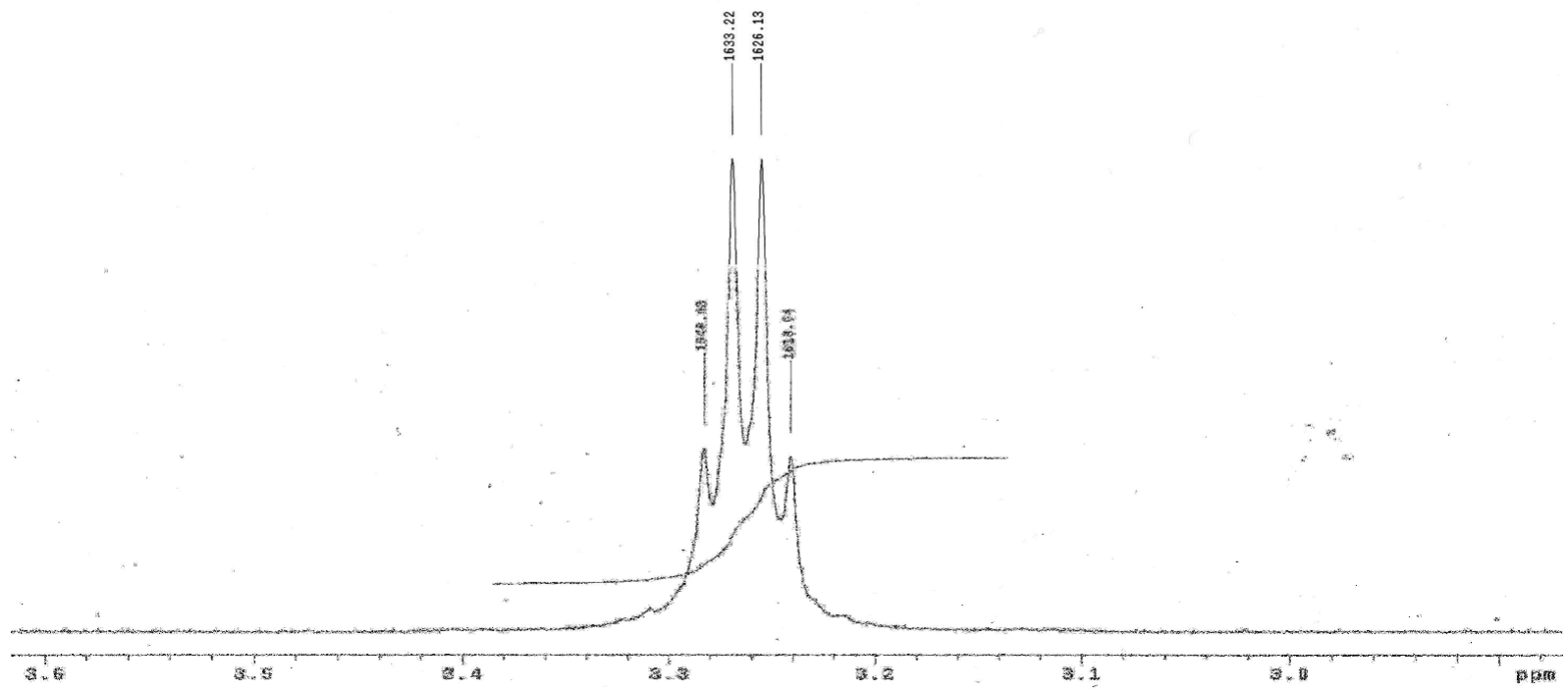




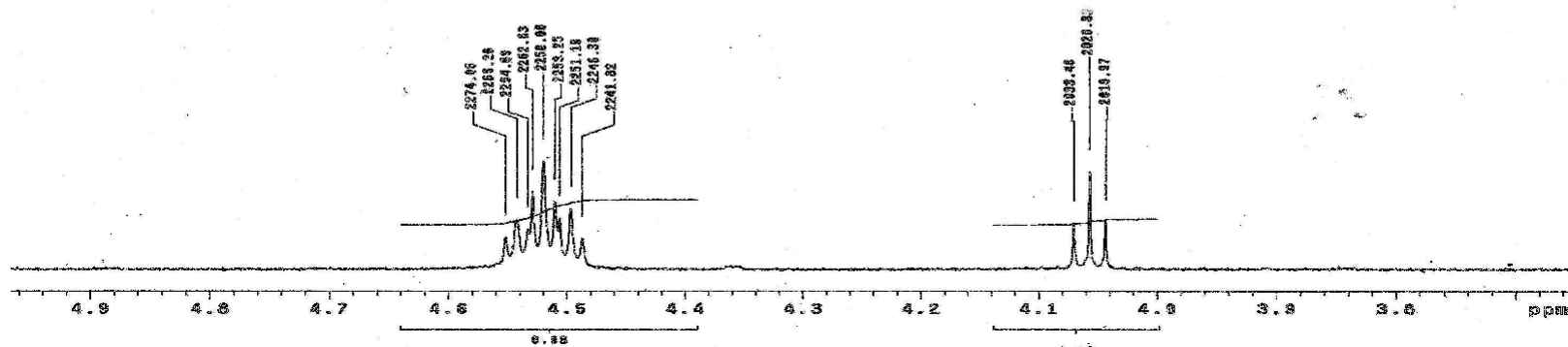
<sup>1</sup>H-NMR spectra of sodium cholesteryl carbonate (SCC)



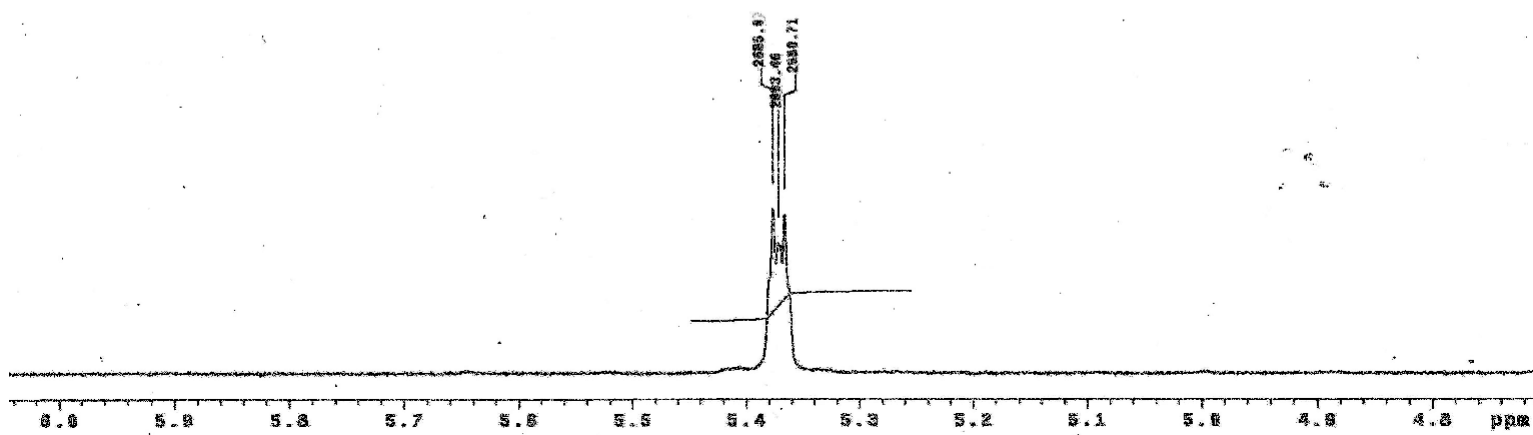
<sup>1</sup>H-NMR spectra of sodium cholesteryl carbonate (SCC)



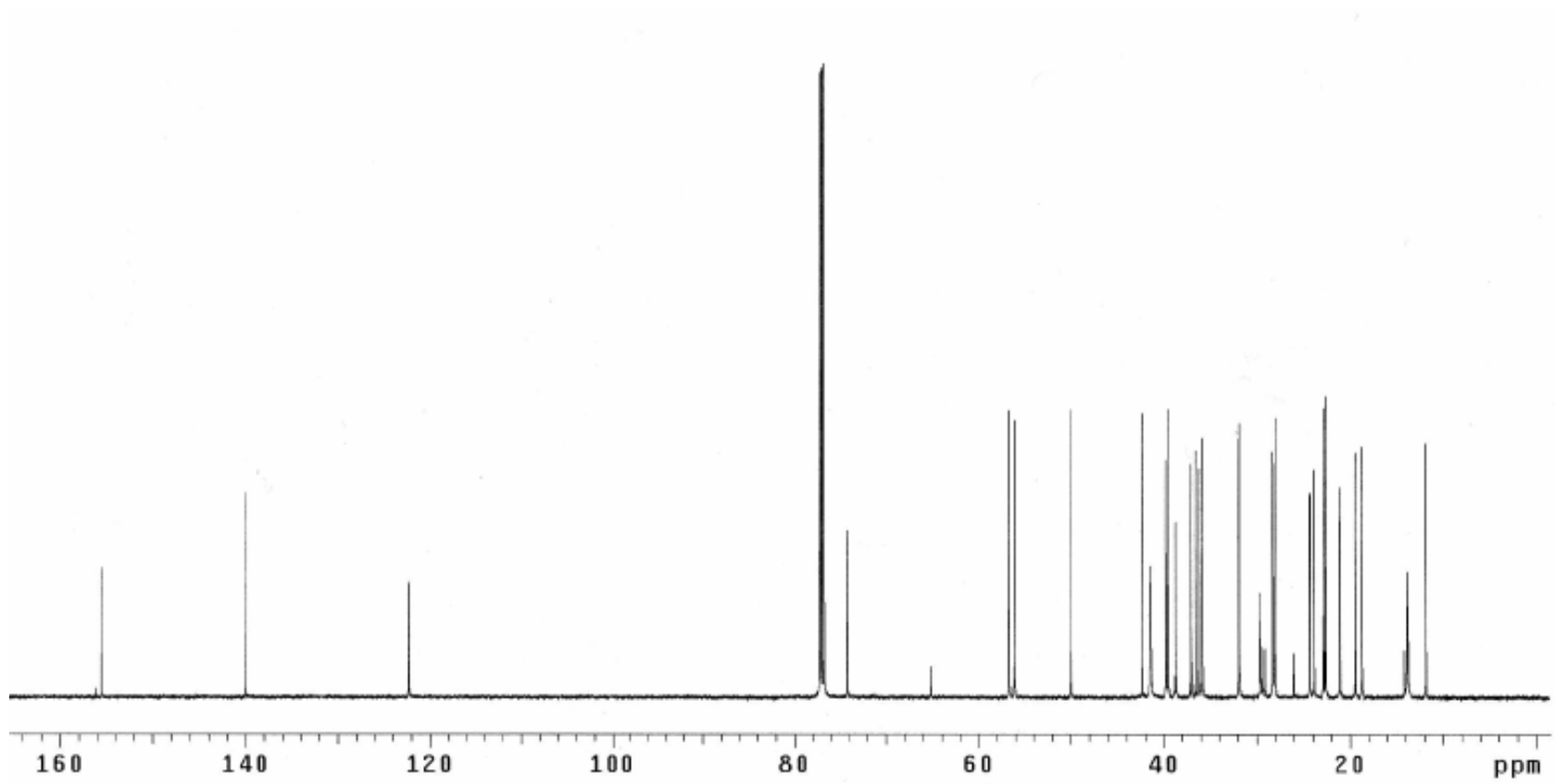
<sup>1</sup>H-NMR spectra of sodium cholesteryl carbonate (SCC)



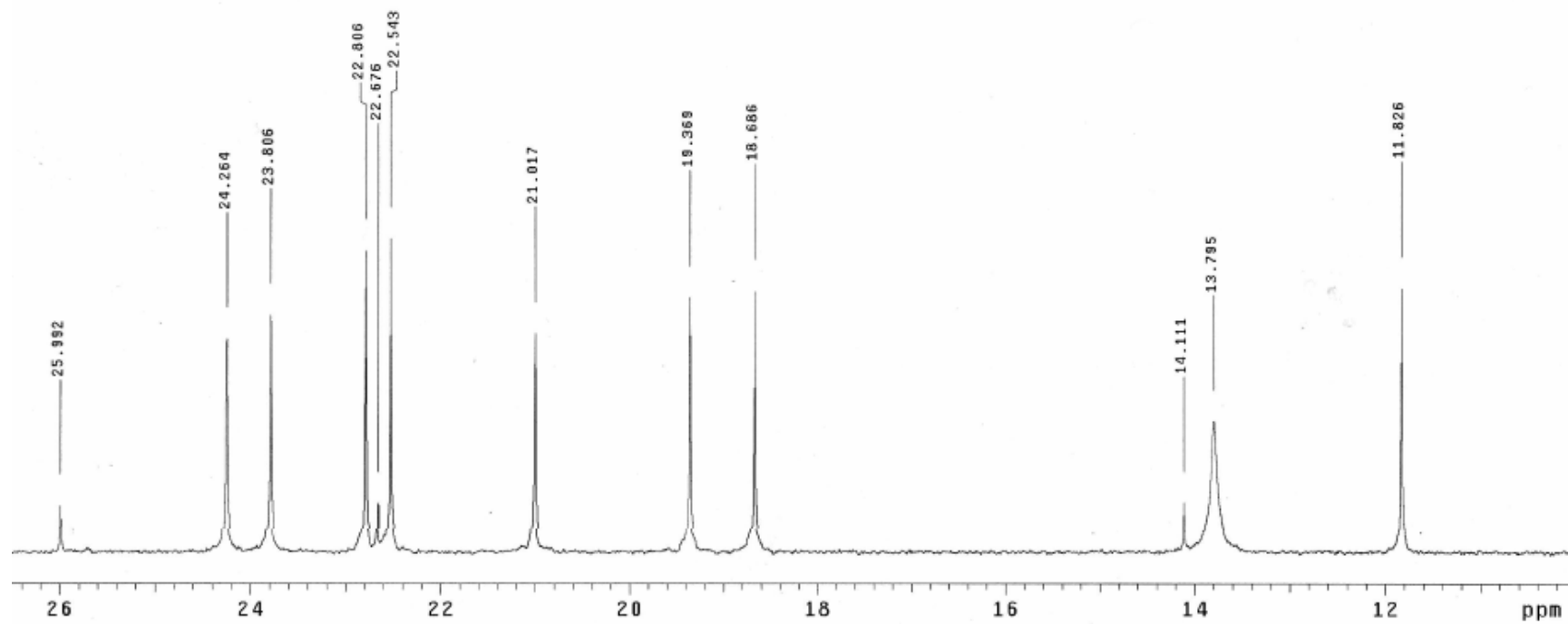
$^1\text{H-NMR}$  spectra of sodium cholesteryl carbonate (SCC)



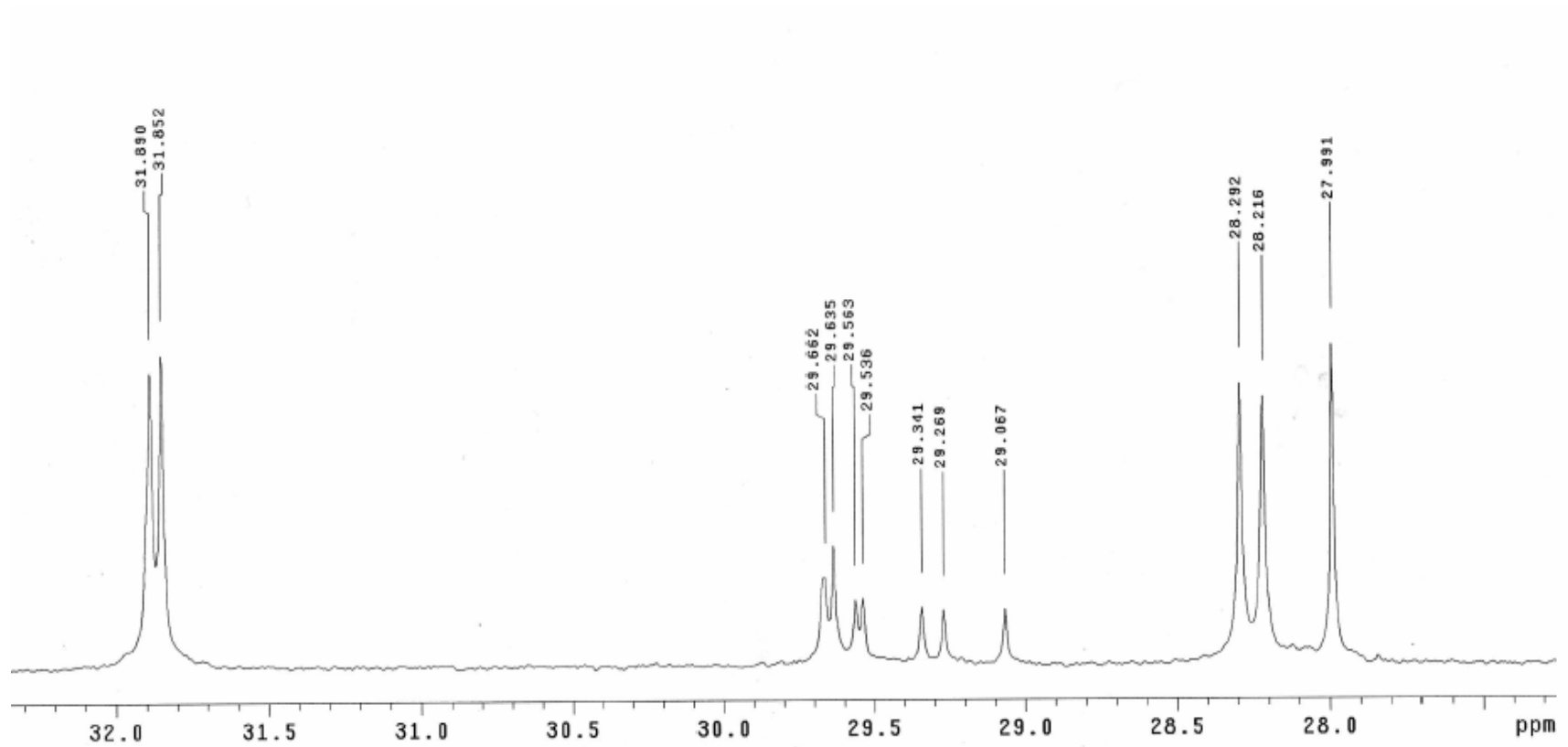
$^1\text{H-NMR}$  spectra of sodium cholesteryl carbonate (SCC)



$^{13}\text{C}$ -NMR spectra of sodium cholesteryl carbonate (SCC)

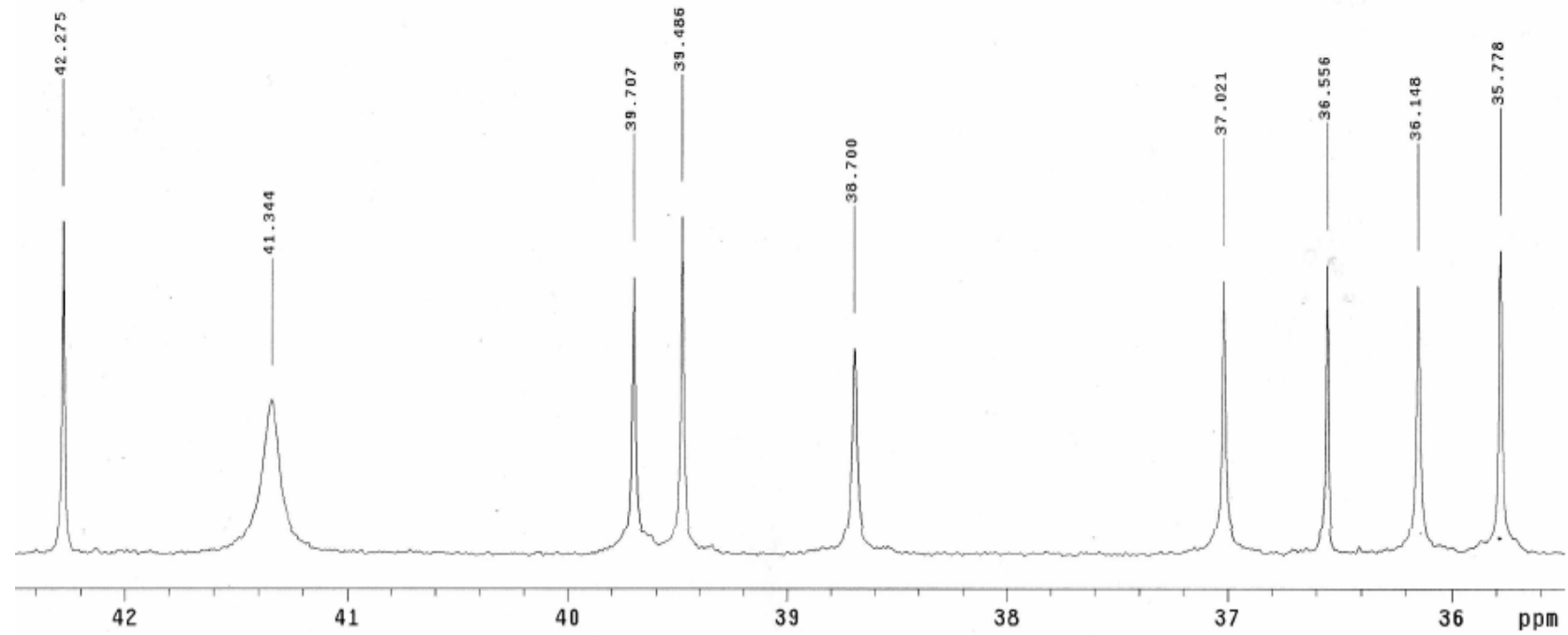


$^{13}\text{C}$ -NMR spectra of sodium cholesteryl carbonate (SCC)

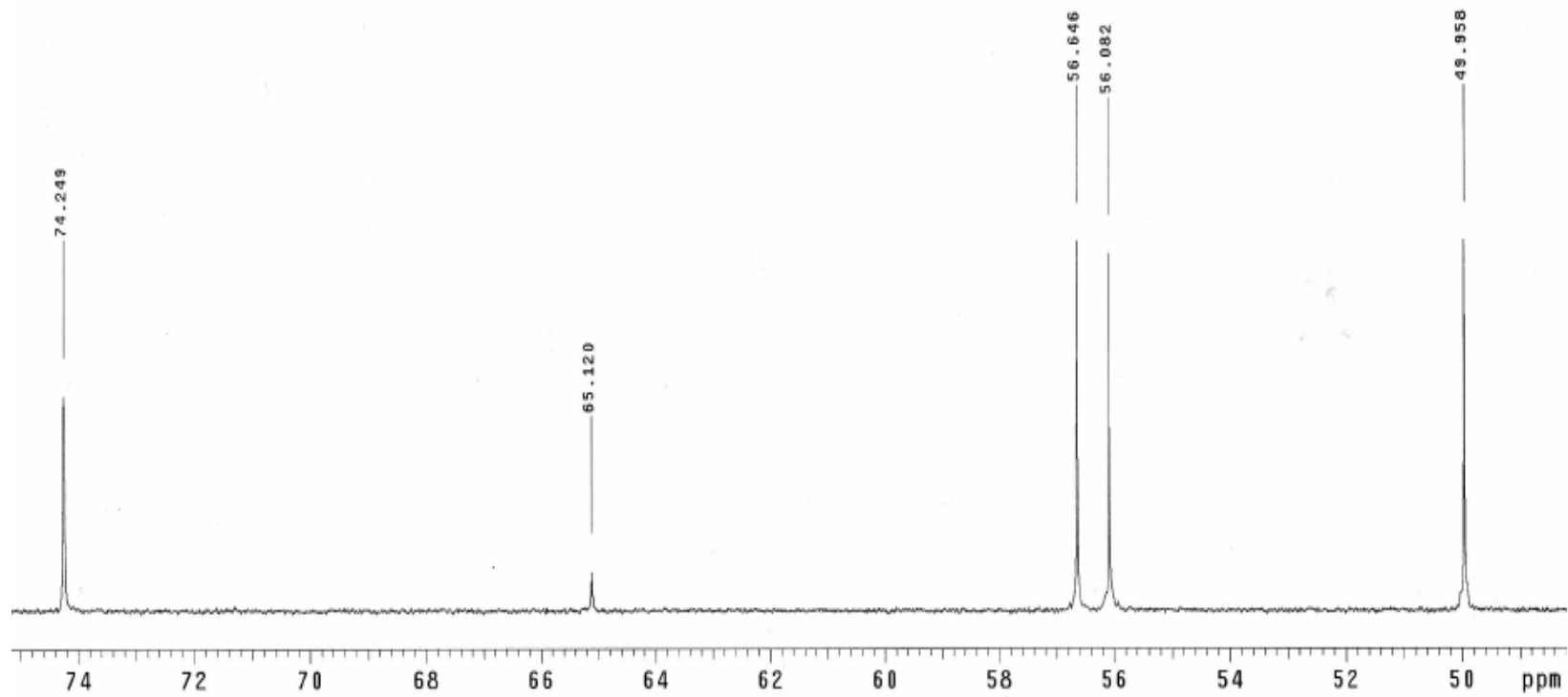


$^{13}\text{C}$ -NMR spectra of sodium cholesteryl carbonate (SCC)

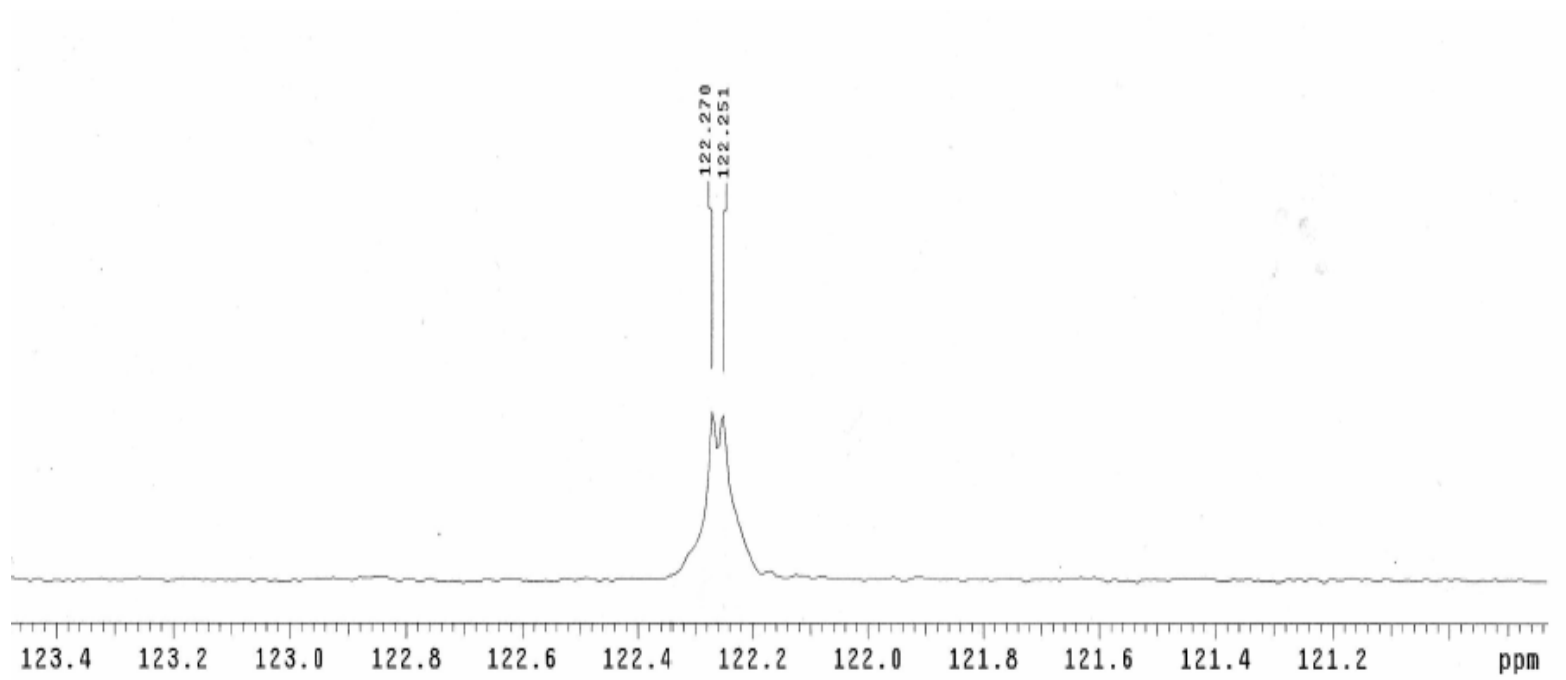




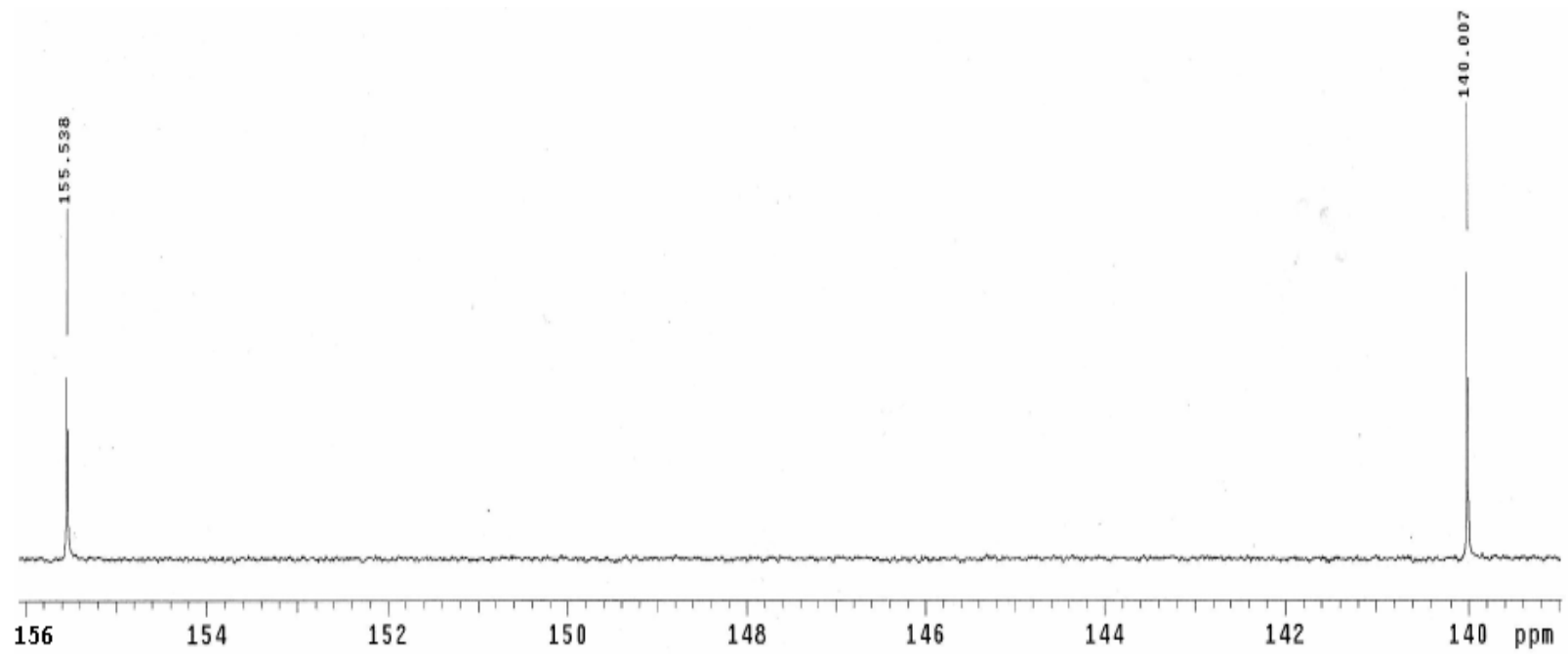
$^{13}\text{C}$ -NMR spectra of sodium cholesteryl carbonate (SCC)



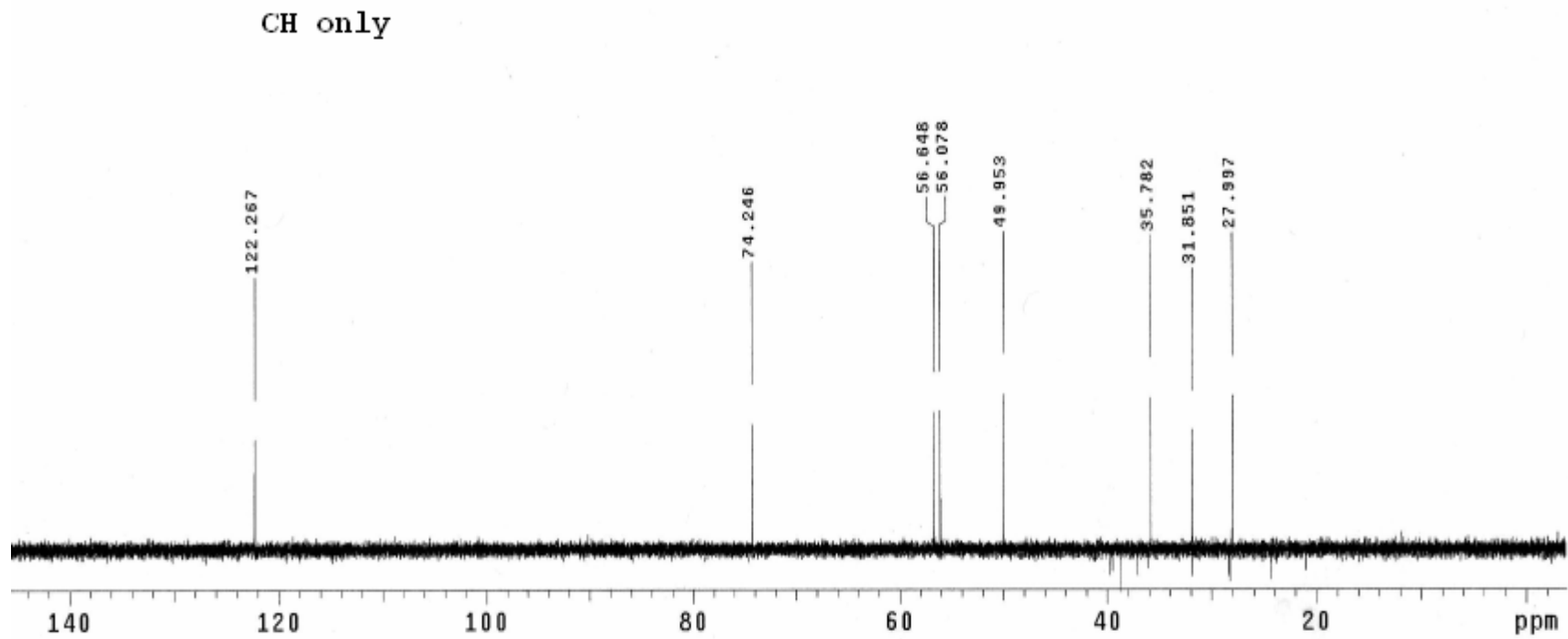
$^{13}\text{C}$ -NMR spectra of sodium cholesteryl carbonate (SCC)



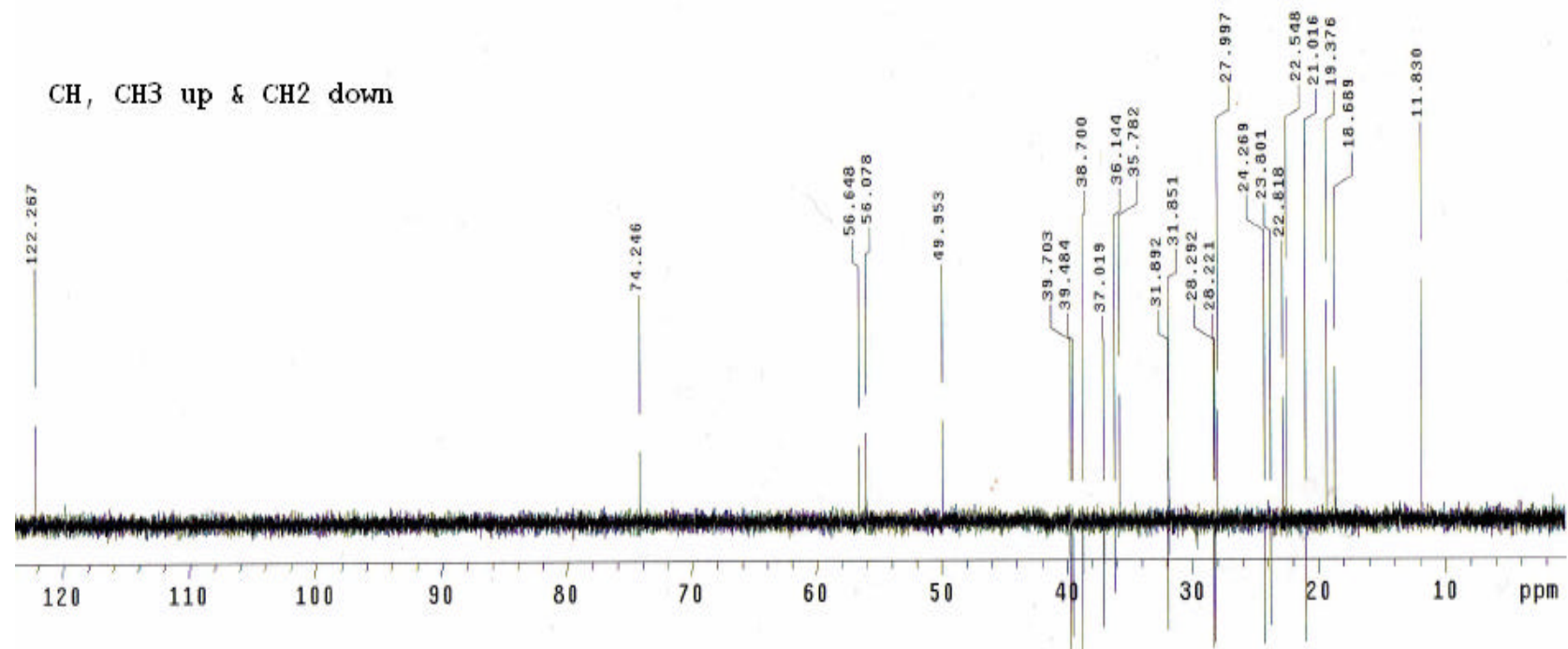
$^{13}\text{C}$ -NMR spectra of sodium cholesteryl carbonate (SCC)



$^{13}\text{C}$ -NMR spectra of sodium cholesteryl carbonate (SCC)

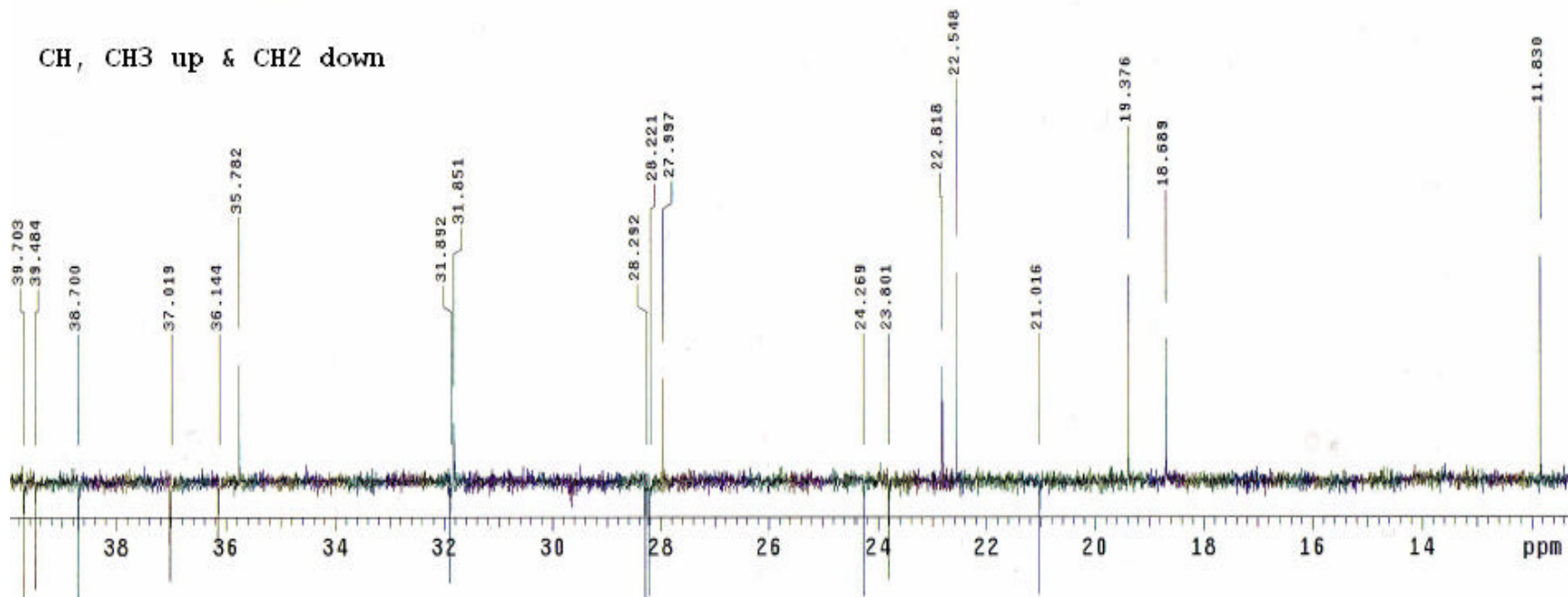


DEPT 90 spectra of sodium cholesteryl carbonate (SCC)



DEPT135 spectra of sodium cholesteryl carbonate (SCC)

CH, CH3 up & CH2 down



DEPT135 spectra of sodium cholesteryl carbonate (SCC)

## VITAE

**Name** Mrs. Rabkwan Chuealee

**Student ID** 4753001

### Education Attainment

Degree	Name of Institution	Year of Graduation
Bachelor of Science in Pharmacy	Khon Kaen University	2000

### Scholarship Award during Enrollment

Royal Golden Jubilee Ph.D. Program, Grant No. PHD/0098/2547, Thailand Research Fund, 2004-2008.

### List of Publications and Proceedings

1. Rabkwan Chuealee, Timothy S. Wiedmann and Teerapol Srichana. 2009. Thermotropic behavior of sodium cholesteryl carbonate. J. Mater. Res. Vol. 24 No. 1. Jan 2009. pp. 156-163. (doi: 10.1557/JMR.2009.0027).
2. Rabkwan Chuealee, Pornanong Aramwit and Teerapol Srichana. 2005. Amphotericin B incorporated in cholesteric liquid crystal. Proceeding of Pharma Indochina IV: Pharmacy in cooperation for development and integration. pp. 275-282.
3. Rabkwan Chuealee, Pornanong Aramwit and Teerapol Srichana. 2007. Characteristics of cholesteryl cetyl carbonate liquid crystals as drug delivery systems. Proceeding of the 2nd IEEE International conference on Nano/Micro



engineered and molecular systems. pp. 1098-1103 (available online IEEE explore and Scopus).

4. Rabkwan Chuealee and Teerapol Srichana. 2007. Amphotericin B in cholesteryl cetyl carbonate mixture as dry powder formulations. Proceeding of the Fifth Pharma-Indochina Conference on Pharmaceutical Sciences: Pharmacy for sustainable development. pp. 1-11.
5. Rabkwan Chuealee and Teerapol Srichana. 2008. Safety of cholesteryl cetyl carbonate mixture nanosystems containing amphotericin B antifungal dry powders formulations. Proceeding on 2008 2<sup>nd</sup> IEEE International Nanoelectronics Conferences. pp. 1478-1483.
6. Rabkwan Chuealee, Sanae Kaewnopparat, Pornanong Aramwit and Teerapol Srichana. 2009. Aerosolization properties, bioactivity and safety of amphotericin B dispersion in cholesteryl carbonate. Proceeding on Respiratory drug delivery (RDD) Europe 2009 Conferences. pp. xx-xx.